ЖУРНАЛ
ПРИКЛАДНОЙ ХИМИИ

Volume 32, No. 1

January 1959

JOURNAL OF
APPLIED CHEMISTRY
OF THE USSR

(ZHURNAL PRIKLADNOI KHIMII)

IN ENGLISH TRANSLATION

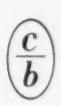

CONSULTANTS BUREAU, INC.

SYNTHESES OF HETEROCYCLIC COMPOUNDS

Volumes 1 and 2 Edited by

A. L. MNDZHOIAN

TRANSLATED FROM RUSSIAN

THE lack of a practical guide to the laboratory preparation of heterocyclic compounds is being met by this series of collections of synthesis methods, originally published by the Armenian Academy of Sciences.

The translation of Volumes 1 and 2 of this series is combined in this convenient handbook, devoted exclusively to the synthesis of furan derivatives.

Subsequent volumes in the series will be published in translation by Consultants Bureau promptly after their appearance in the original Russian.

1959 cloth 6 x 9 155 pp. illus. $6.00

Book Division

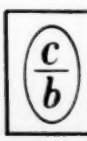

CONSULTANTS BUREAU, INC.

227 WEST 17TH STREET, NEW YORK 11, N. Y.

Volume 32, No. 1

January 1959

JOURNAL OF
APPLIED CHEMISTRY
OF THE USSR

(ZHURNAL PRIKLADNOI KHIMII)

A publication of the Academy of Sciences of the USSR

IN ENGLISH TRANSLATION

Year and issue of first translation:
Vol. 23, No. 1 January 1950

	U. S. and Canada	*Foreign*
Annual subscription	*$60.00*	*$65.00*
Annual subscription for libraries of non-profit academic institutions	*20.00*	*25.00*
Single issue	*7.50*	*7.50*

Copyright 1959

CONSULTANTS BUREAU, INC.
227 W. 17th St., NEW YORK 11, N.Y.

Editorial Board
(ZHURNAL PRIKLADNOI KHIMII)

P. P. Budnikov, S. I. Vol'fkovich, A. F. Dobrianskii,
O. E. Zviagintsev, N. I. Nikitin (Editor in Chief),
G. V. Pigulevskii, M. E. Pozin, L. K. Simonova
(Secretary), V. V. Skorchelletti, N. P. Fedot'ev

Note: The sale of photostatic copies of any portion of this copyright translation is expressly prohibited by the copyright owners.

Printed in the United States of America

JOURNAL OF APPLIED CHEMISTRY OF THE USSR

Volume 32, Number 1 January 1959

CONTENTS

	PAGE	RUSS. PAGE
Stepan Nikolaevich Danilov (on his 70th birthday)	1	3
New Polymer Materials, Their Properties, and Fields of Practical Utilization. M. M. Koton	5	6
Interaction of Calcium Aluminates and Aluminoferrites with Calcium Sulfate. P. P. Budnikov and V. S. Gorshkov	20	21
Sulfoaluminate Cements from the Products of Solid-Phase Reactions. V. I. Kotov	25	26
Properties of Silica Gels Made by the Drying of Silicic Acid Gels in Vacuum. Z. Z. Vysotskii and V. V. Shalya	34	35
Role of the Liquid Phase in the Sintering of Forsterite Refractories. G. V. Kukolev and S. I. Shcheglov	39	40
Thermodynamic Study of Solid-Phase Reactions in the System Calcium Oxide – Alumina. V. I. Babushkin and O. P. Mchedlov-Petrosyan	45	46
Production of Water-Resistant Sand – Silicate Filtration Equipment. M. A. Matveev and V. P. Dyatlova	50	50
Preparation of the Highest Carbide of Chromium. T. Ya. Kosolapova and G. V. Samsonov	55	55
Production of Powdered Iron from Pyrite Cinders in a Fluidized Bed. I. G. Lesokhin	61	60
Phase Diagram of the System NaOH – Na_2CO_3 – NaCl. M. F. Lantratov and A. F. Alabyshev	66	65
Vapor Pressure of SO_2 Over Zinc Bisulfite Solutions. I. L. Peisakhov and V. D. Karmazina	71	70
Effects of Temperature and Partial Pressure of Oxygen in the Gas on the Oxidation Rate of Ammonium Sulfite – Bisulfite Solutions. B. A. Chertkov	78	78
Equilibrium of Carbon with Liquid Alloys of Fe, Mn, Si, and C. M. S. Petrushevskii and P. V. Gel'd	86	86
Gas-Phase Mass-Transfer Coefficients. G. N. Gasyuk, A. G. Bol'shakov, A. V. Kortnev, and P. Ya. Krainii	95	95
The Solution Rates of Methane and Nitrogen – Hydrogen Mixture in Condensing Ammonia. V. I. Atroshchenko and N. A. Gavrya	100	99
Technology of the Production of Iodine by an Electrochemical Method. Ya. I. Gamzulov	105	105

CONTENTS (continued)

	PAGE	RUSS. PAGE
Graphitized Anodes in the Electrolysis of Aqueous Chloride Solutions. V. V. Stender and O. S. Ksenzhek	111	110
Influence of Electrolyte Composition on the Distribution of Current Inside a Graphite Anode and on Its Internal Wear. B. M. Bulygin	122	121
Production of Iron – Nickel Alloys by Electrodeposition from Chloride Electrolytes. V. V. Sysoeva	129	128
The Discharge Mechanism of a Powdered-Zinc Electrode. V. N. Flerov	133	132
The Protective Action of Volatile Inhibitors and Anticorrosion Greases at Tropical Temperatures and High Humidities. B. E. Piskorskii and E. M. Il'ina	139	138
Study of the Protective Action of Mixtures of Corrosion Inhibitors in Neutral Media. A. S. Afanas'ev and G. V. Zhuk	143	141
Sulfonated Ion-Exchange Resins Based on Polyvinyl Chloride and Other Vinyl Polymers. A. A. Vasil'ev and A. A. Vansheidt	151	150
Acid Condensation of Lignin. D. Tishchenko	158	157
Methods for the Separation of Lignosulfonic and Carbohydrate Sulfonic Acids. M. N. Tsypkina and I. M. Balashova	167	166
Determination of the Percentages of 1 – 4, 3 – 4, and 1 – 2 Units in Synthetic Isoprene Rubbers from the Curves for their Rates of Oxidation by Benzoyl Hydroperoxide. N. G. Kasatkina	171	170
Oxidation of Paraffin, Initiated by Chlorine at the First Reaction Stage. I. V. Berezin, G. Vagner, and N. M. Émanuél'	175	173
Effect of Esters of Unsaturated Phosphonic Acids on the Antioxidant Properties of Mineral Oil. K. K. Papok, K. N. Anisimov, B. S. Zuseva, and N. E. Kolobova	181	180
Foam Hydrogenation of Fats. S. Yu. Elovich, G. M. Zhabrova, P. G. Krivenkova, and T. D. Semenovskaya	188	187
Chemical Conversions of Mercury Salts and Their Role in the Hydrofluorination of Vinylacetylene. I. M. Dolgopol'skii, I. M. Dobromil'skaya, and B. A. Byzov	195	194
Direct Synthesis of Phenyltrichlorosilane in a Fluidized Bed. K. A. Andrianov, S. A. Golubtsov, N. N. Tishina, and I. V. Trofimova	203	201
Synthesis of β-Methylnaphthalene. I. L. Kotlyarevskii and A. S. Zanina	209	207
Synthesis of Isodecyl Alcohol and Production of Esters from it. A. I. Kutsenko, V. I. Lyubomilov, and R. A. Abramova	213	211
Brief Communications		
Decomposition Potentials of NaCl in the Fused Electrolytes NaCl – $CaCl_2$ and NaCl – $CaCl_2$ – $BaCl_2$. K. Ya. Grachev and V. Ya. Zhuryutina	216	214
Reduction of Potassium Sulfate by Methane. S. V. Kushnir	219	216
Processes Leading to Generation of Droplets in the Rupture of Bubbles at Liquid – Gas Interfaces. V. G. Gleim, I. K. Shelomov, and B. R. Shidlovskii	222	218

CONTENTS (continued)

	PAGE	RUSS. PAGE
Solubility of Peat Humic Acids. S. E. Burkat.	227	222
Simultaneous Condensation of Substituted Orthosilicate Esters and an Orthosilicate Ester with a Polyester. V. B. Losev	231	225
Purification of Adiponitrile. A. E. Kulikova, E. N. Zil'berman, Ts. N. Roginskaya, and M. M. Smirnova	234	227
Production of Methyl Chloride by Catalytic Hydrochlorination of Dimethyl Ether. R. M. Flid, K. S. Minsker, and N. F. Skvortsova	238	230
Production of Anhydrous Sodium Acetate from an Aqueous Methanol Solution of Methyl Acetate. A. G. Sayadyan and A. E. Akopyan.	241	233
Synthesis of Quaternary Ammonium Salts from a Broad Fraction of High-Molecular Aliphatic Alcohols made by Oxidation of Paraffinic Hydrocarbons from Petroleum. V. P. Érekaev and M. P. Gerchuk	244	235
All-Union Conference on the Chemistry and Practical Uses of Organosilicon Compounds. V. B. Losev	247	238
Errata	251	

STEPAN NIKOLAEVICH DANILOV

(On His 70th Birthday)

January 1959 marks the 70th birthday and 45 years of scientific and teaching activity of that most eminent chemist and remarkable teacher, Corresponding Member AN SSSR, Director of the Institute of High-Molecular Compounds AN SSSR, S. N. Danilov.

S. N. Danilov was born January 6, 1888 in Vitebsk. His scientific activity began in the University of Peterburg, where he graduated in 1914, in the Department of Organic Chemistry. Since that time, Academician Favorskii's outstanding pupil Danilov has been successfully developing the scientific teachings of the Butlerov – Favorskii school for 45 years.

From 1918 he was first deputy editor of the Journal of the Russian Physicochemical Society, and then editor of the Journal of General Chemistry. He still holds the latter post. He devotes much attention to the Leningrad Section of the D. I. Mendeleev Chemical Society, and has been its chairman since 1951.

In 1930 he was appointed professor and Head of the Chair of Chemical Conversion of Cellulose in the Lensoviet Technological Institute, Leningrad; he has held this position to the present day.

Danilov's earliest researches were concerned with the course of dehydration of α-glycols and their reactions with acid reagents. His discovery of the isomeric conversion of aldehydes into ketones, made in 1916, was of great scientific importance.

In studying the dehydration of α-glycols, Danilov showed that the reaction conditions have a greater influence than the structure of the original α-glycol on the reaction products. It was found that by variations of the reaction conditions it is possible to vary the composition of the product so that it contains increasing amounts of ketones, and to obtain as many carbonyl compounds as there are possible ways of splitting a water molecule from the hydroxyl groups of the α-glycol. It was found that an aldehyde is converted into the ketone which is formed from the glycol under the harshest reaction conditions. Together with E. D. Venus-Danilova, S. N. Danilov made detailed studies of the isomerization conditions of different classes of aldehydes. It was found that α-hydroxyaldehydes are isomerized to hydroxyketones and carboxylic acids under the action of catalysts. This new discovery was confirmed by numerous examples of conversion of hydroxy and halo aldehydes and of primary halo ketones into hydroxy ketones and acids.

The systematic relationships in the isomeric conversions of aldehydes and hydroxy aldehydes accounted for the mechanism of ketone formation in the dry distillation of wood, the formation of butyric acid in the fermentation of sugar-containing materials, etc.

These reactions are of considerable interest in relation to biochemical conversions of organic compounds.

A further development of work on the conversion of α-halo and α-hydroxy aldehydes into acids was the research of S. N. Danilov and his pupil, presently Professor of the Tbilisi Pedagogic Institute, A. M. Gakhokidze on the regrouping of halogenated monoses to orthosaccharic acids. Danilov devised a scheme representing the formation of all theoretically possible saccharic acids. Further investigations performed by A. M. Gakhokidze with galactose, L-arabinose, and other substances showed that the new type of saccharic regrouping discovered by S. N. Danilov is general for all sugars. Danilov made extensive use of acid – base – salt catalysis in reactions of isomeric conversion.

S. N. Danilov, jointly with E. D. Venus-Danilova and P. S. Shantarovich, effected the epimeric transformation of glucose to frutose by a new method. Instead of the formerly used mineral hydroxides, a dry organic base (pyridine or quinoline) was used as the reaction medium. It was found that under these new conditions – in absence of moisture – the reaction proceeds somewhat differently: only glucose and fructose were isolated from the reaction medium. Neither mannose nor organic acids were found. This convenient method for epimerization of glucose to fructose is widely used in this country and abroad. Danilov has performed a series of interesting researches in the Institute of High-Molecular Compounds of the Academy of Sciences USSR. He has prepared new amino and guanidino derivatives of monoses and of polyhydric alcohols and various derivatives of xylitol and xylitan, which are starting materials for new high polymers.

During his tenure of the Chair of Chemical Conversion of Cellulose in the Lensoviet Technological Institute of Leningrad, and during his work in the Plastics Institute from 1930 to 1938 and in the Institute of High-Molecular Compounds of the Academy of Sciences USSR since 1949, Danilov with his pupils has done much work on the chemistry of cellulose and its derivatives and on the chemistry of chitin.

The hydrolysis of alginic acid was studied and a series of new derivatives of mannuronic acid was prepared.

Danilov's outstanding work, a research of great significance, was his study of the theory of cellulose nitration. This work developed the Mendeleev – Sapozhnikov theory of nitration.

The properties of cellulose nitrates have been studied in detail in a series of investigations, and the chemistry of the action of weak and strong bases and acetic acid on cellulose nitrate has been elucidated. The causes of the viscosity decrease produced by ammonia were studied.

In his studies of the synthesis and properties of cellulose nitrates he also investigated the properties of other cellulose derivatives. Danilov and his associates were the first to prepare and describe the hydroxybutyl ethers of cellulose, and investigated glycerol ethers of cellulose and carboxymethylcellulose.

In addition to his work in the field of the chemistry of cellulose and its derivatives, Danilov worked on chitin, a natural polysaccharide which had been studied little. Conditions for activation of chitin and its dissolution in alkali were found. The glycerol, hydroxyethyl, and ethyl ethers of chitin were prepared and described for the first time. Ethylated chitin, which is soluble in organic solvents and yields viscous solutions, is of practical interest.

An extensive range of investigations has been carried out by Danilov and his associates on cuprammonium solutions of cellulose and on the chemistry of xanthates and viscose.

Investigations of the formation of basic copper salts and copper hydroxide showed that the preparation conditions and the composition of the salts and impurities have an important influence on the solubility of cellulose and the properties of the spinning solutions. Danilov devised a coagulation method as a test for ripeness of the spinning solution.

In a study of oxidation processes in cuprammonium cellulose solutions in presence of organic and mineral additives Danilov showed that sulfites act as oxidation inhibitors.

The results of physicochemical investigations of cuprammonium solutions of cellulose and other polyhydroxy compounds refuted the concept of the alcoholate nature of the copper – cellulose compound in solution. Studies of the composition of precipitates isolated from cuprammonium cellulose solutions by addition of salts and alkalies showed that the precipitates did not contain chemical compounds of constant composition which had previously been supposed to exist.

Studies of the composition of viscose and of the ripening process led Danilov and his associates to the development of a new branch of viscose chemistry – polysulfide compounds – and made it possible to advance new views on the processes taking place in viscose.

In 1934 Danilov prepared the thioanhydride of cellulosexanthic acid for the first time. In further work, first with model compounds and then with cellulose derivatives, the conversion of dixanthates into thioanhydrides by the action of sulfur acceptors: cyanides, sodium sulfide, sodium sulfite, and sodium arsenite was demonstrated.

Studies of the properties of cellulosexanthic acid thioanhydrides showed that they are readily decomposed in presence of alkali and therefore cannot exist in viscose, although the possibility is not excluded that they can

be formed during viscose ripening from cellulose dixanthides by the action of sulfur acceptors present in viscose. Cellulose dixanthides are formed by oxidation of isolated cellulose xanthates and of viscose by atmospheric oxygen; their formation in viscose and subsequent decomposition by alkali accelerate the ripening of viscose. It was shown in this investigation that dixanthides do not differ in structure from dixanthides of simple alcohols. Studies of the composition of viscose revealed the presence of the disulfide of sodium perthiocarbonate, and the accumulation of polysulfide compounds during ripening.

S. N. Danilov

Danilov elucidated the action mechanism of sulfite. It was found that it acts not only as an antioxidant for viscose, but also as a sulfur acceptor. Potassium cyanide and sodium arsenite act similarly to sulfite in viscose.

New techniques and methods of viscose analysis were needed for studies of the composition of viscose, the chemical conversions of cellulose xanthates, and the distribution of carbon disulfide during xanthation.

Danilov and his associates developed new methods for analysis of cellulose xanthate and viscose. They were the first to use the tracer atom method for determination of the distribution of carbon disulfide between the components of viscose and for determination of the loss of sulfur by polysulfide compounds.

In addition to theoretical problems, Danilov worked on current industrial questions. He developed a method of conferring the properties of wool to viscose fibers by means of wool hydrolyzates, and studied the effects of various factors in the first stage of the process — mercerization — on the distribution of carbon disulfide in xanthation in continuous processes of viscose production. A method of emulsion xanthation (with direct and reverse emulsions) with the object of producing viscose in a single apparatus was developed and viscoses of production quality were obtained. Several investigations were performed on the composition of spinning baths and on the removal of organic impurities from spent alkali.

S. N. Danilov has published numerous reviews of organic chemistry and chemical technology.

His work in the field of intramolecular oxidation — reduction reactions of carbonyl compounds, investigations of cellulose and its derivatives, viscose, and cuprammonium solutions, and numerous other researches have won world fame for S. N. Danilov.

Danilov's talents as a scientist and teacher, his love of science and his personal charm have always attracted young scientists; he has trained more than 50 graduates and doctors of science.

In this brief review it is not possible to do full justice to all the wide range of problems to which S. N. Danilov devoted his varied scientific activities.

The Soviet Government has placed a high value on the services rendered by S. N. Danilov to our science and industry, and in training students and scientists, and has rewarded his with two Orders of Lenin, the Order of the Red Banner of Labor, the "Badge of Honor" order, and various medals.

A. Anikeeva and E. Plisko.

NEW POLYMER MATERIALS, THEIR PROPERTIES, AND FIELDS OF PRACTICAL UTILIZATION

M. M. Koton

The science of high polymers is undergoing continuous development, and each year brings new discoveries in the field of new polymer materials with new and often quite unexpected properties. We are witnessing rapid progress in methods of synthesizing new polymers, of modifying the properties of known polymer materials by the use of fundamentally new polymerization processes, and also of improving methods for the conversion of polymers into various articles.

By the use of stereospecific catalysts it is possible to obtain polymers of a high degree of crystallinity ("isotactic" polymers) of increased heat resistance, and capable of yielding fibers with valuable technical properties. The development of copolymerization methods, with wide use of mechanochemical methods and irradiation, makes it possible to obtain block and graft copolymers of improved physical and mechanical properties. Studies of the fine structure of polymers by means of new physical methods (light scattering, nuclear and electronic paramagnetic resonance, mass spectroscopy) provide new approaches to the problem of producing new polymers with predetermined properties. Plastics, synthetic rubbers, artificial and synthetic fibers are being more widely and boldly used in various branches of technology, agriculture, medicine, and the production of consumer goods with improved properties (lighter footwear, crease-resistant and waterproof fabrics, abrasion-resistant tires, and many others). Problems of house building can be solved in new ways by the use of reinforced and laminated plastics, and honeycomb and foam plastics. The rapid development of the chemical industry specified by the May Plenary Session of the Central Committee of the C. P. S. U. will make it possible to create an abundance of various polymer materials in a short time. It is therefore necessary to make the workers of our industry familiar with the properties of new polymers, so that these can be adopted in the national economy as soon as possible.

Polymers of Unsaturated Hydrocarbons

Polyethylene and its derivatives. An exceptionally valuable polymer material is polyethylene, made by polymerization of ethylene. The main raw materials for production of ethylene are by-product gas from the processing of heavy oils, gases made by pyrolysis of ethane and propane, and natural gas. Different types of polyethylene are now available with properties which differ in accordance with the polymerization method.

High-pressure polyethylene is made at temperatures of 200° and over and pressures from 500 to 1500 atmos, in the presence of 0.03 – 0.1% of oxygen in the gas; this is necessary for the formation of peroxides from oxygen and ethylene, which give rise to free radicals which initiate ethylene polymerization [1]. The polymers have molecular weights from 2,000 to 20,000, and occasionally up to 50,000. High-pressure polyethylene contains about 3 methyl side groups per 100 methylene groups. The presence of side chains confers elasticity on polyethylene. Unsaturated and oxygen-containing groups are also present in the polymer. The crystallinity of high-pressure polyethylene is 55 – 60% (sp. gr. 0.92, m.p. 110°, frost resistance – 70°, elongation at break 600%, elasticity modulus 2500 kg/cm^2). In absence of oxygen polyethylene is stable up to about 200°; at higher temperatures degradation is very rapid with formation of products of low molecular weight.

In 1953 Ziegler discovered a catalytic method for production of low-pressure polyethylene [2] which has been marketed in Germany since 1954 under the name of "Hostalen" [3]. Ethylene is passed at normal pressure (760 mm) and at slightly elevated temperature through a suspension of a catalyst based on titanium and aluminum compounds (1% on the weight of ethylene) in xylene, mineral oil, or other organic solvents. The polymer,

formed in almost quantitative yield, is precipitated as a white powder which is then washed free from catalyst. Low-pressure polyethylene differs from the high-pressure product in having strictly linear macromolecules without side chains. This polymer has high crystallinity (77 – 80% crystalline phase), high density (sp. gr. 0.94 – 0.95) a higher softening temperature (120°) and a lower elongation at break (150%);the elasticity modulus is 5,500 – 11,000 kg/cm^2. Its gas and vapor permeability is low [4].

The molecular weight of low-pressure polyethylene is from 10,000 to 3,000,000, according to the polymerization conditions. The transparency of a film 0.1 mm thick is 70%.

Relatively recently a new type of polyethylene, "Marlex-50", has appeared; it is made by the Phillips process, by polymerization of ethylene in a diluent in presence as a suspended catalyst under a pressure of 10 – 30 atmos at 100 – 150°. The catalyst consists of chromium oxides on aluminosilicate. Polyethylene made by this process has few side chains, is highly crystalline (90%) has density 0.96 and m.p. 113 – 127°. "Marlex-50" has a tensile strength of 310 kg/cm^2 at 350% elongation [5].

Distinctive properties of all types of polyethylene are chemical inertness, impermeability to water, and exceptionally good dielectric properties. Polyethylene is resistant to HCl, dilute HNO_3, and alkali solutions, it is insoluble in organic solvents at 10° but at 60 – 70° dissolves readily in aromatic and chlorinated solvents.

Its dielectric constant is 2.3, its volume resistivity is 10^{16} ohm·cm, the tangent of the dielectric loss angle is 0.0001, and the breakdown voltage is 40 – 60 kv/mm. Polyethylene films and sheets can be welded. Polyethylene is easily machined on lathes.

Polyethylene is now being produced in the USSR, USA, England, Germany, Italy, and a number of other countries in increasing amounts, and its practical applications are continuously growing. Polyethylene is used extensively for the production of tubes, pipes, containers, bottles, beakers, and other domestic articles; for cable insulation, manufacture of films and expanded plastics, and for packaging and protective coatings. Polyethylene is suitable for use as a low-loss dielectric for high-frequency apparatus used in television and radar.

Irradiated polyethylene, marketed under the trade name "Irrathene", is of interest as an insulating material. The action of high-energy electrons, neutrons, or γ-rays on polyethylene causes cross linking with liberation of hydrogen. The polymer so formed retains its amorphous structure and differs from ordinary polyethylene in being transparent, flexible, and stable for a long time at temperatures up to 200°. It is recommended for use at 120 – 150° [6]. Films 0.25 mm thick have 600% elongation, the density is 0.92 g/cc, and the volume resistivity is 10^{15} ohm·cm. It is resistant to acids and alkalies [7].

Polyethylene irradiated by high-energy electrons, produced under the name "Hyrad", has high thermal stability, can be used indefinitely at 150°, for a limited time at 200°, and for several hours at 300°; it decomposes at about 450°. Its dielectric constant is 2.3, and the tangent of the dielectric loss angle is $5 \cdot 10^{-4}$; these values are retained up to 150° [8].

The production of graft copolymers based on polyethylene by the action of ionizing radiations should be mentioned. For example, vinylcarbazole can be grafted to polyethylene films. The softening temperature is increased from 80 – 104° for the original polyethylene to 165 – 220° for a graft polymer containing 53% vinylcarbazole. The elongation at break is decreased from 700 to 45%.

Cation-exchange membranes with good characteristics can be made by sulfonation of a graft copolymer of styrene and polyethylene [9].

Low-pressure polyethylene is now being used for the production of two types of fibers: "Courlene" and "Courlene X-3". The threads are resistant to acids and alkalies and are not attacked by bacteria. They are superior to polyamide fibers in abrasion resistance. Poor light resistance and dyeability are disadvantages [10].

PROPERTIES OF COMMERCIAL POLYETHYLENE [11]

Properties	High-pressure polyethylene	Low-pressure polyethylene
Molecular weight	22,000 – 25,000	60,000 – 200,000
Melting point (°C)	111	133

Properties	High-pressure polyethylene	Low-pressure polyethylene
Crystallinity (%)	60	80 – 85
Specific gravity	0.92	0.96 – 0.97
Refractive index	1.51	–
Heat conductivity (cal/cm^2 · sec · degree · cm)	$8 \cdot 10^{-4}$	–
Water absorption in 24 hours at 25° (%)	0.01	–
Brittle point (°C)	–70	–70
Tensile strength (kg/cm^2)	133	120
Elongation (%)	600	100
Tearing strength (kg/cm^2)	42	70
Shore hardness	D 53	D60-70
Shearing strength (kg/cm^2)	126	–
Softening point, Vicat test (°C)	91	–

Properties of polyethylene films 1 – 1.5 mm thick

Properties	Average value
Longitudinal tensile strength (kg/cm^2)	15.4
Transverse tensile strength (kg/cm^2)	1600
Longitudinal elongation (%)	350
Transverse elongation (%)	615
Longitudinal abrasion resistance (kg/cm^2)	28.3
Transverse abrasion resistance (kg/cm^2)	19.6
Water absorption in 24 hours (%)	0.0
Vapor permeability (g/m^2/ 24 hours)	0.06
Impact strength (kg/cm · sec^2)	12 – 15
Frictional coefficient	0.30 – 0.35

A new rubberlike polymer "Hypalon S-2" has been produced from polyethylene

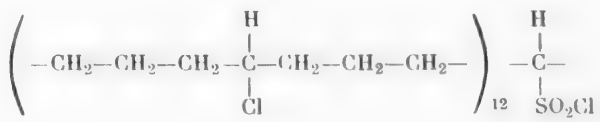

by the action of Cl_2 and SO_2 on polyethylene (number-average molecular weight 20,000). This chlorosulfonated polyethylene contains 1 chlorine atom per 7 carbon atoms, and one SO_2Cl group per 100 carbon atoms. Its density is 1.1 g/cc; it is soluble in aromatic and chlorinated hydrocarbons. It has high resistance to ozone, light, and heat, and is very resistant to abrasion; it is chemically inert to chlorine and nitric acid. It is elastic at low temperatures (–56 to –62°), is nonflammable and can be vulcanized; it is superior to all other rubbers in fatigue strength; its elongation at break is 400 – 500%. Hypalon coatings can withstand over 160,000 flexing cycles without cracking [12].

Hypalon is suitable for insulation of low-voltage leads carrying up to 1000 v. It is used as a packing material in generators, for cable insulation, for chemically resistant hose, conveyor belts, etc.

Polypropylene. Propylene is present in the products of cracking of petroleum hydrocarbons; these products contain more propylene than ethylene, and it polymerized more readily in presence of metal-containing catalysts to yield a polymer with very valuable properties [13].

The Montecatini Company (Italy) has produced a new thermoplastic material "Moplen", which is "isotactic" polypropylene. Natta et al. [14] showed that catalytic polymerization of α-olefins and styrene yields crystalline linear polymers, termed "isotactic", with a strictly regular "head to tail" structure formed by alternation of the tertiary carbon atoms with the same spatial configuration in the principal chain:

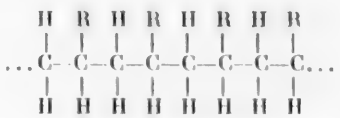

All the R groups lie on one side of the plane of the principal chain. This distinguishes them from ordinary or "atactic" amorphous polymers, which do not have a regular structure in the polymer chain:

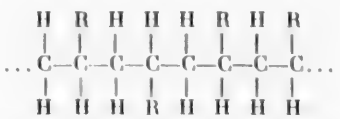

where the R groups are partly below and partly above the plane of the principal chain.

The chains are of spiral form in the crystalline state. The identity period of the unit cell along the chain axis is 6.4 – 6.6 A, which corresponds to these monomer units.

In "isotactic" polymers all the structural elements of the chain rotate the plane of polarization of light in one direction, owing to the equal configuration of the carbon atoms in the chain. According to Natta, the polymerization mechanism is anionic, so that polymerization can be effected under the most favorable conditions for an ordered spatial arrangement of the monomer units, i.e., without branching due to chain transfer or to copolymerization of the monomer with the low-molecular polymers formed.

"Isotactic" polypropylene is formed by the polymerization of propylene in heptane in presence of $TiCl_3$ + $Al(C_2H_5)_3$ catalyst at 30 – 70° for 20 – 40 hours. The polymer is insoluble in heptane, and is precipitated in the form of a powder. Its molecular weight is 270,000 – 485,000 [15]. The activation energy of propylene polymerization is 11.3 ± 0.5 kcal/mole [16].

Polypropylene has a fibrous structure and is therefore suitable for fiber production. Its softening temperature is 150°. Polypropylene films are superior to polyamide in mechanical properties. Polypropylene articles have higher resistance to heat and chemical attack than articles made from low-pressure polyethylene. Polypropylene is highly promising as a dielectric of high chemical resistance and very low moisture absorption. Its dielectric constant is 2.0 – 2.1, the tangent of the dielectric loss angle is $2 \cdot 10^{-4}$, the resistivity is $8 \cdot 10^{15}$ ohm · ·cm, and the breakdown voltage is 30 kv/mm. The dielectric properties of polypropylene are almost independent of atmospheric humidity [17]. Because of the high elasticity modulus, polypropylene articles retain their shape under considerable loads, and have high impact strength; they can be worked at temperatures close to the melting point. The specific gravity of Moplen at 20° is 0.90, the melting point is between 164 and 168°, the tensile strength is 330 – 360 kg/cm^2, the elongation at break is 400 to 800%, and the bending strength is from 8,000 to 10,000 kg/cm^2.

Moplen is resistant to 80% H_2SO_4, 50 – 94% HNO_3 and 40% NaOH. It is insoluble in organic solvents at 20° and does not swell in oils. In absence of atmospheric oxygen it can be heated to 300° without depolymerization for many hours.

The action of sunlight makes it brittle after several months. High-energy radiation results in the formation of cross-linked polymers. Moplen can be easily extruded at 175 – 220°, blown at 170 – 210°, cast under pressures of 700 – 1200 kg/cm^2, and molded by direct pressure (into plates and blocks) at 200 – 250° under 100 – 120 kg/cm^2 pressure. Pipes are made by the centrifugal method. Metal articles can be coated by spraying or by immersion of the articles, heated to 250 – 300°, into the melted polymer. Moplen can be welded [18].

Moplen is used for refrigerator parts, storage cell containers, and automobile parts. Films are suitable as insulating coatings for leads and cables. Polypropylene yields fibers with good electrical and thermal insulation properties, similar to wool or silk in appearance.

Polypropylene is being produced in the USSR, Italy, France, USA, England, and Germany.

The copolymerization of ethylene with propylene in presence of trihexylaluminum + vanadyl chloride catalyst should be mentioned. The copolymers are completely amorphous, have rubberlike elasticity, and are good nonvulcanizable elastomers [19].

Rubbers. The development of modern technology demands a wide range of rubbers with different properties. It is not possible to describe within the limits of this article all the new types of rubbers developed in recent years. Therefore only the most outstanding achievements in this field are mentioned; fuller details are given in special reviews [20, 21].

Natta et al. [22] studied the stereospecific polymerization of diolefins and obtained four polymers of butadiene, crystalline at room temperature (see scheme): III polybutadiene ("isotactic"), with 1, 2 chain configuration, sp. gr. 0.96, m. p. 125°; IV polybutadiene, with 1, 2 chain configuration ("syndiotactic"), sp. gr. 0.96, m. p. 155°; II polybutadiene with 1,4-trans chain configuration, sp. gr. 1.02, m. p. 140°, and I polybutadiene with 1,4-cis chain configuration

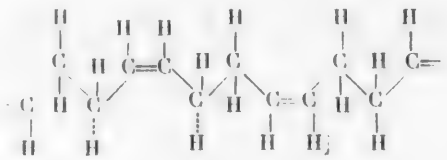

I

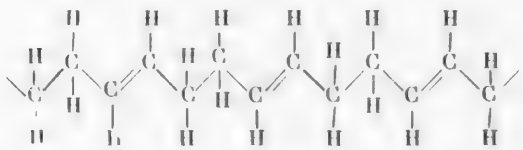

II

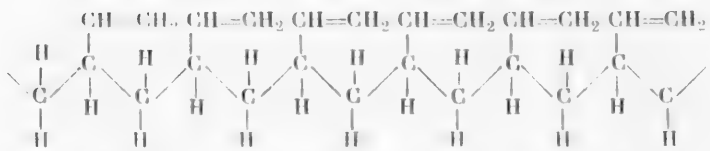

III

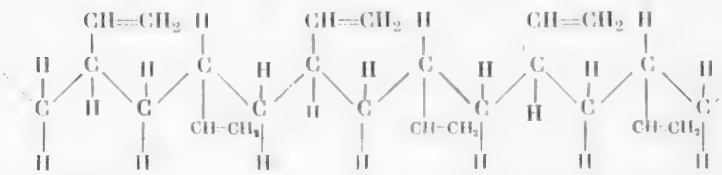

IV

"Syndiotactic" polybutadiene differs from other isomeric polybutadienes in that the vinyl groups are arranged alternately above and below the plane of the principal chain.

The "isotactic" polymer of butadiene-1,2 has a spiral structure in the crystalline state. The "syndiotactic" polymer of butadiene-1,2 differs greatly from it in structure. It is a high-melting crystalline polymer of linear structure, not rubberlike. It is an example of a polymeric hydrocarbon of high molecular weight, containing asymmetric carbon atoms with relatively larger substituent groups, and remaining crystalline.

The polymer of 1,4-cisbutadiene has a lower glass-transition temperature and greater chain mobility that other stereoisomeric polybutadienes. The 1,4-cis polymers are of interest owing to their better elastic properties.

Synthetic cis-1,4-polyisoprene rubber, close in structure and properties to natural rubber, is of great interest. This type of rubber is made in the USSR under the name of SKI, and in the USA it is known as "Ameripol SN".

1,4-transpolyisoprene has a crystalline structure characteristic of the γ and β forms of natural gutta-percha. Noteworthy among the new copolymers of butadiene are Philprenes P-15 and P-25, which copolymers of butadiene with 2-methylvinylpyridine (the numbers indicate the percentage contents of the latter in the copolymer). These copolymers are highly resistant to oils, are readily vulcanized, have excellent low-temperature properties, and are suitable for the production of tires with high wear resistance [23].

Of great interest are the polyurethane rubbers from glycol polyesters and diisocyanates, which have exceptional resistance to thermal aging and the action of oxygen, ozone, and oils [24].

A new group of rubbers consists of carboxylated elastomers, made by copolymerization of acrylic or methacrylic acid with dienes. Introduction of carboxyl groups increases their hardness and strength and makes them more easily vulcanized by bivalent metals, the process being complete in 48 hours at 20°. The vulcanizates have high strength (175 – 400 kg/cm^2) and extensibility (400 – 600%), and are more resistant to ozone and oils. The chief defect is poor resistance to repeated deformation [25].

A very interesting copolymer is a new fluorine-containing rubber, Viton A. Viton A is a linear copolymer of vinylidene fluoride and hexafluoropropylene, containing about 65% fluorine. Its molecular weight is relatively low (~60,000) in comparison with other elastomers. The vulcanizates have high strength and elasticity after prolonged exposure to air or oils at high temperatures. At 315 – 370° specimens retain their shape and do not char or burn. Viton A is stable up to 350°, has high resistance to heat and chemical attack, and excellent mechanical properties [26].

Polysiloxane rubbers

$$\left(\begin{array}{c} CH_3 \\ | \\ -Si-O- \\ | \\ CH_3 \end{array} \right)_n,$$

have high heat resistance; they can be heated to 250° and retain constant elastic modulus and elasticity over a wide temperature range owing to the considerable flexibility of the –Si–O– bond. Their average molecular weight is 600,000 – 900,000 [27], and they can withstand temperatures down to –65°. The introduction of a small quantity of phenyl groups in place of methyl in the molecule of polydimethylsiloxane rubber improves its frost resistance, raising it to –90° [28].

Introduction of fluorine atoms into the molecule of polysiloxane rubber (Silastic LS-53) yields a rubber which combines the properties of polysiloxane rubber with those of solvent-resistant fluorinated plastics [29].

Polystyrene and its derivatives. Styrene polymer, first made in 1839, is one of the first synthetic polymers. The first attempts to use polystyrene for technical purposes met considerable difficulties, owing to its rapid aging, spontaneous degradation, and brittleness. It was only gradually, as the various difficulties associated with the production of the pure monomer and with the introduction of modern polymerization methods were overcome, that polymers with standard and consistent properties could be obtained. Since then polystyrene has been used not only in electrical and radio engineering, but also in other branches of industry. The extensive use of polystyrene in industry is hindered by its low softening temperature (80°) and inadequate strength characteristics. To increase the resistance to heat and to cracking ("silvering"), styrene is now being cross linked by the introduction of p-divinylbenzene in the polymerization process (this gives a maximum heat resistance of 105°), or by the action of atomic radiation. Irradiated polystyrene can withstand temperatures up to 250° without appreciable changes.

Styrene with 1 methyl group introduced in the benzene ring (vinyltoluene)

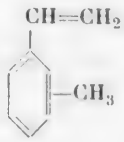

yields polymers with higher heat resistance, especially if the substituent group is in the ortho position relative to the double bond. The maximum heat resistance is 110°. It has been reported that polymethylstyrenes are more stable than polystyrene to the action of boiling water [31]. The heat resistance is increased further by the introduction of two methyl groups in the benzene ring:

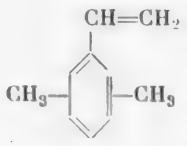

Dimethylstyrene (vinylxylene) polymers are colorless, transparent, hard thermoplastic masses, soluble in aromatic and chlorinated hydrocarbons. The heat resistance of polydimethylstyrenes is 144 — 148°, i.e., nearly double the heat resistance of unsubstituted polystyrene. Of the three isomeric dimethylstyrenes, 2,5-dimethylstyrene (p-vinylxylene) has the greatest polymerization rate and the best properties.

The dielectric properties of dimethylstyrene polymers are similar to those of polystyrene, and change little with temperature up to 145° [32].

Polymers of even higher heat resistance are formed if fluorine atoms are introduced into the vinyl group. The monomer α, β, β-trifluorostyrene, containing the $CF=CF_2$ group,

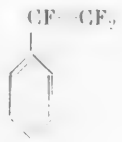

can be polymerized in emulsion to yield a very interesting polymer which combines the properties of polystyrene and Teflon. It is very heat-stable material with softening point 240° and low dielectric loss: the dielectric constant is 2.56, and the tangent of the dielectric loss angle is $(1-3)\cdot 10^{-3}$. It resembles the fluoroethylene polymers in this respect. In addition, it resembles polystyrene in its solubility in a number of organic solvents. The copolymers of α, β, β-trifluorostyrene with styrene soften at 160°, and with trifluorochloroethylene, at 195° [33].

Natta [34] showed that when styrene is polymerized in presence of Ziegler catalyst [$TiCl_4$+$(i\text{-}C_4H_9)_3$ Al] under the conditions described for the polymerization of α-olefins it yields a crystalline polymer. By taking advantage of the different solubilities of amorphous (soluble) and crystalline (difficultly soluble) polystyrenes, it is possible to obtain "isotactic" polystyrene, with m.p. 230° and molecular weight 100,000 — 1,000,000, in the pure state. Very little information on the properties of the new polystyrene is available as yet, and therefore it is difficult to define the fields of its practical applications.

The production of high-strength polystyrene by mechanochemical methods is of great interest. Polymer mixtures (styrene, nitrile rubber) are ground in special equipment in a nitrogen atmosphere, with rupture of the polymer chains. The free ends of such broken chains join to the ends of other broken chains, from the other polymer, forming new polymeric materials consisting of individual "blocks" or pieces of two different polymers. The strength of the copolymer (impact and bending strength) is 1.5 times that of polystyrene [35].

These examples illustrate the possibilities of modifying the properties of known polymers by the use of fundamentally new polymerization methods.

Polyparaxylylene. The development of modern technology calls for new polymer materials with high softening temperatures and adequate thermal stability. Therefore in recent years there has been increased interest in polymers containing cyclic groups in the principal chains [36]. Polymers consisting entirely of benzene rings

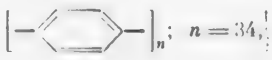

have very high thermal stability. Condensation of p-dichlorobenzene with a liquid melt of potassium and sodium yielded a polymer of a dark brown color, probably due to the presence of a quinoid structure in the benzene rings. This polyphenylene did not melt up to 550°, but lost hydrogen at 500°. Polymers containing only ring structures in the principal chain have the disadvantage of brittleness. Therefore investigators directed their attention to searches for methods for production of new polymers containing elastic units (CH_2 groups, oxygen atoms, etc.) in addition to rings in the principal chains. An example of a compound of this type is polyparaxylylene, formed by pyrolysis of paraxylene in vacuum at 1000°.

First 1,4-dimethylene-2,4-cyclohexadiene is formed:

and this polymerizes to yield polyparaxylylene [37]:

This is a crystalline infusible polymer, insoluble in the common organic solvents, and with very high heat resistance. The polymer does not soften in vacuum at 380°; at 400° it melts with decomposition. Thus, polyparaxylylene is close to Teflon in its heat resistance. Plasticized polyparaxylylene has up to 600% extensibility, and is an excellent heat-resistant dielectric, having tan $\delta = 8.10^{-4}$, dielectric constant 3.3, and volume resistivity 2.10^{15} ohm·cm.

Polymers of fluorine compounds. A large number of different fluoroethylene polymers with very valuable technical properties can be obtained by the introduction of different numbers of fluorine atoms into the ethylene molecule. Polymers of tetrafluoroethylene (Ftoroplast-4 in the USSR, Teflon in the USA) and trifluorochloroethylene (Ftoroplast-3 in the USSR, Kel-F in the USA, and Hostaflon in Federal Germany) are widely known. The copolymer of vinylidene fluoride and hexafluoropropylene (Viton A) is a new and very thermostable rubber with high chemical resistance and excellent mechanical properties. Various fluorinated butadienes have been prepared, including 1,1-difluorobutadiene and hexafluorobutadiene. 1,1-Difluorobutadiene polymerizes on standing to yield a rubber [38]. By regulation of the copolymerization [39] of perfluorovinyl and perfluorobutadiene it is possible to obtain various polymers, ranging from solid thermoplastic resins to waxes and oils. Solid thermoplastic and heat-resistant polymers have been obtained from α, β, β-trifluorostyrene, β, β-difluorostyrene, and α, β-difluorostyrene. A vinyl trifluoroacetate polymer has been described; this is harder and has a higher softening temperature than polyvinyl acetate [40]. Various fluorinated organosilicon compounds of high thermal stability have also been prepared [41]. Modification of siloxane rubbers with Ftoroplast-4 improves their properties; the tearing strength and oil resistance at elevated temperatures are increased 2 to 3-fold [42]. Ftoroplast-4 has exceptional chemical resistance to almost all corrosive media, including powerful oxidizing agents up to 250–300°.

Ftoroplast-4 is one of the most thermostable polymers; it decomposes at temperatures above 400°, yielding tetrafluoroethylene as the primary decomposition product [43]. The remarkable dielectric properties of Ftoroplast-4, which are virtually independent of temperature and frequency, together with its high thermal stability,

make it an indispensable insulating material, especially at high and ultrahigh frequencies. Especially important characteristics of Ftoroplast-4 are that it is not wetted or swollen by water. Insulating materials made from Ftoroplast-4 can therefore be used in conditions of high humidity, as its dielectric properties are not affected [44]. However, it also has important disadvantages: its adhesion to metals and other materials is poor, so that its uses for lining equipment are restricted. Neither can it be used for coatings, because it is insoluble in all known organic solvents. It has been reported that satisfactory adhesion may be produced by surface treatment of Ftoroplast-4 with a solution of metallic sodium in liquid ammonia. There are also reports of good adhesion of Ftoroplast-4 to aluminum, carbon steel, and wood.

Aqueous suspensions of Ftoroplast-4 are used for film casting, and impregnation of fibers and porous metals [45]. A process for the production of a new synthetic fiber, "Ftorlon", from fluorinated copolymers has been worked out in the USSR. The strength of Ftorlon is unaffected by prolonged treatment with concentrated nitric acid or hydrogen peroxide. It is stronger than nylon or capron.

Ftoroplast-3 is used for much the same purposes as Ftoroplast-4. Ftoroplast-3 has extremely high volume resistivity and good dielectric strength. It can therefore be used as a dielectric in high-current technology and in particularly important components. Ftoroplast-3, like Ftoroplast-4, does not exhibit flow in the cold, and has high hardness. Ftoroplast-3 decomposes at 300 – 315°.

Films of Ftoroplast-3, 130 – 150 μ thick, have tensile strength 290 – 350 kg/cm^2 and relative elongation 140 – 180%. Ftoroplast-3 is also difficult to apply in the form of coatings to metal surfaces. In recent years the Scientific Research Institute of the Plastics Industry and the State Institute of Applied Chemistry have developed a technique for applying it from suspensions. The coatings withstood the action of concentrated nitric acid at 50° for at least 6 months. The production of oils, greases, and powders based on Ftoroplast-3 polymers has also been achieved in the USSR [46].

PHYSICAL AND MECHANICAL PROPERTIES OF FLUORINATED PLASTICS [44]

Properties	Ftoroplast-4	Ftoroplast-3
Density (g/cc)	2.1 – 2.3	2.09 – 2.16
Melting point of crystals (°C)	327	208
Glass-transition point of amorphous phase (°C)	–120	55
Maximum working temperature in use (°C)	from – 269 to + 250°	from – 195 to + 100°
Heat conductivity ($\frac{\text{cal}}{\text{cm} \cdot \text{sec} \cdot °\text{C}} \cdot 10^4$)	6	1.4
Specific heat (cal/g·°C)	0.25	0.22
Water absorption in 24 hours (%)	0.00	0.00
Tensile strength (kg/cm^2):		
not hardened	140 – 200	350 – 400
hardened	160 – 250	300 – 350
Relative elongation at break (%)	250 – 500	100 – 200
Static bend strength (kg/cm^2)	110 – 140	600 – 800
Elastic bending modulus (kg/cm^2)	4700 – 8500	11600 – 14500
Specific impact viscosity (kg·cm/cm^2)	> 100	20 – 160
Brinell hardness (kg/mm^2)	3 – 4	10 – 13
Volume resistivity (ohm·cm)	> 10^{17}	10^{18}

Properties	Ftoroplast-4	Ftoroplast-3
Dielectric strength (kv/mm), for thickness:		
4 mm	25 – 27	—
2 mm	–	13
Dielectric constant:		
at 60 cps	1.9 – 2.2	3.0
at 10^6 cps	1.9 – 2.2	2.5 – 2.7
Tangent of dielectric loss angle:		
at 60 cps	0.0002	0.015
at 10^6 cps	0.0002	0.010

Polymers of Oxygen-Containing Compounds

Polyformaldehyde. A new method of formaldehyde polymerization has recently been developed, yielding polymers with fiber-forming and film-forming properties; the fibers have satisfactory strength and thermal stability.

It is known that formaldehyde is a very reactive compound, capable of polymerization. Formaldehyde polymers were first prepared by Butlerov. Much work on the polymerization of formaldehyde was done by Staudinger, but the polymers obtained did not have sufficiently high molecular weight, and had poor mechanical properties. The chemists of the Du Pont Company (USA) have found that formaldehyde polymerizes by an ionic mechanism:

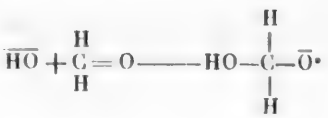

Therefore the formation of formaldehyde polymers $(-CH_2-O)_n$ of high molecular weight requires the use of dry formaldehyde, containing very little water, and free from methanol; polymerization is then quite simple.

For preparation of pure and dry formaldehyde, a solid polymer of the usual type is prepared by the action of acids on aqueous formaldehyde solutions. This polymer, containing 99.7 – 99.9% formaldehyde, is warmed; gaseous formaldehyde is formed, which is purified, dried, and used for polymerization. The gaseous formaldehyde is passed into a thoroughly stirred solvent containing catalyst (0.1%). The formaldehyde rate must correspond to the polymerization rate. Primary amines and other compounds are used as catalysts [47]. A white precipitate is formed, which can be converted into fibers and strong transparent films of high thermal stability. Films are made by casting at 190 – 250° under 105 atmos pressure.

Fibers are formed by melt spinning followed by hot drawing. Polyformaldehyde has the trade name Delrin; it is a linear highly crystalline polymer melting at 163°. It resembles nylon, but absorbs less moisture. Its tensile strength is 700 – 1030 kg/cm^2; the bending strength is 1000 kg/cm^2; water absorption in 24 hours, 0.4%; extensibility at 20°, 13 – 38%, and at 70°, 330 – 461%; sp. gr. 1.425; bending modulus 28,700 kg/cm^2.

The following products made from Delrin have become widely used in recent years: pipelines for gasoline, bearings, rods, clutches, sheets, shaped articles, cable insulation, and domestic goods (plates, cups, etc.) [48].

This new and interesting polymer is likely to find extensive uses in various branches of technology.

Ethylene oxide polymers. In the USA polymers are being made from ethylene oxide; they are soluble in water and are used as emulsifiers and thickeners in the textile industry. The method used for the production of high-molecular polyformaldehyde was applied to the production of ethylene oxide polymers, and polymers of high molecular weight were obtained; these are known as "Polyox" and have the structure $(-CH_2-CH_2-O-)_n$.

Ethylene oxide is polymerized at 70 – 110° for 90 minutes in presence of strontium carbonate (0.1 – 0.5%). This yields a crystalline polymer (~95%); its molecular weight reaches 3,000,000, m. p. 66°, density 1.15 – 1.26 g/cc. The polymer is soluble in chloroform and dichloroethane, and is miscible with water in all proportions. The intrinsic viscosity of aqueous solutions reaches 20, so that the solutions have unusual properties. The polymer gives rise to flexible films which have high crystallinity when dried [49].

Poly-3,3'-bischloromethyloxacyclobutane. A new thermoplastic polymer, produced experimentally by the Du Pont Company under the name of "Penton", has recently attracted the attention of scientists and technologist, "Penton" is a chlorinated polyether with interesting physical, mechanical, and dielectric properties. In studies of the reactivity of four-membered oxacyclobutane rings it was found that compounds of this type can be converted into linear polyethers by the action of electrophilic agents [50]. A compound of special interest is 3,3'-bischloromethyloxacyclobutane

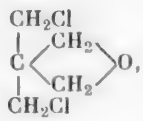

which undergoes cationic polymerization with rupture of the oxide ring to form a linear crystalline polymer

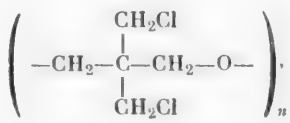

containing 45.5% chlorine. This polymer, known as "Penton", was made in the USA in 1955, and in England, USSR, and Japan in 1956.

In 1957 nearly all the polymer journals contained articles on "Penton", with descriptions of the properties of this new material. The starting material for the synthesis is pentaerythritol. The synthesis of 3,3'-bischloromethyloxacyclobutane is effected according to the following scheme:

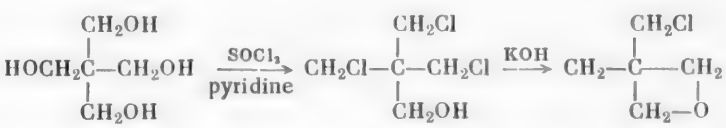

The yield at the first stage of the process is 60 – 70%, and at the second 85%; the product has b.p. 83° (11 mm) and m.p. 18.75°. The bulk polymerization of 3,3'-bischloromethyloxacyclobutane proceeds very vigorously and is difficult to control, and therefore the polymerization is performed in solvents in presence of gaseous BF_3 or BF_3 etherate at low temperatures (from 0 to –70°). Water inhibits the polymerization process, but traces of water are necessary as a co-catalyst. The crystalline polymer has m.p. 180° and molecular weight 30,000. The polymer is insoluble in the usual organic solvents and is not flammable.

The chloromethyl group in 3,3'-bischloromethyloxacyclobutane is linked to a carbon atom which enters the principal polymer chain. Therefore the β position does not contain any hydrogen atoms capable of forming HCl. Consequently the polymer must be thermostable. In fact, Penton can be worked at temperatures up to 285°. Penton can be used for the production of articles of strictly predetermined dimensions, without internal stresses and capable of retaining their dimensions. The water absorption of Penton is 0.01%. Because of this, Penton articles are dimensionally stable even if they pass from a dry to a moist medium. The tensile strength at 100° is 245 kg/cm², and in boiling water is is 210 kg/cm². This property, in conjunction with the very low creep, makes Penton very promising for industrial purposes. The extensibility at 23° is 35%, and at 100°, 200 – 250%. Penton is one of the most chemically-resistant plastics, occupying an intermediate position between the

fluorinated plastics and vinyl chloride and styrene polymers. It can be converted into fibers of good chemical resistance and high tensile strength. Penton is intermediate between polyethylene and polyamides in its dielectric properties. Tests on Penton showed that after exposure to water for one year its surface resistivity fell from $5 \cdot 10^{15}$ ohms to $3 \cdot 10^{15}$ ohms. The dielectric constant of Penton is 2.9, and the tangent of the dielectric loss angle is 0.015.

No changes of any kind were found in a valve made from Penton after exposure to steam at 27 atmos and 160° for 18 months. Penton gear wheels underwent only slight deformation after 1000 hours of rotation at 1000 r.p.m. Penton is recommended for chemical equipment, separator rings, bearings, watch mechanisms, films, and for production of ropes and cables [51].

Polycarbonates. Polycarbonates are aromatic polyesters derived from carbonic acid. They form a new group of thermoplastics with valuable properties. Polycarbonates are made from the very highly reactive 4,4'-dihydroxydiphenyl alkanes by interaction with phosgene or carbonate diesters, according to the following equations [52]:

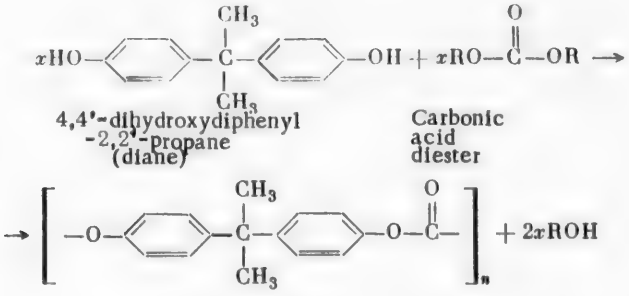

(1)

(the reaction is effected at 150 – 300°; it is useful to add catalysts such as PbO, ZnO, etc.; the molecular weight of the polycarbonates formed is 50,000).

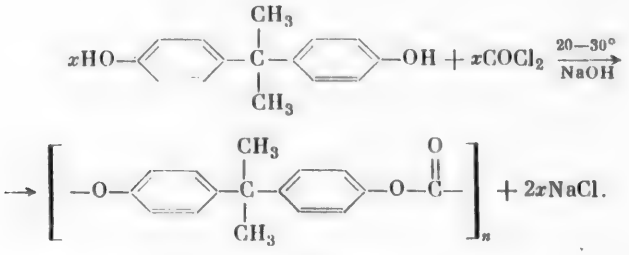

(2)

In this case the molecular weight of the polycarbonates is 150,000 (measured by the osmotic method).

The solid polycarbonates have high melting points: 170 – 260° and 300°. They are soluble in aromatic and chlorinated hydrocarbons; they are stable for a long time in melt form; cooled melts yield colorless transparent films.

Polycarbonates are used in the form of fibers, films, and coatings. They are molded by pressing and casting.

Polycarbonates are crystalline polymers of density 1.17 – 1.22; they can be readily oriented. Polycarbonates are water-repellent and have high chemical resistance, especially to acids (HF, NHO_3) and solutions of strong oxidizing agents; the water absorption is 0.16%, and the gas absorption is low; they are resistant to aliphatic and cycloaliphatic hydrocarbons, higher alcohols, oils, and fats.

A film of Lexan (USA, Federal Germany) polycarbonate did not become colored and its mechanical properties were unchanged after 72 hours of exposure to ultraviolet light. No significant changes were produced by the action of heat at 150° for 26 weeks in air, or at 170° for 8 weeks. A polycarbonate film was unchanged after 4 weeks of exposure to boiling water.

Polycarbonates have good mechanical properties: bending strength 800 – 1000 kg/cm^2, modulus 22,000 kg/cm^2, tensile strength 890 kg/cm^2, elongation at break 180%; their resistance to aging is very high. Polycarbonates also have good dielectric properties: dielectric constant 2.6, volume resistivity 2.10^{16} ohm·cm, tangent of the dielectric loss angle $(9-10)\cdot10^{-4}$. It should be noted that tan δ remains constant up to 150°. The breakdown voltage is 100 – 120 kv/mm [53].

Polycarbonate articles, made by injection molding, are transparent and colorless, and resemble articles of organic glass. The properties of polycarbonates suggest that these materials, which are cheaper than nylon or Terylene, will be widely used in industry, particularly in machine building and in all kinds of electrical equipment.

Reinforced polymer materials. Reinforced plastics are excellent constructional materials, and are widely used in building, car body production, for boat building, etc. Glass-reinforced plastics based on various unsaturated polyester resins are of particular practical importance. Unsaturated polyester resins are condensation products of dihydric alcohols (ethylene glycol, propylene glycol) and dibasic acids (maleic, adipic, etc.), containing unsaturated bonds and capable of being hardened by copolymerization with vinyl monomers (styrene, methyl methacrylate, etc.) in presence of catalysts (2% benzoyl peroxide) to form cross-linked space polymers. These resins are effective bonding agents for glass fibers and are therefore valuable binders for the production of glass-reinforced plastics. Glass fabrics, mats, or other glass fiber materials are impregnated with polyester resins in special molds and formed into laminates. The impregnated layers are pressed against the mold surface. After some time the finished article is formed in the mold, in the shape of a solid, hard, infusible and insoluble material with high mechanical strength. This process for forming plastics articles at room temperature and without the use of pressure (or at very low pressures) in presence of special accelerators is known as "contact molding"; it can be used for the production of large articles by a simple technique.

Glass plastics have high mechanical strength, high chemical resistance, and good dielectric properties. They have the following characteristics: sp. gr. 1.5 – 2.1, tensile strength 2800 – 3500 kg/cm^2, elasticity modulus in extension, from 70,000 to 200,000 kg/cm^2, compressive strength 2100 – 4200 kg/cm^2, bending strength 3500 – 4400 kg/cm^2, impact strength 3500 – 4400 kg/cm^2; tangent of the dielectric loss angle 0.01 – 0.04, dielectric constant 4.0 – 4.8, water absorption in 24 hours 0.3 – 0.9%.

The most outstanding feature of glass-reinforced polyester plastics is the high strength – weight ratio. If reinforced polyesters replace steel, the weight advantage exceeds 50%, and in the case of aluminum it exceeds 30%. The impact strength of glass-reinforced plastics exceeds that of aluminum or steel. They also have good dielectric properties, and high resistance to water, salt solutions, dilute acids and alkalies, and organic solvents. The disadvantages of glass-reinforced plastics include loss of strength with increase of temperature, low abrasion resistance, and a tendency to flow under prolonged loading.

Glass-reinforced plastics are widely used in the aircraft industry (for radio and radar equipment and highly-stressed members such as fuselage parts and other portions of complex outlines, etc.) and in boat building; the production time is thereby decreased 11 to 20-fold, and the cost of equipment is very much lower. The service life of the boats is also increased owing to absence of corrosion and rotting. At the end of 1953 the production of sports cars with glass-reinforced plastic bodies was started in the USA; the cost of equipment is lowered 9-fold as a result. Such bodies are more resistant to impacts than steel bodies. Glass-reinforced plastics are widely used in railroad transport (car equipment, tank cars for milk and oil products, crossties, etc.). They are widely used in building, mainly as architectural panels and translucent sheets for roofs, verandas, and greenhouses. All kinds of furniture can be made from glass-reinforced plastics [54]. It seems likely that in the near future they will become fully developed and even more widely used in various branches of our national economy.

It is not possible in a brief review to describe all the new polymers, the numbers of which are increasing continuously. Successful advances are being made in the field of silicones; silicon-containing heat-resistant plastics, reinforced plastics, rubbers, and oils have been invented and have added considerably to the range of new polymer materials. New metal-containing silicones are being produced; these should have even greater thermal endurance [55]. The first incombustible plastics have been produced by the introduction of phosphorus atoms into their molecules [56]. The thermal and chemical stability of polymers is increased by the introduction of titanium [57]. Various polycondensation materials such as polyethylene terephthalate (Lovsan, Terylene) and polyurethanes are being used with success; the range of epoxy resins has been greatly extended by modification with polyamides, phenol – formaldehyde, and other resins [58]. Advances have been made in the fields of cellulose derivatives.

There are extensive practical uses for ion-exchange resins from various cross-linked space polymers and copolymers; these are used not only for the purification of water, chemicals, and medical preparations, but also in chemical synthesis [59].

We may be confident that rapid development of polymer science will lead to the production of numerous polymer materials, and on a scale which would ensure abundant supplies for all branches of industry and the national economy, helping the progress of modern technology and raising further the living standards of the workers.

LITERATURE CITED

[1] Rubb. and Plast. Age, 36, 733 (1955).

[2] K. Ziegler and H. Martin, Makrom, Ch., 18 – 19, 186 (1956).

[3] G. Schulz, and K. Mehnert, Kunst., 45, 410 (1955).

[4] E. Borrows and E. Lelyveld, Brit. Plast., 137 (1957).

[5] I. Staudinger, Rubb. and Plast. Age, 37, 844 (1956).

[6] A. Charlesby, Brit. Plast., 146 (1957).

[7] Ang. Ch., 69, 741 (1957).

[8] Rubb. and Plast. Age, 37, 678 (1956).

[9] R. Mesrobian, J. Pol. Sci., 23, 903 (1953).

[10] Express Information 29 (1958).

[11] S. Aggarwal and O. Sweeting, Chem. Rev., 57, 665 (1957).

[12] R. Wagner, Rubb. Age, 71, 205 (1952); Ch. Ztg., 81, 203 (1957).

[13] Plastics, 21, 224, 67 (1956).

[14] G. Natta, P. Pino and F. Danusso, Ch. et. Ind., 38, 124 (1956).

[15] A. V. Topchiev, B. A. Krentsel', I. M. Tolchinskii, and G. V. Garnishevskii, Proc. Acad. Sci. USSR 114, 113 (1957);* Bull. Acad. Sci. USSR, Div. Chem. Sci. 500 (1958).*

[16] G. Natta, I. Pasquon, and E. Giachetti, Makrom. Ch., 24, 258 (1957).

[17] Brit. Plast., 30, 305 (1957).

[18] Express Information 8, SVM-30 (1958).

[19] G. Natta, and G. Mazzanti, Ch. et Ind., 39, 733, 743 (1957).

[20] S. Bolam , Plast. 22, 241, 419 (1957).

[21] B. A. Dolgoplosk, Chem. Sci. and Ind. 3, 391 (1957).

[22] G. Natta and P. Corradini, J. Pol. Sci., 20, 251 (1956); Ang. Ch., 68, 615 (1956).

[23] H. Railsback and C. Biard, Ind. Eng. Ch., 49, 1043 (1957).

[24] F. Hill, Ind. Eng. Ch., 48, 927 (1956).

[25] H. Brown and C. Gibbs, Ind. Ch., 47, 1006 (1955).

[26] I. Rugg, and A. Stevenson, Rubb. Age., 82, 102 (1957).

[27] A. S. Novikov and K. F. Kaluzhnina, Chem. Ind. 1, 24 (1954).

[28] M. Wick and W. Dietz, Kunst., 44, 127 (1954).

* Original Russian pagination. See C. B. Translation.

[29] Rubber World 135, 124 (1956).

[30] Kunst., 47, 530 (1957).

[31] J. Melchor, Mod. Plast., 33, 163 (1956).

[32] M. M. Koton, K. N. Kryukova, V. A. Paribok, and T. G. Smolyuk, Trans. Sci. Res. Inst. Radio Components 1 (4), 45 (1957).

[33] D. Livingston, P. Kamath and R. Corley, J. Pol. Sci., 20, 485 (1956).

[34] G. Natta and F. Danusso, Makrom. Ch., 20, 37 (1956).

[35] W. Wentworth, Brit. Plast., 12, 507 (1955).

[36] G. Edwards and G. Goldfinger, J. Pol. Sci., 16, 589 (1955).

[37] L. Schaefgen, J. Pol. Sci., 15, 203 (1955).

[38] P. Tarrant, J. Am. Chem. Soc., 76, 944 (1954).

[39] Polymer Chemistry and Technology 6, 124 (1954).

[40] H. Haas, J. Pol. Sci., 22, 291 (1956).

[41] Rubb. and Plast. Age, 38, 321 (1957).

[42] A. Irby, Rubb. World 133, 2 (1955).

[43] C. Patrick, Nature, 181, 698 (1958).

[44] D. D. Chegodaev, Fluorinated Plastics [in Russian] (Goskhimizdat, 1956).

[45] I. Ya. Klinov, Chem. Sci. and Ind. 3, 497 (1958).

[46] T. N. Nikolaeva, Summaries of Papers and Communications at the All-Union Scientific and Technical Conference on Corrosion and Metal Protection, No. 6 [in Russian] (Profizdat,* 1958).

[47] Ch. Eng. News, 34, 48, 5926 (1956).

[48] G. Kline, Plastics, 35, 153 (1957).

[49] F. Hill, Ind. Eng. Ch., 50, 5 (1958); Ang. Ch., 70, 275 (1958).

[50] A. Farthing, J. Chem. Soc., 3648 (1955); J. Appl. Chem., 8, 186 (1958).

[51] G. Kline, Mod. Plast., 34, 149 (1957).

[52] H. Schnell, Ang. Ch., 68, 633 (1956).

[53] Brit. Plast., 31, 312 (1958).

[54] G. A. Shtraikhman, Bull. Leningrad Council of National Economy 6 (1958).

[55] K. A. Andrianov and A. A. Zhdanov, Proc. Acad. Sci. USSR 112, 1050 (1957).**

[56] T. M. Frunze and V. V. Korshak, Bull. Acad. Sci. USSR, Div. Chem. Sci. 783 (1958).**

[57] W. English and L. Sommer, J. Chem. Soc., 77, 170 (1955).

[58] H. Jahn, Plaste and Kautschuk, 5, 6 (1958); Ind. Eng. Ch., 49, 7 (1957).

[59] De Cat, Ind. Chim. Belg., 21, 457 (1956); Polymer Chemistry and Technology 3, 106 (1957).

Received October 14, 1958

* Trade-Unions' Publishing House.

** Original Russian pagination. See C. B. Translation.

INTERACTION OF CALCIUM ALUMINATES AND ALUMINOFERRITES WITH CALCIUM SULFATE

P. P. Budnikov and V. S. Gorshkov

In certain papers [1, 2] dealing with the characteristics of hardened cement pastes the view is put forward that the hydration products of calcium aluminates and aluminoferrites in presence of calcium sulfate have a crystalline structure in the metastable state only; with time they are converted into multicomponent gels containing all the oxide components of the cement and including calcium sulfate. The conversion of calcium hydrosulfoaluminate and hydrosulfoferrite, which have a crystalline structure which "reinforces" the hardened cement, into a multicomponent gel should in the first instance influence the physicomechanical properties of thehardened cement.

The purpose of the present investigation was to study the products of simultaneous hydration of calcium aluminates and aluminoferrites with calcium sulfate, and to use differential thermal analysis and x-ray phase analysis for determining the nature of the phase conversions in the sulfate-containing compounds formed in clinker minerals during hydration at normal and elevated temperatures.

It is known that $4CaO \cdot Al_2O_3 \cdot Fe_2O_3$ is not an individual chemical compound in cement clinker, but is an intermediate member in the series of solid solutions of $3CaO \cdot Al_2O_3$ and $2CaO \cdot Fe_2O_3$. Therefore, for our studies of the reaction products of calcium sulfate with calcium aluminoferrites, we synthesized $6CaO \cdot 2Al_2O_3 \cdot Fe_2O_3$, $4CaO \cdot Al_2O_3 \cdot Fe_2O_3$, $6CaO \cdot Al_2O_3 \cdot 2Fe_2O_3$, $2CaO \cdot Fe_2O_3$ and $3CaO \cdot Al_2O_3$; these were fired until the lime was completely assimilated and then ground down to a specific surface of about 5000 cm^2/g.

For studies of the kinetics of the interaction between clinker minerals and calcium sulfate, and for determination of the products formed in their simultaneous hydration, 5 g of each of the above-named minerals was put into glass vessels and covered with 1000 ml of a lime – calcium sulfate solution. The calcium sulfate concentration in the saturated lime solution corresponded to 0.927 g SO_3 per liter. To ensure thorough interaction of the individual mineral grains with the lime – sulfate solution, and to equalize the concentration of $SO_4^{=}$ anions during absorption by the mineral, the contents of the vessels were mixed at intervals throughout the hydration period. Variations of the $SO_4^{=}$ anion concentration were determined at definite intervals; for this, 100 ml samples of solution were taken from the vessels, and the unreacted sulfate was precipitated by addition of 10% barium chloride.

The results of these determinations are given in Table 1.

After 3 months of hydration the solid phase was separated from the solution, washed with ethyl alcohol, and separated into two fractions by means of a heavy liquid (bromoform, sp. gr. 2.890). The clinker minerals which had not reacted with calcium sulfate, which had a higher specific gravity than bromoform, settled out on the bottom of the tube when centrifuged, while the sulfate-containing compounds formed by interaction between calcium sulfate and the minerals remained on the surface of the bromoform. The crystals of the sulfate-containing compounds, separated from bromoform, were washed with ethyl alcohol and ether; they were then subjected to x-ray phase analysis by the powder method and to thermal analysis by means of the Kurnakov differential pyrometer.

The interplanar distances and intensities of the diffraction lines of the analyzed x-ray patterns are given in Fig. 1. For comparison, this figure also shows the x-ray patterns (at 20°) of calcium hydrosulfoaluminate

TABLE 1

Kinetics of the Interaction of Clinker Minerals with Calcium Sulfate

Clinker minerals	Amount of sulfate combined (in g SO_3 per liter) in time (days)				
	1	3	7	28	90
$3CaO \cdot Al_2O_3$	1.803	2.110	2.405	2.862	2.989
$6CaO \cdot 2Al_2O_3 \cdot Fe_2O_3$	0.854	1.432	1.797	2.115	2.321
$4CaO \cdot Al_2O_3 \cdot Fe_2O_3$	0.835	1.343	1.604	1.936	2.086
$6CaO \cdot Al_2O_3 \cdot 2Fe_2O_3$	0.268	0.392	0.786	1.097	1.391
$2CaO \cdot Fe_2O_3$	0.043	0.112	0.498	0.694	0.872

prepared by the following two methods: 1) interaction of saturated $3CaO \cdot Al_2O_3$ solution with $CaSO_4 \cdot 0.5H_2O$ solution; 2) solid-phase interaction of finely divided $3CaO \cdot Al_2O_3$ and $CaSO_4 \cdot 0.5H_2O$ (specific surface about 7000 cm^2/g) taken in the calculated proportions to give the high-sulfate form of calcium hydrosulfoaluminate.

Comparison of the interplanar distances and intensities found in the x-ray patterns of the hydration products of $6CaO \cdot 2Al_2O_3 \cdot Fe_2O_3$, $4CaO \cdot Al_2O_3 \cdot Fe_2O_3$ and $6CaO \cdot Al_2O_3 \cdot 2Fe_2O_3$ formed in lime sulfate solution reveals, in addition to lines corresponding to calcium hydrosulfoaluminate, supplementary lines corresponding to the lines obtained in the x-ray pattern of the products of hydration of $2CaO \cdot Fe_2O_3$ in lime – sulfate solution. The following supplementary lines (in addition to the calcium hydrosulfoaluminate lines) are found in the x-ray patterns of the respective hydration products:

For $6CaO \cdot 2Al_2O_3 \cdot Fe_2O_3$ — 3.61, 3.03, 2.60, 2.38, 2.13, 1.50 A;
For $4CaO \cdot Al_2O_3 \cdot Fe_2O_3$ — 3.61, 3.00, 2.62, 2.36, 2.13, 1.50 A;
For $6CaO \cdot Al_2O_3 \cdot 2Fe_2O_3$ — 3.59, 3.00, 2.65, 2.37, 2.13, 1.49 A.

The presence of the supplementary lines indicates that the hydration products of the iron-containing clinker minerals contain calcium hydrosulfoferrite in addition to calcium hydrosulfoaluminate. Hence it is clear that when iron-containing clinker minerals are hydrated in lime – sulfate solution, i.e., in a medium in which the CaO and SO_4'' concentrations are close to those existing in hydrating cement before the calcium sulfate has been completely combined, the formation of calcium hydrosulfoaluminate is accompanied by formation of calcium hydrosulfoferrite, the latter being formed at a considerably lower rate than calcium hydrosulfoaluminate (Table 1).

Thermal analysis of calcium hydrosulfoaluminate made by the two different methods indicated above revealed the existence of two distinct endothermic effects (Fig. 2). Determinations of the amount of water of crystallization liberated in the heating of calcium hydrosulfoaluminate, performed by dynamic weighings on a torsion balance, showed that in the ~40 – 120° range the water loss is 28.4%, corresponding to 20 molecules of water of crystallization. The total water loss on heating to 1050° is 45.97%. The amount of water of crystallization calculated theoretically on the assumption that calcium hydrosulfoaluminate contains 32 water molecules is 45.93%, which is in good agreement with the experimental value. The remaining 12 molecules of water of crystallization are mainly removed before 250° when calcium hydrosulfoaluminate is heated; this corresponds to the second endothermic effect at 270 – 280°.

The dehydration of calcium hydrosulfoferrite formed by the interaction of $2CaO \cdot Fe_2O_3$ with lime – sulfate solution and separated from the unchanged mineral by centrifuging, as revealed by thermal analysis, took a different course from that of calcium hydrosulfoaluminate (Fig. 3). Whereas in the heating of calcium hydrosulfoaluminate the first effect, corresponding to the removal of most of the bound water (20 molecules out of 32), occurs below 120°, in the dehydration of calcium hydrosulfoferrite the first endothermic effect, corresponding to the removal of a smaller amount of water (as shown by the depth of the effect), is found in the 170 – 180° range. The second effect on the heating curve of calcium hydrosulfoferrite is found in the 315 – 330° range, whereas in the dehydration of calcium hydrosulfoaluminate the residual water of crystallization is lost at a lower temperature (in the 270 – 280° range).

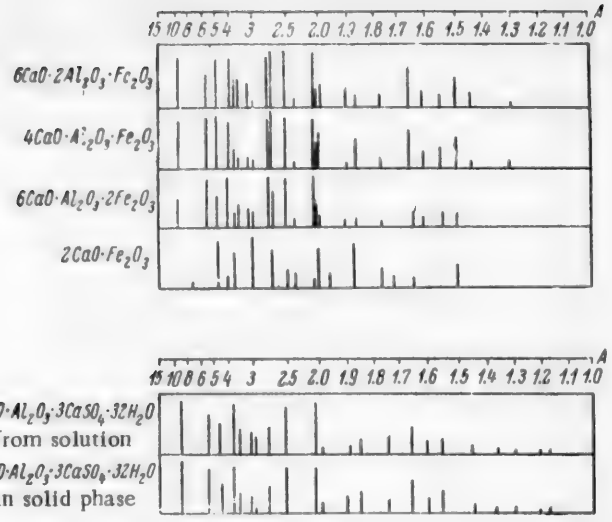
15 10 8 6 5 4 3 2.5 2.0 1.9 1.8 1.7 1.6 1.5 1.4 1.3 1.2 1.1 1.0 A
6CaO·2Al2O3·Fe2O3
4CaO·Al2O3·Fe2O3
6CaO·Al2O3·2Fe2O3
2CaO·Fe2O3
3CaO·Al2O3·3CaSO4·32H2O from solution
3CaO·Al2O3·3CaSO4·32H2O in solid phase

Fig. 1. Analyzed x-ray patterns of the products of hydration of clinker minerals in lime – sulfate solution.

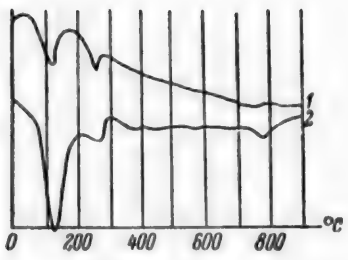

Fig. 2. Thermogram of calcium hydrosulfoaluminate: 1) $3CaO \cdot Al_2O_3 \cdot 3CaSO_4 \cdot 32H_2O$ from solution, 2) $3CaO \cdot Al_2O_3 \cdot 3Ca\,SO_4 \cdot 32H_2O$ in solid phase.

For comparison with the nature of the dehydration of calcium hydrosulfoferrite formed by the reaction of $2CaO \cdot Fe_2O_3$ with lime – sulfate solution, synthetic calcium hydrosulfoferrite made by the treatment of ammonium ferric alum – $(NH_4)_2SO_4 \cdot Fe_2(SO_4)_3 \cdot 24H_2O$ – with saturated lime solution for 3 days at 20±2° with continuous stirring was subjected to thermal analysis.

After separation from the mother liquor, the crystals, from 0.05 × 0.01 to 0.03 × 0.005 mm in size, had a weak polarization color, direct extinction, positive elongation, and an average refractive index of 1.490±0.003.

The optical constants of calcium hydrosulfoferrite crystals formed by the reaction of $2CaO \cdot Fe_2O_3$ with lime – sulfate solution were similar to those of the synthetic calcium hydrosulfoferrite, but the crystals were considerably smaller.

It is clear from the thermograms for synthetic hydrosulfoferrite, shown in Fig. 3, that the principal heat effects in its dehydration lie in the same temperature ranges as those of calcium hydrosulfoferrite made by hydration of $2CaO \cdot Fe_2O_3$.

The nature of the heating curves of the products formed by hydration of iron-containing clinker minerals – $6CaO \cdot 2Al_2O_3 \cdot Fe_2O_3$, $4CaO \cdot Al_2O_3 \cdot Fe_2O_3$ and $6CaO \cdot Al_2O_3 \cdot 2FeO_3$ – in lime – sulfate solutions for six months (Fig. 3) indicates the formation of sulfate-containing compounds which decompose in temperature ranges intermediate between the temperatures of the corresponding decomposition effects of calcium hydrosulfoaluminate and hydrosulfoferrite.

When $6CaO \cdot Al_2O_3 \cdot 2Fe_2O_3$ is hydrated in lime – sulfate solution, the calcium hydrosulfoaluminate formed loses part of its water of crystallization over a fairly wide temperature range (from 40° to 115 – 120°). The initial dehydration of calcium hydrosulfoferrite formed in the hydration of $6CaO \cdot Al_2O_3 \cdot 2Fe_2O_3$ under the same conditions occurs over a narrower temperature range (from 160° to 175 – 180°), which almost coincides with the first dehydration effect of hydrosulfoaluminate, and therefore these effects are superposed in the thermogram. The second endothermic effect at 270 – 280° on the same curve corresponds to total dehydration of calcium hydrosulfoaluminate. The total dehydration of hydrosulfoferrite present in the same hydration products of $6CaO \cdot Al_2O_3 \cdot 2Fe_2O_3$ occurs at 315 – 330°.

TABLE 2

Effect of Moist Heat Treatment on the Rate of Binding of Calcium Sulfate by Clinker Minerals

Clinker minerals	SO_3 content before treatment (%)		SO_3 content after treatment (%)			
			steamed at 100°		steamed at 8 atmos	
	free	bound	free	bound	free	bound
$3CaO \cdot Al_2O_3$	2.61	32.89	4.80	30.70	5.96	29.54
$6CaO \cdot 2Al_2O_3 \cdot Fe_2O_3$	8.04	27.46	7.32	28.18	6.71	28.79
$4CaO \cdot Al_2O_3 \cdot Fe_2O_3$	12.38	23.12	10.14	25.36	9.46	26.04
$6CaO \cdot Al_2O_3 \cdot 2Fe_2O_3$	27.58	7.92	23.64	11.86	21.67	13.83
$2CaO \cdot Fe_2O_3$	33.79	1.71	30.50	5.00	23.36	12.14

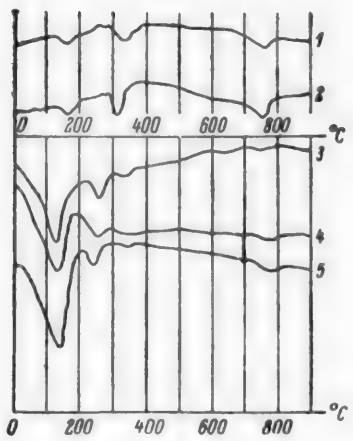

Fig. 3. Thermograms of the products of hydration of clinker minerals in lime – sulfate solution:
1) calcium hydrosulfoferrite prepared from $2CaO \cdot Fe_2O_3$; 2) synthetic calcium hydrosulfoferrite prepared from ammonium ferric alum; 3) hydration products of $6CaO \cdot Al_2O_3 \cdot 2Fe_2O_3$;
4) hydration products of $4CaO \cdot Al_2O_3 \cdot Fe_2O_3$; 5) hydration products of $6CaO \cdot 2Al_2O_3 \cdot Fe_2O_3$.

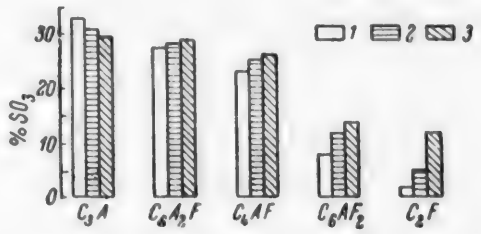

Fig. 4. Interaction of calcium sulfate with clinker minerals in moist heat treatment: contents of bound SO_3 (%): 1) before treatment, 2) after treatment at 100°, 3) after autoclave treatment.

The thermograms of the hydration products of $4CaO \cdot Al_2O_3 \cdot Fe_2O_3$ and $6CaO \cdot 2Al_2O_3 \cdot Fe_2O_3$ (Fig. 3) are almost identical with the heating curve of the hydration products of $6CaO \cdot Al_2O_3 \cdot 2Fe_2O_3$ by the number of effects and their temperature ranges. They are distinguished by the different magnitudes of the thermal effects, which are a quantitative measure of the presence of different phases.

The magnitude of the effect at 315 – 330° increases with increasing $2CaO \cdot Fe_2O_3$ content in the series of solid solutions from $6CaO \cdot 2Al_2O_3 \cdot Fe_2O_3$ to $6CaO \cdot Al_2O_3 \cdot 2Fe_2O_3$; this corresponds to an increasing content of calcium hydrosulfoferrite in the products formed by their hydration jointly with calcium sulfate.

Thermal analysis of calcium hydrosulfoaluminate and hydrosulfoferrite therefore shows that calcium hydrosulfoferrite is the more stable to the action of elevated temperatures. This fact suggests that calcium aluminates and aluminoferrites present in cement clinker should behave differently with calcium sulfate, and that the stabilities of the hydration products formed from them during moist heat treatment should be different.

To test this hypothesis, mixtures with calcium sulfate hemihydrate and calcium oxide were prepared from iron-containing clinker minerals and from $3CaO \cdot Al_2O_3$ ground to a specific surface of 5000 cm^2/g. The amount of calcium sulfate hemihydrate in each mixture corresponded to 33.5% SO_3; the amount of added calcium oxide was 3.0% on the mineral weight.

The mixtures were mixed with 50% of water and made into specimens 1 × 1 × 3 cm; these were removed from the molds after 24 hours and kept in a moist atmosphere at 20±2°. After 28 days of hardening and preliminary determination of the unreacted calcium sulfate, some of the specimens were subjected to moist heat treatment at 100° for 8 hours, while the rest were steamed in an autoclave at 8 atmos under the following conditions: pressure increase for 2 hours, exposure for 4 hours, pressure decrease for 2 hours.

The free calcium sulfate was determined in the specimens after the moist heat and autoclave treatments. The results are given in Table 2 and Fig. 4.

It follows from Table 2 that in 28 hours of hydration of specimens under humid conditions the amount of calcium sulfate bound by the minerals decreases with increasing calcium ferrite content. Moist heat treatment at 100° of specimens made from a mixture of $3CaO \cdot Al_2O_3$, calcium sulfate, and calcium oxide, the hydration of which for 28 days yielded about 93% of calcium hydrosulfoaluminate, resulted in an increase of the free SO_3 content from 2.61 to 4.80%; this shows that part of the calcium hydrosulfoaluminate was decomposed. Autoclave treatment of these specimens results in more intensive decomposition of calcium hydrosulfoaluminate, the amount of free SO_3 increasing from 2.61 to 5.96%.

The presence of iron compounds in aluminoferrite minerals makes them more stable in moist heat treatment. For example, the amount of calcium sulfate combined with $2CaO \cdot Fe_2O_3$ in 28 days of hydration corresponds to 1.71% SO_3, whereas after treatment of these specimens at 100° for 8 hours the amount of combined calcium sulfate increases to 5.0% SO_3, while after autoclave treatment at 8 atmos it increases to 12.14% SO_3.

SUMMARY

The results indicate that in the moist heat treatment of cements with a high content of calcium aluminoferrites, decomposition of calcium hydrosulfoaluminate with liberation of free calcium sulfate is accompanied by the formation of a more heat-resistant compound, calcium hydrosulfoferrite, which combines with the liberated calcium sulfate.

LITERATURE CITED

[1] G. L. Kalousek and M. Adams, J. Am. Concrete Inst., 23, 77 (1951).

[2] T. C. Powers and T. L. Brownyard, J. Am. Concrete Inst., 688 (1947).

Received June 13, 1957

SULFOALUMINATE CEMENTS FROM THE PRODUCTS OF SOLID-PHASE REACTIONS

V. I. Kotov

It is known that the cement industry of the future must be based on other processes in addition to those carried out at high temperatures, which involve enormous consumption of fuel and considerable losses of heat to the surroundings [1].

At the present time two types of cement are known the production of which requires less heat than the production of Portland cement clinker: 1) lime – burned-clay ("glinit") cements (GOST 2544-44), made by the mixing of clay calcined at 700 – 900° with lime; and 2) alite-free cements, made by the grinding of clinker formed at 1000 – 1200°.

The characteristic feature of the first type of cement is that during calcination of the clay the clay minerals (kaolinite, montmorillonite, hydromica, etc.) decompose into oxides, among which silica has considerable activity and forms a hydraulic binding material – calcium silicate – when mixed with lime and hydrated.

The characteristic feature of the second type of cement is that its clinker is formed only as the result of reactions in the solid state, and therefore it consists predominantly of belite, which is the main binding material in hydration.

Both types of cement have fairly low ratings.

The purpose of the present investigation was to find whether it is possible to produce a hydraulic cement with a lower expenditure of heat, by a study of the activity of calcined Belgobskii clay.

The material used for the investigation was clay of the type used for brick production, consisting mainly of montmorillonite minerals which, according to Belyankin and Ivanov [2], are completely dehydrated when heated to 700°, so that the montmorillonite lattice is destroyed. Since native montmorillonite is a substituted compound, its decomposition products will evidently be, in accordance with its composition $n(Mg, Ca)O \cdot Al_2O_3 \cdot (4-5)SiO_2 \cdot H_2O \cdot 5aq$ (Sedletskii [3]):

$$nMgO \cdot Al_2O_3 \cdot 4SiO_2 \cdot nH_2O \xrightarrow{700^\circ} Al_2O_3 + 4SiO_2 + nMgO.$$

In the clay used, the argillaceous material comprised about 45%; the remaining components were quartz (35%), calcium and magnesium carbonates (14%), and iron oxides (6%).

Repeated experiments performed to determine the optimum burning temperature showed that the most active material is obtained when the clay is heated in the 600 – 650° range. The activity of the product is lowered if a higher temperature is used.

The effects of the cement composition on its compressive strength are given in Table 1. The compressive strength was determined by means of the Amsler press. Cubes 7×7×7 cm were made from the cement with sand by tamping in a Klebe impact machine, the expenditure of work for each cube being 80 kg-meters. The cubes were stored over water under a cover with a hydraulic seal. Each sample consisted of 3 cubes. The average of the 2 highest values are given in the Table.

TABLE 1

Effects of Calcium Sulfate, Lime, and Clay Preparation on the Compressive Strength Under Moist Storage Conditions

Expt. No.	Composition of cement (%)				W/C ratio (%)	Setting time (hours)		Compressive strength (kg/cm^2) after	
	burned clay	lime	calcium sulfate: hemihydrate	calcium sulfate: dihydrate		start	end	7 days	28 days
1	82	15	3	—	—	5.9	17.0	18.2	47.0
2	82	15	-	3	—	4.0	13.0	38.4	93.0
3	72	25	--	3	55	5.5	14.5	26.6	78.0
4	82	15	-	3	50	4.0	13.5	38.7	93.0
5	87	10	--	3	50	4.0	12.0	41.0	97.0
6	92	5	-	3	48	6.5	17.5	22.0	—
7	82	15		3	53	3.8	11.0	23.0	57.0
8	87	10	-	3	51	3.9	11.5	24.0	68.0
9	87	10	---	3	35	4.3	14.6	30.0	51.0
10	87	10	- -	3	42	—	—	4.6	15.0

TABLE 2

Effect of Additions of Burned Clay Cement on Portland Cement Mortars

Mortar	Composition by weight	W/C ratio (%)	Plasticity by the StroiTsNILA cone test (cm)	Compressive strength (kg/cm^2) after	
				7 days	28 days
M-300 Portland cement + sand	1 : 3	0.58	6	121	150
M-300 Portland cement + M-50 burned clay cement + sand	0.8 : 0.2 : 3	0.61	6	112	145

Tests showed that the highest activity in clay calcined at 600 — 650° is produced by additions of 3% $CaSO_4 \cdot 2H_2O$ and 10% $Ca(OH)_2$ (Table 1, Experiments 1 — 6).

Activity tests on waste products from brick works showed that "underburned" wastes, formed when bricks are fired in annular furnaces in the 550 — 700° range (Table 1, Experiments Nos. 7 — 9), have considerable activity, whereas wastes from bricks fired normally (at about 1000°) have considerably lower activity (Table 1, Experiment No. 10).

Frost resistance tests on burned-clay cement showed that 7×7×7 cm cubes can withstand 15 cycles of alternate freezing (−15°) and thawing in water (20°) without any outward signs of destruction. However, after 15 freezing cycles the compressive strength falls to 26 kg/cm^2.

Concrete cubes 20×20×20 cm, made from grade 50 burned-clay cement, of the composition 1 : 1.5 : 2, cone sag of the concrete mix 4 cm determined by the vibration method, were also rated "50" after 28 days of aging in a moist medium.

For fuller characterization of the burned-clay cement, its influence on Portland cement mortars was tested (Table 2).

The results in Table 2 show that replacement of 20% of Portland cement rated "300" (rating "150" in the plastic mortar) by "50" grade burned-clay cement has almost no effect on the rating of the mortar (145 kg/cm^2).

TABLE 3

Effect of Storage Conditions of 7×7×7 cm Cubes on Compressive Strength

Expt. No.	Storage conditions	Storage time			Compressive strength (kg/cm²)	
		months	days	hours	Series "A"	Series "B"
1	Air at 20°	—	7	—	22.4	18.2
2	" " "	—	28	—	22.8	19.2
3	" " "	3	—	—	21.0	19.0
4	Humid at 20°	—	7	—	38.0	18.2
5	" " "	—	28	—	93.0	47.0
6	Humid at 20°, then in water	2	28	—	97.0	51.0
7	Humid at 20°, then in air	2	28	—	81.0	43.0
8	Humid at 20°, then in water	—	2	1	Destroyed	Destroyed
9	Humid at 20°, then steamed* at 90°	—	3	4	16.7	—
10	Humid at 20°, then steamed	—	3	6	52.0	—
11	Humid at 20°, then steamed	—	3	9	108.0	—
12	Humid at 20°, then steamed	—	3	12	192.0	—

* Steamed over boiling water in a closed vessel.

However, burned-clay cement is not used to any great extent in construction work, mainly on account of its low rating.

The hardening rate of burned-clay cement is considerably less than the hardening rates of alite and even of belite cements, and therefore the ultimate strength of burned-clay cement constructions can be determined even less reliably from its 28-day strength. It is known that in the case of low-strength belite cements the strength increase is greatest as the result of hydrothermal treatment [4]. This property is even more pronounced in burned-clay clinkerless cement. The results of tests of burned-clay cement under different hardening conditions are given in Table 3.

Storage of the specimens in water after 28 days under moist conditions does not result in any appreciable strength increase (Table 3, Experiments Nos. 5 and 6). The strength increases rapidly if the cubes are steamed; after 12 hours of steaming the compressive strength is more than doubled (Experiment No. 12) relative to the compressive strength of 28-day cubes.

Hardening of burned-clay cement in air produces little effect at 7 days, after which the strength does not increase during further exposure to air owing to drying of the specimens (Experiments Nos. 1 — 3).

Many workers (Baikov [5], Budnikov [6], Zhuravlev [7], Yung [1], Aleksandrovskii [8], and Zaporozhets [9]) consider that the processes which take place during the hardening of mixtures of lime and active silica are purely chemical. Other workers consider hardening processes of pozzolana cements only in relation to adsorption processes.

It was noted at the 1937 All-Union Conference on Concrete Corrosion held by the Academy of Sciences USSR that definite chemical compounds are formed between active silica and lime; later Zhuravlev [7], in a study of the kinds of hardening of lime — pozzolana cements with many different metal oxides and active silica of different origins, showed that "a chemical reaction occurs here, leading to the formation of a calcium hydrosilicate of the general type $xCaO \cdot ySiO_2 \times nH_2O$". The hydrosilicate formed is amorphous during the early stages

of its existence, but later crystallizes slowly. It is highly probable that under normal conditions the hardening of burned-clay cement results in the formation of monocalcium hydrosilicates with variable amounts of water:

$$SiO_2 + Ca(OH)_2 + nH_2O \rightleftarrows CaO \cdot SiO_2 \cdot nH_2O.$$

If colloidal silica and saturated lime solutions are used, the composition of the hydrosilicates formed approaches $2CaO \cdot SiO_2 \cdot H_2O$, i.e., calcium silicate, which is, of course, the predominant component (up to 40%) of Portland cement.

In the production of ordinary cement clinker the liquid phase is formed in the 1280 – 1300° temperature range. As the result of solid-phase reactions, the mixture at the start of sintering consists of C_2S, C_3A, C_4AF, C_2F and excess of calcium oxide, and after passing the sintering zone (1300 – 1480°) the cement clinker has the composition C_2S, C_3S, C_3A, C_4AF.

To ensure assimilation of the lime during burning of cement clinker, additives which lower the temperature at which a liquid is formed are used. Yung [1], Makashev [10], and Zhuravlev [11] note that fluorides are the best mineralizers. In particular, in presence of NaF (0.95%) the reaction between 2CaO and SiO_2 begins at 500°, and at 1100° the conversion reaches 98.9%. The acceleration of the process is attributed to formation of catalytically-active $CaO \cdot 3NaF$ and transition of quartz to cristobalite. Kukolev [12] observed accelerated interaction between finely ground quartz and $CaCO_3$ (without added mineralizers), which started at 600°. This effect is also explained by earlier breakdown of the reacting components in the mixture, and partial polymorphism of SiO_2. Ormont [13] noted that when quartz is heated, up to 600° there is strong expansion, from 600 to 1100° there is considerable contraction, and above 1100° expansion returns. These volume changes are due to breakdown of the hexagonal quartz lattice and formation of cristobalite with a cubic lattice (Fig. 1).

The breakdown of the rhombohedral $CaCO_3$ lattice, which occurs in practice at 900 – 1000° and is accompanied by decarbonation, also leads to formation of a cubic lattice of active calcium oxide.

If the second component is not limestone, but calcium hydroxide with its hexagonal lattice, the latter breaks down at 547° as the result of dehydration, with formation of the cubic lattice characteristic of calcium oxide (Fig. 2).

The reason why silica and limestone are suitable for synthesis of $2CaO \cdot SiO_2$, and why clay and limestone are suitable for cement production is that these substances become activated in the same temperature range (900 – 1000°). If $Ca(OH)_2$ is used for this synthesis, it is appropriate to use silica in a form which becomes active at the breakdown temperature of the $Ca(OH)_2$ lattice. Such a form can only be amorphous SiO_2, which does not have a crystal lattice. Slaked lime and amorphous silica are the best starting materials, which ensure a considerable reaction rate at the lowest temperatures and the optimum conditions for a solid-state reaction. These require: 1) the minimum expenditure of energy for loosening the $Ca(OH)_2$ lattice; 2) very fine grinding of the components; 3) high mobility of ions in the CaO lattice, so that the diffusion of ions through the newly-formed reaction products is accelerated; 4) presence of highly active amorphous silica.

The scheme for the reaction of $2CaO + SiO_2$ in the solid state at 400 – 1200° shows that the formation of the crystalline reaction product, $2CaO \cdot SiO_2$, is preceded by a number of periods in which intermediate states are present (Fig. 3).

The known process for dehydration and breakdown of clay minerals by the action of heat at about 500 – 700° is not the only method for this. We treated clay with sulfuric acid of sp. gr. 1.61. It was found that the optimum conditions for decomposition of the clay and separation of amorphous silica are obtained when the clay is treated with sulfuric acid at 360 – 400° for 2 hours. The adsorption activity of the SiO_2 formed in the process was checked from the rate at which sulfates formed simultaneously with the amorphous silica are washed out by water (Fig. 4).

The chemical and mineral composition of the clay changes sharply as the result of breakdown of the clay substance and other reactions of H_2SO_4 with the clay components.

The mineral composition of the clay (in %) before and after the sulfuric acid treatment is given on page 30.

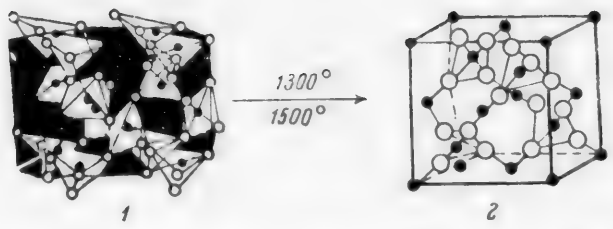

Fig. 1. The change taking place on breakdown of the hexagonal quartz lattice:
1) α-quartz, 2) β-cristobalite.

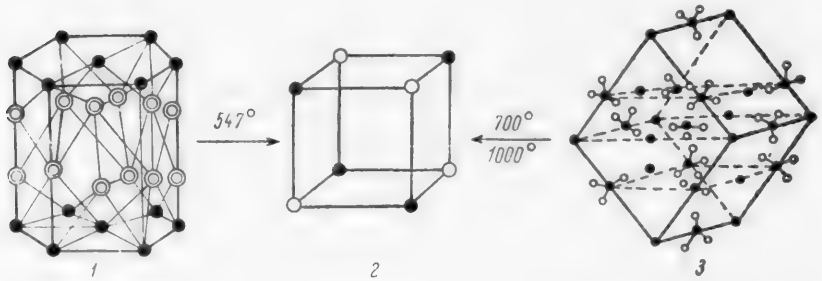

Fig. 2. Changes taking place on breakdown of the rhombohedral calcium carbonate lattice and the hexagonal calcium hydroxide lattice:
1) $Ca(OH)_2$, 2) CaO, 3) $CaCO_3$.

The product was used for the production of cements; it was mixed with the other component (slaked lime) and the mixture was burned at 700 – 1000°. The calcium sulfate formed, together with sulfates of other metals, can take part in the formation of complex compounds.

Lerch and Bogue [14] and Foret [15] have reported that calcium hydrosulfoaluminate can be synthesized under the usual conditions from calcium sulfate and any calcium aluminate.

Calcium hydrosulfoaluminate is known to exist in 2 forms: the trisulfate form, of the composition $3CaO \cdot Al_2O_3 \cdot 3CaSO_4 \cdot 31H_2O$, and the monosulfate form, of the composition $3CaO \cdot Al_2O_3 \cdot CaSO_4 \cdot 12H_2O$. Both hydrosulfoaluminates crystallize in the hexagonal system; the former as fine needles and the latter as plates [16].

According to Astreeva and Lopatnikova [17], calcium hydrosulfoaluminate gradually breaks down, forming calcium sulfate dihydrate, calcium hydroxide, and hydrated alumina. It is broken down more rapidly in sea water. It was also noted that hydrosulfoaluminates of low basicity, obtained from monocalcium aluminate, are the more stable.

Lyubimova [18] and Kalousek [19] noted that the trisulfate form of calcium hydrosulfoaluminate has low heat stability and is dehydrated to the monosulfate form.

The trisulfate form of calcium hydrosulfoaluminate is stable, and persists even at 90° provided that a large excess of calcium sulfate is present in the hydrosulfoaluminate.

However, despite the above-mentioned adverse properties of calcium hydrosulfoaluminate, it is known that in many cases the formation of calcium hydrosulfoaluminate in cements improves the quality of construction made from these cements.

For example, the addition of calcium sulfate to Portland cement, as a regulator of setting (up to 3%), and to slag cement, as activator (up to 15%), is specified by GOST and is not harmful, as in such cases the sulfoaluminate is formed either in the still-unhardened mass, or in the residual liquid phase of the hardened cement, without increase of volume.

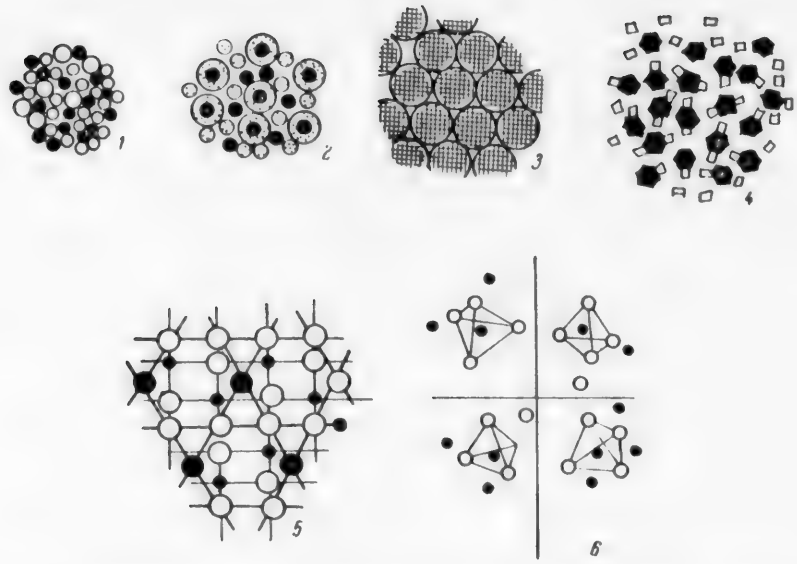

Fig. 3. Scheme for the reaction $2CaO+SiO_2=2CaO \cdot SiO_2$ in the solid state: 1) period of decrease of the sorptional properties of the reacting substances (400°), 2) period of formation of very thin layers on the grain surfaces of the less mobile component, 3) period of decrease of the mobility of particles in the layers owing to their increased bonding with the lattice of the less mobile substance, 4) period of internal diffusion of the particles of the mobile component within the lattice in the grains of the other component (700°), 5) period of formation of crystalline product, 6) period of improvement of the lattice structure of the compound formed (1000 – 1200°).

Before treatment		After treatment	
Clay minerals calculated as kaolinite – $Al_2Si_2O_5(OH)_4$	44.8	Quartz – SiO_2	23.1
Quartz – SiO_2	35.2	Active amorphous SiO_2	14.0
Limestone – $CaCO_3$	9.3	$Al_2(SO_4)_3$	40.5
$MgCO_3$	4.7	$Fe_2(SO_4)_3$	10.0
Fe_2O_3	6.0	$CaSO_4$	8.4
		$MgSO_4$	4.4

Volzhenskii's [20] observation that gypsum with added blast-furnace slag and active tripoli can harden in water with continuous increase of strength without loss of hardening rate can also be attributed to formation of the hydrosulfoaluminate complex.

Yung [1] reported that calcium sulfoaluminate can sometimes even serve as an important structural constituent in certain hydrated hardened cements. In 1950 Mikhailov [21] invented waterproof expanding and noncontracting cements; calcium sulfoaluminate is an active component in the hardening of these cements.

The foregoing data suggest that cements formed in solid-state reactions and containing mainly dicalcium silicate may, in conjunction with calcium hydrosulfoaluminate, be effective as hydraulic cements of fairly high mechanical strength and high resistance to corrosion by water containing dissolved alkali-metal sulfates.

Two kinds of sulfoaluminate cements were made from sulfated clay: burned-clay and belite cements. The raw mixes were made from the above-named components calculated to yield sulfoaluminate burned-clay

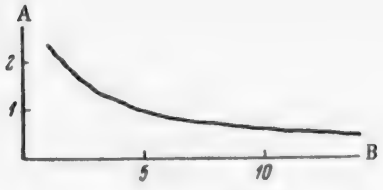

Fig. 4. Effect of time of washing with water on the sesquioxide content of sulfated clay:
A) R_2O_3 content (%), B) time (days).

cement at a firing temperature of 700°, and sulfoaluminate belite cement at a firing temperature of 1000°. The mixes were formed into briquets which were dried and fired in an experimental gas-heated chamber furnace.

The composition of these cements by chemical analysis (in %) is given below.

Cement	SiO_2	Al_2O_3	Fe_2O_3	CaO	MgO	SO_3
Burned clay	25.2	8.1	2.7	34.8	1.1	27.3
Belite	20.6	6.6	2.1	47.1	0.6	22.7

Bulychev's [22] considerations concerning the formation of monocalcium silicate and dicalcium aluminate in mixed plasters when they are mixed with water, and the phase diagrams of the corresponding two- and three-component systems, suggest that the principal structural elements formed in these cements upon hydration are calcium hydrosulfoaluminate and mono- and dicalcium silicates.

The effects of hardening conditions on the compressive strength of hardened cement paste (1 : 0) of normal consistency (about 35%) are shown in Figs. 5 and 6 [23].

The recent work of Budnikov, Kosyreva, and Kuznetsov [24] on the production of alite-free cement from mixtures of low-grade bauxite (40%), chalk (30%) and calcium (30%) fired at 1200° showed that the cement formed has the following chemical composition (%): SiO_2 11.96, Al_2O_3 21.06 Fe_2O_3 5.20, CaO 42.05, MgO 1.23, SO_3 19.12. Evidently the calcium sulfate content of this cement is equivalent to the amount of SO_3 found; i.e., it is 32.50% $CaSO_4$. Therefore the amount of CaO bound with SiO_2, Al_2O_3, Fe_2O_3, must be $42.05 - 13.38 = 28.67\%$. These alite-free cements must therefore be classed with the sulfoaluminate cements, as when they are mixed with water calcium hydrosulfoaluminate, which plays an important role in structure formation, is formed.

The results of determinations of the sulfate resistance of 12-month cements of different mineral compositions, reported by Okorokov, Vol'fson, and Burakova [25], show that only cements which do not contain C_3S and C_3A can be sulfate-resistant ($KS_{12} > 1$). For cements containing relatively small amounts of C_3S, $KS < 1$; it follows that such cements are gradually destroyed in 5% Na_2SO_4 solution. Therefore sulfate-resistant cements have the mineral composition $C_2S = 75\%$, $C_4AF + C_2F = 25\%$.

Alite-free cement contains [24] C_4AF, C_2S, and CA in addition to $CaSO_4$. When such cement is hydrated, monocalcium aluminate reacts with $CaSO_4$ to form calcium sulfoaluminate. The coefficient of sulfate resistance (KS_1) of this cement in 5% Na_2SO_4 and 3% $MgSO_4$ solutions, calculated from these authors' data, is less than unity ($KS_1 = 0.79 - 0.93$ for cement with a rating of $157 - 175$ kg/cm^2).

No attack or changes were found in specimens molded from our belite cement when exposed to 5% solution of $Na_2SO_4 + MgSO_4$ for a year and more.

When burned-clay cement was made from clay burned at 650°, mixed with lime (10%) and calcium sulfate (3%), it was found that the hardening of cubes made from this mixture and sand is accelerated by steaming; therefore the reaction between amorphous silica and calcium hydroxide is accelerated. It is likely that the use of steam in the burning of sulfoaluminate raw mixes should have a similar effect.

Le Chatelier [26] treated calcium chlorosilicate with steam at 600° and obtained tricalcium silicate

$$2CaO \cdot SiO_2 \cdot CaCl_2 + H_2O \xrightarrow{600^\circ} 3CaO \cdot SiO_2 + 2HCl,$$

which is, of course, one of the most valuable components of Portland cement and which is usually formed from 3 CaO and SiO_2 at 1500°.

Budnikov and Berezhnoi [27] also noted the accelerating effect of steam on reactions between certain substances. If a reaction takes place in presence of water vapor, then the value of the constant C, which is a quantitative measure of the possibility of particle diffusion, in the equation $\log K = \log C - \frac{a}{2.3T}$, is increased 8.5-fold.

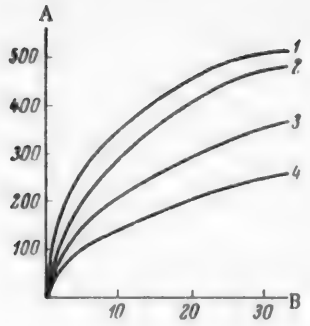

Fig. 5. Effect of hardening time on the compressive strength of belite cement:
A) compressive strength (kg/cm^2),
B) time (days); storage conditions:
1) wet; 2) wet, with 2% $CaCl_2$;
3) humid; 4) in air.

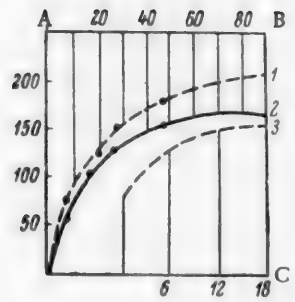

Fig. 6. Effect of hardening time on the compressive strength of burned-clay cement:
A) compressive strength (kg/cm^2),
B) temperature (deg), C) time (hours); storage: 1) wet, 2) humid, 3) steaming.

The accelerating effect of steam on the reaction SiO_2+CaO is due to loosening of the crystal lattice and increase in the dispersity of the reaction product ($2CaO \cdot SiO_2$), which facilitates diffusion of the substances constituting the reaction mixture.

We used the method of firing in presence of steam for the preparation of a cement from a mixture of sulfated clay and calcium oxide (1 : 1), with calcium chloride in an amount calculated to yield calcium chlorosilicate ($2CaO \cdot SiO_2 \cdot CaCl_2$). The experiments were performed in a furnace containing an iron tube filled with lumps of the raw mix. The firing was continued for 2 hours at 600°. Steam was passed continuously through the tube during the firing. The product had the following characteristics: water sorption 35%, start of setting 8-12 minutes, compressive strength of cubes (1 : 0) after 14 days of hardening in water 170 kg/cm^2.

SUMMARY

1) The hydraulic burned-clay ("glinit") cement made by the mixing of dehydrated clay, containing decomposed clay minerals, with lime has a very low rate of hardening. Normal initial hardening of such cement is possible only in a moist medium. Burned-clay cement can be hardened in water only on the 8th day after hardening in a moist atmosphere, when the compressive strength reaches about 20 kg/cm^2. Hardening in air stops as the material dries. In specimens of 28-day burned-clay cement the strength increase is only 50% of that obtained by steaming of the specimens for 12 hours (192 kg/cm^2).

2) The use of hydrosulfoaluminate in conjunction with calcium silicate formed in solid-state reactions confers considerably better properties on the cement and ensures:

a) normal and in some cases accelerated setting,

b) hardening under any conditions — in water, humid atmospheres, air, and steam, c) a fairly high rating in mortars (1 : 3) with sand, about 250 kg/cm^2, and a significantly high rating in paste (1 : 0), 500 kg/cm^2, and

d) sulfate resistance.

3) A specific characteristic of the method of production of sulfoaluminate cements from the products of solid-state reactions is preliminary breakdown of the structure of the clay materials with liberation of free oxides: amorphous silica and alumina. Our method for the breakdown of clay minerals by treatment of clay with sulfuric acid is probably not the only possible method. It is possible that sulfoaluminate cements produced in accordance with the principle discussed in this paper may prove valuable hydraulic cements.

LITERATURE CITED

[1] V. N. Yung, Principles of Cement Technology [in Russian] (Industrial Construction Press, 1951).

[2] D. S. Belyankin and B. V. Ivanov; Data on Studies of Dinas and Its Raw Materials in the USSR [in Russian] (Moscow-Leningrad, 1939).

[3] I. D. Sedletskii, Mineralogy of Colloidal Dispersions [in Russian] (Izd. AN SSSR, 1945).

[4] V. I. Kotov, Advances in Petroleum Technology (Construction and Installation) 4, 43 (1955).

[5] A. A. Baikov, Collected Works, 5 (Izd. AN SSSR, 1948) p. 203. [In Russian].

[6] P. P. Budnikov, A. S. Berezhnoi, I. A. Bulavin, G. V. Kukolev, V. I. Perevalov and I. S. Smenyanskii, Technology of Ceramic Wares (Moscow – Leningrad, State Construction Press, 1946) p. 46. [In Russian].

[7] V. F. Zhuravlev, Chemistry of Cements (Moscow – Leningrad, State Sci. Tech. Press Chem. Lit., 1951) p. 105. [In Russian].

[8] V. A. Kind and N. Aleksandrovskii, Building Materials, 1 (1929).

[9] N. D. Zaporozhets, in the collection: Pozzolana Cements (1936). [In Russian].

[10] S. D. Makashev, Cement 4, 5 (1950).

[11] V. F. Zhuravlev and S. L. Vol'fson, et al. Cement 3, 3 (1950).

[12] G. V. Kukolev, Chemistry of Silicon and Physical Chemistry of the Silicates [in Russian] (1951) p. 310.

[13] B. F. Ormont, Structures of Inorganic Substances [in Russian] (Moscow – Leningrad, GITTL, 1950), p. 510.

[14] W. Lerch and R. H. Bogue, J. Res. Natl. Bur. Standards 54, 715 (1929).

[15] J. Foret, Recherches sur les Combinaisons entre Sels de Calcium et les Aluminate de Calcium (Paris, 1935).

[16] N. A. Toropov, Chemistry of Cements (Moscow, State Constructional Materials Press, 1956) p. 215. [In Russian].

[17] O. I. Astreeva and L. Ya. Lopatnikova, Modern Views on Processes of Cement Hydration (Moscow, State Constructional Materials Press, 1956) p. 40. [In Russian].

[18] T. Yu. Lyubimova, Proc. Acad. Sci. USSR 94, 6 (1954).

[19] G. Kalousek, Proceedings of the Third International Symposium on the Chemistry of Cement (London, 1952).

[20] V. A. Volzhenskii, Coll. Trans. Sci. Res. Inst. Plaster Ind. 27 (1945).

[21] V. V. Mikhailov, Coll. Summaries of Scientific Research Papers on Building Construction (Stroiizdat, 1950) p. 117. [In Russian].

[22] G. G. Bulychev, Mixed Plasters (Moscow, State Construction Press, 1952) p. 87. [In Russian].

[23] V. I. Kotov, Cement 6, 12 (1953).

[24] P. P. Budnikov, Z. S. Kosyreva, and I. P. Kuznetsova, Trans. Mendeleev MKhTI, 21, 157 (1956).

[25] V. N. Yung, Yu. M. Butt, V. F. Zhuravlev, and S. O. Okorokov, Technology of Cements (Moscow, State Constructional Materials Press, 1952) p. 303. [In Russian].

[26] H. Le Chatelier, Silica and Silicates (Leningrad, Sci. Chem. Tech. Press, 1929) [Russian translation].

[27] P. P. Budnikov and A. S. Berezhnoi, Solid-Phase Reactions [in Russian] (Industrial Construction Press, 1949).

Received March 22, 1957

PROPERTIES OF SILICA GELS MADE BY THE DRYING OF SILICIC ACID GELS IN VACUUM

Z. Z. Vysotskii and V. V. Shalya

The significance of silica gels as adsorbents and catalyst supports is well known and increases year by year, and therefore searches for new methods for production of silica gels with different pore structures on the one hand, and the theory of formation of such pore structures during preparation of the gels on the other, are of definite interest.

Veselovskii and Selyaev [1] were the first to formulate clearly and to confirm experimentally the view that the capillary forces which compress the gel framework of silicic acid during dehydration mainly depend on the surface tension of the intermicellar liquid; this surface tension is therefore of decisive significance in the formation of the pore structure of silica gels. This viewpoint was subsequently accepted by Neimark et al. [2], who presented additional experimental data in its support.

However, even the experimental data so far obtained in this field indicate that the above interpretation is by no means conclusive. Moreover, in the case of the microheterogeneous systems – gels – in question, it could be assumed that the surface tension of the intermicellar liquid should in general be of subsidiary importance, while the main factor determining the magnitude of the capillary forces during the drying of a silica gel is the intensity of interaction between the intermicellar liquid and the silicic acid micelles. This factor is formally taken into account as the term $\cos\theta$ in the formula for capillalry forces, $p = 2\gamma \cdot \cos\theta / r$.

One possible way of testing experimentally the effect of the surface tension of the intermicellar liquid would be to dry a gel, both at atmospheric pressure and room temperature, when the intermicellar phase is liquid, and also under reduced pressure and with cooling of the gel, when the intermicellar phase is solid and capillary forces are ineffective.

This paper contains the results of such a comparative study of silica gels prepared from silicic acid gels in water, alcohol, and benzene. A method, developed in the course of the investigation, for vacuum drying of silicic acid gels at low temperatures is also described.

EXPERIMENTAL

Preparation of silica gels. Silicic acid hydrogels were made by the usual method – addition of a solution of sodium or potassium silicate to a solution of sulfuric acid; the acid sol formed passed after a few hours into a hydrogel, which was then washed free from salts. The details of the preparation and washing of the gels are given in the table.

The alcogel was made from hydrogels, water being replaced by ethanol by repeated treatment of the hydrogels with alcohol at room temperature, and the aqueous alcohol was decanted off every 24 hours.

Two methods were used for preparation of the gels in benzene: 1) at room temperature, water being replaced by alcohol and alcohol by benzene, as described above, and 2) at the boiling point of benzene, directly from the hydrogel which was boiled in benzene with continuous distillation of water – benzene mixture and additions of pure benzene.

All the gels were dried in the simple vacuum apparatus shown schematically in Fig. 1. (In every case a part of the gel was separated and dried at room temperature in air as a control). The apparatus consists of a glass

Preparation and Adsorption Capacity of Silica Gels

Series No.	Hydrogel preparation and washing	Sample No.	Drying conditions	Static activity for C_6H_6 (%)	Sorbent pore volume V_s (cc/g)	
					by adsorption of C_6H_6	from H_2O adsorption isotherm
I	2 volumes of Na_2SiO_3 (d = 1.15) + 1 volume of H_2SO_4 (1.18); washed with acidified running water (pH ~ 3.5); Hydrogel A	11	In air at room temperature	23.2	0.26	—
		12	In vacuum, externally cooled to −15°	24.6	0.28	0.28
		13	Partly dried in air, then in vacuum without external cooling	23.7	0.27	—
		14	Deposit in vacuum condenser	23.2	0.26	—
II	2 volumes of K_2SiO_3 (1.19) + 1 volume of H_2SO_4 (1.22); tap water (pH ~ 7.5); Hydrogel B	21	In air at room temperature	41.2	0.46	—
		22	In vacuum, frozen by self-cooling	61.9	0.71	—
III	2 volumes of Na_2SiO_3 (1.19) + 1 volume of H_2SO_4 (1.22); tap water (pH ~ 7.5); Hydrogel C	31	In air at room temperature	36.1	0.41	—
		32	In vacuum, frozen by self-cooling	53.7	0.61	0.69
IV	Hydrogel C, with water replaced by ethyl alcohol, by repeated decantation at room temperature	41	In air at room temperature	39.6	0.45	—
		42	In vacuum, frozen by self-cooling	68.3	0.78	—
V	Hydrogel A, with water replaced at room temperature, by repeated decantation, with ethyl alcohol, and the latter with benzene	51	In air at room temperature	35.1	0.40	—
		52	Partly dried in air, then in vacuum, frozen by self-cooling	39.1	0.45	—
		53	In vacuum, frozen by self-cooling	41.2	0.46	—
VI	Hydrogel C, with water replaced by benzene; gel boiled in benzene, with distillation and addition of fresh benzene	61	In air at room temperature	72.0	0.82	—
		62	In vacuum, frozen by self-cooling	72.0	0.82	—

ampoule 1 with the sample, contained in a Dewar flask 2 with a suitable freezing mixture, or without, as vacuum drying (especially of hydrogels) is accompanied by intensive self-cooling of the samples. The ampoule is connected through the three-way cock 3 and intermediate stopcock 4 to a condenser 5, immersed in liquid air in the Dewar flask 6 and joined to a vacuum pump through the stopcock 7. After the sample had been put into the ampoule, the apparatus was evacuated, the stopcock 7 was closed, and the condenser was immersed in liquid air; as a result, vapor of the intermicellar substance began to distill over into the condenser. In most cases the gels were converted into powders with 0.1 — 0.5 mm grains by vacuum drying. When hydrogels were used, the condenser was found to contain a suspension of fine silica gel powder after thawing; these particles were probably entrained with the water vapor, although the possibility is not excluded that they were formed in the condenser

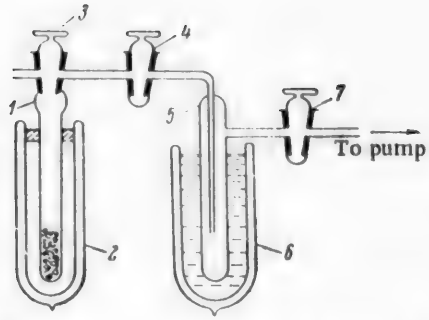

Fig. 1. Apparatus for vacuum drying of silica gels.

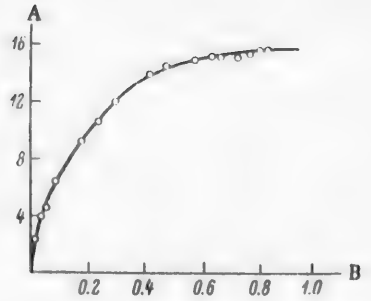

Fig. 2. Adsorption isotherm of H_2O vapor on silica gel 12: A) adsorption of water vapor (millimoles/g), B) relative pressure $(\frac{P}{P_s})$.

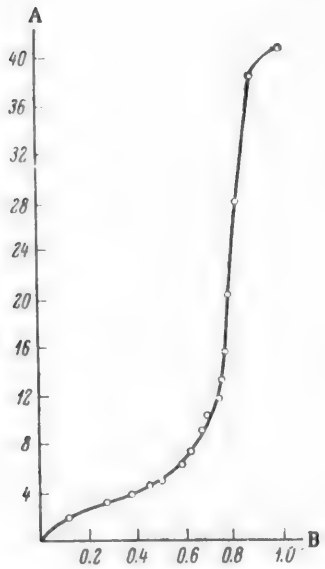

Fig. 3. Adsorption isotherm of H_2O vapor on silica gel 32: A) adsorption of water vapor (millimoles/g), B) relative pressure $(\frac{P}{P_s})$.

as the result of condensation of monomeric silicic acid molecules distilled under vacuum from the ampoule with the hydrogel into the condenser.

Investigation of the adsorption properties of the silica gels. The sorption of benzene vapor at room temperature by all the samples was studied by the desiccator method. The sorptive pore volumes of the samples were calculated from the static activities determined by this method. In some cases the isotherms for adsorption of water vapor in vacuum at 20° were determined by the quartz spring balance method.

RESULTS AND DISCUSSION

The results of the investigation are given in the table and in Figs. 2 and 3. Three series of hydrogels (I, II, and III), one series of alcogels (IV), and two series of benzene gels (V and VI) were prepared.

It follows from the data in the table that the control sample 11 and samples 12 – 14 of Series I, made from sodium silicate, have the same sorptive pore volume V_s, irrespectively of the very different dehydration conditions. Fig. 2 shows the isotherm for adsorption of H_2O vapor on sample 12; it is seen that the samples of this series are typical microporous silica gels. The common feature of Series I is that the original hydrogel A was washed free from salts with acidified tap water of pH~3.5.

However, it was found in Series II, the hydrogels of which were prepared from potassium silicate and washed with tap water at pH~7.5 (hydrogel B), that the vacuum-dried sample 22 has a much higher adsorption capacity than the control sample 21. To determine the cause of this difference between Series I and II – to find whether it was due to the nature of the silicate or to the pH of the wash water – Series III was prepared from sodium silicate (Hydrogel C), the samples being washed, as for Series II, by tap water with pH~7.5. It follows from the table that in this case, as in Series II, control sample 31 is less porous than the vacuum-dried silica gel 32. The isotherm in Fig. 3 shows that this sample is coarsely porous.

This leads to the conclusion that the control and vacuum-dried samples differ in porosity only if washed with water at pH~7.5 (Series III and IV), regardless of the nature of the original silicate.

The control (41) and vacuum-dried (42) alcogels differ in pore structure. Comparison of the porosity of control sample 31 with that of the control alcogel 41 shows that they are almost the same in structure, although the surface tensions of water and ethanol differ considerably. However, these hydroxylic compounds are similar in chemical structure. The situation is different if the hydrogel water is replaced by benzene (compare control samples 11 and 51, and 31 and 61 respectively). This result should evidently be attributed to differences between the chemical properties of water and benzene.

The benzene gels of Series V, prepared at room temperature, have approximately the same pore structure, despite the different drying conditions. Similarly, the adsorptive power of benzene gels of Series VI (control sample 61, and vacuum-dried sample 62, made by boiling in benzene) is also the same in the two cases, although comparison of the porosities of the gels in the two series shows that gels of Series VI have coarser pores than gels of Series V. Thus, despite the fact that the control benzene gels (Series V and VI) were dried under conditions such that the surface tension of liquid benzene could have an effect, whereas this possibility was excluded in vacuum drying, benzene gels made by the same method, with water replaced at the same temperature, had the same porosity. In this case the surface tension of benzene apparently has a subordinate role, and the structure of silica gels obtained from benzene gels is determined by the interaction of the intermicellar liquid, benzene, with the surface of the silicic acid micelles; this interaction differs for series V and VI respectively, prepared by different methods and at different temperatures, and therefore the gels of Series V differ in porosity from gels of Series VI.

It follows from the results of these experiments, in which the control samples were dried under conditions in which the intermicellar phase was liquid, while the test samples were dried by sublimation of the intermicellar substance from the solid state, that in some cases (Series II, III, and IV) the porosity differs in accordance with the drying conditions, while in others (Series I, V, and VI) it is the same. Therefore the surface tension of the intermicellar substance is not the sole and decisive factor determining the magnitude of the capillary forces. The above comparison of the properties of control silica gels made from gels in water, alcohol, and benzene shows that the observed facts are explained more satisfactorily if it is assumed that the degree of interaction between the dispersion medium and the disperse phase has the decisive influence on the structure of silica gels.

SUMMARY

1. Microporous silica gels of the same pore structure are formed when silicic acid hydrogels, washed with acidified water (pH~3.5) are dehydrated either in air at room temperature or under vacuum (with or without cooling).

If hydrogels washed with tap water (pH~7.5) and alcogels made by replacement of water at room temperature are dried in vacuum, the silica gels formed are more coarsely porous than air-dried silica gels.

Benzene gels formed by replacement of water by benzene, the hydrogel being boiled in benzene with continuous distillation of the liquid, and benzene gels formed from alcogels at room temperature, do not differ in pore structure from the corresponding control samples; i.e., the structure of benzene gels is almost independent of the drying method.

However, the porosity of benzene gels depends significantly on the method used for replacement of water by benzene.

2. Replacement of water in a hydrogel by ethyl alcohol at room temperature, followed by drying of the alcogel, produces almost no change in the pore structure of the dry gel, despite the difference between the surface tensions of water and ethanol. The gel structure is altered by replacement of water by benzene.

3. The surface tension of the intermicellar liquid is not, in general, decisive in the formation of the pore structure of silica gels.

The pore structure of a silica gel depends primarily on physicochemical processes taking place on the surface of the micellar framework of the silicic acid gel and on differences in the molecular structure of the disperse phase and dispersion medium, which influence the intensity of their interaction and therefore the rate and degree of formation of the microheterogeneous structure of the hydrogel (or benzene or alcohol gel).

LITERATURE CITED

[1] V. S. Veselovskii and I. A. Selyaev, J. Phys. Chem. 6, 1171 (1935).

[2] I. E. Neimark, Trans. Commission Anal. Chem. Acad. Sci. USSR 6 (9), 77 (1955); I. E. Neimark and F. I. Khatset, Colloid J. 9, 289 (1947); I. E. Neimark and R. Yu. Sheinfain, Colloid J. 15, 50 (1953).*

Received December 28, 1956

* Original Russian pagination. See C. B. Translation.

ROLE OF THE LIQUID PHASE IN THE SINTERING OF FORSTERITE REFRACTORIES

G. V. Kukolev and S. I. Shcheglov

The V. I. Lenin Polytechnic Institute, Khar'kov

The purpose of our investigation was a study of the sintering of forsterite refractories in relation to phase-equilibrium data.

Goldschmidt [1], Arshinov [2, 3], Basilevich [4 – 6], Andreev [7, 8], Berezhnoi [9 – 12], Tsynkina [13, 14], Mamykin [15] and others have published papers on the sintering of forsterite refractories.

However, no systematic investigations of the liquid-phase sintering of forsterite refractories have been carried out as yet, although in practice the production of dense forsterite refractories involves considerable difficulties.

Our investigations were performed with various mixtures in the systems: $MgO - SiO_2$, $MgO - Al_2O_3 - SiO_2$, $2MgO \cdot SiO_2 - SiO_2 - CaO \cdot Al_2O_3 \cdot 2SiO_2$ and $Na_2O - MgO - SiO_2$.*

The compositions of the original mixtures required to give definite amounts of liquid phase at particular temperatures in the field of primary crystallization of forsterite were calculated by analysis. The calculations were checked graphically.

The samples were prepared from mixtures yielding 5, 15 and 25% of melts of the same composition, for a given system and temperature, in equilibrium with solid forsterite. The initial bulk density of all the mixtures was 1.54 g/cc (porosity about 48%).

The degree of sintering was determined from changes of bulk density, apparent and true porosity, and compressive strength of the samples.

The melt viscosity, and in some instances the surface tension, was determined by the method developed by Ermolaeva in the All-Union Scientific Research Institute of Refractories (Khar'kov). The surface tension of the melts was calculated from Appen's data [16] in most cases. Magnesium oxide of analytical-reagent grade, and quartz sand ground and washed in 10% HCl solution, were used for studies of the phase equilibria.

Oxides in amounts of 0.01 mole per 100 g of the principal mixture were added. The effects of the following additives were studied: V_2O_5, B_2O_3, P_2O_5, Fe_2O_3, Li_2O, ZrO_2, WO_3, TiO_2, Al_2O_3, MnO_2, CuO, Bi_2O_3, Na_2O, Cr_2O_3, K_2O, BaO, PbO, CdO, CoO, ZnO and NiO.

It is clear from the curves in Fig. 1 (changes of true porosity) that sintering of mixtures in the system $MgO - SiO_2$ proceeds very slowly, but is more rapid at 1700° if 15% of melt is formed in the samples. However, it does not go to completion even in the latter case. Increases of the amount of melt above 15% have little effect on the sintering process.

Sintering of the mixtures is much more intensive in the systems M – A – S and $M_2S - S - CAS_2$. Even at 1500°, with the same amounts of melt, it approaches to the sintering of the system $MgO - SiO_2$ at 1700°. Increase of the firing temperature of mixtures in the systems M – A – S and $M_2S - S - CAS_2$ to 1700° improves sintering a little (Figs. 2 and 3).

* The following abbreviated notation is used below in most cases: SiO_2 – S, Al_2O_3 – A, MgO – M, CaO – C, Na_2O – N.

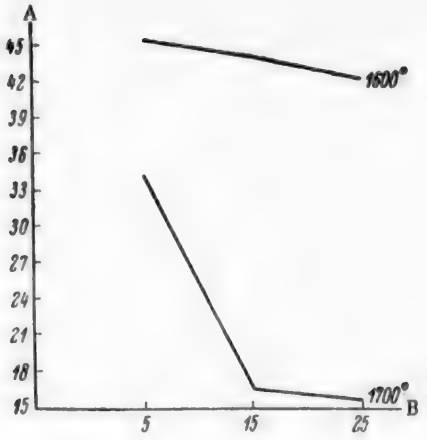

Fig. 1. Sintering of forsterite in the system $MgO - SiO_2$:
A) true porosity (%), B) content of melt (%).

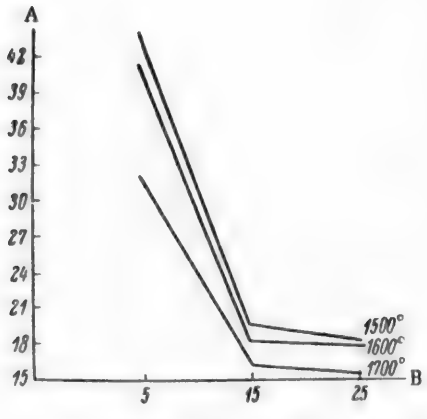

Fig. 2. Sintering of forsterite in the system $MgO - Al_2O_3 - SiO_2$:
A) true porosity (%), B) content of melt (%).

It follows from the curves in Fig. 4 that sintering of mixtures in the system N – M – S increases considerably with increase of the amount of melt from 5 to 15%, and to a smaller extent with increase of temperature.

We found that the mixtures giving the best sintering are those for which the point representing the composition of the melts lie within the primary crystallization field of forsterite. In the system M – A – S the point 1 for the melt composition was taken in the 1500° isotherm at the boundary curve between the primary crystallization fields of forsterite and clinoenstatite, and the point 2 – within the primary crystallization field of forsterite, and the point 3 – at the boundary curve between the primary crystallization fields of forsterite and periclase in the same system. The mixtures formed 15% of melt during firing. It was found that samples containing a melt of the composition corresponding to point 1 had 27.4% porosity, those corresponding to point 2, 19.6%, and those corresponding to point 3, 23.9% (Fig. 5). Similar relationships were found for other systems.

At 1600° the sintering of mixtures worsens from left to right in the series M – A – S → M_2S – S – CAS_2 → M – S. With regard to the sintering rate, which is already considerable at 1400°, the system N – M – S could be placed before the system M – A – S.

The degree of sintering of the solid phase and its tendency to recrystallization are closely associated with the structure of the melt present in the mixture. They increase with increase of the amount of the cybotactical regions forming in the melt, corresponding to the crystal lattice of the sintering solid phase [17, 18].

The better sintering of mixtures in the systems M – A – S, M_2S – S – CAS_2 in comparison with mixtures in the system M – S is the consequence of the more favorable melt structures in the former two systems. Melts of mixtures in these two systems contain many more cybotactical regions corresponding to the forsterite crystal lattice. For example, at 1600° the selected melts of the systems M – A – S and M_2S – S – CAS_2 contained 38.2 and 37.7% of forsterite respectively (by calculation), and the O: Si ratios in them were 3.51 and 3.48, i.e., close to 4, which corresponds to forsterite.

In presence of Mg^{2+}, Al^{3+} cations have a coordination number of 6 [19], and do not enter the silicon – oxygen complexes. In the system M – S, on the other hand, the melt contains only 9% forsterite and its O: Si ratio is only 3.

Increase of the O: Si atomic ratio in the melt to approximate to 4 creates conditions in which the concentration and formation of individual SiO_4^{4-} tetrahedrons and Mg^{2+} cations (not surrounded by free O^{2-}) necessary for formation of the forsterite lattice are greatest.

In the systems M – A – S and M_2S – S – CAS_2 at 1500° the melt viscosity was 13.6 and 18.5 poises respectively, i.e., considerably lower than in the system M – S (35.7 poises). The formation of individual SiO_4^{4-} groups in the melt, important for sintering and building of the forsterite lattice, lowered the melt viscosity, and this in turn favored diffusion and accelerated sintering.

As SiO_2 is replaced by Al_2O_3, the oxygen – silicon complexes in the melt are broken down and the melt viscosity falls [20]. The bonds between O^{2-} and Al^{3+} ions are less stable than between O^{2-} and Si^{4+}; the oxygen

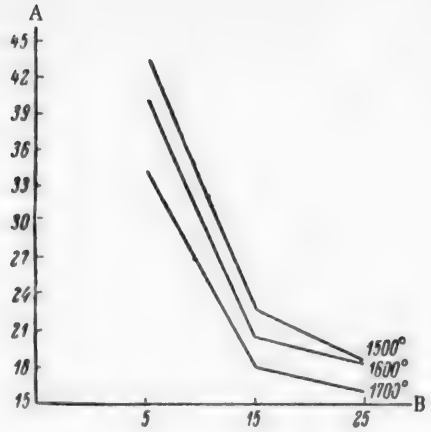

Fig. 3. Sintering of forsterite in the system $2MgO \cdot SiO_2 - SiO_2 - C_2O \cdot Al_2O_3 \cdot 2SiO_2$:
A) true porosity (%), B) content of melt (%).

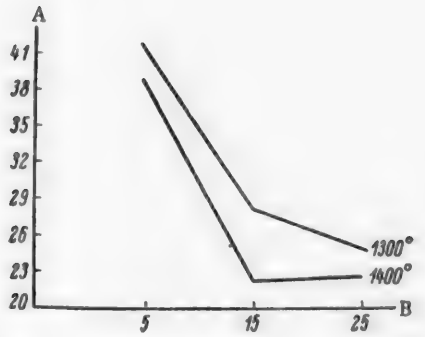

Fig. 4. Sintering of forsterite in the system $Na_2O - MgO - SiO_2$:
A) true porosity (%), B) content of melt (%).

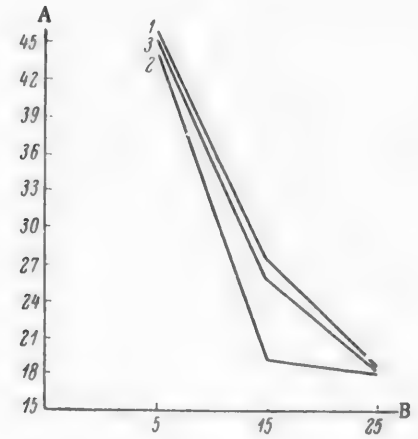

Fig. 5. Sintering of forsterite in the system $MgO - Al_2O_3 - SiO_2$ in relation to the position of the point for the melt composition:
A) true porosity (%), B) content of melt (%); the numbers of the curves correspond to the points for melt composition.

anions, in passing to Si^{4+}, break down the complexes of the latter. This is also favored by the fact that in presence of Mg^{2+} and Ca^{2+} aluminum acquires sixfold coordination completely or partially. The complex silicon – oxygen groups present before this in the surface layer of the melt pass into the depth of the melt when broken down because of the increase of their generalizing moment, and the surface tension of the melt at its air interface increases as a result. If the surface tension at the forsterite – melt boundary decreases in the process (which may be assumed to be the case if the contact angles are similar), this should be unfavorable for recrystallization of forsterite through the melt. At the same time, the high surface tension at the melt – air interface should result in a decrease in the size of pores with a liquid coating.

In the system N – M – S the melt viscosity at 1400° is considerably higher (56.4 poises) than in the system M – – S at 1500° (35.7 poises). The surface tension at the melt – – air boundary is considerably lower in the former system than in the M – S system; however, sintering is rapid at 1400°, differing little from sintering in the systems M – – A – S and M_2S – S – CAS_2 even at 1600°. There is no doubt that in this case also the structure of the melt has a favorable effect on recrystallization and sintering, despite the high melt viscosity in the system N – M – S. The low surface tension at the melt – air boundary, determined by the melt structure, should have little effect in decreasing pore size. At the same time (if the wettability is the same) the surface tension at the solid – melt boundary should increase, thus favoring recrystallization.

According to Esin [21, 22] in presence of Na^{1+} cations (these are weak cations, as their charge – radius ratio is low) $Si_xO_y^{z-}$ ions are grouped around them with formation of SiO_4^{4-} ions from the weakly-bound oxygen surrounding the Na^{1+} ions. This creates favorable conditions for the formation of cybotactical groups corresponding to the forsterite lattice, and therefore for sintering.

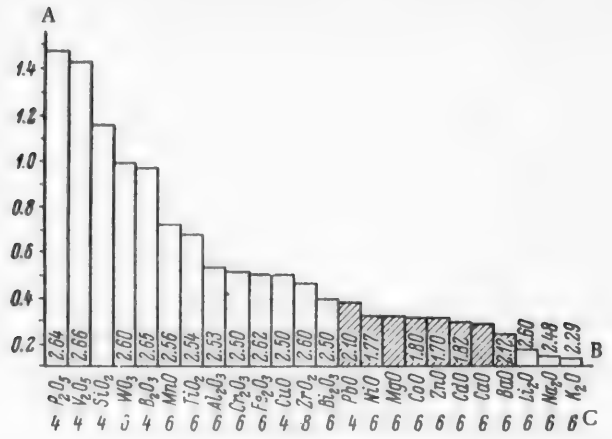

Fig. 6. Energy of interaction ($\frac{E}{e^2}$) between oxygen and cations added to mixtures in the system $MgO - SiO_2$, and their influence on the sintering of forsterite:
A) interaction energy of cation and oxygen, B) bulk density (g/cc), C) possible coordination number of the cation; shaded columns represent additives which either improve slightly, or worsen, the sintering of mixtures in the system $MgO - SiO_2$.

The surface tension of the melt in alkaline systems is decreased because MgO in melts of the M – S system is partially replaced by sodium oxide with displacement of Na^{1+} into the surface layer of the melt. The influence of Na^{1+} on the melt structure and sintering of forsterite is also great because in melts of this system the (calculated) concentration of forsterite at 1400°, as indicated by the MgO content, is the highest – 45.3%. An interesting fact is that sintering in this system cannot be retarded by the relatively low ratio of O: Si = 2.93.

The effects of additives on the sintering of forsterite were studied with mixtures the melt-composition points of which were within the primary-crystallization field of forsterite; in the M – S system at 1600 and 1700°, in the M – A – S system at 1500°, in the $M_2S - S - CAS_2$ system at 1500°, and in the N – M – S system at 1300°. The action of some additives was tested at other temperatures.

In the system N – M – S sintering is not improved by additives. In the systems M – A – S and $M_2S - S - CAS_2$ additives significantly improve the sintering of mixtures which contain only small amounts of melt. In the system M – S most additives improved sintering, even in mixtures containing 15% of melt.

Additions of NiO, ZnO, and CoO either have little effect on sintering in the system M – S or worsen it. The greatest improvements of sintering in these systems were produced by additions of V_2O_5, B_2O_3, P_2O_5 and Li_2O. Thus, in the system M – S at 1600° samples containing 15% melt without additives had true porosity of 43.9%, and compressive strength 288 kg/cm^2.

On addition of V_2O_5 the porosity decreased to 17.3%, on addition of B_2O_3, it decreased to 17.9%, with P_2O_5 to 18.3%, and with Li_2O to 19.3% (the compressive strength was 1300 – 1800 kg/cm^2). On the other hand, addition of ZnO increased the porosity to 47.7%, and of NiO to 45.2%.

In the system M – A – S sintering is improved by considerably smaller amounts of additives (including V_2O_5, B_2O_3, P_2O_5 and Li_2O). Additives have a similar effect on sintering of mixtures in the system $M_2S - S - CAS_2$.

Thus, sintering is intensive in presence of additives which ensure either the greatest breakdown of the oxygen – silicon groups or the greatest removal of surrounding oxygen ions from around the Mg^{2+} cations and displacement of these cations toward the SiO_4^{4-} groups, which is necessary to build the forsterite lattice. The existence of these two ways for intensification of sintering is clear from an examination of our calculated values for

Sintering of Finely Ground Dunite and Talcomagnesite with Additives at 1500°

Material	Additive, 1% by weight	True porosity (%)
Talcomagnesite + 25% caustic magnesite	without additive	21.0
	P_2O_5	11.7
	B_2O_3	12.0
Dunite + 15% caustic magnesite	without additive	24.0
	P_2O_5	16.2
	B_2O_3	14.2

the electrostatic energy of interaction of oxygen with Mg^{2+}, Si^{4+} and cations of the additives [18] (Fig. 6). The interaction energies are referred to the possible coordination numbers of the cations.

In the system M — S the best sintering effects are produced by additives which have either much greater energy of interaction (V^{5+}, P^{5+}, B^{3+}) than Mg^{2+}, or much lower (Li^{1+}). V^{5+}, P^{5+}, B^{3+} cations, having a much greater energy of interaction with O^{2-} than Mg^{2+}, take oxygen from the latter and displace it toward the SiO_4^{4-} groups, thus favoring formation of the forsterite lattice.

The addition of Li_2O, which has a cation which interacts less actively than Mg^{2+} with oxygen, acts on complex oxygen — silicon groups with a small generalizing moment and breaks them down, giving up its available O^{2-}

In the systems M — A — S and M_2S — S — CAS_2 sintering is improved by additives which have a greater interaction energy with oxygen than the Al^{3+} cation (V^{5+}, P^{5+}, B^{3+}). The presence of Al^{3+} cations in the melt itself favors the formation of cybotactical regions in it, corresponding to the forsterite lattice, as their energy of bonding with oxygen is greater than that of Mg^{2+} but less than that of Si^{4+}. If cations with a greater bonding energy with oxygen than that of Al^{3+} are introduced, they take oxygen from Mg^{2+}, and even from Al^{3+} if there are not enough oxygen anions around the Mg^{2+}. In this process Mg^{2+}, being the weaker cation, is displaced toward the oxygen — silicon tetrahedrons.

In the system N — M — S the Na^{1+} cation is itself effective in favoring sintering and formation of cybotactical regions corresponding to the forsterite lattice in the melt, and additives do not improve sintering.

It is seen that additives which improve sintering lower the viscosity and surface tension of the melts. Thus, in the system M — S at 1600° the melt without additives had a viscosity of 21.2 poises, while with V_2O_5 the viscosity was 15.2, with P_2O_5 it was 16.4, with B_2O_3 it was 17.5, and with LiO_2 it was 19.6 poises. In the system M — A — S the melt viscosity without additives was 25.3 poises, while with P_2O_5, B_2O_3, and Li_2O it was 15.4, 17.2, and 17.1 poises respectively. Similar effects are produced in the systems M_2S — S — CAS_2 and N — M — S. However, despite this, sintering is not improved in the latter system.

The particularly effective sintering action of these additives can be attributed to a simultaneous improvement of the structure, and decreases of the viscosity and surface tension of the melts. The latter, if the wettability is similar, indicates an increase of the surface tension at the solid — liquid boundary and should therefore accelerate recrystallization of forsterite. It was found, in fact, that the forsterite crystals are considerably larger if any of these additives are used.

A check of the above results in sintering tests with ground native forsterite materials containing additives confirmed these conclusions (see table).

Articles made from the fired mixtures without additives had a true porosity of 23.7% (with talcomagnesite as the principal material) or 26% (with dunite).

Specimens made from mixtures containing 1% additives had true porosity of 10.5 — 11.4 (talcomagnesite) and 21.6 — 22.1% (dunite).

LITERATURE CITED

[1] W. M. Goldschmidt, British Patent 283,791.

[2] V. V. Arshinov, Mineral Raw Materials 2, 165 (1930).

[3] V. V. Arshinov, Mineral Raw Materials 3, 258 (1931).

[4] A. S. Bazilevich, Refractories 4, 385 (1935).

[5] A. S. Bazilevich, Refractories 6, 373 (1939).

[6] A. S. Bazilevich, Mineral Raw Materials 2, 27 (1935).

[7] N. V. Andreev, Mineral Raw Materials 8 – 9, 822 (1931).

[8] N. V. Andreev, Mineral Raw Materials 1, 33 (1931).

[9] A. S. Berezhnoi and M. A. Uralov, Collected Data on Problems of the Refractories Industry [in Russian] (ONTI, People's Commissariat of the Heavy Industry, 1937).

[10] A. S. Berezhnoi, Proc. 1st Conference on Refractories [in Russian] (Moscow, Izd. AN SSSR, 1940) p. 84.

[11] A. S. Berezhnoi, Coll. Trans. Ukrainian Sci. Res. Inst. Refractories [in Russian] (Khar'kov, Metallurgy Press, 1941) 56, p. 87.

[12] A. S. Berezhnoi, Refractories 4, 147 (1955).

[13] V. M. Tsynkina, Refractories 12, 1682 (1938).

[14] V. M. Tsynkina, Trans. Ukrainian Sci. Res. Inst. Refractories [in Russian] (Khar'kov, Metallurgy Press, 1938) 54, p. 78.

[15] P. S. Mamykin, V. V. Samarov, and P. N. D'yachkov, Proc. 2nd Conference on Refractories [in Russian] (Moscow, Izd. AN SSSR, 1941) p. 85.

[16] A. A. Appen, J. Appl. Chem. 24, No. 9, 907 (1951).*

[17] A. A. Appen, J. Phys. Chem. 16, No. 8, 1132 (1952).

[18] G. V. Kukolev and E. N. Leve, J. Appl. Chem. 28, No. 8, 807 (1955).*

[19] G. V. Kukolev and I. A. Kryzhanovskaya, J. Appl. Chem. 29, No. 10, 1502 (1956).*

[20] O. A. Esin, Bull. Acad. Sci. USSR, Div. Chem. Sci. 6, 561 (1948).

[21] O. A. Esin, J. Phys. Chem. 21, No. 4, 479 (1947).

[22] O. A. Esin, J. Phys. Chem. 22, No. 5, 617 (1948).

Received May 20, 1957

* Original Russian pagination. See C. B. Translation.

THERMODYNAMIC STUDY OF SOLID-PHASE REACTION IN THE SYSTEM CALCIUM OXIDE – ALUMINA

V. I. Babushkin and O. P. Mchedlov-Petrosyan

The system calcium oxide – alumina plays an important role in burning processes during the production of various types of cements: hydraulic lime, Portland cement, and aluminous cement. Therefore many workers have studied the kinetics of solid-phase reactions in this system [1 – 6].

The system $CaO - Al_2O_3$ was originally found to contain four compounds: $3CaO \cdot Al_2O_3$, $5CaO \cdot 3Al_2O_3$, $CaO \cdot Al_2O_3$ and $3CaO \cdot 5Al_2O_3$ [7]. Later it was established that the compound $5CaO \cdot 3Al_2O_3$ has the true composition of $12CaO \cdot 7Al_2O_3$ [5, 8], while the compound $3CaO \cdot 5Al_2O_3$ must be actually $CaO \cdot 2Al_2O_3$ [9]. Finally, it was suggested that the compound $3CaO \cdot 16Al_2O_3$ [10] may exist, but later this was shown to be $CaO \cdot 6Al_2O_3$ [11].

The aim of the present investigation was to determine the thermodynamic conditions for the occurrence of possible reactions, and to correlate these conditions with the above-mentioned studies of the kinetics of calcium aluminate formation in this system.

Thermodynamic studies of the systems $MgO - SiO_2$, $CaO - SiO_2$ and $Al_2O_3 - SiO_2$ [12] showed that if reliable initial thermodynamic data are available this method can provide a fundamental explanation of the kinetics of the series of solid-phase reactions under consideration, revealing the sequence in which the compounds are formed and explaining the reasons for the discrepancies between the experimental results of different workers.

TABLE 1

Thermodynamic Data on Certain Compounds

Compounds	ΔH_{298} (cal/mole)	ΔZ_{298} (cal/mole)	ΔH_{trans} (cal/mole)	T_{trans} (°K)
CaO	— 151790	— 144400	—	—
γ-Al_2O_3	— 391340	— 368390	7750	>1200
α-Al_2O_3	— 399090	— 376770	—	—
$CaO \cdot Al_2O_3$	— 554800	— 526800	—	—
$12CaO \cdot 7Al_2O_3$	—4617000	—4365720	—	—
$3CaO \cdot Al_2O_3$	— 850000	— 809100	—	—

It was noted [13] that an urgent task in relation to cement technology is to carry out an investigation of this type for the system $CaO - Al_2O_3$. With the publication of new experimental data the solution of this problem has become more reliable [14, 15], but because of the absence of thermal data on high-alumina compounds these could not be considered in the calculations.

Our starting data are presented in Table 1, which has been compiled from a number of sources [14, 16 – 18].

TABLE 2

Results of Thermodynamic Calculations for Certain Reactions

Reaction	ΔH_{298}	ΔZ_{298}	ΔZ_{1000}	ΔZ_{1200}	ΔZ_{1400}	ΔZ_{1600}	ΔZ_{1700}	ΔZ_{1800}
1	—11670	— 14010	— 21550	— 23940	— 13260	— 14600	—	— 15950
2	—56140	— 54190	— 62200	— 65020	+ 25250	+ 30300	+33010	—
3	— 3290	— 7510	— 19760	— 23600	— 14530	— 17530	—	— 20520
4	—31720	— 34520	— 45460	— 49260	— 25790	— 26930	—	— 27900
5	—83900	—113930	—200600	—226670	—209760	—243000	—	—275050
6	—42980	— 24150	+ 16330	+ 27170	+ 47970	— 51690	—	+ 53910
7	+33110	+ 1620	— 76800	—100650	—126680	+151770	—	—180990
8	+25550	+ 43880	+ 90320	+104580	+119220	+134190	—	+149360
9	+ 8380	+ 6500	+ 2030	+ 850	— 410	+ 1540	—	— 3780
10	+ 9200	+ 55260	+170880	+204860	+242620	+279790	—	+319670

We now consider the following reactions with the aid of the data in Table 1.

$$CaO + Al_2O_3 \rightarrow CaO \cdot Al_2O_3,$$
$$12CaO + 7Al_2O_3 \rightarrow 12CaO \cdot 7Al_2O_3, \quad (1)$$
$$3CaO + Al_2O_3 \rightarrow 3CaO \cdot Al_2O_3,$$

$$3CaO \cdot Al_2O_3 + 2Al_2O_3 \rightarrow 3(CaO \cdot Al_2O_3),$$
$$12CaO \cdot 7Al_2O_3 + 5Al_2O_3 \rightarrow 12(CaO \cdot Al_2O_3),$$
$$4(3CaO \cdot Al_2O_3) + 3Al_2O_3 \rightarrow 12CaO \cdot 7Al_2O_3,$$
$$12CaO \cdot 7Al_2O_3 + 9CaO \rightarrow 7(3CaO \cdot Al_2O_3),$$
$$7(CaO \cdot Al_2O_3) + 5CaO \rightarrow 12CaO \cdot 7Al_2O_3,$$
$$CaO \cdot Al_2O_3 + 2CaO \rightarrow 3CaO \cdot Al_2O_3,$$
$$5(3CaO \cdot Al_2O_3) + 9(CaO \cdot Al_2O_3) \rightarrow 2(12CaO \cdot 7Al_2O_3).$$

The calculated results for these reactions are given to an accuracy of 10 calories (Table 2).

Variations of ΔZ with temperature were determined by means of the formula

$$\Delta Z = \Delta H_0 - \Delta\Gamma_0 \cdot T \ln T - \frac{1}{2}\Delta\Gamma_1 \cdot T^2 - \frac{1}{2}\Delta\Gamma_2 \cdot T^{-1} + y \cdot T,$$

the coefficients in which are found from the equation for the heat capacity of the system as a function of temperature:

$$\Delta C_p = \Delta\Gamma_0 + \Delta\Gamma_1 \cdot T + \Delta\Gamma_2 \cdot T^{-2},$$

while ΔH_0 is found from the equation for ΔH as a function of T and a known value of ΔH_{298}:

$$\Delta H_0 = \Delta H_{298} - \Delta\Gamma_0 \cdot T - \frac{1}{2}\Delta\Gamma_1 \cdot T^2 + \Delta\Gamma_2 \cdot T^{-1}.$$

For determination of variation of heat capacity of the reaction components with increase of temperature we used equations which give errors of 2 – 5% in the 1000 – 1700° K range. The results are given below:

Substance	Heat capacity
CaO	$c_p = 11.67 + 1.08 \cdot 10^{-3}T - 1.56 \cdot 10^5 T^{-2}$,
γ-Al_2O_3	$c_p = 16.37 + 11.1 \cdot 10^{-3}T$,
α-Al_2O_3	$c_p = 27.43 + 3.06 \cdot 10^{-3}T - 8.47 \cdot 10^5 T^{-2}$,
$CaO \cdot Al_2O_3$	$c_p = 34.62 + 6.75 \cdot 10^{-3}T - 0.76 \cdot 10^5 T^{-2}$,
$12CaO \cdot 7Al_2O_3$	$c_p = 291.32 + 50.3 \cdot 10^{-3}T - 5.25 \cdot 10^5 T^{-2}$,
$3CaO \cdot Al_2O_3$	$c_p = 52.34 + 15.8 \cdot 10^{-3}T + 0.55 \cdot 10^5 T^{-2}$.

The first and third equations are taken from the summary by K. Kelley [19], while all the others were obtained by calculations of heat capacities from entropy data [20].

The data were used to derive equations for Reactions (1 – 10), the first three being independent; the heat of transition of γ-Al_2O_3 to α-Al_2O_3 at temperatures above 1200° K was taken into account in the calculations.*

Reaction (1)

$$\Delta Z = -13120 - 6.58T \cdot \ln T + 2.71 \cdot 10^{-3}T^2 - 0.4 \cdot 10^5T^{-1} + 34.4T \text{ — to } 1200^\circ \text{ K};$$
$$\Delta Z = +409 + 4.48T \cdot \ln T - 1.3 \cdot 10^{-3}T^2 - 4.63 \cdot 10^5T^{-1} - 40.1T \text{ — to fusion.}$$

Reaction (2)

$$\Delta Z = -60760 - 36.73T \ln T + 20.17 \cdot 10^{-3}T^2 - 6.72 \cdot 10^5T^{-1} + 232T \text{ —to } 1200^\circ \text{ K};$$
$$\Delta Z = +33950 + 40.69T \cdot \ln T - 7.96 \cdot 10^{-3}T^2 - 36.37 \cdot 10^5T^{-1} - 288T \text{ —to fusion.}$$

Reaction (3)

$$\Delta Z = -1890 - 0.96T \ln T - 0.73 \cdot 10^{-3}T^2 - 2.61 \cdot 10^5T^{-1} - 10.25T \text{ — to } 1200^\circ \text{ K};$$
$$\Delta Z = +11660 + 10.1T \ln T - 4.74 \cdot 10^{-3}T^2 - 6.85 \cdot 10^5T^{-1} - 84.8T \text{ —to fusion.}$$

Reaction (4)

$$\Delta Z = -37470 - 18.78T \ln T + 8.87 \cdot 10^{-3}T^2 + 1.41 \cdot 10^5T^{-1} + 112.5T \text{ — to } 1200^\circ \text{ K};$$
$$\Delta Z = -10410 - 3.34T \ln T + 0.83 \cdot 10^{-3}T^2 + 7.05 \cdot 10^5T^{-1} - 36T \text{ — to fusion.}$$

Reaction (5)

$$\Delta Z = -96700 - 42.47T \ln T + 12.47 \cdot 10^{-3}T^2 + 1.93 \cdot 10^5T^{-1} + 176.5T \text{ — to } 1200^\circ \text{ K};$$
$$\Delta Z = -36790 - 13.03T \ln T - 7.7 \cdot 10^{-3}T^2 + 19.24 \cdot 10^5T^{-1} - 20.2T \text{ —to fusion.}$$

Reaction (6)

$$\Delta Z = -53140 - 32.86T \ln T + 23.1 \cdot 10^{-3}T^2 + 3.72 \cdot 10^5T^{-1} + 273T \text{ to } 1200^\circ \text{ K};$$
$$\Delta Z = -15140 + 0.33T \ln T - 17.4 \cdot 10^{-3}T^2 + 8.98 \cdot 10^5T^{-1} + 67.5T - \text{ to fusion.}$$

Reaction (7)

$$\Delta Z = +47650 + 29.97T \ln T - 25.29 \cdot 10^{-3}T^2 - 11.57 \cdot 10^5T^{-1} - 305T \text{ — to fusion.}$$

Reaction (8)

$$\Delta Z = +31080 + 9.37T \ln T - 1.17 \cdot 10^{-3}T^2 - 3.93 \cdot 10^5T^{-1} - 6.34T \text{ —to fusion.}$$

Reaction (9)

$$\Delta Z = +11290 + 5.84T \ln T - 3.44 \cdot 10^{-3}T^2 - 2.21 \cdot 10^5T^{-1} - 45.9T \text{ — to fusion.}$$

Reaction (10)

$$\Delta Z = +5990 - 9.36T \ln T - 19.57 \cdot 10^{-3}T^2 + 3.2 \cdot 10^5T^{-1} + 209T.$$

The results of the calculations are summarized in the diagram.

Examination of the data in Table 2 and the diagram shows that the primary reaction product of the oxides must be $12CaO \cdot 7Al_2O_3$ [Reaction (2)], but this is immediately converted, with a large change of free energy, into $CaO \cdot Al_2O_3$ or $3CaO \cdot Al_2O_3$, depending on which is present in excess — Al_2O_3 or CaO [Reactions (5) and (7)].

In the range of the alumina γ-α transition (900°) the free energy of Reaction (2) decreases sharply, and the formation of $CaO \cdot Al_2O_3$ by Reaction (4) also becomes possible.

Whereas in presence of excess Al_2O_3, $CaO \cdot Al_2O_3$ is formed readily both from $12CaO \cdot 7Al_2O_3$ [Reaction (5)] and from $3CaO \cdot Al_2O_3$ [Reaction (4)], by saturation with alumina, according to the observations of Belyankin et al. [6] in presence of excess lime saturation to compounds richer in calcium oxide proceeds only by way of $12CaO \cdot 7Al_2O_3$ [Reaction (7)] and not by absorption of lime by monocalcium aluminate [Reaction (9)].

* Analogous calculations performed by Coughlin [14] are of no practical interest, as the starting data were for α-Al_2O_3 and CaO, whereas we are concerned with more active forms of alumina for most types of aluminous materials (bauxites, kaolin).

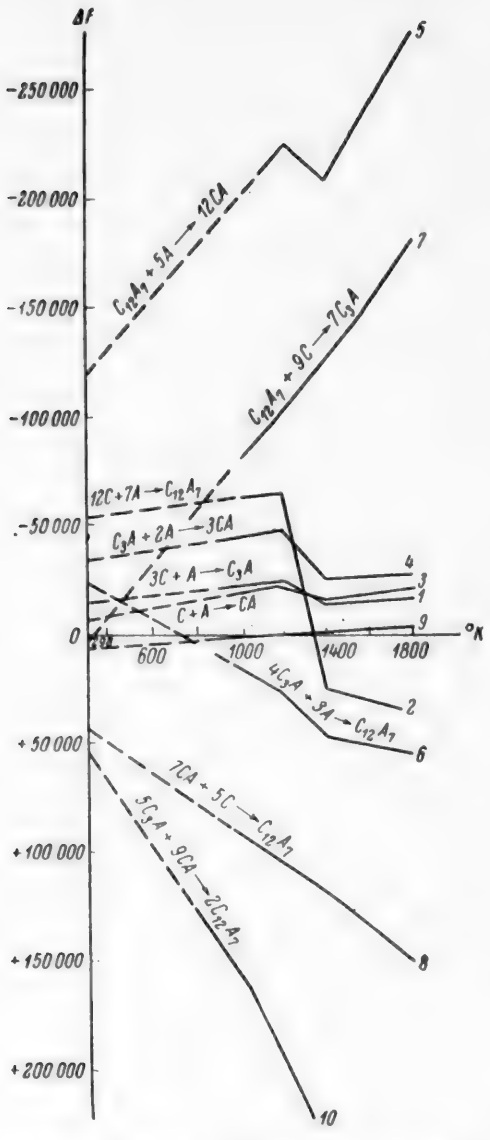

Free energy change $\Delta F = f(T)$ in reactions (F in cal/mole) in the system $CaO - Al_2O_3$ as a function of temperature.

The complete decomposition of $3CaO \cdot Al_2O_3$ in presence of 0.5% of calcium fluoride into $12CaO \cdot 7Al_2O_3$ and CaO [5, 21, 22] may be attributed to the fact that this additive makes the compound $12CaO \cdot 7Al_2O_3$ stable.

The known fact that $12CaO \cdot 7Al_2O_3$ does not decompose on fusion does not contradict the results of these calculations, as the calculations are based on the assumption of the γ-$Al_2O_3 \rightarrow \alpha$-$Al_2O_3$ transition at 900°. If 1200° is regarded as the limit of the $\gamma \rightarrow \alpha$ transition, then $12CaO \cdot 7Al_2O_3$ must become unstable only near the fusion point.

Attention must also be drawn here to the need for correcting the erroneous statements [23] found in the technical literature on the burning of Portland cement clinker, according to which the formation of $CaO \cdot Al_2O_3$ is followed by saturation with lime to yield aluminates with higher lime contents. Even if such saturation does take place, it occurs only owing to the presence of mineralizers such as iron oxides, etc., in the raw mix [23].*

SUMMARY

Thermodynamic calculations were used to provide a quantitative interpretation of the sequence in which different compounds are formed in solid-phase reactions involving lime in the system $CaO - Al_2O_3$; equations are given for calculation of the free energies for ten possible reactions in the system $CaO - Al_2O_3$; a scheme of aluminate formation is presented, and attention is drawn to some erroneous points in the theory of the burning of Portland cement.

LITERATURE CITED

[1] W. Dyckerhoff, Dissertation, Frankfurt a. M. (1925).

[2] Sh. Nagai and R. Naito, J. Soc. Chem. Ind. Japan (Suppl.), 33, 4, 133 (1930).

[3] F. N. Strokov, V. A. Musyakov, and P. D. Katsenelenbogen, Trans. State Inst. Appl. Chem. 32, 15 (1940).

[4] V. F. Zhuravlev, I. G. Lesokhin, and R. G. Tempel'man, J. Appl. Chem. 21, No. 9, 887 (1948).

[5] H. Kühl. Zement-Chemie, 2, Berlin, 76 (1952)

[6] D. S. Belyankin, N. A. Toropov, and N. A. Dyuko, Coll. Trans. All-Union Sci. Res. Inst. Cement 18 (1937).

[7] E. S. Shepherd, G. Rankin and F. E. Wright, Am. J. Sci., series 4, 28, 293 (1909).

[8] W. Büssem and W. Eitel, Z. Krist., 95, 175 (1936).

* At the end of 1957 G. M. Matveev published a paper entitled "Thermodynamic analysis of solid-phase reactions in the system $CaO - Al_2O_3$" [24]. Unfortunately, certain new experimental data [14, 15] are not taken into account in that paper, and therefore not all of the author's conclusions are in agreement with ours.

[9] B. Tavasci, La Chem. e. L'Industria 17, 461 (1935).

[10] K. Lagerquist, S. Walmark and A. Westgren, Z. anorg. allg. Ch. 234, 1, 1 (1937).

[11] N. E. Filonenko, Proc. Acad. Sci. USSR 48, No. 6, 456 (1945).

[12] O. P. Mchedlov-Petrosyan et al., J. Phys. Chem. 24, No. 11, 1299, 1755 (1950); J. Appl. Chem. 25, No. 2, 216 (1952).*

[13] O. P. Mchedlov-Petrosyan, in the collection: Physicochemical Principles of Ceramics [in Russian] (Moscow, Industrial Construction Press, 1956) p. 499.

[14] J. P. Coughlin, J. Am. Chem. Soc. 78, 5479 (1956).

[15] P. T. Carter and T. G. Macfarlane, J. Iron and Steel Inst., 185, 1, 54 (1957).

[16] F. D. Rossini et al., Selected values of Chemical Thermodynamic Properties Nat. Bur. Stand., Circ., Washington, 500 (1953).

[17] E. J. Huber and C. E. Holley, J.Phys. Chem., 60, 498 (1956).

[18] M. Kh. Karapetyants, Chemical Thermodynamics [in Russian] (Moscow, Goskhimizdat, 1953) p. 557.

[19] K. K. Kelley, Bull. Bureau of Mines, 476 (1949).

[20] N. A. Landiya, J. Phys. Chem. 25, 927 (1951).

[21] W. Eitel, Zement, 30, 31, 127; 2, 17; 3, 29 (1941).

[22] V. I. Satarin, Bull. Tech. Inf. Southern State Inst. Planning and Research Cement Ind. 20 – 21, 3 (1956).

[23] V. N. Yung, Principles of Cement Technology [in Russian] (Moscow, Industrial Construction Press, 1951) pp. 220, 235.

[24] G. M. Matveev, Coll. Trans. Chem. Technol. Silicates [in Russian] (Industrial Construction Press, 1957) p. 94.

Received May 22, 1957

* Original Russian pagination. See C. B. Translation.

PRODUCTION OF WATER-RESISTANT SAND – SILICATE FILTRATION EQUIPMENT

M. A. Matveev and V. P. Dyatlova

Sand – silicate filtration equipment (plates, disks, pipes, etc.) are now being used in various branches of industry. They are used for pneumatic conveying of powders and dustlike materials, for pulp aeration, for air purification, for filtration of suspensions, etc. Such porous products, in the form of pipes and gutters, could be widely used for drainage of soils and building sites.

Sand – silicate filters are made from sand cemented by water glass (of 3 : 1 ratio). The articles are made by molding of the filter and binder. When hardened and dried, they are fired at 950°. A small amount of sodium fluosilicate (3 – 4%) is added to the water glass. This accelerates hardening and facilitates drying of the articles. If fluosilicate is added, the water glass does not swell when dehydrated during firing [1].

Our investigation [2] showed that sodium fluosilicate is almost completely dissociated during the firing of sand – silicate articles: $Na_2SiF_6 \rightarrow SiF_4 + 2NaF$. Sodium fluoride remains in the binder, while SiF_4 is volatilized.

Sodium fluosilicate has no advantages over sodium fluoride for articles made by the firing process. Moreover, silicon tetrafluoride is highly toxic. Sodium fluoride, on the other hand, is virtually nonvolatile up to 1000° (its vapor pressure at 1130° is 0.001 atmos). Therefore sodium fluosilicate may be replaced by sodium fluoride in fired articles.

Sodium fluoride added to the mix coagulates the alkali silicate solution, and the silicic acid liberated in the process firmly cements the sand grains together. Moisture is easier to remove from such coagulated solutions, and the articles do not swell during firing. Sodium fluoride lowers the viscosity of the melt and thus assists its uniform distribution in the form of fine films over the filler grains.

An important defect of silicate products cemented by alkali silicate with added sodium fluosilicate or fluoride is their low water resistance. The binder in such products is almost completely dissolved when they come in contact with water, and they gradually disintegrate.

It is known that the solubility of alkali silicates falls sharply on addition of alumina [3]. However, the introduction of aluminum into the silicate binder, for example by addition of alumina, is impracticable, as very high temperatures are required. Alumina does not dissolve to any appreciable extent in a high-ratio alkali silicate even at 1300°. At such temperatures the viscosity of sodium aluminate is low, so that the aluminate readily flows out of the porous articles which remain without binder. To overcome these difficulties, we have devised a new method for the production of water-resistant binder, by addition of aluminum fluoride, which is a substitute both for sodium fluoride and for alumina, to sodium silicate.

Addition of aluminum fluoride at the initial stages of the process assists hardening of the binder, and makes it possible to prepare the pressed articles for firing without complications. It was found by x-ray investigations of the binder that at this stage of the process aluminum fluoride acts as a coagulant and itself remains unchanged. During the subsequent firing it reacts chemically to form sodium fluoride and an aluminosilicate glass.

$$2AlF_3 + Na_2O \text{ (in sodium silicate)} \rightarrow 6NaF + Al_2O_3 \text{ (in glass)}.$$

Results of Experiments on the Water Resistance of the Binder

Amount of AlF_3 added (%)	Weight loss of powdered binder (%) when boiled in water during time (hours):					Amount of Na_2O (%) dissolved out of the powdered binder when boiled for (hours):				
	1	2	3	4	5	1	2	3	4	5
0	85.2	—	—	—	—	21.2	—	—	—	—
5	2.45	5.00	7.79	10.2	12.6	0.95	1.96	2.85	—	—
10	1.20	2.02	3.20	4.2	5.1	0.10	0.19	0.28	0.37	0.46
15	0.58	0.80	0.96	1.10	1.25	0.065	0.095	0.117	0.135	0.15
20	0.38	0.51	0.60	0.68	0.76	0.04	0.057	0.07	0.08	0.09
25	0.50	0.71	0.88	1.00	1.14	0.034	0.054	0.06	0.07	0.071

The heat ΔH of this reaction is 400 kcal per mole of Al_2O_3 [4]. Because of this chemical reaction the aluminosilicate glass is formed at a relatively low temperature (not above 900°).

The aluminosilicate binder formed by this method has considerably higher water resistance. The water resistance was estimated from the loss in weight of the powdered binder when boiled in water for 1 — 5 hours. The results of the tests are given in the table.

The solubility of the silicate binder is at a minimum with addition of 20% Al_2F_3. Whereas the weight loss of the alkali silicate is 85.2%, in presence of 20% AlF_3 it is 0.38%. Thus, the water resistance of the binder is increased more than 200-fold in this case.

It is clear from the data in the table that although the total weight loss of the binders is decreased sharply by addition of aluminum fluoride, the loss nevertheless is in excess of that due to dissolution of alkali. To determine the composition of the dissolved compounds, we analyzed the solutions obtained after the powders had been boiled for 3 hours. The filtrate contained sodium fluoride and silicate in addition to alkali. Their concentrations decrease with increasing amount of added aluminum fluoride. The results of these determinations are plotted in Fig. 1.

The solubility of the silicate binder is decreased considerably in presence of 5 — 10% of aluminum fluoride. However, as for binders without aluminum, the solution rate remains constant. This means that these binders are also soluble in water, although the solution rate is lower. With higher contents of aluminum fluoride the solubility changes sharply in character. The solution rate no longer remains constant, but decreases rapidly with time. The curves in Fig. 2 are parabolas (they are linear if the square of the weight loss is plotted against time). These results lead to the conclusion that binders with higher aluminum contents are virtually insoluble in water.

The optimum addition of aluminum fluoride to the binder is 15 — 20%, and the total amount of binder relative to the filler does not exceed 12%. Therefore, for the production of water-resistant sand — silicate filters it is recommended to add 2 — 2.5% of AlF_3 on the weight of the dry mixture.

The recommended optimum molding pressure in the production of sand — silicate filters is 200 kg/cm^2. Such products must be fired at 900° with an exposure time of 3 hours, the total cycle being 8 — 10 hours. Under such conditions the sand — silicate articles acquire good mechanical strength (ultimate compressive strength 370 — 400 kg/cm^2) and high porosity (45%).

A comparative x-ray and microscopic investigation of binders of different compositions was carried out. The x-ray patterns of binders made from mixtures of water glass and sodium fluosilicate and fired at 950° show only lines characteristic of sodium fluoride. Their intensity increases with the amount of fluosilicate added. Under the microscope sodium fluoride is seen in the form of branched dendrites which permeate the entire binder (Fig. 3). Thermographic investigation of the system $Na_2O \cdot 3SiO_2$ — NaF showed that the fusion curves have minima corresponding to a eutectic at the temperature 680± 10°, containing 25± 5% NaF (Fig. 4).

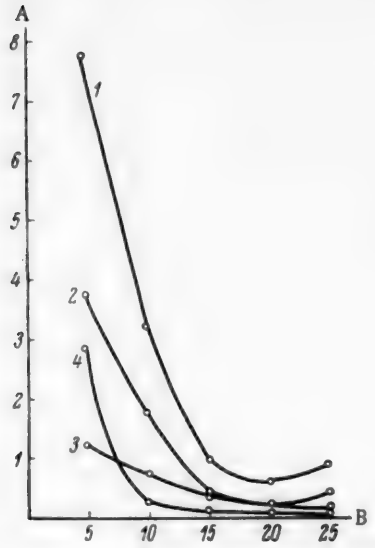

Fig. 1. Effects of the amount of aluminum fluoride added to water glass on the contents of Na_2O, SiO_2, and NaF in solution and on the weight loss:
A) weight loss (%), B) AlF_3 content (%); curves: 1) total weight loss, 2) SiO_2, 3) NaF, 4) Na_2O.

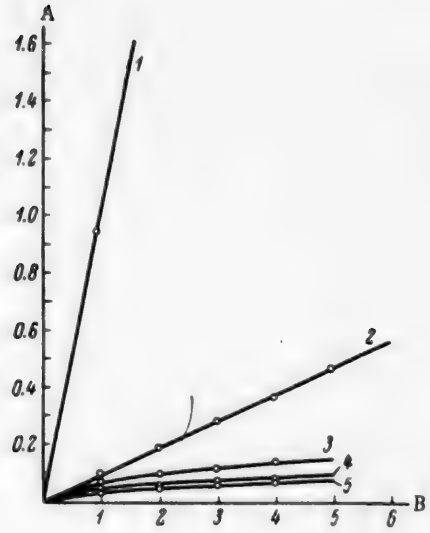

Fig. 2. Effect of boiling time on weight loss:
A) loss of Na_2O (%), B) time (hours), AlF_3 contents (%): 1) 5, 2) 10, 3) 15, 4) 20, 5) 25.

Fig. 3. Microphotograph of binder 20×17.

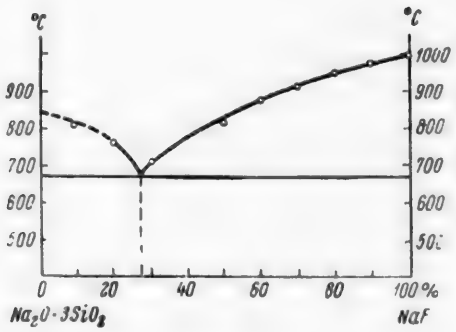

Fig. 4. Phase diagram for the system in the section NaF — $Na_2O \cdot 3SiO_2$.

It is clear from these results that when this binder crystallizes from a melt it forms a mixture of two water-soluble substances (sodium fluoride and sodium silicate). This accounts for the poor water resistance of sand—silicate filters made with water glass and sodium fluosilicate by the firing method.

When the binder is made under similar conditions from sodium silicate with added aluminum fluoride, the sodium fluoride lines on the x-ray pattern are weaker. The sodium fluoride concentration, determined from the intensities of the lines in the x-ray patterns, decreases with increase of the amount of aluminum fluoride

added, although its total content increases. This result shows that a considerable part of the sodium fluoride is retained in the structure of the glass and does not form an independent phase. No lines characteristic of aluminum fluoride or other crystalline phases were found in the x-ray patterns.

The water resistance of filters with aluminosilicate binder was compared with the water resistance of similar specimens made under the same conditions with a binder of alkali silicate with added sodium fluosilicate. Filters made with the aluminosilicate binder did not change in mechanical strength when boiled in water for 12 hours. Filters made with alkali silicate and fluosilicate binder were destroyed completely when boiled for the same time.

DISCUSSION OF RESULTS

The solubility of aluminosilicate binders is selective in character. This is because alkali silicate and alumina form a glass. When it comes in contact with water, protective films of silica and alumina form on its surface and hinder leaching of sodium compounds. This explanation is consistent with Grebenshchikov's theory of the nature of the chemical resistance of glasses [5].

The increase in the water resistance of silicate binders by additions of aluminum fluoride can be explained as follows. In aluminosilicate glasses aluminum replaces silicon isomorphously in the vertices of the silicon – oxygen tetrahedrons. It then has coordination number 4. Since the valence of aluminum is 3, and that of silicon 4, uncompensated oxygen valences with an effective negative charge arise in the structure of the aluminosilicate glass [6, 7]. Therefore replacement of some of the silicon by aluminum is accompanied by strengthened bonding of positive ions (Na^+, K^+, or Ca^{++}) in the structure of the aluminosilicate glass as the result of purely electrostatic forces. The structural bonding of the cations in aluminosilicate glass is the cause of its increased water resistance. This is primarily reflected in a sharp decrease of the alkali solubility (Fig. 1). The solubility of sodium fluoride also decreases, because in this case the cations are bound in the glass structure. Therefore, despite increasing NaF concentration, the content of free fluoride decreases with increase of the amount of AlF_3 added. Microscope studies confirm this result.

SUMMARY

1. The low water resistance of sand – silicate filters made by the firing process from sand cemented by water glass with added sodium fluosilicate is the consequence of the solubility of the binder. The binder is a mixture of sodium silicate and fluoride.

2. A mixture of sodium silicate (3 : 1 ratio) and 15 – 20% of aluminum fluoride is recommended for the production of sand – silicate filters. In this case firing results in the formation of aluminosilicate glass, which firmly cements the grains of sand or other filters.

3. Thus new binder has considerable water resistance. The water-soluble sodium compounds (Na_2O and NaF) present in it are firmly held in the structure of the aluminosilicate glass in order to balance the negative charges which arise when a part of the 4-valent silicon is replaced by 3-valent aluminum in the silicon – oxygen tetrahedrons of sodium silicate.

4. Chemical interaction between alkali silicate and aluminum fluoride yields aluminosilicate glasses at moderate temperatures directly, during single diring of filtration equipment.

5. The high quality of the new binder is confirmed by the results of structural and microscopic investigations and by water stability and mechanical strength tests on sand – silicate filters.

LITERATURE CITED

[1] K. A. Smirnova, Trans. Sci. Res. Inst. Construction Ceramics 3, 93 (1950).

[2] M. A. Matveev and V. P. Dyatlova, J. Phys. Chem. 28, No. 10, 1713 (1954).

[3] I. I. Kitaigorodskii and L. S. Lande, Influence of Chemical Composition on Certain Physicochemical Properties of Glass [in Russian] (1934).

[4] E. V. Britske, and A. F. Kapustinskii, et al. Thermal Constants of Inorganic Substances [in Russian] (Izd. AN SSSR, 1949).

[5] I. V. Grebenshchikov, Bull. Acad. Sci. USSR, Div. Chem. Sci. 1, 3 (1937).

[6] V. V. Sobolev, Introduction to Silicate Mineralogy [in Russian] (L'vov State Univ. Press, 1949).

[7] N. V. Belov, Proc. 4th Conference on Experimental Mineralogy and Petrography, 2 [in Russian] (Izd. AN SSSR, 1953) p. 133.

Received June 8, 1956

PREPARATION OF THE HIGHEST CARBIDE OF CHROMIUM

T. Ya. Kosolapova and G. V. Samsonov

Chromium carbide of the formula Cr_3C_2 is a solid infusible compound, superior to almost all other carbides in oxidation resistance. It is therefore used for the preparation of cemented carbide alloys with special properties – heat-resisting, chemically stable, cutting and surfacing alloys.

The formation of the carbide Cr_3C_2 was first observed by Moissan on reduction of chromium oxide in an arc furnace; the carbide contained 86.72% Cr and 13.21% C [1].

Conditions for the formation of Cr_3C_2 in the fusion of chromium with carbon were studied by Ruff and Foehr [2]. In these experiments, when chromium was melted in a carbon crucible at 2000°, a carbide containing 13.7 – 14.2% C was formed in 15 minutes. A carbide of similar composition was formed in a study of the chromium – carbon system [3 – 6]; in addition to Cr_3C_2, the lower carbides Cr_7C_3 and $Cr_{23}C_6$ were also found.

Cr_3C_2 is made under industrial conditions by the reduction of chromic oxide by carbon:

$$3Cr_2O_3 + 13C = 2Cr_3C_2 + 9CO,$$

the process is effected in a charge of the stoichiometric composition at 1600° in a tubular graphite furnace in a hydrogen atmosphere [1].

However, the production of pure Cr_3C_2 without admixtures of free carbon and lower carbides is difficult by this process; this prompted the present study of the conditions for the production of Cr_3C_2.

EXPERIMENTAL

Our study of the conditions for the production of Cr_3C_2 was based on the above reaction of reduction of chromic oxide by carbon taken in the excess necessary for the formation of carbide after removal of oxygen.

To determine the effects of excess and deficiency of carbon in the charge on the formation of carbide, charges containing 23.08, 25.38, 26.33 and 29.67% C were used (the calculated theoretical carbon content is 25.5%).

The charges were moistened with dextrin solution, dried, and molded into briquets 20 × 20 mm.

In the first series of experiments, briquets of the stoichiometric composition were heated in graphite boats placed in a resistance furnace with a graphite tube, in a hydrogen atmosphere, at temperatures from 900 to 1800° (in 100° steps), with exposures of 1 hour at each temperature.

The weight loss of the briquets was determined, and the extent of reaction was estimated from the ratio of the weight of the products formed to the calculated theoretical weight of carbide.

In addition, the reaction products were chemically analyzed for total chromium, total carbon, and free carbon, and the particle size of the carbide formed was determined microscopically.

The total chromium content was determined by the persulfate – silver method [7] after fusion of 0.1 g of the product with sodium peroxide in a nickel crucible.

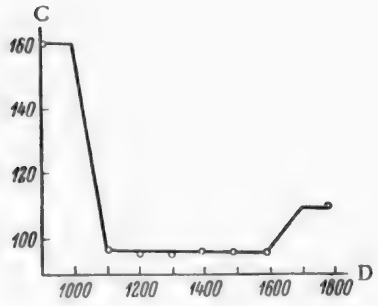

Fig. 1. Completeness of the reaction of chromium carbide formation:
C) yield ($\frac{A}{B} \cdot 100\%$), D) temperature (°C).

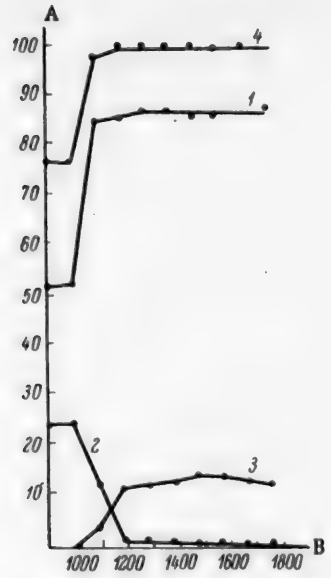

Fig. 2. Effects of temperature on Cr_{total} (1), C_{free} (2), C_{bound} (3), and the sum of Cr_{total} + C_{total} (4):
A) contents (%), B) temperature (°C).

The total carbon was determined by the volumetric absorption method after combustion of a weighed sample in a furnace of the Mars type in a current of oxygen at 1300° with cupric oxide as a flux [7, 8].

Free carbon was determined by the volumetric absorption method after combustion in a Mars furnace in a current of oxygen at 600°. Chromium carbide is not oxidized appreciably at this temperature.

The results of this series of experiments are summarized in Table 1 and plotted in Figs. 1 and 2.

Table 1 also contains data on the amount of residue insoluble in hydrochloric acid.

It is sometimes believed that when chromium carbide is heated with 1:1 hydrochloric acid the lower carbides are dissolved, while Cr_2C_3 remains as an insoluble residue.

We do not agree with the view that Cr_3C_2 is completely insoluble in HCl.

However, as a first approximation, the amount of insoluble residue may be taken as a measure of the amount of the highest chromium carbide present.

It follows from these results that the degree of reduction increases sharply to the calculated value at 1100° and then remains virtually constant to 1600°; the sum of Cr_{total} + C_{total} also becomes 100% from 1200°, and then remains constant within the temperature range studied.

The content of bound carbon approaches the calculated value (13.33%) at 1400°, remains constant to 1600°, and then falls regularly at 1700 and 1800°.

The content of the insoluble residue is also greatest at 1400 – 1600°. It should be noted that the content of free carbon falls to 0.10 – 0.16% in this temperature range.

It is interesting to note that above 1600° the degree of reduction calculated for Cr_3C_2 changes (the ratio $\frac{A}{B} \cdot 100\%$ in Fig. 1 increases), the contents of total carbon and insoluble residue decrease, while the free carbon content increases. The average size of the carbide particles decreases at the same time.

TABLE 1

Results of Experiments on the Preparation of Chromium Carbide (stoichiometric mixture, exposure time 1 hour)

Expt. No.	Temperature (°C)	Weight of briquet (g)		Loss of briquet weight (%)	Calculated weight of carbide (g) (B)	A/B	Chemical composition (%)						Average size of carbide particles (μ)
		before heating	after heating (A)				Cr_{total}	C_{total}	C_{free}	C_{bound}	sum of $Cr+C_{total}$	insoluble residue	
1	900	9.8033	9.5120	2.97	5.7839	1.64	52.10	24.82	24.78	—	76.92	—	—
2	1000	9.8100	9.4840	3.32	5.7879	1.63	52.23	24.80	24.71	—	77.03	—	—
3	1100	9.6807	5.6287	42.9	5.7116	0.98	85.35	12.53	9.06	3.80	97.88	69.0	—
4	1200	9.3208	5.2930	43.2	5.4993	0.96	86.54	12.59	0.63	11.72	99.13	74.0	0.66
5	1300	9.8929	5.6255	43.1	5.8368	0.96	87.64	12.74	0.63	12.19	100.38	89.1	1.15
6	1400	9.8660	5.6289	42.9	5.8174	0.97	87.24	13.30	0.16	13.16	100.54	97.5	7.09
7	1500	9.9407	5.6687	43.0	5.8650	0.97	87.00	13.48	0.16	13.34	100.48	98.6	6.94
8	1600	9.5397	5.4084	43.3	5.6284	0.96	86.79	13.32	0.10	13.22	100.11	98.7	7.53
9	1700	14.9835	9.8585	34.2	8.8403	1.11	87.46	12.91	0.18	12.75	100.37	86.5	6.56
10	1800	9.8110	6.5441	33.4	5.7885	1.12	87.71	12.31	0.25	12.09	100.02	76.0	5.41

• The free carbon content is related to the carbide phase, i.e., $C_{bound} = \frac{C_{total} - C_{free}}{100 - C_{free}} 100\%$.

This effect may be explained on the assumption that at temperatures above 1600° the lower carbides — Cr_7C_3 and $Cr_{23}C_6$ — are formed together with Cr_3C_2. These carbides are formed as small segregations from the Cr_3C_2 grains, leading to subdivision of the carbide particles.

When Cr_3C_2 molecules recombine in presence of hydrogen in the furnace, part of the carbon is released in the free state and forms hydrocarbons which are swept out of the furnace by the hydrogen stream.

This liberation of carbon is not of an equilibrium but of a purely kinetic character.

The principal admixture in the carbide Cr_3C_2 at temperatures above 1600°, according to the phase diagram [1], is the carbide Cr_7C_3.

The presence of an admixture of the carbide Cr_7C_3 in the reaction products obtained at temperatures above 1600° can be confirmed by the following calculation. For example, at 1800° a product weighing 6.5441 g was obtained (Table 1); according to analytical data, it contained 5.7398 g Cr and 0.8043 g C. If it is assumed that the carbide Cr_3C_2 was the insoluble residue (76.0%), it follows that 4.9735 g of it was present in the product, including 0.0164 g of free carbon. This leaves 6.5441 − 5.9735 = 1.5706 g for the lower carbides, inclusive of 1.4443 g of chromium and 0.1263 g of carbon. This corresponds to 8.10% C in the carbide, which is in satisfactory agreement with the C_{bound} content of the carbide Cr_7C_3 (9.01% by calculation), and differs sharply from the C contents in Cr_3C_2 (13.3%) and $Cr_{23}C_6$ (5.68%).

Thus, the optimum temperature for the production of the carbide Cr_3C_2 from a stoichiometric mixture is 1400 − 1500° (the optimum temperature of 1600° recommended in the literature [1] is technologically dangerous, as active formation of the carbide Cr_7C_3 begins immediately beyond this temperature).

For more precise determination of the exposure time at the optimum temperatures, and of the time required to raise the temperature to 1500 and 1600°, experiments

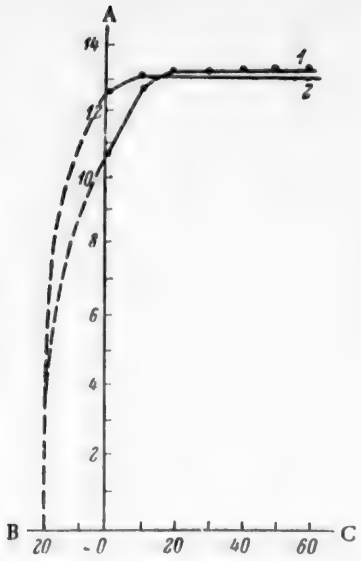

Fig. 3. Effect of heating time on the bound carbon content; carbon content of mixture 25.38%, temperature raised for 20 minutes:
A) C_{bound} (%), B) heating-up time (minutes), C) heating time (minutes); temperature (°C): 1) 1500, 2) 1600.

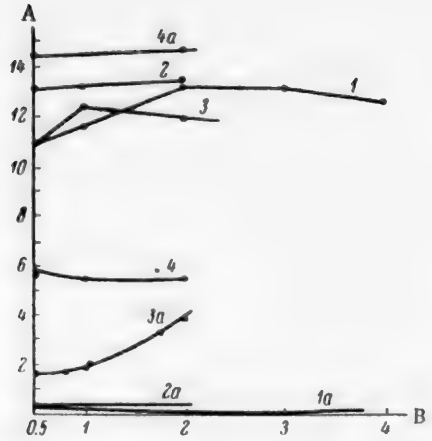

Fig. 4. Variations of the C_{bound} and C_{free} contents with the heating time and carbon content of mixture (temperature 1550°):
A) carbon content (%), B) time (hours); Contents of C_{bound} and C_{free} respectively for mixtures containing C (%):
1 and 1a) 23.08; 2 and 2a) 25.38;
3 and 3a) 26.33; 4 and 4a) 29.67.

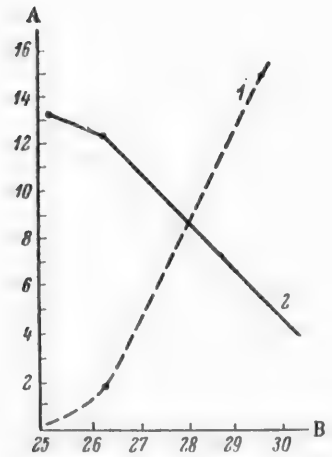

Fig. 5. Effect of carbon content of the charge on the C_{free} (1) and C_{bound} (2) contents (temperature 1550°, exposure time 1 hour):
A) carbon contents (%), B) carbon in charge (%).

were performed in which the temperature was raised from 1000 to 1500 or 1600° over a period of 20 minutes, with exposure times of 0, 10, 20, 40 and 60 minutes at these temperatures.

According to the data in Fig. 3, an exposure time of 20 minutes is sufficient for the formation of the carbide with the calculated composition (13.33% C) at 1500°, while at 1600° 10 minutes is enough. The effects of a deficiency and an excess of carbon in the mixtures were studied at 1550°; the heating times at this temperature were 0.5, 1, and 2 hours, and for mixtures with a deficiency of carbon, also 3 and 4 hours.

The results are presented in Table 2 and in Figs. 4 and 5.

The contents of total and free carbon rise sharply, while the bound carbon content decreases, with increase of the carbon content of the charge. With 29.67% C in the charge, most of the carbon is in the free state. This may be attributed to decarbonization of carbide during carbon transfer (through the hydrocarbon medium in the tube furnace) from the particles of chromium carbide with a relatively high hydrocarbon pressure over them to the particles of excess carbon black, which in turn react continuously with hydrogen, with the hydrocarbons formed being carried out of the furnace.

TABLE 2

Carbon Contents of Carbides Formed from Mixtures with Excess and Deficiency of Carbon (temperature 1550°)

Carbon in carbides	C_{total} in charge (%)													
	23.08					25.38 (stoichiometric mixture)			26.33			29.67		
	time (hours)													
	0.5	1	2	3	4	0.5	1	2	0.5	1	2	0.5	1	2
C_{total}	11.18	11.90	13.29	13.19	12.56	13.53	13.67	13.66	12.57	14.30	16.31	19.68	19.36	19.72
C_{free}	0.17	0.09	0.07	0.09	0.04	0.36	0.31	0.35	1.65	1.96	3.94	14.66	14.69	14.87
C_{bound}	11.12	11.82	13.22	13.12	12.51	13.22	13.41	13.36	10.96	12.39	11.88	5.89	5.48	5.69

TABLE 3

Contents of C_{bound} and C_{free} for Different Heating-Up Times (exposure time 1 hour, charge with 24.7% C)

Time for heating up from 1000 to 1550° (min)	Carbon content (%)		
	C_{total}	C_{free}	C_{bound}
80	12.48	Traces	12.48
40	12.47	"	12.47
20	12.32	"	12.32

Thus, most of the carbon in this process is in the free state, and transfer of carbon from the carbide particles to the carbon black particles is probably accelerated by removal of carbon from the furnace in the form of hydrocarbons.

Such "equilibrium-kinetic" systems in the furnace tube are also characteristic of the production of other carbides (those of titanium, zirconium, tungsten, molybdenum, tantalum, and niobium), with some specific differences.

On decrease of the carbon content of the charge (23.08% as against the calculated 25.5%) the carbon content increases with increase of the exposure time up to 3 hours due to the carbon-containing atmosphere of the furnace, and then begins to decrease somewhat.

Variations of the heating-up time from 1000 to 1500° between 20 and 80 minutes have no effect on the carbon content of carbide formed from a charge with a carbon deficiency (Table 3).

Thus, for briquets 10 – 15 g in weight the optimum conditions for production of the highest carbide Cr_3C_2 are: temperature in the 1400 – 1600° range, heating-up time from 1000 to 1400 – 1600°, 20 minutes, exposure time at 1400 – 1600°, 30 minutes.

A larger batch of chromium carbide, 200 g in weight, made under these conditions with an exposure time of 1 hour had the following chemical composition (%): C_{total} 13.43, C_{free} 0.09, C_{bound} 13.36, insoluble residue 99.06.

Structure investigation by the x-ray method* with CuKα radiation in an RKD camera 57.3 in size (taken asymmetrically) showed that the reduction product contained the carbide Cr_3C_2 with lattice constants a = 11.44, b = 5.51, c = 2.79 A (according to published data [9]: a = 11.46, b = 5.52, c = 2.82 A).

The microhardness of Cr_3C_2 sintered by hot pressing was found to be 1314 ± 70 kg/mm²; this is also close to the published figure [10], according to which the microhardness of Cr_3C_2 is 1300 kg/mm².

SUMMARY

Conditions for the preparation of chromium carbide Cr_3C_2 as close as possible in composition to the calculated value, with minimum contents of lower carbides and free carbon, were studied and it was found that the optimum conditions for preparation of this chromium carbide are obtained if 10 – 15g briquets made from a

* The x-ray analysis was performed by V. P. Dzeganovskii.

charge of the calculated composition corresponding to the reaction $3Cr_2O_3 + 13C = 2Cr_3C_2 + 9CO$ are heated in hydrogen at 1400 – 1500° for 30 minutes, the heating-up time being 20 minutes; the corresponding exposure time for 200 – 300 g of charge is 1 hour.

Increase or decrease of the carbon content of the charge has an adverse effect on the chemical and phase composition of the carbide.

LITERATURE CITED

[1] G. V. Samsonov and Ya. S. Umanskii, Solid Compounds of Infusible Metals [in Russian] (Metallurgy Press, 1957).

[2] O. Ruff and T. Foehr, Z. anorg. allg. Ch., 104, 27 (1918).

[3] A. Westgren and G. Phragmen, Z. anorg. allg. Ch., 187, 401 (1930).

[4] E. Friemann and F. Sauerwald, Z. anorg. allg. Ch., 203, 64 (1932).

[5] M. Hansen, Structures of Binary Alloys 1 (1941) [Russian translation].

[6] H. Goldschmidt, J. Iron and Steel Inst., 160, 4, 345 (1948).

[7] W. F. Hillebrand, G. E. Lundell, H. A. Bright and J. I. Hoffman, Practical Manual of Inorganic Analysis (Goskhimizdat, 1957) [Russian translation].

[8] A. M. Dymov, Technical Analysis of Ores and Metals [in Russian] (Metallurgy Press, 1949).

[9] K. Hellström and A. Westgren, Svensk. Kem. Tids. 45, 141 (1933).

[10] R. Kieffer and F. Kölbl, Powd. Metall. Bull., 4, 4 (1949).

Received June 21, 1957

PRODUCTION OF POWDERED IRON FROM PYRITE CINDERS IN A FLUIDIZED BED*

I. G. Lesokhin

The Lensoviet Technological Institute, Leningrad

Pyrite cinders from sulfuric acid plants are an iron-rich material which also contains nonferrous metals. Before the cinders can be used for pig-iron production, they must be treated to extract nonferrous metals, as they contain copper and zinc in excess of the permitted amounts for pig iron. Moreover, their granulometric composition and sulfur content is such that cinders cannot be used directly in the blast-furnace process. It is therefore necessary not only to remove nonferrous metals but also to agglomerate the cinders in order to improve the physical properties and to remove sulfur.

However, pyrite cinders may be used not only for pig-iron production but also for production of iron powder, which is becoming increasingly important in technology. An example of the use of powdered iron is the conversion of oxidized copper ores by the Mostovich process [1]. Steel smelted from iron powder has good mechanical properties. With addition of only 10% of iron powder to the open-hearth furnace charge, the mechanical strength of steel is increased by 15 – 20% [2].

Iron powder can be made by reduction of iron oxides at moderate temperatures (700 – 1000°), followed by separation of the iron powder from gangue by means of a magnetic separator. The reduction may be effected by gaseous fuels, such as illuminating, producer, or natural gases, coke-oven gas, etc., or any solid fuel such as peat, charcoal, brown coal, anthracite, etc. Therefore, in contrast to the blast-furnace process, the use of coke or wood charcoal is not obligatory for solving the problem of reduction of pyrite cinders to metallic iron. The process can therefore be developed in different regions of the country.

It is known from the literature [3 – 14] that the rate and degree of reduction of iron from oxide ores depends on the following factors: nature of the original ore, particle size, temperature, time, composition of the reducing agent, and velocity of the gas stream. Many investigators have shown that native oxides ores can be reduced to metallic iron by various gaseous and solid reducing agents. All these investigations were performed with static material. There have been very few studies related to determinations of the optimum conditions for the reduction of pyrite cinders to metallic iron in general, and in a fluidized bed in particular.

The purpose of the present investigation was to study the reduction of iron from pyrite cinders by means of various gaseous and solid reducing agents. This investigation is of practical interest, as pyrite, mainly obtained by flotation, will remain the principal raw material for sulfuric acid production, and the amounts used will increase because of the development of nonferrous metallurgy.

This paper contains the results of a study of the reduction of iron from pyrite cinders in a fluidized bed by a gaseous reducing agent (illuminating gas).

EXPERIMENTAL

Pyrite cinders made by the roasting of flotation pyrite in the mechanical furnace of the Neva Chemical Works was used for the reduction. The sample was from the lowest shelf of the burner before the quenching stage.

* N. A. Shilova took part in the experimental work.

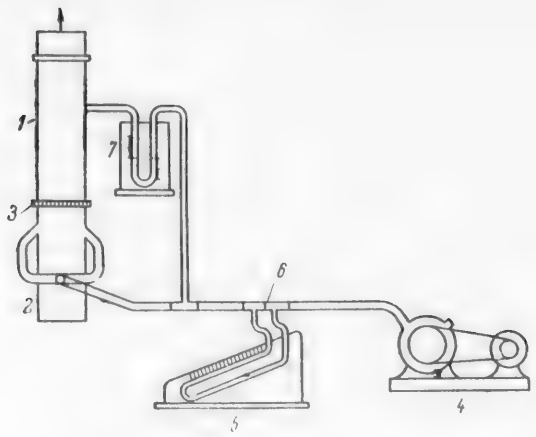

Fig. 1. Diagram of apparatus for determination of pressure drop (explanation in text).

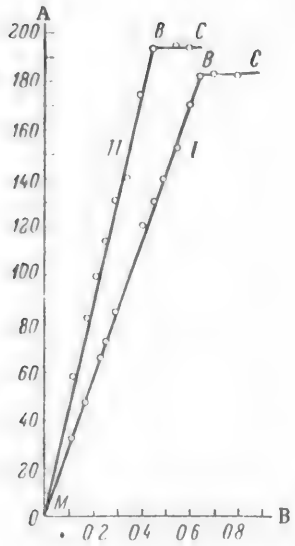

Fig. 2. Effect of air velocity on pressure drop:
A) static pressure drop (mm H_2O), B) air velocity (m/second); pyrites: I) d = 0.37 mm, H_0 = 100 mm; II) d = 0.75 mm, H_0 = 100 mm.

The cinders contained 44% iron, 3.18% total and 2.74% sulfide sulfur, 15.84% FeO, 42.25% Fe_2O_3, 33.73% gangue. The grain composition of the cinders is given below.

Grading, mesh size (mm)	+0.2	+0.12	+0.102	+0.088	+0.075	−0.060
Contents in sample (%)	35.15	41.65	4.8	14.66	0.54	4.2

The illuminating gas contained 2.8% CO_2, 12.0% CO, 45.7% H_2, 18.0% CH_4.

An important factor in studies of the reduction of pyrite cinders to metallic iron in a fluidized bed is determination of the velocity of the reducing gas at which the layer of solid material passes from the solid (filtering) state into the fluidized state. One of the most important elements in the control of this process is measurement of the pressure drop [14]. Changes of the pressure drop give an indication of the state and character of the formation of a suspended layer of solid particles. Experimental data on the pressure drop were obtained in a cold model shown in Fig. 1. Its main part is the glass column 1, 1000 mm high and 34 mm in diameter. The lower part 2 of the column contains a grid 3 on which the solid material was placed; air was fed under the grid from the blower 4. The air velocity was determined by means of the differential manometer 5 connected to the diaphragm 6. The static pressure drop was determined by means of the manometer 7. The experimental data on the pressure drop in the passage of air through the layer of granular material were used to plot the relationship between the pressure drop and air velocity (Fig. 2). The sloping portion of the graph corresponds to a static filtering layer, not yet expanded. The pressure drop increases over this region, and reaches a maximum at the point B. On further increase of the air velocity the pressure drop remains almost unchanged, and the line representing the pressure drop is parallel to the abscissa axis beyond the point B. In the region BC the solid particles are in the suspended state. Thus, the point B separates the stationary from the fluidized layer, and the gas velocity corresponding to this point is the critical velocity at which the layer of solid particles passes into the suspended state. This method for determination of the critical velocity was used throughout the study of the reduction of iron from cinders in a fluidized bed; the apparatus used is shown schematically in Fig. 3.

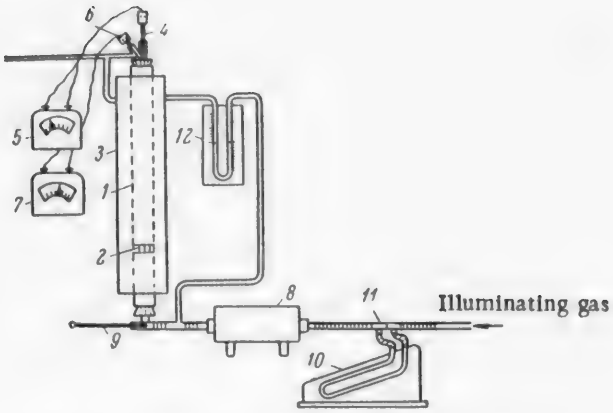

Fig. 3. Diagram of apparatus for reduction of iron from cinders in a fluidized bed (explanation in text).

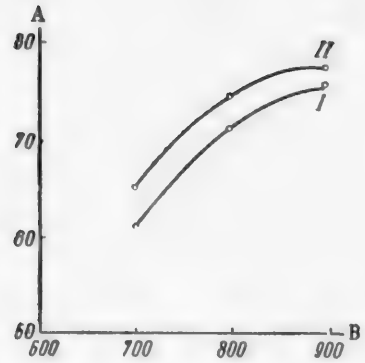

Fig. 4. Effect of temperature on the degree of reduction of iron by illuminating gas, with a reduction time of 60 minutes:
A) degree of reduction (%), B) temperature (°C) (explanation in text).

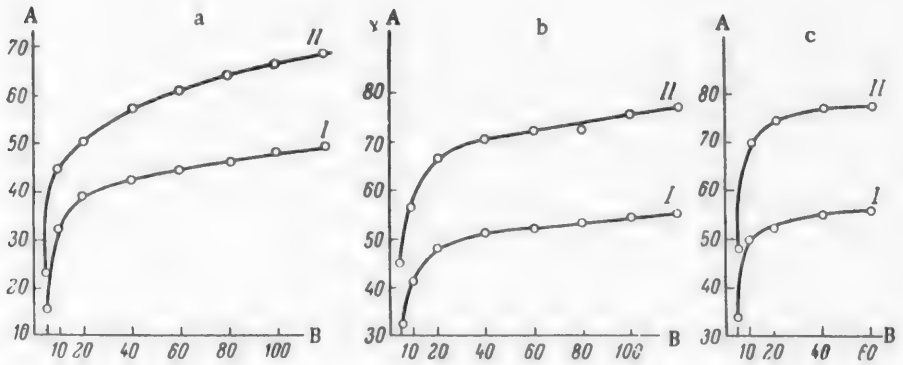

Fig. 5. Effect of time on the percentage content of iron (I) and the degree of reduction of iron (II) from cinders by illuminating gas:
A) degree of reduction and contents of metallic iron (%), B) time (minutes); temperature (°C): a) 700, b) 800, c) 900.

The principal part of the apparatus was the porcelain tube 1, 760 mm high and 28 mm in diameter. The porcelain tube was wound around with Nichrome wire for electrical heating. 25 cm from the lower end of the tube was the grid 2. The porcelain tube with its winding was inserted in the vertical furnace 3. The temperature inside the tube was measured by a thermocouple 4, the end of which was in the layer of suspended solid particles, and a galvanometer 5. The temperature of the gas leaving the furnace was measured by the thermocouple 6 and galvanometer 7. The illuminating gas was preheated in the furnace 8 before entry into the reaction vessel, and its temperature was measured by the thermometer 9. The amount of the reducing gas fed in for formation of the fluidized layer was found from the readings of the differential manometer 10 connected to the diaphragm 11, and from the pressure difference in the manometer 12. Before the start of an experiment the tube 1 was heated to the required temperature, and the weighed cinders were then fed into the tube from above.

It is clear from Fig. 4 that the degree of reduction increases with temperature at constant time (60 minutes) and gas velocity (0.0376 m/second). At 700° the degree of reduction reaches 61.5%, and at 800 and 900°, 72.0 and 76.0% respectively. These results were obtained for cinders containing 15.84% FeO and 45.25% Fe_2O_3 without preliminary removal of sulfide sulfur (Curve 1). The degree of reduction of iron from cinders at constant temper-

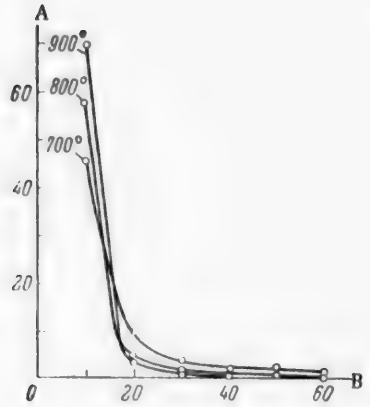

Fig. 6. Variation of the rate of reduction of iron from the cinders during the experiment:
A) degree of reduction in 10 minutes (%), B) time (minutes).

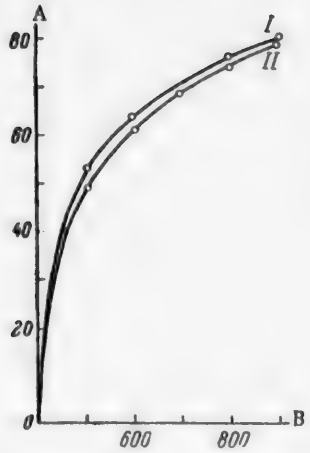

Fig. 7. Effect of temperature and the velocity of the illuminating gas on the degree of reduction of the cinders:
A) degree of reduction (%),
B) temperature (°C); gas velocity (m/second): I) 0.116, II) 0.158.

ature, time, and gas velocity depends on the chemical composition of the original cinder. Fig. 4 (Curve II) shows experimental data on the reduction of iron from cinders, after preliminary removal of sulfur by oxidation by atmospheric oxygen in a fluidized bed, containing 21.62% FeO and 43.85% Fe_2O_3. Under otherwise equal conditions, the degree of reduction increases somewhat after preliminary removal of sulfur from the cinders. Our curves do not differ in principle from published data [10] on the reduction of native iron oxide ores.

Experimental data on the influence of time on the course of reduction of cinders are presented in Fig. 5, and experimental data on variations of the reduction rate of iron from cinders during the experiments (degree of reduction in 10 minutes) at 700, 800, and 900° and at a constant velocity of the reducing gas are plotted in Fig. 6. The fall of reduction rate is due to the continuous decrease of the total reaction surface, and also to worsening conditions of diffusion toward this surface. As the reduction process develops, its rate usually falls because of the continuing decrease of the amount of unreduced iron oxides present, which is accompanied by an increase of the amount of reduced iron, which progressively blocks access to the particles of unreduced oxides [12]. As a result, conditions of contact between the reducing gas and unreduced iron oxides deteriorate, and diffusion conditions worsen. Moreover, when gaseous reducing agents are used at high temperatures there is some sintering and growth of particle size in the iron powder, and this also has an unfavorable effect on the reduction rate. To reduce these effects as much as possible it is necessary to minimize the reduction time, i.e., the cinders should not be reduced completely, as near the end the rate of reduction falls sharply.

The effects of gas velocity on the reduction rate of iron (under otherwise constant conditions) were studied with cinders containing 21.62% FeO and 43.85% Fe_2O_3 after removal of sulfide sulfur. It was found (Fig. 7) that with gas velocity 0.116 m/second, at temperatures of 700, 800, and 900° and reaction time 60 minutes the degree of reduction was 65.0, 74.6, and 77.5% respectively, and with gas velocity 0.158 m/second it was 70.5, 76.0, and 80.2% respectively.

The best conditions for the production of powdered iron from pyrite cinders can be determined from the above results. The process temperature primarily depends on the properties of the ore, and lies in the 850 — 900° range. The kinetic curves show that the best reaction time for the reduction of iron from cinders in a fluidized bed at these temperatures is 15 — 20 minutes. The degree of reduction under these conditions is 72 — 74%. Iron can be reduced from cinders by illuminating gas at a somewhat lower temperature, but the duration of the process must be increased. For example, to attain 72 — 74% reduction 60 — 80 minutes is required at 800°, and over 120 minutes at 700°.

SUMMARY

1. The reduction of iron from cinders in a fluidized bed was studied and it was found that the degree of reduction increases with temperature. At constant gas velocity (0.0376 m/second) and reaction time (60 minutes) the degree of reduction reaches 61.5% at 700°, whereas at 800 and 900° under the same constant conditions it is 72.0 and 76.0% respectively.

2. The degree of reduction of iron from cinders at constant temperature, time, and gas velocity depends on the chemical composition of the original cinders. The degree of reduction can be increased somewhat, under otherwise constant conditions, by preliminary removal of sulfur.

3. It is shown that with increase of the reducing gas velocity (under otherwise constant conditions) the degree of reduction increases. At gas velocity 0.11 m/second, and at temperatures of 700, 800, and 900° the degree of reduction of iron from the cinders is 65.0, 74.6, and 77.5% respectively, and at 0.158 m/second it is 70.5, 76.0, and 80.2% respectively.

LITERATURE CITED

[1] S. I. Mitrofanov, Conversion of Oxidized Copper Ores by the V. Ya. Mostovich Process [in Russian] (State Ferrous and Nonferrous Metallurgy Press, 1956).

[2] A. P. Egorov, A. I. Shereshevskii, and I. V. Shmanenkov, Course of Mineral Technology [in Russian] (Goskhimizdat, 1950).

[3] M. Borin, P. Emery, and M. Tambe, Reduction Roasting with Subsequent Concentration in Magnetic Separators of Low Field Intensity [Russian translation]. Min. of Nonferrous Metallurgy, No. 448.

[4] Prangé and Ziegler, Ref. Zhur. Khim. 1 (1956).

[5] I. A. Sokolov, Reduction of Iron Ores [in Russian] (ONTI, 1933).

[6] I. A. Sokolov, Raw Materials for the Blast-Furnace Process, 1 [in Russian] (ONTI, 1935).

[7] G. I. Chufarov and A. P. Lokhvitskaya, J. Phys. Chem. 5, 1103 (1934).

[8] V. S. Krym, Theory of Metallurgical Processes [in Russian] (ONTI, People's Commissariat of the Heavy Industry, 1936).

[9] Warren K. Lewis, Chem. Eng. 398 (1953) [Russian Translation].

[10] V. A. Vanyukov and A. V. Vanyukov, Nonferrous Metals 3 (1949).

[11] A. V. Vanyukov and G. F. Ivanov, Nonferrous Metals 4 (1949).

[12] A. P. Lyuban and V. G. Lapchinskii, Steel 12 (1952).

[13] S. I. Vol'fkovich, A. P. Egorov, V. N. Kuskov, and I. V. Shmanenkov, General Chemical Technology II [in Russian] (1946).

[14] G. Ya. Leizerovich, Roasting in a Fluidized Bed [in Russian] (Metallurgy Press, 1956).

Received March 20, 1957

PHASE DIAGRAM OF THE SYSTEM NaOH – Na_2CO_3 – NaCl

M. F. Lantratov and A. F. Alabyshev

The V. I. Ul'yanov (Lenin) Institute of Electrical Engineering, Leningrad

The phase diagram of the system NaOH – Na_2CO_3 – NaCl has not been investigated, although it is of practical importance in relation to the production of metallic sodium by electrolysis of fused caustic soda.

We have studied the temperatures of the start of crystallization for a number of compositions in the system NaOH – Na_2CO_3 – NaCl, rich in NaOH and containing up to 60 wt.% of sodium chloride or carbonate.

The visual polythermal method was used in the investigation. The temperature of the start of crystallization was determined by means of a Chromel – Alumel thermocouple to an accuracy of ±1°. The hot junction of the thermocouple, protected from the action of alkali by a thin silver cover, was immersed in the melt to a depth of 15 – 20 mm. The thermocouple was calibrated against a standard platinum/platinum – rhodium thermocouple and by the crystallization temperatures of tin, zinc, lead chloride, and potassium chloride. The start of crystallization was determined visually and from the cooling curves. The temperatures found by these two methods agreed within ±1°.

The vessel used was a silver crucible about 20 ml in capacity. 25 g of the components was put into the crucible. The thermocouple was used as stirrer. The cooling rate was less than 5° per minute. The crucible containing the salts was in a nitrogen atmosphere.

The components, of chemically pure grade, were dehydrated before use. The sodium carbonate was calcined at 800°. Sodium chloride was dried and fused. Caustic soda was dehydrated by heat in a silver crucible at 450 – 500° in an inert atmosphere for 1 – 5 hours. The sodium carbonate content of the melt was determined by titration of samples with hydrochloric acid solution. The original caustic soda contained from 0.3 to 2.2 wt.% Na_2CO_3. Caustic soda containing 0.3 wt% Na_2CO_3 was used in determinations of the crystallization temperatures of pure NaOH and of the NaOH – NaCl system.

The system NaOH – NaCl. The system NaOH – NaCl was studied in detail by Scarpa [1] and by Antropoff and Sommer [2]. Phase changes in this system were also studied later [3]. Lines for the start of crystallization, according to the data of these workers, are plotted in Fig. 1. The following values have been given for the melting point of caustic soda: 310° [1], 322° [2], and 327° [3]; the melting point of sodium chloride is given as 806° [1] and 798° [2]. According to Heves [4], the melting point of NaOH is 318.4° ± 0.2°, according to Neumann and Bergve [5] it is 300°, and according to Khitrov [6] it is 322°. Our value for the melting point of sodium hydroxide is 318.2 ± 1°.

The results of our determinations of the start of crystallization in the system NaOH – NaCl are given below and in Fig. 1 (Curve 3).

Crystallization Temperatures in the System NaOH – NaCl

NaCl content (wt.%)	0	10	20	30	40	50	60	100
Start of crystallization (°C)	318.2	332	331	355.5	431	518	585	804

Our results are in good agreement with Scarpa's data [1]. We did not detect a sharp break in the liquidus curve in the region of 40 wt.% of sodium chloride, which was reported by Antropoff and Sommer (Fig. 1, Curve 2).

Temperatures of the Start of Crystallization in the System $NaOH - Na_2CO_3 - NaCl$

Point No.	Contents (wt %)			Temperature of start of crystallization (°C)	Point No.	Contents (wt %)			Temperature of start of crystallization (°C)
	NaOH	Na_2CO_3	NaCl			NaOH	Na_2CO_3	NaCl	
1	99.7	0.3	—	318.2	18	70	20	10	327
2	89.7	0.3	10	322	19	60	20	20	355
3	87.7	2.3	10	320	20	40	20	40	498
4	79.7	0.3	20	331	21	70	30	—	370
5	77.7	2.3	20	328	22	60	30	10	379
6	69.7	0.3	30	356	23	40	30	30	445
7	59.7	0.3	40	431	24	60	40	—	433
8	49.7	0.3	50	518	25	40	40	20	490
9	39.7	0.3	60	585	26	40	60	—	559
10	—	—	100	804	27	90	5	5	306.6
11	90	10	—	303	28	80	5	15	311
12	80	10	10	305	29	80	15	5	291
13	70	10	20	321	30	70	15	15	312
14	60	10	30	376	31	55	20	25	357
15	40	10	50	569	32	60	15	25	348.5
16	83	17	—	293	33	78.2	15	6.8	282
17	80	20	—	307					

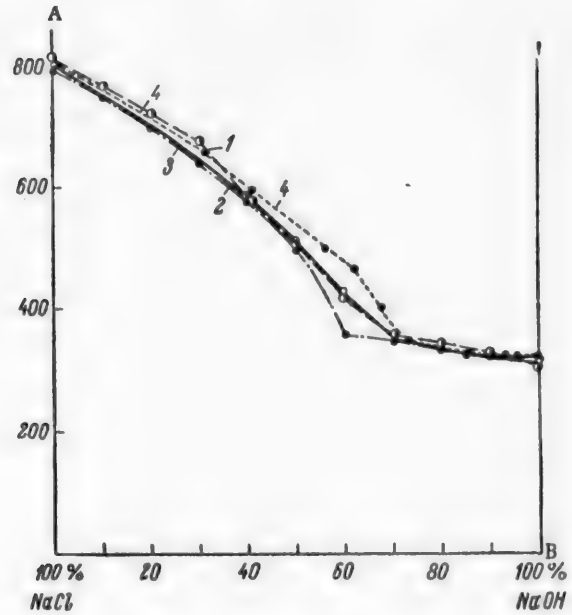

Fig. 1. Phase diagram for the system NaOH – NaCl: A) temperature (°C), B) composition (wt.% NaOH); data of: 1) Scarpa, 2) Antropoff and Sommer, 3) ourselves, 4) Ravich and Elenevskaya.

The system $NaCl - Na_2CO_3$. The system $NaCl - Na_2CO_3$ was studied by Amadori [7] and by several Soviet workers [8]. The system has a eutectic at 58.5 molar % (43.8 wt.%) NaCl, and starts to crystallize at 636° [7].

The system $NaOH - Na_2CO_3$. The binary system $NaOH - Na_2CO_3$ was first studied by Le Blanc and Carrier [9]. It was later studied in detail by Maksimenko [10], who used thermal analysis; he demonstrated the existence

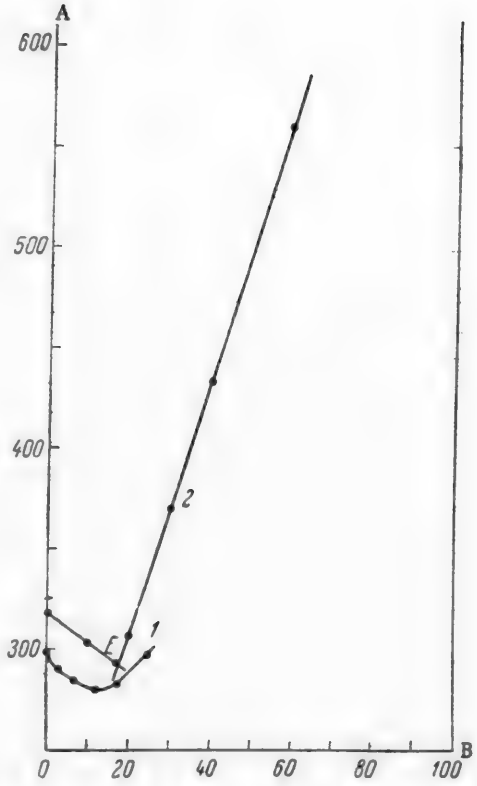

Fig. 2. Phase diagram for the system $NaOH - Na_2CO_3$:
A) temperature (°C), B) composition (wt.% Na_2CO_3); data: 1) Neumann and Bergve, 2) ours.

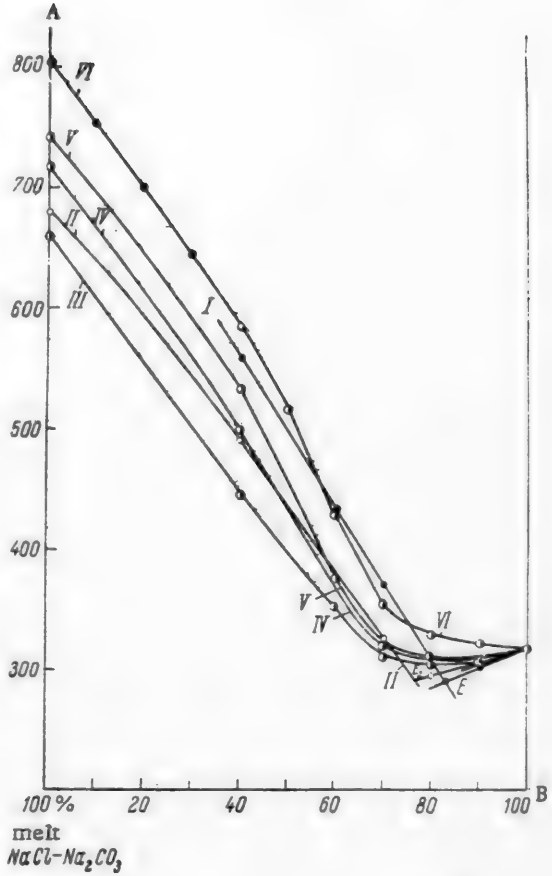

Fig. 3. Phase diagram for the system $NaOH - Na_2CO_3 - NaCl$:
A) temperature (°C), B) composition (wt.% NaOH); lines for Sections I – VI.

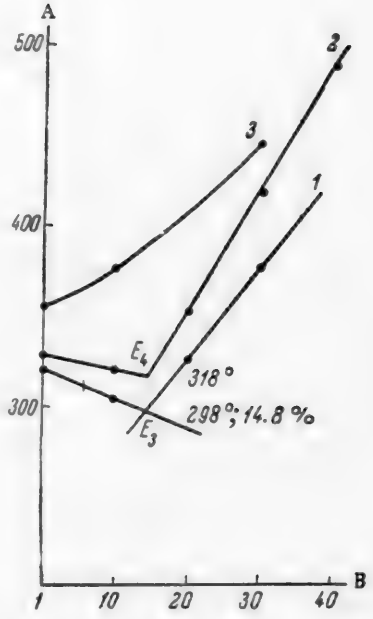

Fig. 4. Phase diagram for the system $NaOH - Na_2CO_3 - NaCl$:
A) temperature (°C), B) composition (wt.% Na_2CO_3); lines for Sections 1, 2, 3.

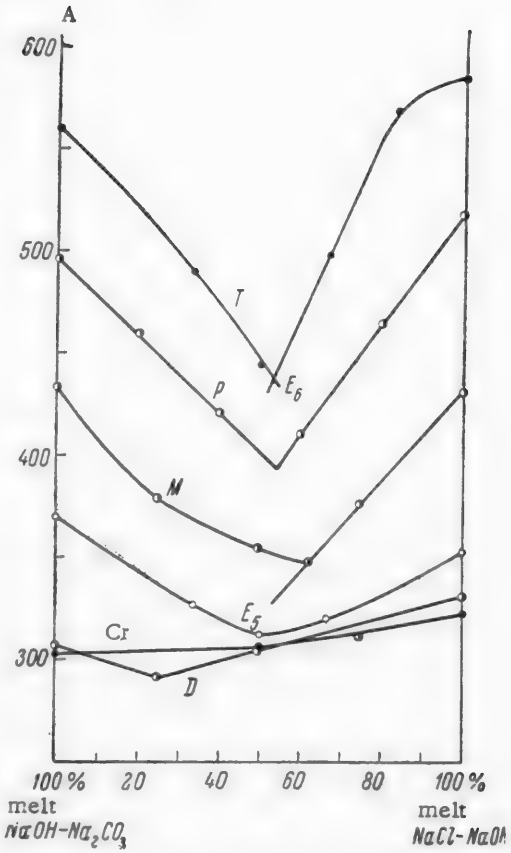

Fig. 5. Phase diagram for the system NaOH — Na_2CO_3 — NaCl:
A) temperature (°C); lines for Sections G, D, M, P, and T.

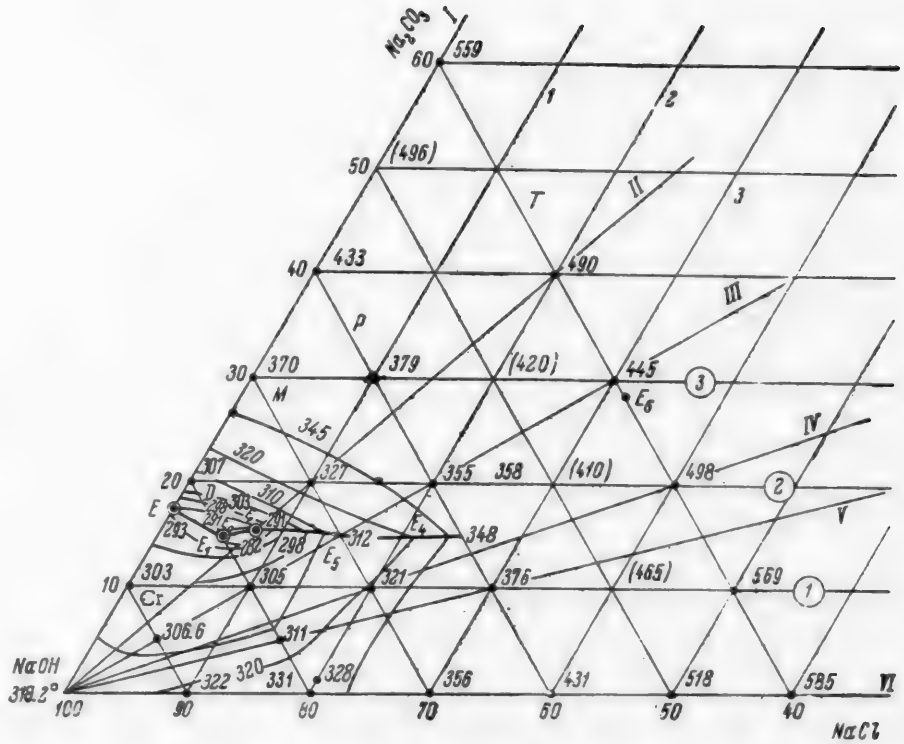

Fig. 6. Phase diagram for the system NaOH — Na_2CO_3 — NaCl.

of a eutectic at 300° and 11.6 wt.% Na_2CO_3. Neumann and Bergve [5] discovered the existence of solid solutions in the system, with a minimum at 280° and 17 wt.% Na_2CO_3. According to Amadori, the system forms a eutectic at 300° with 13 molar % carbonate. Finally, Khitrov [6] found that NaOH and Na_2CO_3 form a eutectic melting at 284°, with 11.5 molar % Na_2CO_3. The results of our determinations are given below and in Fig. 2, Curve 2 (Curve I represents Neumann and Bergve's data [5]).

Crystallization Temperatures in the System NaOH – Na_2CO_3

Na_2CO_3 content (wt.%)	0	10	17	20	30	40	60
Start of crystallization (°C)	318.2	303	293.5	307	370	433	559

We found a eutectic at 17.6 wt.% Na_2CO_3 and 291.8° (Fig. 2, point E).

The system NaOH – Na_2CO_3 – NaCl. The results of our determinations of the crystallization temperatures in the system NaOH – Na_2CO_3 – NaCl are given in the table and in Figs. 3 – 6.

Fig. 3 shows the crystallization curves along the Sections I – VI (Fig. 6). It is clear from Fig. 3 that Section II resembles Section I. The eutectic E_2 is found at 291° and 7.7 wt.% NaCl, 15.5 wt.% Na_2CO_3, and 76.8 wt.% NaOH. No eutectics are found on the lines for Sections III (wt.% ratio of Na_2CO_3 to NaCl = 1), IV, and V (wt.% ratio of Na_2CO_3 to NaCl = 3), and these are similar to Section VI, i.e., the system NaOH–NaCl.

Fig. 4 shows the curves for the start of crystallization along the lines of the three Sections 1 – 3 (Fig. 6), for constant sodium chloride contents of 10, 20, and 30 wt.% respectively. The eutectic point E_3 corresponds to 14.8 wt.% Na_2CO_3, 10 wt.% NaCl, and 75.2 wt.% NaOH; the eutectic point E_4 corresponds to 14.8 wt.% Na_2CO_3, 20 wt.% NaCl, and 65.2 wt.% NaOH.

Fig. 5 shows curves for the start of crystallization in the sections G, D, M, P, and T for lines corresponding to constant caustic soda contents (Fig. 6). It is clear from Fig. 5 that addition of sodium chloride to NaOH – Na_2CO_3 melts at constant caustic-soda content lowers the melting point of the ternary melt.

Part of the triangular diagram for the system NaOH – Na_2CO_3 – NaCl is given in Fig. 6. The point E_0 corresponds to the composition: 15 wt.% Na_2CO_3, 6.8 wt.% NaCl, and 78.2 wt.% NaOH, with melting point 282°. The temperature of the start of crystallization of the binary NaOH – Na_2CO_3 eutectic of variable composition decreases from the point E through the point E_1. Further, the crystallization temperature increases along the line E_0, E_2, E_4, and E_5. It also follows from Fig. 6 that under production conditions with an electrolysis temperature of 300° up to 10 – 20% of sodium chloride can build up with the same content of sodium carbonate in the melt.

LITERATURE CITED

[1] G. Scarpa, Atti della reale accademia nazionale dei Lincei, 24, 955 (1915).

[2] A. Antropoff and W. Sommer, Z. phys. Chem., 123, 161 (1926).

[3] M. I. Ravich and V. I. Elenevskaya, Ann. Sector Phys.-Chem. Analysis 24, 280 (1954).

[4] G. Hevesy, Z. phys. Chem., 73, 667 (1910).

[5] B. Neumann and E. Bergve, Z. Elektroch., 20, 271 (1914).

[6] V. A. Khitrov, Ann. Sector Phys.-Chem. Analysis 25, 236 (1954).

[7] M. Amadori, Atti della reale accademia nazionale dei Lincei, 22, 366 (1913).

[8] V. P. Radishchev, J. Gen. Chem. 3, 7, 852 (1933); N. N. Volkov and A. G. Bergman, Proc. Acad. Sci. USSR 27, 967 (1940); I. N. Belyaev and M. L. Sholokhovich, Collected Papers on General Chemistry [in Russian] (Moscow – Leningrad, Izd. AN SSSR, 1953) 1.

[9] M. Le Blanc and C. F. Carrier, Z. Elektroch., 10, 569 (1904).

[10] M. Maksimenko, Bull. Electrotech. Inst. 9, 87 (1913).

Received March 21, 1958

VAPOR PRESSURE OF SO_2 OVER ZINC BISULFITE SOLUTIONS

I. L. Peisakhov and V. D. Karmazina

A method has been developed in the State Institute of Nonferrous Metals, under the guidance of the authors of this paper, for removal of sulfur dioxide from metallurgical gases by means of a pulp containing zinc oxide and sulfite.

Calculations relating to equipment design, and evaluation of the technical process conditions, require data on the SO_2 pressure over the pulp containing solid $ZnSO_3$ and dissolved $Zn(HSO_3)_2$. I. N. Kuzminykh and A. G. Kuznetsova determined SO_2 pressures, but their data were largely concerned with the region of high $Zn(HSO_3)_2$ concentrations, and the influence of $ZnSO_4$ in the solution was studied only at 20°.

In the purification of metallurgical gases the region of low $Zn(HSO_3)_2$ concentrations and the influence of temperature in presence of $ZnSO_4$ are of interest, as $ZnSO_4$ is formed continuously during the gas purification and is therefore present in dissolved form in the absorption liquid.

The equilibrium pressure of SO_2 over aqueous solutions of zinc bisulfite and sulfate was determined by the dynamic method generally used for such purposes.

The apparatus is shown schematically in Fig. 1.

Nitrogen from a cylinder passed through a rheometer and then through five consecutive absorption flasks containing the solution. The experimental procedure was essentially the same as that used by Kuzminykh and Kuznetsova [1], but the liquid over which the SO_2 pressure was determined was not pure zinc bisulfite solution but a pulp containing solid zinc sulfite, as preliminary experiments showed that in absence of solid zinc sulfite in the solution the reproducibility of the SO_2 pressure determinations is often poor. Therefore crystalline zinc sulfite was added to the zinc bisulfite solution in each flask.

The gas emerging from the last flask was analyzed for its SO_2 content and then passed through an absorption flask containing iodine solution. The nitrogen rate was maintained at about 0.5 liter/minute.

It was shown in preliminary experiments that iodine was not volatilized from the flask during the determinations.

In all cases the solutions in the last three flasks were analyzed for SO_2 and Zn after the end of each experiment. As a rule the solutions in them were all of the same composition, which did not differ from the original.

The SO_2 pressure was calculated as follows. Let v_{SO_2} be the volume of SO_2 under standard conditions (in ml) in the gas entering the flask containing iodine solution during sampling of the gas for analysis; v_{N_2} is the volume of inert gas under standard conditions (in ml) entering the aspirator during the experiment.

We have:

$$\frac{v_{SO_2}}{p_{SO_2}} = \frac{v_{H_2O}}{p_{H_2O}} = \frac{v_{N_2}}{p_{N_2}} = \frac{v_{0\,total}}{p_{0\,total}} \qquad (1)$$

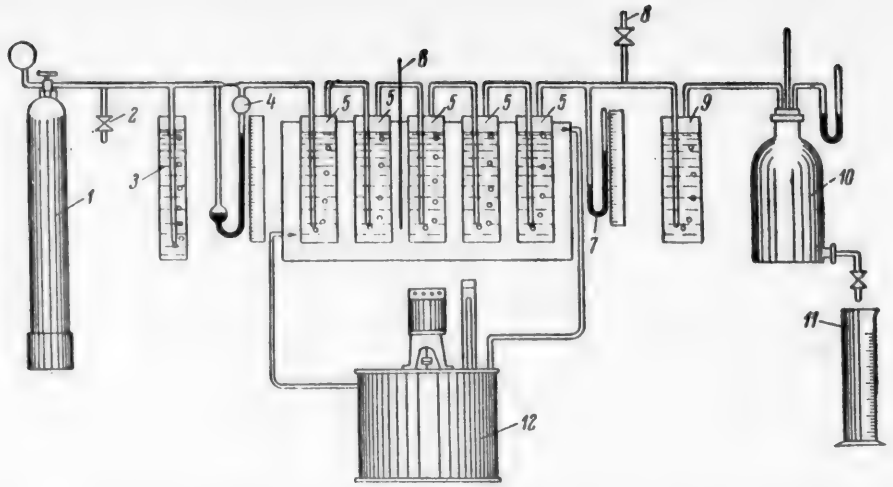

Fig. 1. Laboratory apparatus for determination of SO_2 pressure over zinc bisulfite solutions: 1) N_2 cylinder, 2) outlet valve for excess N_2, 3) mercury manostat, 4) rheometer, 5) absorption flasks with zinc bisulfite solution, 6) thermometer, 7) manometer for determination of rarefaction in the last absorption flask, 8) valve for release of gas into the air, 9) flask with iodine solution, 10) aspirator, 11) measuring cylinder, 12) ultrathermostat for keeping the temperature constant.

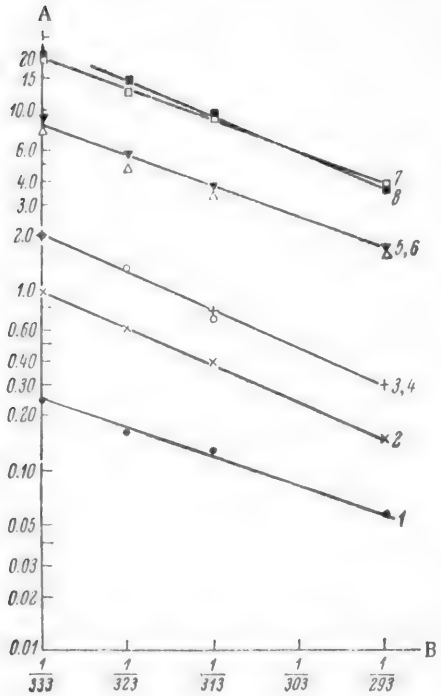

Fig. 2. Variations of SO_2 pressure with temperature at $ZnSO_4$ concentrations below 12 g/liter: A) log SO_2 pressure (mm Hg), B) 1/T; the numbers of the curves correspond to the solution compositions represented by the same numbers in Table 1.

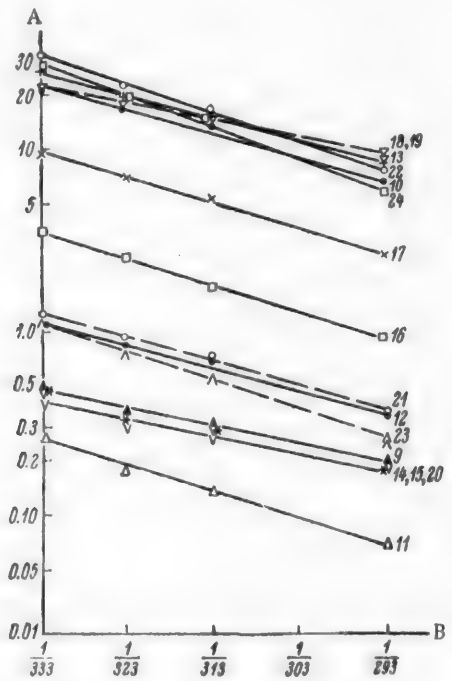

Fig. 3. Variations of SO_2 pressure with temperature at $ZnSO_4$ concentrations above 12 g/liter: A) log SO_2 pressure (mm Hg), B) 1/T; the numbers of the curves correspond to the solution compositions represented by the same numbers in Table 2.

TABLE 1

Values of SO_2 Pressure over Zinc Bisulfite Solutions with Zinc Sulfate Concentrations < 12 g/liter

Expt. No.	Contents in solution (g/liter)					Solution pH		Density of solution	SO_2 pressure (mm Hg) at temperature (°C):				Formula for calculation of log P_{SO_2} (mm Hg)
	$Zn(HSO_3)_2$	$ZnSO_4$	Zn^{++}	SO_2 total	SO_2 free	before experiment	calculated from formula		20	40	50	60	
1	5.32	4.52	3.38	2.98	0	4.8	–	1.006	0.057	0.126	1.160	0.241	3.94 – 1520/T
2	10.2	3.52	4.44	5.84	0	4.2	4.3	1.009	0.149	0.393	0.597	0.954	4.88 – 1960/T
3	13.9	8.1	7.25	7.97	0.19	4.2	4.1	1.016	0.465	0.679	1.29	2.00	6.43 – 2040/T
4	13.9	4.44	5.79	7.83	0	3.9	4.1	1.012	0.302	0.767	1.26	2.02	6.23 – 2040/T
5	24.2	3.71	8.47	14.0	0.26	3.6	3.8	1.018	1.68	3.34	4.61	8.77	7.28 – 2110/T
6	25.6	6.6	10.05	15.0	0.58	3.6	3.7	1.025	1.67	3.74	5.70	7.62	5.77 – 1620/T
7	39.3	11.4	15.9	23.65	1.54	3.15	3.3	1.041	3.8	8.52	12.2	18.5	6.04 – 1600/T
8	41.4	9.35	15.6	25.0	1.73	3.4	3.3	1.04	3.6	9.34	14.57	19.73	6.92 – 1865/T

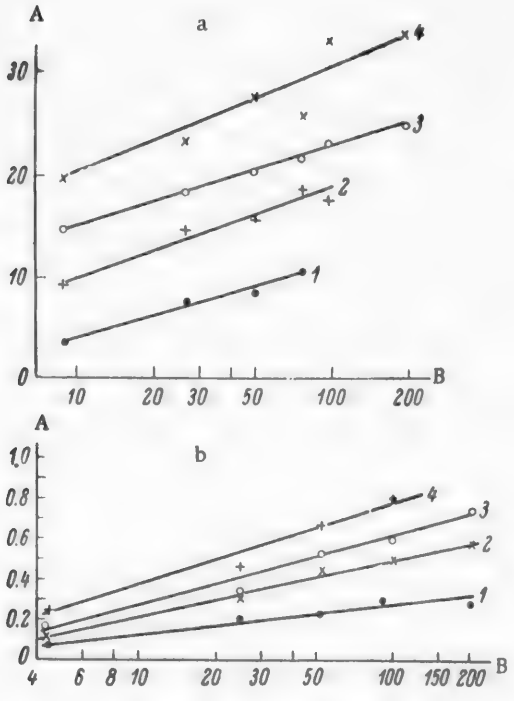

Fig. 4. Variations of SO_2 pressure with $ZnSO_4$ concentration at different temperatures: total SO_2 contents of solutions (g/liter): a) 25, b) 3; A) SO_2 pressure (mm Hg), B) $ZnSO_4$ concentration (g/liter); temperature (°C): 1) 20, 2) 40, 3) 50, 4) 60.

where p is the pressure of each component (mm Hg), and v is the volume;

hence:

$$p_{SO_2} = v_{SO_2} \frac{P_{total}\, p_{H_2O}}{v_{total}\, v_{H_2O}} = (P_{total}\, p_{H_2O}) \frac{v_{SO_2}}{v_{SO_2} + v_{N_2}} \quad (2)$$

Further,

1) v_{SO_2} is the number of milliliters of decinormal iodine solution consumed, multiplied by 1.095;

$$2)\quad v_{N_2} = \frac{v_{water}\, 273\,(B - p - b)}{760 \cdot T}, \quad (3)$$

where v_{water} is the volume of water displaced from the aspirator (ml); B is the barometric pressure (mm Hg); p is the rarefaction in the aspirator (mm Hg); b is the water vapor pressure at the temperature of the water in the aspirator;

$$3)\quad p_{H_2O} = \frac{100 p'_{H_2O}}{100 + c_{SO_2} + c_{SO_4} + c_{Zn}}, \quad (4)$$

where p' is the pressure of water vapor over pure water at the temperature of the experiment (mm Hg); c are the concentrations of SO_2, $SO^{=}_4$, Zn (in moles per 100 moles of water in the solutions used);

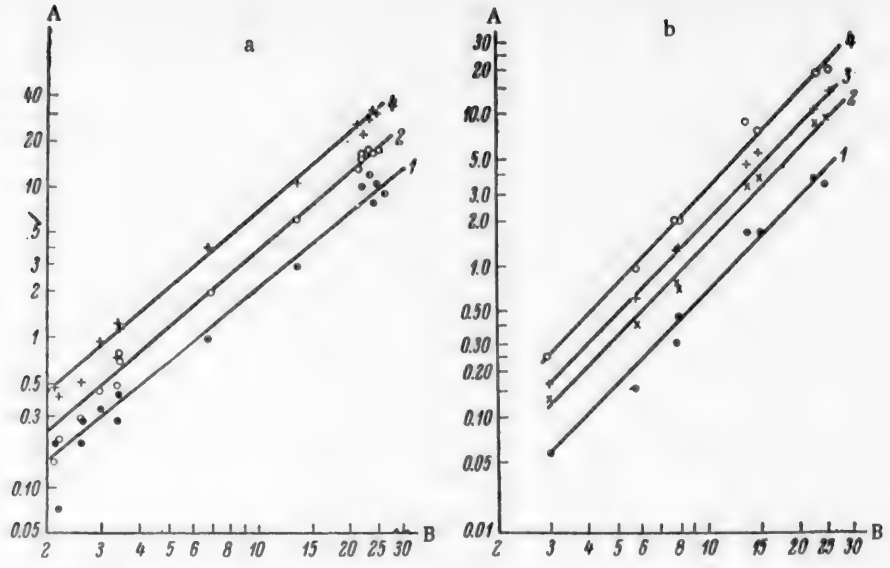

Fig. 5. Effect of total SO_2 concentration in solution on the SO_2 pressure at different temperatures:
$ZnSO_4$ contents (g/liter): a) 100, b) 12; A) SO_2 pressure (mm Hg), B) total SO_2 concentration (g/liter); temperature (°C): 1) 20, 2) 40, 3) 50, 4) 60.

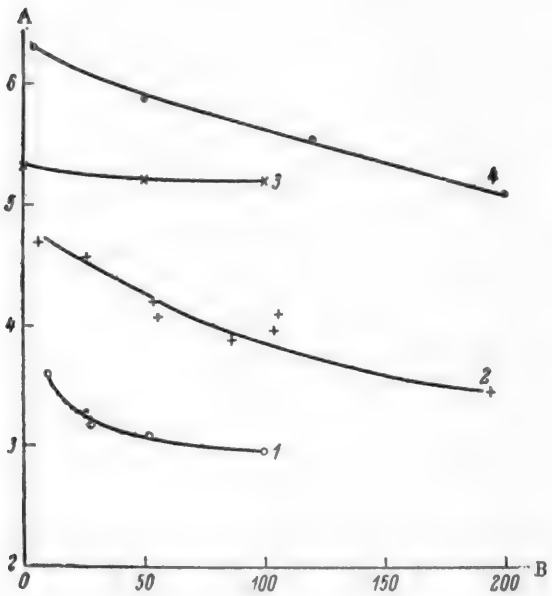

Fig. 6. Effect of $ZnSO_4$ concentration on solution pH with different total SO_2 contents:
A) pH, B) $ZnSO_4$ concentration (g/liter); total SO_2 contents (in g/liter): 1) 22 – 25, 2) 1.7 – 3.5, 3) 0.7 (zinc bisulfite absent), 4) solution contains $ZnSO_4$ only.

4) p_{total} is the barometric pressure ± the pressure in the last flask.

The values obtained for the SO_2 pressure over solutions of different compositions are given in Tables 1 and 2. The results are grouped according to $ZnSO_4$ concentration, and are presented in order of increasing $SO_{2\,total}$ concentration in each group.

The effect of temperature on the SO_2 pressure is given by the Clapeyron – Clausius equation, which can be written in the simplified general form:

$$\lg p = a - \frac{b}{T}, \qquad (5)$$

where a and b are constants; T is the absolute temperature.

Our experimental results were presented in graphical form (Figs. 2 and 3).

It is clear from Figs. 2 and 3 that nearly all the points lie on straight lines, i.e., conform to Equation (5).

For $ZnSO_4$ concentrations < 12 g/liter most of the lines have the same slope, corresponding to an average value of 1900 for the coefficient b.

For $ZnSO_4$ concentrations > 12 g/liter most of the lines also have the same slope; we could not determine the cause of the existing deviations, but they may be caused by the effect of considerable concentrations of $ZnSO_4$ on the solubility of $ZnSO_3$ and $Zn(HSO_3)_2$.

TABLE 2

Values of SO_2 Pressure over Zinc Bisulfite Solutions with Zinc Sulfate Concentrations > 12 g/liter

Expt. No.	Contents in solution (g/liter)					Solution pH			Density of solution	SO_2 pressure (mm Hg) at temperature (°C)				Formula for calculation of $\log P_{SO_2}$ (mm Hg)
	$Zn(HSO_3)_2$	$ZnSO_4$	Zn^{++}	SO_2 total	SO_2 free	before experiment	after experiment	calculated from formula		20	40	50	60	
9	5.56	24.8	11.62	3.36	0.23	4.3	4.5	4.2	1.026	0.206	0.319	0.356	0.50	$2.22 - \frac{880}{T}$
10	41.3	26.8	22.7	23.7	0.45	3.0	3.2	3.25	1.051	6.70	13.2	16.8	21.5	$5.06 - \frac{1240}{T}$
11	3.86	55	23.4	2.21	0.32	4.05	—	4.4	1.055	0.07	0.134	0.175	0.259	$1.85 - \frac{850}{T}$
12	6.14	53.2	23.3	3.5	0.05	3.45	4.1	4.1	1.057	0.363	0.723	0.843	1.035	$3.5 - \frac{1150}{T}$
13	42.3	49.6	32.2	25.0	1.15	2.8	3.1	3.1	1.080	8.44	15.7	20.5	27.5	$5.38 - \frac{1300}{T}$
14	3.64	88.2	36.7	2.63	0.58	4.1	—	4.2	1.088	0.256	0.289	0.30	0.395	$2.09 - \frac{830}{T}$
15	3.64	88.2	36.7	2.63	0.58	4.1	—	4.2	1.088	0.188	0.258	0.311	0.468	
16	10.9	82.6	36.8	6.9	1.21	3.9	—	3.9	1.090	0.948	1.78	2.52	3.58	$4.76 - \frac{1400}{T}$
17	22.9	82.0	39.6	13.7	1.02	3.8	—	3.6	1.10	2.68	5.46	6.96	9.41	$4.92 - \frac{1320}{T}$
18	35.4	77.5	41.5	22.2	2.3	3.2	—	3.2	1.106	9.35	16.77	18.73	21.3	$3.88 - \frac{850}{T}$
19	35.4	77.5	41.5	22.2	2.3	3.2	—	3.2	1.106	8.64	14.78	17.6	22.3	
20	3.64	104	43.5	2.06	0	4.1	—	4.2	1.088	1.187	0.299	0.329	0.472	$2.68 - \frac{1000}{T}$
21	5.67	103	43.6	3.44	0 24	3.4	4.0	4.0	1.099	0.373	0.726	0.933	1.25	$4.01 - \frac{1300}{T}$
22	42.7	101.4	53.1	24.5	0.45	2.8	3.0	3.1	1.122	7.83	17.0	22.5	32.5	$6.16 - \frac{1550}{T}$
23	3.28	194	77.8	3.01	1.65	3.5	—	4.1	1.185	0.274	0.573	0.740	1.08	$4.38 - \frac{1450}{T}$
24	38.1	198	91.6	21.5	0	3.4	—	3.2	1.216	5.93	14.94	20.53	28.7	$6.66 - \frac{1700}{T}$

Fig. 4 (a and b) shows the effect of the concentration of $ZnSO_4$ in solution on the SO_2 pressure. It may be represented by the equation:

$$p = A + B \lg c_{ZnSO_4}. \qquad (6)$$

To determine the effect of total SO_2 content in solution (determined directly by iodometric titration of the solution) on the SO_2 pressure, a graph was plotted (Fig. 5,a and b), with corrections for the effect of $ZnSO_4$ concentration in accordance with Fig. 4 applied to the experimental data.

These corrections were not applied for $ZnSO_4$ concentrations below 12 g/liter.

Plotted in log – log coordinates, the points lie satisfactorily on straight lines, and the relationship between P_{SO_2} and $c_{SO_2\,total}$ may be represented by the following formulas.

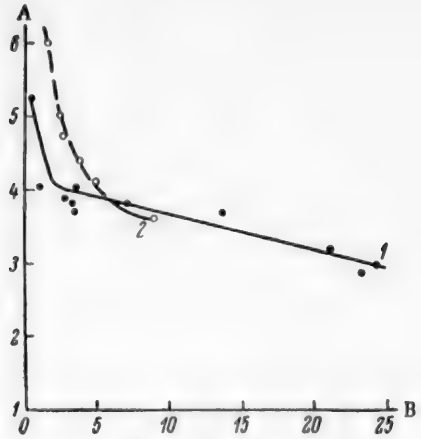

Fig. 7. Effect of total SO_2 concentration in solution on the solution pH:
A) pH, B) total SO_2 concentration in solution; curves: 1) laboratory results for 100 g $ZnSO_4$ per liter, 2) results obtained in pilot unit with variable $ZnSO_4$ concentration.

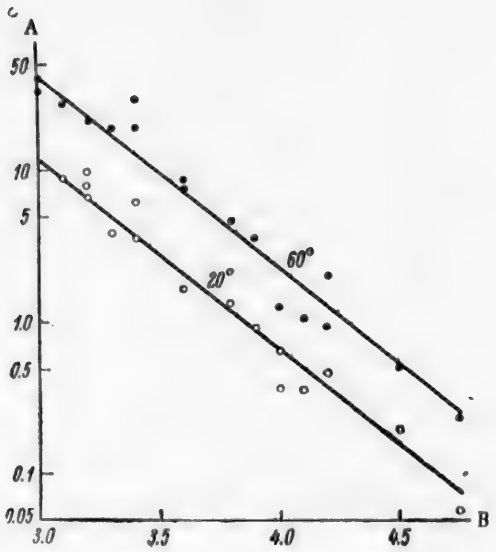

Fig. 8. Effect of solution pH on the SO_2 pressure:
A) log SO_2 pressure (mm Hg), B) pH.

For solutions containing less than 12 g $ZnSO_4$ per liter,

$$\lg p_{SO_2} = 4.06 + 2.13 \lg c_{SO_2,\ total} - \frac{1900}{T} \tag{7}$$

For higher $ZnSO_4$ concentrations, we combine the relationships represented by Equations (5) and (6) and the graphs in Figs. 4 and 5 to obtain the following approximate formula:

$$\lg p_{SO_2} = 2.15 + 1.75 \lg c_{SO_2,\ total} + 0.43 \lg c_{ZnSO_4} - \frac{1300}{T}. \tag{8}$$

The presence of a particular amount of $SO_{2\,total}$ in the solution is closely associated with the solution acidity. Therefore the SO_2 pressure over the solution must depend on the H^+ concentration. It must be pointed out, however, that the H^+ concentration can itself be influenced by the concentration of $ZnSO_4$ in the solution.

The variations of solution pH with the $ZnSO_4$ concentration are plotted in Fig. 6.

Fig. 7 shows variations of solution pH with $c_{SO_{2\,total}}$ at $ZnSO_4$ concentration of 100 g/liter.

It should be noted that: 1) equilibrium between the components of a pulp containing solid $ZnSO_3$ and a high concentration of dissolved $ZnSO_4$ is established very slowly, and the solution pH therefore fluctuates for several hours; 2) the scattering of the points is possibly due to the fact that some solutions contained relatively large amounts of sulfurous acid (in addition to bisulfite), about 2 – 3 g/liter, which might have a somewhat different effect to the presence of bisulfite only on the pH.

pH values less than 4 can be represented by the formula:

$$pH \approx 4.6 - 0.2 \lg c_{ZnSO_4} - 0.045 c_{SO_2,\ total} \tag{9}$$

and pH values above 4, by formula:

$$pH \approx 9.5 - 0.005c_{ZnSO_4} - 2c_{SO_2\ total}. \quad (10)$$

The experimental values of log p_{SO_2} are plotted against the solution pH in Fig. 8. It is seen that the points lie around lines satisfying the equation

$$\lg p_{SO_2} \approx 9.25 - 1.25pH - \frac{1300}{T} \quad (11)$$

for the pH range from 3 to 4.8.

The data found for the SO_2 pressure over various solutions can be used to calculate the percentage purification of a gas containing SO_2 if it is washed with a pulp containing ZnO, $ZnSO_3$, $ZnSO_4$ and $Zn(HSO_3)_2$.

SUMMARY

1. It is shown that the SO_2 pressure over a pulp containing $ZnSO_3$, $ZnSO_4$ and $Zn(HSO_3)_2$ depends on the temperature (in accordance with the Clapeyron – Clausius equation), the total SO_2 concentration in the solution, and the $ZnSO_4$ concentration.

2. The solution pH approximately corresponds to the formula: $pH = 4.6 - 0.2 \log c_{ZnSO_4} - 0.045\, c_{SO_2 total}$ for pH values below 4, while at higher pH it is represented by the formula:

$$pH = 9.5 - 0.005c_{ZnSO_4} - 2c_{SO_2\ total}.$$

3. The SO_2 pressure can be roughly calculated from the formulas:

$$\lg p_{SO_2} = 4.06 + 2.13 \lg c_{SO_2\ total} - \frac{1900}{T}$$

at $ZnSO_4$ concentrations below 12 g/liter, and

$$\lg p_{SO_2} = 2.15 + 1.75 \lg c_{SO_2\ total} + 0.43 \lg c_{ZnSO_4} - \frac{1300}{T}$$

at $ZnSO_4$ concentrations above 12 g/liter; or, for all cases at pH below 4.8

$$\lg p_{SO_2} \approx 9.25 - 1.25pH - \frac{1300}{T}.$$

LITERATURE CITED

[1] I. N. Kuzminykh and A. G. Kuznetsova, J. Appl. Chem. 27, No. 8, 816 (1954).*

Received February 11, 1957

* Original Russian pagination. See C. B. Translation.

EFFECTS OF TEMPERATURE AND PARTIAL PRESSURE OF OXYGEN IN THE GAS ON THE OXIDATION RATE OF AMMONIUM SULFITE – BISULFITE SOLUTIONS

B. A. Chertkov

Oxidation of sulfite – bisulfite solutions, and in particular, of ammonium sulfite – bisulfite, plays an important role when such solutions are used as absorbents in the extraction of SO_2 from dilute gaseous mixtures. In most cases, and especially in circulation processes of SO_2 extraction, the aim is to create conditions in which the absorbent solution is oxidized as little as possible. However, this cannot always be achieved, as the degree of oxidation of any particular solution depends on a whole series of factors, some of which can intensify the process while others retard it. Determination of the influence of individual factors on the oxidation of the absorbent solution with variations of the conditions for absorption of SO_2 from gases, with the appropriate quantitative data, would make this problem considerably easier to solve.

In our preceding paper [1] the influence of the composition of the absorbent solution on its oxidation rate was considered. The data on the influence of temperature and the partial pressure of oxygen in the gas on the oxidation rate of sulfite – bisulfite solution, presented in this paper,* may also be of definite interest in relation to SO_2 absorption.

It is known that the reversible cyclic process of SO_2 extraction from gases is most complete at low temperatures (about 20 – 25°). However, it is very difficult to cool considerable volumes of contaminated industrial gases, especially boiler-house flue gases, to such temperatures, and in the summer time it is impossible. Therefore in practice SO_2 is absorbed from gases at a higher temperature (30 – 35°).

If, however, a cyclic process is not required or if other and nonvolatile bases are used rather than ammonia, absorption of SO_2 can be effected without preliminary cooling of the gases. In such cases the temperature of the absorbent solution is established at a level close to 50 – 55°.

Thus, the possible temperature range of the absorbent liquors in the removal of SO_2 from gases is 20 – 55°.

The partial pressure of oxygen can vary from 8 – 10% in flue gases of electrical power stations, to 18 – 20% in very dilute exit gases in the nonferrous metals industry and other industries.

The extensive literature on the oxidation of sulfite and bisulfite solutions** contains much information on the influence of various factors, including temperature and oxygen concentration in the gas phase, on the oxidation rate. However, such information is often contradictory and, as has already been pointed out [1], the cause of the discrepancies lies in the different experimental conditions, and in particular, in differences of the concentrations of the solutions studied.

* The experimental work was performed by D. L. Puklina, T. I. Pekareva, and T. T. Spiridonova.

** The fullest literature reviews on this subject are given in an old paper by Vol'fkovich, and Belopol'skii [2], in a relatively recent paper by Abel [3], who suggested a new mechanism of sulfite oxidation, and in Rozenknop's monograph [4].

The oxidation conditions and the influence of individual factors on the oxidation rate in dilute solutions differ substantially from those in concentrated sulfite – bisulfite solutions used for removal of SO_2 from gases.

For example, Titov [2], who used very dilute sodium sulfite solutions, found that the oxidation rate is independent of the oxygen concentration in the gas phase over a wide range.

Reinders and Vless [2], who also worked with dilute solutions, confirmed that the oxidation reaction is independent of the oxygen concentration, and also found that the reaction rate is doubled with a 10° rise of temperature. Miyamoto [2], on the contrary, found that the influence of temperature on the oxidation rate is very small.

Vol'fkovich and Belopol'skii [2] improved the experimental technique and found that the oxidation rate of potassium sulfite increases with increasing concentration of dissolved oxygen. According to their results, increase of the solution temperature from 0 to 10° almost doubled the oxidation rate (the potassium sulfite concentration was 0.5 M).

In a stronger solution of ammonium sulfite (1.2 M) the effect of temperature on the oxidation rate, according to the results of Vol'fkovich and Tsirlin [5], was less pronounced. Thus, with increase of temperature from 20 to 80° the percentage oxidation of ammonium sulfite rose from 4.45 to 11.1%.

Terres and Heinsen [6], who studied the oxidation of highly concentrated ammonium sulfite and bisulfite solutions, found that the oxidation rate of ammonium sulfite changes only very slightly with increase of temperature. In the case of ammonium bisulfite, on the other hand, the oxidation rate increased considerably with temperature, the greatest increase being found for ammonium bisulfite solutions of the highest concentrations. For example, when the temperature was increased from 25 to 50°, the rate coefficient for the oxidation of 30% NH_4HSO_3 solution increased 1.15-fold, while for a 78% solution it increased 4-fold.

It is clear from this brief survey that the available literature data cannot provide a basis for quantitative estimation of the effects of temperature and partial pressure of oxygen in the gas on the oxidation rates of sulfite – bisulfite solutions, and in particular of ammonium sulfite – bisulfite, used for extraction of SO_2 from gases.

The influence of these factors on the rate of the oxidation process can be deduced on the basis of the most general considerations which follow from the theory of absorption of gases with chemical reactions in the liquid phase.

As is noted in Ramm's monograph [7] the general equation for absorption accompanied by irreversible reactions in the liquid phase, for the absorption of a sparingly soluble gas, when the gas-film resistance may be disregarded, is of the form

$$N = \beta H k_L \left(P - \frac{1}{\coth \gamma} P^* \right), \qquad (1)$$

where N is the amount of the component absorbed (in kg/m^2·hour), H is the Henry coefficient (in kg/m^3·atmos) (in the equation C = Hp), k_L is the liquid-film mass-transfer coefficient (in m/hour), P is the partial pressure of the absorbed component in the gas phase (in atmos), P^* is the equilibrium pressure of the absorbed component, corresponding to its concentration in the liquid phase (in atmos), and β is the factor representing the decrease of the liquid-film resistance in presence of a chemical reaction, given by the expression

$$\beta = \frac{\gamma}{\tanh \gamma}, \quad \text{where} \quad \gamma = \sqrt{\frac{k_1}{D}} \cdot z_L$$

here k_1 is the rate constant of the chemical reaction (tentatively assumed to be of the 1st order) (in sec^{-1}), D is coefficient of diffusion of the absorbed component through the liquid film (in m^2/hour), z_L is the thickness of the liquid film (in m), and coth and tanh are hyperbolic functions.

The values of all the quantities in Equation (1) except P can vary with the temperature.

The value of γ should undergo the greatest changes, as the rate constant k_1 of the chemical reaction may increase severalfold in the 20 – 55° range, while the coefficient of diffusion of oxygen in the liquid D, increases approximately 1.5-fold. The film thickness z_L remains almost unchanged.

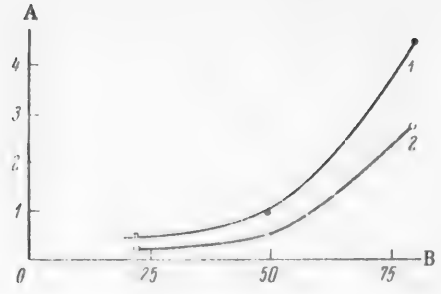

Fig. 1. Effect of temperature on the rate of absorption of oxygen by ammonium sulfite – bisulfite solutions:
A) oxygen absorbed (in g/m²·hour), B) temperature; solutions: 1) prepared artificially, 2) liquor from sulfur recovery unit.

With the remaining conditions constant, the driving force of absorption ($P - \frac{1}{\coth \gamma} P^*$) and the value of the factor β increase with increasing γ.

Increase of temperature also results in increase of the liquid-film mass-transfer coefficient k_L; the latter can be determined, say for wetted-wall apparatus, from the following general equation [7]

$$k_L = A \frac{D^{0.5}}{(\mu d)^{0.107}}, \qquad (2)$$

where A is a coefficient combining a group of hydrodynamic factors, μ is the viscosity of the liquid (in kg·second/m²), and d is the density of the liquid (in kg/m³).

It is clear from Equation (2) that k_L is determined mainly by the diffusion coefficient of oxygen D, which, as already stated, increases approximately 1.5-fold in the temperature range under consideration.

On the other hand, the Henry coefficient H decreases with rise of temperature. When oxygen is dissolved in water, the value of H decreases approximately 1.5-fold in the 20 – 55° range. Therefore, with all the factors taken into account, the rate of oxygen absorption, and therefore the total oxidation rate, should increase with temperature.

By Henry's law, increase of the oxygen partial pressure in the gas results in an increase of the dissolved oxygen concentration in the liquid. Since the rate of the chemical reaction is a function of the concentrations both of sulfite – bisulfite, $C_{SO_3^{--}+HSO_3^-}$, and of the dissolved (but not yet reacted) oxygen, C_{O_2}, increase of the the concentration of the latter should in general increase the over-all rate of the process. However, the case in which the chemical reaction is very slow and controls the over-all oxidation rate must be distinguished here. In this case increase of the oxygen partial pressure in the gas and corresponding increase of C_{O_2} should not lead to any significant change in the oxidation rate of the solution.

Since the concentration of dissolved oxygen at any given instant is unknown, and the relationship between the rate of chemical reaction and the diffusion rate is also unknown, the rate of the oxidation process cannot be calculated, but must be determined experimentally in each instance.

EXPERIMENTAL

As in the preceding investigation [1], the influence of temperature on the oxidation rate was studied by a static method, in which samples of solution in open vessels were oxidized by oxygen of the surrounding air. The static method, which takes much time, gives more reliable and reproducible results than the dynamic method. The reason is that in the static method the phase contact area remains strictly constant, and diffusion processes in the liquid phase occur freely, without external influences. In contrast, in the dynamic method the nature and area of the gas – liquid interface vary with the experimental conditions, and in particular with the temperature of the liquid. For example, ammonium sulfite – bisulfite solution froths considerably more at low than at higher temperatures when air is passed through it; this is due to changes in the solution viscosity and surface tension with changes of temperature. As this results in different interfacial areas, it may lead to totally erroneous conclusions concerning the influence of a particular factor, in this instance the temperature, on the rate of the process in question.

Vessels with duplicate samples of solution were kept at room temperature and in a thermostat at 50° respectively. The partial pressure of oxygen remained constant, while the solution compositions were so chosen that the changes of composition as the result of oxidation and the simultaneous desorption of SO_2 and NH_3 were as

TABLE 1

Comparative Experiments on Oxidation of Ammonium Sulfite – Bisulfite Solutions in Air at 22 and 50°

Type of solution	Duration of experiment (hours)		Solution sample	Solution composition (moles/liter)				$\frac{S}{C}$	G_{O_2} rate of oxygen absorption ($g/m^2 \cdot hour$)	Notes
	total	heating time		total SO_2 (S)	total NH_3 eff (C)	$(NH_4)_2SO_4$	$(NH_4)_2S_2O_6 + (NH_4)_2S_3O_6$			
Artificially prepared			Initial	5.210	6.64	0.26	0	0.785		
	320	—	Final at 22°	4.460	5.99	0.61	0	0.745	0.45	
	320	300	Final at 50°	3.810	4.86	0.97	0	0.785	0.95	
			Initial	5.525	7.00	0.125	0	0.790		
	369	—	Final at 22°	4.660	5.86	0.563	0	0.796	0.49	F_{vessel} = 78.5 cm^2,
	369	347	Final at 50°	3.960	5.50	0.969	0	0.785	0.962	$V_{solution}$ = 200 ml
			Initial	5.210	6.640	0.255	0	0.785		
	320	—	Final at 22°	4.600	6.25	0.550	0	0.738	0.378	
	320	300	Final at 50°	3.860	4.96	0.940	0	0.780	0.906	
Liquor from sulfur recovery unit			Initial	2.517	3.320	1.945	0.194	0.758		
	319	—	Final at 22°	2.268	2.972	2.110	0.203	0.765	0.215	
	319	276	Final at 50°	1.400	2.102	2.300	0.248	0.670	0.505	F_{vessel} = 38.4 cm^2,
			Initial	2.517	3.320	1.945	0.194	0.758		$V_{solution}$ = 100 ml
	319	—	Final at 22°	2.268	2.972	2.110	0.203	0.765	0.215	
	319	276	Final at 50°	1.487	2.756	2.240	0.211	0.700	0.410	
			Initial	2.616	3.141	2.016	2.217	0.833		
	475	—	Final at 22°	2.220	2.550	2.343	0.227	0.870	0.285	F_{vessel} = 78.5 cm^2,
	475	280	Final at 50°	1.462	1.792	2.556	0.230	0.804	0.590	$V_{solution}$ = 200 ml

TABLE 2

Oxidation of Ammonium Sulfite – Bisulfite Solutions in Air at 80° Heating Time 140 Hours in All Experiments (F_{vessel} = 40.7 cm², $V_{solution}$ = 200 ml)

Type of solution	Solution sample	Sol. comp. (moles/liter)				S/C	S/C average for experiment	G_{O_2} rate of oxygen absorption (g/m²·hour)
		total SO_2 (S)	total NH_3 eff (C)	$(NH_4)_2SO_4$	$(NH_4)_2S_2O_3$ + $(NH_4)_2S_3O_6$			
Artificially prepared	Initial	4.98	6.11	1.58	0.28	0.815		
	Final	3.61	4.67	2.41	0.34	0.774	0.795	4.65
	Initial	6.25	6.80	0.20	0	0.920		
	Final	4.15	5.25	1.02	0.04	0.791	0.855	4.60
	Initial	5.51	6.12	1.43	0.26	0.900		
	Final	3.49	4.45	2.38	0.29	0.787	0.842	5.35
Liquor from sulfur recovery unit	Initial	2.93	3.47	2.12	0.21	0.845		
	Final	1.81	2.32	2.62	0.33	0.783	0.814	2.80
	Initial	3.56	3.71	2.28	0.22	0.960		
	Final	1.96	2.56	2.98	0.31	0.765	0.862	3.95

TABLE 3

Effect of Oxygen Concentration in the Gas on the Oxidation Rate of Ammonium Sulfite – Bisulfite (experimental temperature 20°, volume of solution in vessels 50 ml, gas rate 400 cc/minute)

Duration of experiment (hours)	Composition of gas mixture (%)	Samples	Sol. comp. (moles/liter)				S/C
			total SO_2 (S)	total NH_3 eff (C)	$(NH_4)_2SO_4$	$(NH_4)_2S_2O_3$	
27	12.5 O_2, 87.5 N_2	Original solution No. 1	5.00	5.98	0.085	0	0.835
		Final solution	4.73	5.70	0.224	0	0.830
	25 O_2, 75 N_2		4.57	5.47	0.336	0	0.836
	50 O_2, 50 N_2		4.28	5.01	0.571	0	0.855
	100 O_2, 0 N_2		3.53	3.77	1.190	0	0.935
20	12.5 O_2, 87.5 N_2	Original solution No. 2	1.74	2.16	2.345	0	0.806
		Final solution	1.63	2.04	2.400	0	0.803
	25 O_2, 75 N_2		1.60	1.98	2.440	0	0.809
	50 O_2, 50 N_2		1.48	1.71	2.560	0	0.865
	100 O_2, 0 N_2		1.36	1.55	2.650	0	0.878

small as possible. To maintain the S/C ratio,* which has an appreciable influence on the oxidation rate [1], at a constant level, small amounts of SO_2 or NH_3 were added to the solutions as necessary.

The results are given in Table 1. The oxidation rate was found from the increase of the ammonium sulfate present in solution, and was calculated as the equivalent rate of oxygen absorption G_{O_2} (in g/m²·hour).

* The S/C or SO_2/NH_3 eff ratio is a measure of the relative proportions of bisulfite and sulfite in solution. When S/C = 1, the solution contains bisulfite only.

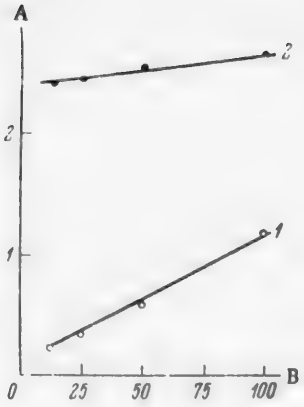

Fig. 2. Effect of partial pressure of oxygen in the gas on the oxidation rate of ammonium sulfite – bisulfite solutions: A) concentration of $(NH_4)_2SO_4$ (moles/liter), B) oxygen content of gas (%). Initial NH_3 concentration of solution (moles/liter): 1) 5.98, 2) 2.16.

It follows from Table 1 that in the oxidation of a pure artificial solution, free from ammonium thiosulfate and trithionate,* consistent results were obtained, showing that the rate of absorption of oxygen by a solution of the given composition is 0.45 g/m²·hour at 22°, and 0.95 g/m²·hour at 50°. In the oxidation of liquor from a sulfur recovery unit, which contained appreciable amounts of thiosulfate and trithionate and also p-phenylenediamine which inhibits their catalytic action, consistent results were also obtained, showing that G_{O_2} is 0.25 g/m²·hour at 22°, and 0.5 g/m²·hour at 50°. Thus, in both cases increase of temperature from 22 to 50° had a positive effect, in agreement with theory, on the rate of oxygen absorption.

For confirmation of this result over a wider temperature range, experiments on the oxidation of solutions at 80° were performed. The results are presented in Table 2. At this temperature it is very difficult to keep the S/C ratio at a constant level owing to strong desorption of SO_2 and NH_3, and here we can speak only of an average value of S/C for the duration of each experiment.

All the values found for G_{O_2}, both with the artificial solution and the works liquor, are logically interrelated but the essential fact is that at 80° the oxidation process can no longer be separated from the spontaneous decomposition of the solution. The two processes occur together, and the thiosulfate and trithionate formed have a catalytic effect in causing additional oxidation of the sulfite – bisulfite solution.

It is clear from the data in Table 2 that G_{O_2} in these experiments increased severalfold in comparison with the values obtained at 50°.

The oxidation rates of solutions with the same S/C ratio at 22, 50, and 80° are compared in Fig. 1. It follows from the curves in Fig. 1 that the influence of temperature on the oxidation rate is much more complicated than the literature survey indicates. This relationship (at temperatures above 50°) deviates strongly from linearity, and is best represented by an equation of the form

$$[G_{O_2}]_{t^\circ} = [G_{O_2}]_{22^\circ} + at + bt^2. \qquad (3)$$

The constant coefficients of t and t^2 are:

for the artifical solution

$$a = -0.0565,\ b = 0.0013,$$

for the works liquor

$$a = -0.0400,\ b = 0.0009.$$

Thus, if the oxidation rate of a particular solution is known at any one temperature, the curves in Fig. 1 can be used to find its oxidation rate at any other temperature if all the other process conditions remain unchanged.

The influence of oxygen concentration in the gas on the oxidation rate of ammonium sulfite – bisulfite solutions was studied by a dynamic method since the static method is by its nature inapplicable for this purpose. To avoid the errors inherent in the dynamic method, all possible measures were taken to ensure an equal contact area in each reaction vessel. The vessel dimensions, solution volumes, amounts of gas passed, size of the gas bubbles, temperature, and other experimental conditions were the same for all the vessels, and remained strictly constant during each experiment. Only the composition of the incoming gas mixture was varied.

* These impurities are formed by spontaneous decomposition of bisulfite, and they have a catalytic effect on the oxidation process.

Gas mixtures of the required composition were prepared by measurement and mixing of oxygen and nitrogen from cylinders in definite proportions. For convenience, the following four gas mixtures were made:

% O_2		% N_2
12.5	and	87.5
25	and	75
50	and	50
100	and	0

The oxygen concentration of the mixtures was varied over a considerably wider range than that corresponding to the usual oxygen contents of industrial gases. This was necessary in order to establish a more general relationship, within the limits of which it would be possible to determine more precisely the influence of oxygen concentration on oxidation in the narrow region with which we were concerned.

The results of these experiments are presented in Table 3.

Increase of the ammonium sulfate concentration in each vessel can serve as a measure of the oxidation rate in these experiments. The value of G_{O_2} (in $g/m^2 \cdot$ hour) cannot be found, as the phase-contact area in the reaction vessel is not known.

As is seen in Table 3, two original solutions were oxidized: with a high and a low concentration of ammonium sulfite – bisulfite (C = 5.98 moles/liter and 2.16 moles/liter respectively). These concentrations were chosen because they lie on either side of the optimum concentration at which the oxidation proceeds at the highest rate. We showed earlier [1] that there is an optimum concentration of ammonium sulfite – bisulfite (C ~ 3 moles/liter) above and below which the oxidation rate falls continuously. At higher sulfite – bisulfite concentrations the rate of the chemical reaction is high, but the over-all oxidation process is limited by access of oxygen, the solubility of which falls with increase of the salt concentration. In the region of low sulfite – bisulfate concentrations the rate of the process begins to be determined by the rate of the chemical reaction, and access of oxygen is no longer decisive.

This is additionally confirmed by the data in Table 3. In the oxidation of Solution No. 1, when the process is limited by the rate of oxygen access, increase of the oxygen concentration in the gas produced an appreciable and almost directly proportional increase of the ammonium sulfate concentration in solution. In the oxidation of Solution No. 2, when the rate of the chemical reaction is the determining factor, increase of the oxygen concentration in the gas had, on the whole, only a slight effect, although the increase of the ammonium sulfate content was still proportional to it. These results are presented graphically in Fig. 2.

From the results of these experiments it may be concluded that increase of the partial pressure of oxygen in the gas always results in an increase in the oxidation rate of sulfite – bisulfite solutions.

Accordingly, in the extraction of SO_2 from dilute waste gases from nonferrous metallurgical processes the oxidation of the absorbent solution should be greater (approximately double) than oxidation in the extraction of SO_2 from power-station flue gases, under the same conditions. However, the oxidation rate may differ in accordance with the concentration of the ammonium sulfite – bisulfite solution, being at a minimum with the use of highly concentrated or very dilute solutions.

SUMMARY

1. The effects of temperature and partial pressure of oxygen in the gas on the oxidation rate of ammonium sulfite – bisulfite solutions used for extraction of SO_2 from industrial gases were studied, and an empirical relationship was derived which can be used for determination of the oxidation rate of the solution at any given temperature if the oxidation rate of this solution at any other temperature is known.

2. It is shown that increase of the oxygen partial pressure in the gas increases the oxidation of the solution. However, the increase of the ammonium sulfate concentration may be greater or less; this depends on whether the oxidation process is determined by the access of oxygen to the liquid phase or the rate of the chemical reaction between sulfite – bisulfite and dissolved oxygen.

LITERATURE CITED

[1] B. A. Chertkov, J. Appl. Chem. 30, No. 10, 1496 (1957).*

[2] S. I. Vol'fkovich and A. P. Belopol'skii, J. Appl. Chem. 5, No. 5, 504-566 (1932).

[3] E. Abel, Monatsh. 82, 815 (1951).

[4] Z. P. Rozenknop, Extraction of Sulfur Dioxide from Gases [in Russian] (Goskhimizdat, 1952).

[5] S. I. Vol'fkovich and D. L. Tsirlin, J. Chem. Ind. 18, 1323 (1929).

[6] E. Terres and A. Heinsen, Gas and Wasserfach, 994 (1929).

[7] V. M. Ramm, Absorption Processes in Chemical Industry [in Russian] (Goskhimizdat, 1951).

Received June 17, 1957

* Original Russian pagination. See C. B. Translation.

EQUILIBRIUM OF CARBON WITH LIQUID ALLOYS OF Fe, Mn, Si, and C

M. S. Petrushevskii and P. V. Gel'd

It is known that silicon considerably lowers the solubility of carbon in its alloys with iron, chromium, and certain other metals. This is equally true of both solid and liquid systems. The influence of silicon on the activity coefficient of carbon in the system Fe – Si – C has been studied in considerable detail. Far fewer data (mainly on melts) are available on alloys of Cr, Si, and C. Information on manganese alloys is extremely scanty, and relates mainly to certain technological samples. Nevertheless the technology of smelting of silicon – manganese alloy and of a number of other alloys with high manganese contents requires the determination of relationships characterizing the thermodynamic properties of the carbon present in them.

These considerations prompted the present investigation, which had a limited objective – determination of the solubility of carbon in manganese and its alloys with iron and silicon at 1460°.

The starting materials were Armco iron, electrolytic manganese, and technical silicon (~98.5% Si).

The solubility of carbon in alloys of different composition was determined as follows.

A weighed sample of the materials (about 200 g) was put in a graphite crucible (internal diameter 50 mm, height 90 mm) heated in Kryptol furnace. To avoid oxidation, the crucible and furnace were carefully closed, while during the control experiments purified argon was passed into the heated portion of the apparatus. The temperature was measured by means of an optical pyrometer. Samples of the melt were sucked into quartz tubes. They were analyzed for carbon in the Ströhlein apparatus; the silicon and manganese contents were determined by usual methods of chemical analysis.

In order to determine the time required for saturation of alloys with carbon, preliminary kinetic investigations were performed in which samples of metal were taken in the course of the process. It is clear from Fig. 1 (Curves 1, 2) that saturation of pure metals (Mn and Fe) with carbon is fairly rapid, and is complete after about 20 minutes. The time is approximately the same for silicon alloys. As Fig. 1 shows, if manganese is added to fused silicon (Curve 3), the equilibrium concentration of carbon in the alloy (~14% Si, ~83% Mn, ~3% C) is reached after about 15 minutes. Much longer time is required to reach equilibrium if silicon is added to a previously melted metal, saturated with carbon (Fig. 1, Curve 4). In this case the time required for removal of excess carbon is 40 – 50 minutes. Moreover, there is then an increased risk that a suspension of carbon (or SiC) particles may be formed and lead to erroneous results. Therefore all the subsequent experiments were performed by simultaneous fusion of the charge containing silicon and its saturation with carbon during about 40 minutes.

The partial system Fe – Si – C. It has long been known that the properties of carbon dissolved in iron depend considerably on the concentration of silicon in the alloy. The ternary system Fe – Si – C has therefore been studied by a number of investigators; this work (up to 1936) is reviewed in the monograph by Greiner, Marsh, and Stoughton [1]. It has been found that silicon considerably increases the activity coefficient of carbon, i.e., it lowers its solubility. The system Fe – Si – C was studied in greater detail by Smith [2], who determined the thermodynamic characteristics of carbon at 1000° both in ferrite and in austenite. Samarin and Shvartsman [3] put forward the semiempirical formula

$$\gamma_C = \frac{1}{1 - 5\,(N_C - N_{Si})},$$

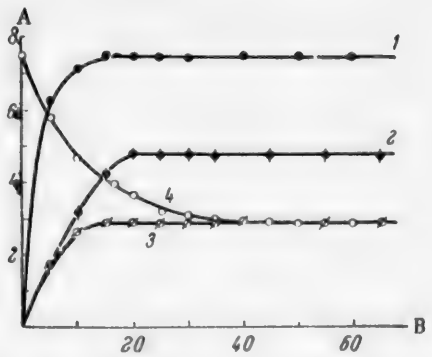

Fig. 1. Solution kinetics of carbon in iron, manganese, and manganese – silicon alloys at 1460°:
A) carbon content (wt.%), B) time (minutes); 1) Mn, C; 2) Fe,C; 3, 4) Mn, C, Si.

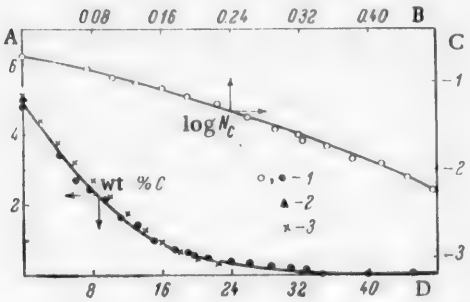

Fig. 2. Solubility of carbon in iron – silicon alloys at 1460°:
A) carbon content (wt.%), B) N_{Si}, C) log N_C, D) silicon content (wt.%); 1,2) from the results of this study; 3) from Chipman's data [9].

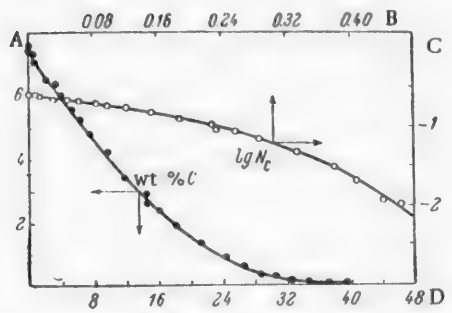

Fig. 3. Solubility of carbon in manganese – silicon alloys at 1460°:
A) carbon content (wt.%), B) N_{Si}, C) log N_C, D) silicon content (wt.%).

which gives fair agreement with experimental data, for calculation of the activity coefficient of carbon. However, there is a systematic discrepancy ($\gamma_{expt.} > \gamma_{calc.}$) between experimental results and the values given by this formula; in the authors' opinion this indicates that the silicon atoms not only displace carbon from the interstices, but are electrostatically repelled by carbon atoms.

Decrease of the solubility of carbon with increasing silicon concentration is observed not only in austenite, but also in liquid alloys. This is shown by numerous early observations [4 – 7] and by the results of more thorough investigations [8, 9]. The most reliable data are probably those of Chipman and Fulton [9]; according to their results, the presence of, say, 10% of silicon lowers the solubility of carbon in Fe – Si – C alloys to 2.2% (at 1460°).

To test the method chosen for the investigation, and to obtain experimental data on this most important system, we measured the solubility of carbon in alloys of Fe, Si, and C containing from 0.02 to 49.72% Si (at 1460°). The results are plotted in Fig. 2. For comparison, interpolated data from the paper by Chipman and Fulton [9] are also shown; it is seen that the agreement is not bad. It is true that for low-silicon alloys our values for the solubility of carbon are roughly 0.1 – 0.15% lower than those found by Chipman.

Experimental data on the solubility of carbon in melts containing Fe, Si, and C at 1460° can be satisfactorily represented by the empirical equation

$$\lg N_C^{Fe,\,Si} = -0.70 - 2.15N_{Si} - 2.25N_{Si}^2.$$

The activity coefficient of carbon can easily be calculated if, for example, we assume $\gamma_C^{Fe} = 1$ for saturated solution of carbon in pure iron ($\log N_C^{Fe} = -0.70$). Value gives

$$\lg \gamma_C^{Fe,\,Si} = \lg \frac{N_C^{Fe}}{N_C^{Fe,\,Si}} = 2.15N_{Si} + 2.25N_{Si}^2.$$

These expressions are in fair agreement with the results of other authors [8].

The partial system Mn – Si – C. As far as we know, there are no systematic data on the influence of silicon on the solubility of carbon in alloys of Mn, Si, and C.

The results of our determinations are given in Fig. 3. These results are confirmed to some extent by comparison of our data for pure manganese with literature data. According to our results, the solubility of carbon in manganese at 1460° is 7.62% (experiments in an argon atmosphere). This is in satisfactory agreement with values found by extra-

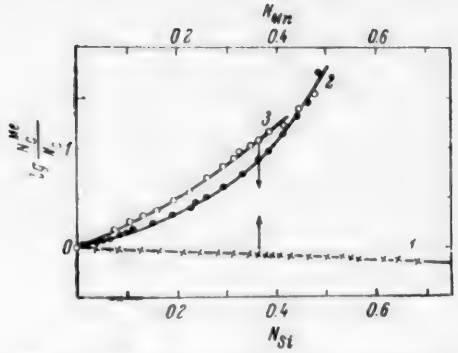

Fig. 4. Effects of silicon (and manganese) on the activity coefficient of carbon in Fe – Si – C and Mn – Si – C (and also Fe – Mn – C) alloys at 1460°:

Alloys: 1) Fe – Mn – C ($\gamma_C^{Fe}=1$), 2) Mn – Si – C ($\gamma_C^{Mn}=1$), 3) Fe – Si – C($\gamma_C^{Fe}=1$).

sume that $\gamma_C^{Mn}=1$ for the binary system Mn – C.

Since at 1460°

polation of Chipman and Thomson's results [9] for iron – manganese alloys (consistent results to ~ 65% Mn) to pure manganese. This value is about 7.58% C for 1460°. A somewhat higher value (7.82% C) was found by Turkdogan et al. [10]. The discrepancies between the results are small, and are within the permissible error limits.

Data for Mn – Si – C alloys in the high silicon region are in fair agreement with the results of Esin and Vatolin [11]. At low silicon concentrations (< 12% Si) their solubility values are somewhat lower than those found in the present study.

As in the case of Fe – Si – C alloys, silicon lowers the solubility of carbon considerably in this system. The data plotted in Fig. 3 can be satisfactorily represented by the empirical equation

$$\lg N_C^{Mn,\,Si} = -0.56 - 0.8N_{Si} - 4.5N_{Si}^2,$$

valid at 1460°.

For estimation of the influence of silicon on the thermodynamic characteristics of dissolved carbon, we may as-

$$\lg N_C^{Mn} = -0.56, \text{ therefore}$$

$$\lg \gamma_C^{Mn,\,Si} = \lg \frac{N_C^{Mn}}{N_C^{Mn,\,Si}} = 0.8N_{Si} + 4.5N_{Si}^2.$$

For illustration of the effect on the activity coefficient of carbon in Fe – Si – C and Mn – Si – C alloys, Fig. 4 shows the relationships between $\log \gamma^{Me,\,Si}$ and N_{Si}. It is seen that the action of silicon is of the same type in both systems. When the silicon content is such that $N_{Si} < 0.45$ the activity coefficient of carbon is higher in Fe – Si – C alloys. Conversely, at higher silicon concentrations the latter has a greater effect on the activity of carbon in the Mn – Si – C system. It should be pointed out, however, that conclusions based on data for high-silicon alloys with low concentrations of carbon (0.02 – 0.10%) require further confirmation. This is largely due to the insufficient accuracy of determination of small amounts of carbon in the alloys, and also to the possibility of relatively large errors caused by the presence of suspended carbon particles.

Since it is intended to consider the characteristics of carbon in the quaternary system Fe – Mn – Si – C, it is also desirable to express the activity of carbon in Mn – Si – C alloys on the assumption that $\gamma_C^{Fe}=1$. In this case it is evident that

$$\lg \gamma_C^{'Mn,\,Si} = \lg \frac{N_C^{Fe}}{N_C^{Mn,\,Si}} = -0.14 + 0.8N_{Si} + 4.5N_{Si}^2.$$

The partial system Fe – Mn – C. The effects of manganese on the solubility and activity of carbon in iron – manganese alloys at 1000° was studied by Smith [2] and several others. They showed that, in contrast to silicon, manganese decreases the activity coefficient of carbon in solid solutions. It has a similar effect at higher temperatures, at which Fe – Mn – C alloys become liquid. It must be pointed out that literature data [7, 9, 11]

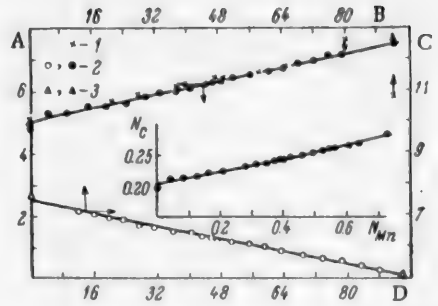

Fig. 5. Solubility of carbon in iron – manganese alloys at 1460°:
A) carbon content (wt.%), B) iron content (wt.%), C) carbon content (wt.%), D) manganese content (wt.%); 1) from Chipman's data [9]; 2,3) from our data.

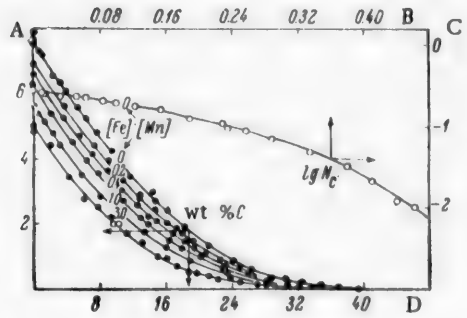

Fig. 6. Effects of silicon and of $N_{Fe} : N_{Mn}$ ratio on the solubility of carbon in Fe – Si – C alloys at 1460°:
A) carbon content (wt.%), B) N_{Si}, C) log N_C, D) silicon content (wt.%).

on the solubility of carbon in liquid alloys were not in good agreement; additional determinations were therefore advisable. Investigations were accordingly performed with a large number of alloys, in which the iron and manganese concentrations were varied within wide limits (up to $N_{Mn_{1,2}} = 0$).

The results of determinations at 1460° are given in Fig. 5. It is clear from Fig. 5 that the solubility of carbon increases linearly with the manganese concentration in the alloy, and can be represented with sufficient accuracy by the equations*

$$[\%\,C]_{Fe,\,Mn} = 5.10 + 0.0265\,[\%\,Mn],$$

$$N_C^{Fe,\,Mn} \cong 0.203 + 0.1N_{Mn} = 0.276 - 0.096N_{Fe}.$$

The latter equation can be used for finding the effect of the composition of liquid Fe – Mn – C alloys on the activity coefficient of carbon. Assuming, as before, that $\gamma_C^{Fe} = 1$ for a solution of carbon in liquid iron (i.e., $a_C^{Fe} = N_C^{Fe}$), we have

$$\gamma_C^{Fe,\,Mn} = \frac{N_C^{Fe}}{N_C^{Fe,\,Mn}}.$$

Since, further, $N_C^{Fe} \cong 0.203$, it follows that

$$\gamma_C^{Fe,\,Mn} = \frac{0.203}{0.203 + 0.1N_{Mn}} = \frac{1}{1 + 0.492N_{Mn}};$$

$$\ln \gamma_C^{Fe,\,Mn} = -\ln (1 + 0.492N_{Mn}).$$

Resolving this last expression into a Taylor series for powers of a small quantity (0.492 N_{Mn}) we have

$$\ln \gamma_C^{Fe,\,Mn} = -0.492N_{Mn} + 0.121N_{Mn}^2 - 0.0396N_{Mn}^3 + \ldots$$

Ignoring terms containing higher powers of the manganese concentration, and converting to common logarithms, we have

$$\lg \gamma_C^{Fe,\,Mn} = -0.214N_{Mn}$$

or

$$\lg N_C^{Fe,\,Mn} \cong -0.700 - 0.214N_{Mn}.$$

* Here and subsequently the expressions in square brackets represent concentrations in weight percentages.

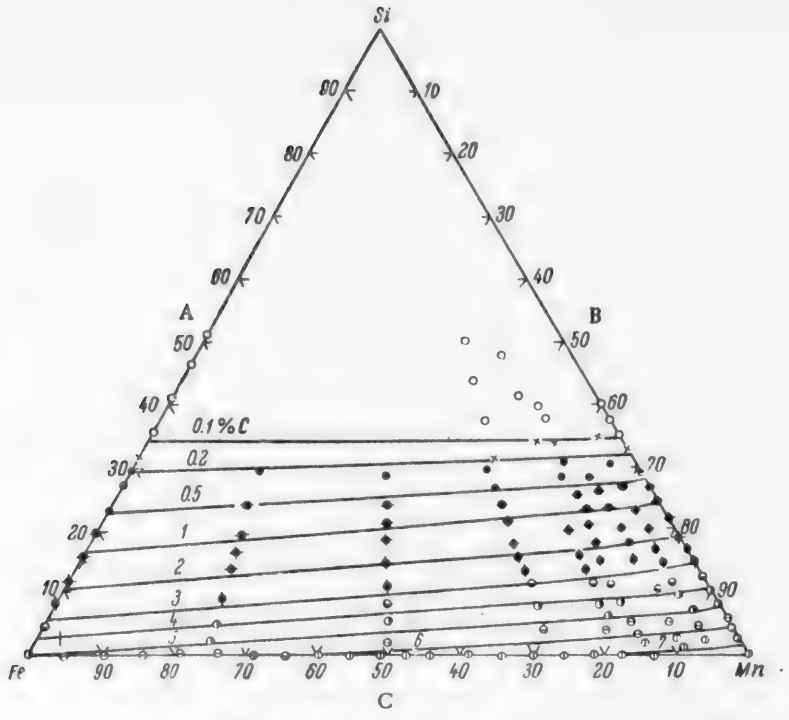

Fig. 7. Parametric graph with [% C] = const. for the solubility of carbon in Fe – Mn – Si alloys at 1460° on the assumption that [% Fe]+[% Mn]+[% Si] = 100%:

A) silicon content (wt.%), B) manganese content (wt.%), C) iron content (wt.%); the different points correspond to variations of carbon content from 0.10 to 7.5%.

Although these last equations are approximate, they can be used for rough calculations of the activity coefficients of carbon in Fe – Mn – Si alloys at 1460°. This is confirmed, in particular, by the good agreement with experimental data (Fig. 4).

It should be noted that the above values for the solubility of carbon are in fair agreement with the data of Chipman and Thomson [9], shown in Fig. 5 for comparison. It is seen that the discrepancy between the values for alloys containing up to 65% Mn does not exceed 0.1 – 0.15%. At higher manganese concentrations the data of Chipman and Thomson have poor reproducibility and show considerable scattering. Moreover, our results confirm the conclusion of Turkgodan and Leake [12] that the influence of manganese in this system may be characterized by the linear expression

$$\Delta N_C^{Mn} = N_C^{Fe,\,Mn} - N_C^{Fe} = 0.1\ N_{Mn}.$$

In view of the large number of experiments, the adequate purity of the materials, and of the results of control experiments in an argon atmosphere, it may be assumed that the above data represent the effect of concentration on the solubility of carbon in iron – manganese alloys to an accuracy of the order of ±0.1% C.

The quaternary system Fe – Mn – Si – C. Studies of ternary and quaternary alloys show that the solubility of carbon in them falls rapidly with increase of silicon content. Therefore only alloys in which the silicon concentration did not exceed 50 wt.% were studied. Some of the results are presented in Fig. 6. It should be noted that the curves in Fig. 6 are approximate, as during the smeltings the initial concentration ratios of iron to manganese in the alloys varied a little. However, the experimental data indicate that the slight fluctuations (of N_{Fe}: N_{Mn}) had relatively little effect on the carbon solubility. Therefore this family of curves can be regarded, with-

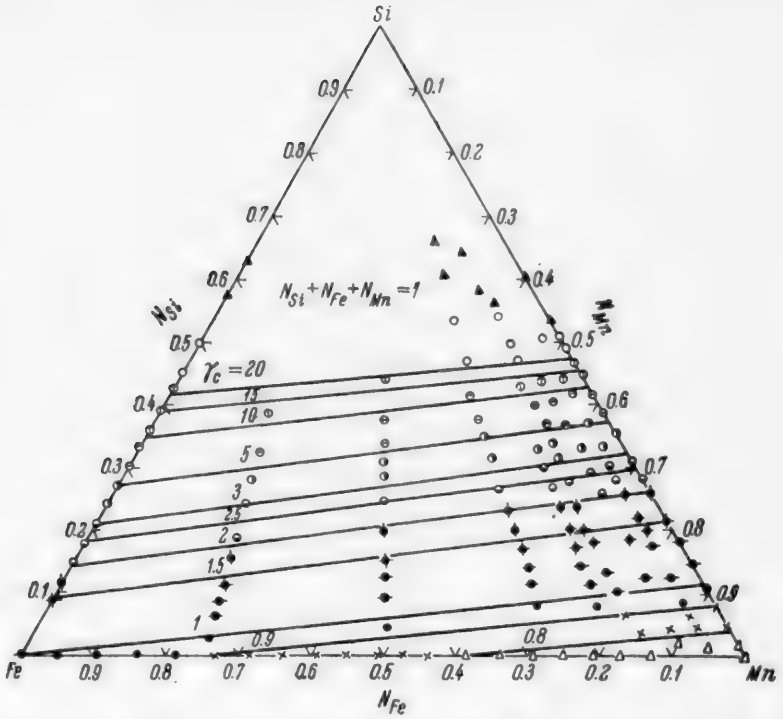

Fig. 8. Curves representing equal activity coefficients of carbon in the quaternary system Fe – Mn – Si – C (saturated at 1460°); the different points correspond to changes of γ_C from 0.70 to 200.

out significant error (in any event, not greater than the error in plotting of the graphs), as sections of the solubility surface of carbon in the quaternary system Fe – Mn – Si – C by planes with $(N_{Fe} : N_{Mn}) = \text{const}$. Further, because of the relatively small changes of N_C with $\frac{N_{Fe}}{N_{Mn}}$, the curves in Fig. 6 can be used for finding easily, by interpolation, the carbon concentration in saturated Fe – Mn – Si – C alloys.

Investigations of the system Fe – Mn – C and of a number of quaternary alloys also showed that replacement of iron by manganese leads to an almost linear variation of carbon solubility. Therefore the carbon content of a saturated 4-component alloy can be determined by the rule of mixtures:

$$[\%\,C]_{Mn,\,Fe,\,Si} = \frac{[\%\,Fe]\,[\%\,C]_{Fe,\,Si}}{[\%\,Fe] + [\%\,Mn]} + \frac{[\%\,Mn]\,[\%\,C]_{Mn,\,Si}}{[\%\,Fe] + [\%\,Mn]},$$

where $[\%\,C]_{Mn,\,Fe,\,Si}$; $[\%\,C]_{Fe,\,Si}$; $[\%\,C]_{Mn,\,Si}$ are the solubilities of carbon (in wt.%) in Mn – Fe – Si, Fe – Si, and Mn – Si alloys respectively, with a fixed silicon concentration.

The solubilities of carbon in binary alloys at 1460° are conveniently found either from the graphs given earlier, or from the interpolation formulas

$$\lg [\%\,C]_{Fe,\,Si} \cong 0.7 - 0.0435\,[\%\,Si],$$

$$\lg [\%\,C]_{Mn,\,Si} \cong 0.886 - 0.0161\,[\%\,Si] - 0.0010\,[\%\,Si]^2.$$

The plotting of quaternary solubility diagrams involves certain difficulties. It is therefore convenient to represent the determination results in the form of parametericgraphs ([% C] = const.), the alloy composition

being recalculated on the assumption that the sum of its iron, manganese, and silicon contents is 100%. It is evident that

$$[\%\, i]_r = \frac{[\%\, i]_t}{100 - [\%\, C]},$$

where $[\%i]_r$ and $[\%i]_t$ are the recalculated and true contents of the alloy components.

The results of such calculations are presented in Fig. 7. It is seen that the solubility of carbon varies almost linearly with changes of the ratio [% Fe]:[% Mn]. Low-silicon alloys are the most sensitive to replacement of iron by manganese. The effect of manganese on the solubility of carbon decreases with increasing silicon content, and at [% Si] > 30% the isoconcentration lines become almost parallel to the (Mn, Fe) base of the triangle.

It should be noted that the activity coefficient of carbon varies similarly with composition (Fig. 8).

The fact that silicon has a greater influence on the solubility of carbon in Fe – Si – C than in Mn – Si – C alloys can probably be ascribed to differences in the degree of microheterogeneity of the melts. Indeed, it is clear both from thermochemical data [13] and the structure of phase diagrams for the systems Mn – Si and Fe – Si [14] that the bonds between Fe and Si atoms are more stable than between Mn and Si atoms. If, moreover, it is taken into account that the bond energy between carbon and manganese atoms is considerably greater than between carbon and iron [13], the cause of the higher microheterogeneity in Fe – Si – C alloys as compared with Mn – Si – C alloys becomes evident. It follows directly from this that silicon has the greater influence on the activity coefficient of carbon in iron – silicon alloys, at least at not excessively high concentrations, when changes in the coordination of the atoms may be disregarded.

In particular, this is consistent with the views of Pearson and Turkdogan [15], according to whom the mutual activity decrease of the components of a melt becomes more pronounced as the decrease of free energy resulting from their interaction becomes greater. It may be noted that in the formation of solutions of different concentrations the ratio of the values of ΔF_{ij} may in the first approximation be estimated from the heat effect of the process ΔH_{ij}.

The same qualitative results are derived more rigorously, for example by the theory of strictly regular solutions [16], in the zero approximation of which

$$\ln \gamma_i = \frac{\omega}{kT} N_j^2,$$

where ω is an energy characteristic of the system which determines the difference between the potential energy of interaction of two pairs on unlike particles (ij) in the solution, and the potential energy of (ii) and (jj) pairs.

Therefore the decrease of the activity coefficient of carbon in its alloys with iron on addition of manganese is due to strengthening of the C – Me bonds, as $\epsilon_{Mn,\,C} > \epsilon_{Fe,\,C}$. The increase of the solubility of carbon with increased manganese content in the alloys is a direct consequence of this. Here, as in a number of other systems [15, 17, 18] there is a linear relationship between $\log \gamma_C$ and silicon concentration.

The increase of the activity coefficients of carbon and the decrease of its solubility on addition of silicon to alloys are due to strengthening of the bonds between the metal and metalloid particles, i.e., formation of cybotactical groups, enriched with Me, Si on the one hand and with Me, C on the other, since $\epsilon_{Me,\,Si} > \epsilon_{Me,\,C}$.

As the replacement of small amounts of iron by manganese has a relatively weak effect on the thermodynamic properties of carbon, it may be assumed that the above considerations are also relevant to discussion of the qualitative characteristics of the quaternary system Fe – Mn – Si – C. In this case, however, it is necessary to take into account the possible formation of more diverse cybotactical groups, which may arise, for example, by increase of the bond energy between silicon and iron atoms in the one hand, and between carbon and manganese atoms on the other.

It is for this reason that the influence of manganese on the solubility of carbon is fairly pronounced only in low-silicon alloys. In such systems silicon atoms are present mainly in pairs with iron atoms. Particles of Fe, Mn, and C accumulate in adjoining regions. In view of the above-mentioned inequality $\epsilon_{Mn, C} > \epsilon_{Fe, C}$ the activity coefficient of carbon decreases with increase of manganese content in the alloy, i.e., with increased strengthening of the bonds between the carbon particles and the metal. Increase of the silicon content of the alloy first changes the composition of the cybotactical groups (a decrease of the content of iron atoms in regions rich in carbon), and then leads to almost complete bonding of iron and manganese atoms in the form of dynamic groupings, analogs of the monosilicides. Under such conditions the formation of carbon-rich cybotactical groups becomes improbable, and the solubility of carbon becomes only slightly sensitive to changes of the $N_{Fe} : N_{Mn}$ ratio, thus, the isoconcentration curves in Fig. 7 become virtually parallel to the (Mn, Fe) base of the triangle.

In conclusion, we must again point out that the above data, according to which $\gamma_{Mn, Si} > \gamma_{Fe, Si}$ (at high silicon concentrations), require further verification. It is quite possible that this result was the consequence of insufficient accuracy in determinations of the solubility of carbon in high-silicon alloys. Otherwise it would be necessary to take into account changes in the coordination of the atoms, and other characteristics of concentrated solutions, to explain this inequality.

SUMMARY

1. The solubility of carbon in binary Fe — Si and Mn — Si alloys at 1460° was studied and it was found that the activity coefficient of carbon increases with increase of silicon concentration, more rapidly in the first system than in the second. In Mn — Fe alloys increase of manganese concentration leads to a slight decrease of γ_C.

2. Studies of the solubility of carbon in Fe — Mn — Si alloys showed that the activity coefficient of carbon increases with the silicon content in this system also. Replacement of Fe by Mn (most sensitive at low N_{Si}) leads to an almost linear decrease of the activity coefficient.

3. The explanation of these variations of γ_C with composition is that the bond energy of silicon is higher with iron than with manganese, whereas the reverse is true for carbon. It was found that these quantitative relationships can be approximately represented by equations which follow from the theory of strictly regular solutions.

LITERATURE CITED

[1] E. S. Greiner, J. S. Marsh, and B. Stoughton, Alloys of Iron and Silicon (GONTI Ukraine, 1936) [Russian translation].

[2] R. P. Smith, J. Am. Ch. Soc., 68, 1163 (1946); 70, 2724 (1948).

[3] A. I. Samarin and L. A. Shvartsman, Bull. Acad. Sci. USSR, Div. Chem. Sci. 11, 1696 (1950).

[4] C. E. Williams and C. E. Sims, Trans. Am. Electroch. Soc., 41, 63 (1922).

[5] K. Honda and T. Murakami, Sci. Rep. Sendai, 12, 257 (1923).

[6] K. Schichtel and E. Piwowarsky, Arch. Eisenhüttenwesen, 3, 139 (1929).

[7] C. H. Hilty and M. B. Royer, U. S. Bur. Mines Inform. Circul., 3230 (1934).

[8] J. Chipman, Disc. Far. Soc., 4, 23 (1948).

[9] J. Chipman et al., Trans. Am. Soc. Metals 44, 1215 (1952).

[10] E. T. Turkdogan, R. A. Hancock and S. T. Herlitz, J. Iron Steel Inst., 182, 274 (1956).

[11] O. A. Esin and N. A. Vatolin, J. Appl. Chem. 27, 1252 (1954).*

[12] E. T. Turkdogan and L. E. Leake, J. Iron Steel Inst., 179, 39 (1955).

* Original Russian pagination. See C. B. Translation.

[13] O. Kubaschewski and E. Evans, Metallurgical Thermochemistry (IL, 1954) [Russian translation].

[14] M. Hansen, Structure of Binary Alloys (Metallurgy Press, 1941) [Russian translation].

[15] J. Pearson and E. Turkdogan, Problems of Modern Metallurgy 6, 53 (1954).

[16] M. I. Shakhparonov, Introduction to the Molecular Theory of Solutions [in Russian] (GITTL, 1956).

[17] J. Chipman, J. Iron Steel Inst., 180, 97 (1955).

[18] N. I. Levenets and A. M. Samarin, Proc. Acad. Sci. USSR 101, 1089 (1955).

Received May 21, 1957

GAS-PHASE MASS-TRANSFER COEFFICIENTS*

G. N. Gasyuk, A. G. Bol'shakov, A. V. Kortnev,

and P. Ya. Krainii

Odessa Polytechnic Institute

Our earlier investigations [1, 2] confirm the results of studies [3, 4] which suggest that gas lifts can be used as highly effective absorption equipment.

In an earlier paper [1] we gave the results of an investigation of the dependence of the liquid-phase mass-transfer coefficient in a gas lift on the volumetric liquid rate and the immersion depth.

If the dependence of the gas-phase mass-transfer coefficient on the volumetric gas rate and the immersion depth is known, the absorption efficiency of gas-lift equipment can be determined more fully. Moreover, if the dependence of the partial mass-transfer coefficients on the principal factors is known, and the relationships are presented as generalized equations in criterial form, it would be possible to perform calculations relating to absorption processes in gas lifts regardless of variations of the gas-liquid system.

The experimental unit described previously [1] was used for experimental determination of gas-phase mass-transfer coefficients in a gas lift.

The gas-phase mass-transfer coefficients were determined for the absorption of the following gases: ammonia from air – ammonia mixture by water, sulfur dioxide from air – sulfur dioxide mixture by caustic potash solutions, and sulfur dioxide from air – sulfur dioxide mixture by water.

Preliminary experiments on the absorption of ammonia by water showed that the gas and liquid phases always reached a state approaching equilibrium, with wide variations of the gas and liquid rates (because of the high efficiency of the gas lift in uniflow). Therefore this system could not be used for determination of the gas-phase mass-transfer coefficient.

In the absorption of sulfur dioxide by caustic potash solutions, the degree of absorption reached 98 – 100% for all the gas and liquid rates used, and therefore satisfactory results could not be obtained with this system either.

Since we did not succeed in determing the gas-phase mass-transfer coefficient by a direct method, we used the system sulfur dioxide – air – water. Sulfur dioxide is a gas of moderate solubility, and therefore the diffusion resistances in the gas and liquid phases are comparable in magnitude. Therefore the over-all mass-transfer coefficients were determined in this case, and the gas-phase coefficients were then calculated from them.

The gas-phase mass-transfer coefficient for the system ammonia – water was determined previously by a similar method [5].

Calculation method. The over-all mass-transfer coefficient was calculated from the equation

$$K_{Gen}{}^{a} = \frac{G}{V_1 \cdot \Delta p_{av}} \left[\frac{kg}{m^3 \cdot hour \cdot atmos}\right], \quad (1)$$

* Communication II in the series on mass transfer in gas-lift equipment.

where G is the quantity of gas absorbed (in kg/hour), V_1 is the volume of the apparatus (in m^3), and Δp_{av} is the logarithmic mean difference between the partial pressures at the apparatus entry and exit (in atmos).

The amount of gas absorbed was calculated from the equation

$$G = \frac{60 v_0 \gamma_t 100 (c_1 - c_2)}{1000 (100 - c_1)(100 - c_2)} \left[\frac{kg}{hr}\right], \quad (2)$$

where v_0 is the volume of inert gas entering the apparatus at the experimental temperature and 760 mm Hg (in liters/minute); c_1 and c_2 are the concentrations of the absorbed gas at the entry and exit of the apparatus, where $c_1 = \frac{p_1}{p} 100$ and $c_2 = \frac{p_2}{p} 100$; γ_t is the density of the absorbed gas at the experimental temperature and 760 mm Hg (in g/liter).

The logarithmic mean difference of the partial pressures in uniflow was found from the equation

$$\Delta p_{av} = \frac{p_1 - (p_2 - p')}{2.303 \log \frac{p_1}{p_2 - p'}}, \quad (3)$$

where $p_1 = \frac{c_1}{100} \cdot \frac{p_3 + p_4}{760}$ is the partial pressure of the absorbed gas at the entry to the apparatus (in atmos); $p_2 = \frac{c_2}{100} \cdot \frac{p_3}{760}$ is the partial pressure (in atmos) of the absorbed gas at the exit from the apparatus (excess gas pressure at the exit was disregarded, as it did not exceed 10 mm H_2O at even the highest gas rates); p_3 is the barometric pressure in mm Hg; p_4 is the gaseous pressure at the entry to the apparatus, in mm Hg; p' is the equilibrium partial pressure of the soluble gas, corresponding to its concentration in water (in atmos).

The equation

$$\frac{1}{K_{Gen} a} = \frac{1}{k_G a} + \frac{1}{k_L a H} \quad (4)$$

was used to calculate, from the value found for the over-all coefficient, the gas-phase coefficient

$$k_G a = \frac{H k_L a \cdot K_{Gen} a}{H k_L a - K_{Gen} a}, \quad (5)$$

where H is the Henry coefficient (in $kg/m^3 \cdot$ atmos). Since the system silfur dioxide – water deviates from Henry's law at low concentrations, the mean integral value of the Henry coefficient was calculated; $k_L a$ is the liquid-phase mass-transfer coefficient (in $hour^{-1}$).

The liquid-phase mass-transfer coefficient was determined from our criterial equation [1], applied to the system sulfur dioxide – water at $Re_L < 1400$ and immersion depth 20%.

$$Nu'_L = 0.0056 Re_L^{0.91} (Pr'_L)^{0.5} \left(\frac{h}{20}\right)^{-0.7} \quad (6)$$

Dependence of the gas-phase mass-transfer coefficient on the volumetric gas rate and immersion depth. Three series of experiments, at 20° and immersion depths of 10, 20, and 30%, were performed for determination of the influence of the gas rate and immersion depth on the gas-phase mass-transfer coefficient.

In each series of experiments the immersion depth was kept constant, and the volumetric gas and liquid rates were varied. For immersion depth of 10% the gas rate was varied approximately 4.2-fold (from 4680 to

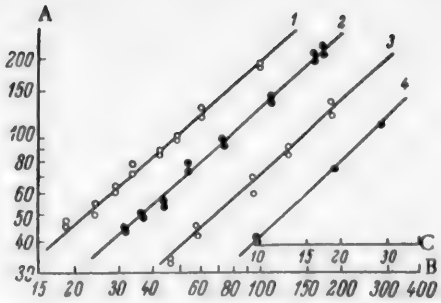

Fig. 1. Variation of the gas-phase mass-transfer coefficient with the volumetric gas rate (1, 2, 3) and with the immersion depth (4):
A) mass-transfer coefficient $k \cdot 10^{-3}$ (kg/m³ · atmos · hour), B) volumetric gas rate $V \cdot 10^{-2}$ (m³/m² · hour), C) immersion depth (%).

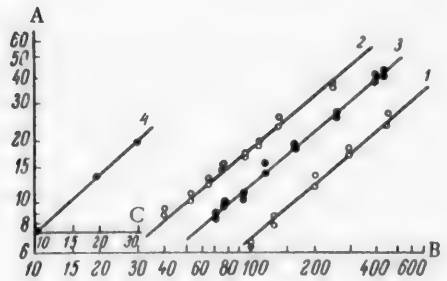

Fig. 2. Variations of $\frac{Nu'_G}{(Pr'_G)^{2/3}}$ with Re_G (1, 2, 3) and variations of $\frac{Nu'_G}{(Pr'_G)^{1/3}}$ with immersion depth (4):
A) $\frac{Nu'_G}{(Pr'_G)^{1/3}}$, B) Re_G, C) immersion depth (%).

19820 m³/m² · hour); at 20%, 5.8-fold (from 3150 to 18520 m³/m² · hour), and at 30%, 5.6-fold (from 1900 to 10730 m³/m² · hour).

The results are plotted in Fig. 1 in logarithmic coordinates.

The values found for the gas-phase mass-transfer coefficients fit satisfactorily on straight lines for $k_G a = f(V)$. Line 1 represents the mass-transfer coefficients for 30% immersion, Line 2, for 20% immersion, and Line 3, for 10% immersion.

The relationship between the mass-transfer coefficient and the gas rate can be represented by the following equation:

$$k_G a = a \cdot V^{0.87} \qquad (6)$$

Line 4 in Fig. 1 represents variations of the gas-phase mass-transfer coefficient with immersion depth. This relationship can be expressed as

$$k_G a = b \cdot h^{0.906}. \qquad (7)$$

If both the gas rate and immersion depth are taken into account, the general expression for the mass-transfer coefficient becomes

$$k_G a = 39.9 V^{0.87} \left(\frac{h}{20}\right)^{0.906}, \qquad (8)$$

where V is the volumetric gas rate (m³/m² · hour), and h is the immersion depth (%).

Analysis of experimental data by means of the similarity theory. The experimental data were analyzed, in order to present the relationship between the gas-phase mass-transfer coefficient and its determining factors in the form of power functions of dimensionless criteria, by Bol'shakov's method [6]:

$$Nu'_G = A Re_G^n (Pr'_G)^m, \qquad (9)$$

where $Nu'_G = \frac{(P_i)_{av} k_G a d}{D_G \gamma_a} \sqrt{\frac{\sigma_L}{\gamma_L}}$ is a gas-phase diffusion criterion of the Nusselt type; $\frac{w \cdot d \cdot \gamma_G}{\eta_G}$ is the Reynolds number for the gas; $Pr'_G = \frac{\eta_G}{\gamma_G D_G}$ is the Prandtl diffusion number for the gas; k_G is the gas-phase mass-transfer coefficient (kg · m³ · hour · atmos), $(P_i)_{av}$ is the average partial pressure of the inert gas in the gas phase (atmos); σ_L is the coefficient of surface tension (in kg/m); γ_L is the density of the liquid (kg/m³); γ_a is the density of the absorbed component (kg/m³); γ_G is the density of the gas stream (mg/m³); η_G is the coefficient of viscosity of the gas stream (kg/m · hour); D_G is the diffusion coefficient of the soluble component in the gas phase (m²/hour), w is the virtual gas velocity in the gas lift (in m/hour), and d is the diameter of the gas lift (m).

The effects of the physical properties of the gas and of the temperature on the gas-phase mass-transfer coefficient were not investigated specially. The influence of the physical properties of the gas-phase on the mass-transfer coefficient is taken into account by the introduction of the Prandtl diffusion criterion raised to the power $^2/_3$.

If the power of the Prandtl diffusion criterion is taken to be $^2/_3$, we have a dimensionless equation of the form

$$Nu'_G = A \cdot Re_G^n (Pr'_G)^{1/3}. \quad (9a)$$

For determination of the constant A and the index n in this equation, the values of Nu'_G Re_G $(Pr'_G)^{2/3}$ were calculated for each series of experiments, and the relationship $Nu'_G/(Pr'_G)^{2/3} = f(Re_G)$ was plotted in logarithmic coordinates (Fig. 2). Line 2 represents values of $Nu'_G/(Pr'_G)^{2/3}$ at 30% immersion, Line 3, at 20% immersion, and Line 1, at 10% immersion.

The equation for these lines is of the form

$$\frac{Nu'_G}{(Pr'_G)^{1/3}} = A \cdot Re_G^{0.87} \quad (10)$$

or

$$Nu'_G = A \cdot Re_G^{0.87} (Pr'_G)^{1/3}. \quad (10a)$$

Line 4 in Fig. 2 represents variations of Nu'_G with immersion depth. The equation for this line is

$$Nu'_G = B \cdot h^{0.906}. \quad (11)$$

The effects of gas rate and immersion depth on Nu'_G can be represented by the following general equation:

$$Nu'_G = 0.032 Re_G^{0.87} \cdot (Pr'_G)^{1/3} \cdot \left(\frac{h}{20}\right)^{0.906}. \quad (12)$$

SUMMARY

A general equation for the similarity criteria, for calculation of the gas-phase mass-transfer coefficient, was derived:

$$Nu'_G = 0.032 Re_G^{0.87} (Pr'_G)^{1/3} \left(\frac{h}{20}\right)^{0.906}$$

this equation, together with the general criterial equations for calculation of the liquid-phase mass-transfer coefficients, derived earlier [1]:

for $Re_L < 1400$

$$Nu'_L = 5.6 \cdot 10^{-5} Re_L^{0.91} (Pr'_L)^{0.5} \left(\frac{h}{20}\right)^{0.7},$$

for $Re_L > 1400$

$$Nu'_L = 246 \cdot 10^{-8} Re_L^{1.98} (Pr'_L)^{0.5} e^{-0.0362(h-20)}.$$

can be used for calculations relating to absorption with different gas – liquid systems in gas-lift equipment.

LITERATURE CITED

[1] G. N. Gasyuk, A. G. Bol'shakov, A. V. Kortnev, and P. Ya. Krainii, J. Appl. Chem. 31, 1019 (1958).*

[2] G. N. Gasyuk, P. Ya. Krainii, and A. G. Bol'shakov, J. Appl. Chem. 31, No. 12, 1787 (1958).*

[3] E. K. Lopatto and L. I. Aleksandrova, Trans. Mechnikov State Univ. Odessa, Coll. Chem. Faculty 2 (1952).

[4] G. O. Grigoryan and A. G. Bol'shakov, Sci. Mem. Odessa Polytech. Inst. 2 (1955).

[5] N. M. Zhavoronkov et al., J. Chem. Ind. 8 (1951); 4 (1953).

[6] A. G. Bol'shakov, Sci. Mem. Odessa Polytech. Inst. 2 (1954).

Received May 8, 1957

* Original Russian pagination. See C. B. Translation.

THE SOLUTION RATES OF METHANE AND NITROGEN – HYDROGEN MIXTURE IN CONDENSING AMMONIA*

V. I. Atroshchenko and N. A. Gavrya

The V. I. Lenin Polytechnic Institute, Khar'kov

Nitrogen – hydrogen mixture made by gasification of low-grade fuel from natural gas and other sources has a high methane content. The presence of methane in the gas mixture entering the ammonia-synthesis cycle leads to high losses of nitrogen – hydrogen mixture with the blow gas, and hence to higher ammonia costs. Losses of nitrogen – hydrogen mixture can be avoided by increase of the methane partial pressure in the gas mixture circulating in the ammonia-synthesis system. Most of the methane coming in with fresh gas mixture is then dissolved in liquid ammonia and is removed with it from the system. The amount of blow gas decreases sharply. Because of the decreased partial pressure of nitrogen – hydrogen mixture, less of it is lost by solution in liquid ammonia.

Several investigators have studied the solubility of nitrogen – hydrogen mixture and methane in liquid ammonia. According to Larson and Black [1], the solubility of 1:3 nitrogen – hydrogen mixture is more than doubled by a temperature rise of 50°. The effect of pressure conforms to Henry's law.

Ipat'ev and Teodorovich [2] studied the solubility of hydrogen in liquid ammonia at 25° and pressures from 15 to 250 atmos. Slight deviations from Henry's law were observed.

Wiebe and Tremearne [3, 4] and Wiebe and Caddy [5] studied the solubility of hydrogen and nitrogen in liquid ammonia over wider pressure and temperature ranges.

Bol'shakov and Lebedeva [6] studied the solubility of nitrogen – methane mixture (78.8% N_2 + 21.2% CH_4) in liquid ammonia. The Krichevskii – Kazarnovskii equation [7] was used to calculate the solubility of pure methane in liquid ammonia. The effects of pressure and temperature on the solubility were determined.

Valuable data on the solubility of 1:3 nitrogen – hydrogen mixture in liquid ammonia at high pressures were also obtained by Bol'shakov [8].

The work of Krichevskii [9] and Krichevskii and Kazarnovskii [7] is of great theoretical and practical significance. Their equations can be used for calculating the solubilities of the components of a gas mixture in liquids at high pressures. These equations were used to calculate the solubilities of nitrogen – hydrogen mixture and methane in liquid ammonia at pressures from 300 to 600 atmos and temperatures of 25 and 40°.

It must be pointed out, however, that the experimental and calculated data on the solubilities of the components of gas mixtures in liquid ammonia were found for equilibrium liquid – gas systems. The experiments were performed by the static method. Equilibrium was attained by prolonged contact, lasting hours or days, between the gas and liquid ammonia in a rocking autoclave or in an autoclave with an electromagnetic stirrer. In industrial processes for ammonia synthesis, however, the components of the gas mixture are dissolved continuously in liquid ammonia during condensation and separation of the ammonia. The contact time of the gas with liquid ammonia is measured in seconds. The composition of the gas over the liquid ammonia remains virtually constant.

* This paper represents a part of the dissertation work performed by N. A. Gavrya.

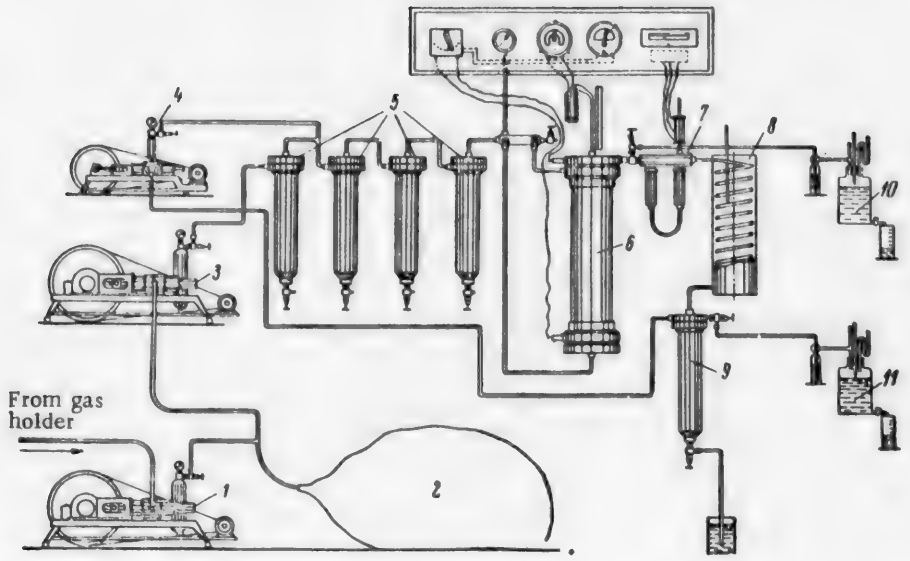

Fig. 1. Diagram of experimental unit:
1) pump, 2) rubber gas holder, 3) compressor, 4) circulating pump, 5) filters, 6) synthesis column, 7) high-pressure rheometer, 8) condenser, 9) separator, 10, 11) aspirators.

In the present investigation the solution rates of methane and nitrogen – hydrogen mixture in condensing ammonia were studied under conditions close to those in the industrial process: pressure 300 atmos, ammonia condensation temperature from 10 to 30°, and space velocities from 30,000 to 60,000 m^3/m^3 of catalyst per hour, corresponding to contact times from 40 to 20 seconds between gas and liquid.

EXPERIMENTAL

The experiments were performed in a large-scale laboratory unit for ammonia synthesis, operating by a circulation scheme (Fig. 1).

Nitrogen – hydrogen mixture was made by decomposition of ammonia and then purified under atmospheric pressure. Methane was added to the gas mixture in a wet gas holder. Methane of Metilopol' origin, previously freed from oxygen, was used.

The gas mixture was compressed to 300 atmos and fed into the unit. The fresh and circulating gases were freed from oil and dried by means of filters packed with activated charcoal, silica gel, fused alkali, and cotton wool. The synthesis column was filled with 100 cc of industrial catalyst. The catalyst was reduced by pure nitrogen – hydrogen mixture at 100 atmos and 500°. The synthesized mixture was condensed in a coil immersed in a thermostat. A double-action pump was used for circulating the gas. The space velocity was measured by means of a high-pressure rheometer with an induction device.

Samples of the circulating gas were taken from the upper part of the separator and analyzed for ammonia, hydrogen, nitrogen, and methane. Samples of liquid ammonia were taken from the lower part of the separator and analyzed as described earlier. The VTI apparatus was used for gas analysis.

The temperature of the medium surrounding the separator was maintained equal to the condensation temperature by thermostatic control. Before samples of liquid ammonia were taken, the separator was blown through, and freshly-formed ammonia was taken for analysis. Under such conditions it was not possible for methane, nitrogen, and hydrogen to pass from the liquid into the gas phase, or from the gas phase into the liquid, while the liquid ammonia was in the separator.

TABLE 1

Amounts of Methane Dissolved in Condensing Ammonia (cc CH_4 at 0° and 760 mm per g NH_3) Pressure 300 Atmos, Contact Time of Gas and Liquid NH_3 40 Seconds (space velocity 30,000 m^3/m^3 catalyst per hour)

Condensation temperature (°C)											
−10		0		10		20		25		30	
CH_4 content of circulating mixture (%)	cc CH_4 / g NH_3	CH_4 content of circulating mixture (%)	cc CH_4 / g NH_3	CH_4 content of circulating mixture (%)	cc CH_4 / g NH_3	CH_4 content of circulating mixture (%)	cc CH_4 / g NH_3	CH_4 content of circulating mixture (%)	cc CH_4 / g NH_3	CH_4 content of circulating mixture (%)	cc CH_4 / g NH_3
2.9	1.346	2.86	1.5	1.75	1.045	2.13	1.79	2.8	2.33	3.23	3.57
4.36	1.8	8.1	4.77	2.8	1.8	6.12	3.6	4.6	3.0	4.2	4.4
5.3	2.29	12.3	6.89	4.74	3.33	10.3	7.8	6.3	5.76	6.3	7.05
5.5	2.58	15.86	8.6	6.2	4.2	11.8	9.4	7.9	7.54	7.85	8.85
7.22	3.38	19.4	11.0	8.2	5.3	14	10.5	8.35	7.8	9.66	10
8.65	4.1	23.6	13.4	9.6	6.2	14.2	10.7	8.75	7.9	10.13	11.26
—	—	25.6	14.1	11.31	7.4	—	—	9.25	8.6	—	—
—	—	27.4	15.5	—	—	—	—	10.5	10.8	—	—
—	—	—	—	—	—	—	—	12.4	11.3	—	—

TABLE 2

Values of the Coefficient k in Equation (1)

Condensation temperature (°C)	−10	0	10	20	25	30
Coefficient k	0.15	0.19	0.22	0.256	0.311	0.357

TABLE 3

Amounts of Methane Dissolved in Condensing Ammonia (cc CH_4 at 0° and 760 mm per g NH_3) Pressure 300 Atmos, Condensation Temperature 0°

Contact time t of gas with liquid ammonia (seconds), and space velocity V (m^3/m^3 catalyst per hour)					
$t = 40$, $V = 30000$		$t = 30$, $V = 45000$		$t = 20$, $V = 60000$	
CH_4 content of circulating mixture (%)	cc CH_4 / g NH_3	CH_4 content of circulating mixture (%)	cc CH_4 / g NH_3	CH_4 content of circulating mixture (%)	cc CH_4 / g NH_3
2.86	1.5	2.39	0.78	5.27	2.88
8.1	4.77	7.21	3.88	6.7	3.95
12.3	6.89	11.0	6.06	11.99	7.2
15.86	8.6	13.4	7.5	19.0	10.9
19.4	11.0	17.25	9.6	20.01	11.8
23.6	13.4	20.1	11.6	22.5	13.3
25.6	14.1	—	—	—	—
27.4	15.5	—	—	—	—

RESULTS AND DISCUSSION

It follows from the experimental data (Table 1 and Fig. 2) that the amount of methane dissolved in liquid ammonia is proportional to the methane content of the circulating mixture.

TABLE 4

Amounts of Nitrogen – Hydrogen Mixture Dissolved in Liquid Ammonia (cc of Gas at 0° and 760 mm per g NH_3). Total Pressure 300 Atmos

Condensation temperature (°C)	−10	0	10	20	25	30
Amount of nitrogen – hydrogen mixture	18.75	20.41	22.46	23.9	24.35	27.79

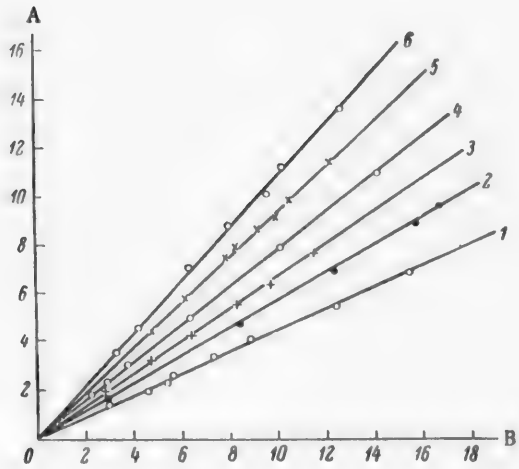

Fig. 2. Variation of the amount of methane dissolved in liquid ammonia with the methane content of the circulating mixture:
A) amount of methane (in cc CH_4 at 0° and 760 mm; per 1 g NH_3), B) CH_4 content of circulating mixture (%); condensation temperature (°C):
1) – 10, 2) 0, 3) 10, 4) 20, 5) 25, 6) 30.

This can be expressed as

$$S = kp, \qquad (1)$$

where S is the amount of methane dissolved in liquid ammonia (in cc CH_4 at 0° and 760 mm per g NH_3); k is a coefficient which depends on the circulation temperature (Table 2); p is the methane partial pressure in the circulating gas, in atmos.

The amount of methane dissolved in liquid ammonia increases linearly with increase of the condensation temperature from −10 to +15°; above 20° the solubility of methane increases sharply (Fig. 3).

It follows from Table 3 and Fig. 4 that the contact time of the gas with liquid ammonia has no effect on the amount of methane dissolved in liquid ammonia during its condensation. The shortest contact time of the gas with liquid ammonia was 20 seconds (at a space velocity of 60,000 m^3/m^3 catalyst per hour). At condensation temperature 25° our experimental results are in good agreement with calculated data for equilibrium in the liquid – gas system (Figs. 3 and 4).

The foregoing data lead to the conclusion that the solution rate of methane in condensing liquid ammonia is high. The contact time of the gas with liquid ammonia is sufficient for equilibrium to be established between the liquid and gas phases at all the condensation temperatures and space velocities studied. In industrial ammonia-synthesis systems methane dissolves in liquid ammonia mainly at the instant when the ammonia passes from the gaseous to the liquid state. The area of contact between the gas and liquid ammonia is very extensive at that instant.

The solubility of nitrogen – hydrogen mixture in liquid ammonia was found from the amounts of nitrogen and hydrogen dissolved. The partial pressures of nitrogen and hydrogen in the circulating mixture varied only slightly, and therefore the solubility of nitrogen – hydrogen mixture in liquid ammonia was determined from the average solubilities of nitrogen and hydrogen over the whole experiment.

The average experimental data on the amounts of nitrogen – hydrogen mixture dissolved in condensing ammonia are presented in Table 4.

It must be noted that the contact time of the gas with liquid ammonia does not effect the amount of nitrogen – hydrogen mixture dissolved in the ammonia.

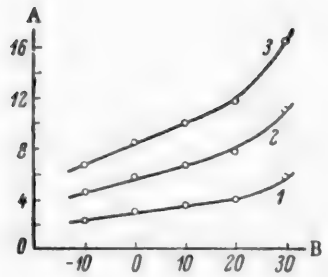

Fig. 3. Effect of ammonia condensation temperature on the amount of methane dissolved in liquid ammonia:
A) amount of methane (in cc CH_4 at 0° and 760 mm per g NH_3), B) temperature (°C); contents of methane in circulating mixture (%): 1) 5, 2) 10, 3) 15.

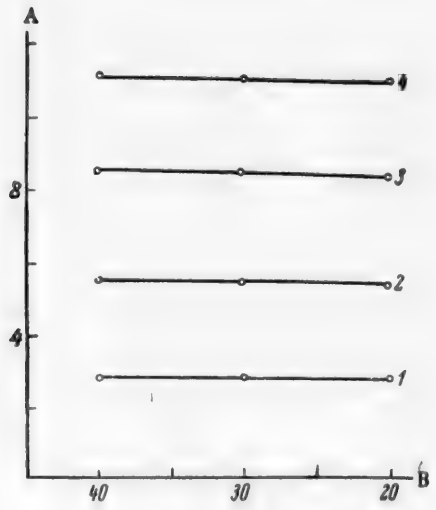

Fig. 4. Effect of contact time between gas and liquid on the amount of methane dissolved in condensing ammonia:
A) amount of methane (in cc CH_4 at 0° and 760 mm per g NH_3), B) contact time (seconds); methane contents in circulating mixture (%): 1) 5, 2) 10, 3) 15, 4) 20.

SUMMARY

1. The solubility of methane and of nitrogen – hydrogen mixture in liquid ammonia during condensation and separation of the ammonia was studied; it was found that the amount of methane dissolved in liquid ammonia is proportional to its partial pressure in the circulating mixture. The proportionality coefficients were calculated.

2. The space velocity has no effect on the amounts of methane or nitrogen – hydrogen mixture dissolved in condensing ammonia. The contact time of the gas with liquid ammonia during condensation and separation of the ammonia is sufficient for a state of equilibrium to be reached between the liquid and gas phases.

LITERATURE CITED

[1] Larson, Black, Ind. Eng. Ch., 17, 715 (1925).

[2] V. V. Ipat'ev and V. P. Teodorovich, J. Gen. Chem. 2, 305 (1932).

[3] Wiebe and Tremearne, J. Am. Chem. Soc. 55, 975 (1933).

[4] Wiebe and Tremearne, J. Am. Chem. Soc. 56, 2357 (1934).

[5] Wiebe and Caddy, J. Am. Chem. Soc. 59, 1984 (1937).

[6] P. E. Bol'shakov and E. S. Lebedeva, J. Phys. Chem. 14, 261 (1940).

[7] I. R. Krichevskii and Ya. S. Kazarnovskii, J. Phys. Chem. 6, 1321 (1935).

[8] P. E. Bol'shakov, Trans. State Sci. Res. Inst. Nitrogen Industry, 4 [in Russian] (Goskhimizdat, 1954).

[9] I. R. Krichevskii, Phase Equilibria in Solutions at High Pressures [in Russian] (Goskhimizdat, 1952).

Received June 10, 1957

TECHNOLOGY OF THE PRODUCTION OF IODINE BY AN ELECTROCHEMICAL METHOD

Ya. I. Gamzulov

The existing methods for extraction of iodine from salt solutions or oil-well brines [1 – 8] are complicated, and in most cases require the use of valuable chemicals.

The present paper deals with an electrochemical process for extraction of iodine from iodine solutions. The process can be used for extraction of iodine in presence of chlorides and other salts.

EXPERIMENTAL

Design and operation of the electrolytic unit. Our problem was the isolation of iodine from oil-well brines containing not more than 30 mg of iodide per liter.

The composition of brines concentrated by the adsorption method* and then treated by the electrolytic process is given in Table 1.

Laboratory experiments on the electrochemical isolation of iodine showed that in absence of a diaphragm the iodine liberated at the carbon anode mixes with the alkali formed at the cathode before it can settle to the bottom of the vessel, and reacts with it by the known reaction [6]

$$6KOH + 3I_2 \rightarrow KIO_3 + KI. \quad (1)$$

A rational method for preventing this reaction is the use of a diaphragm to separate the cathode and anode compartments. If this is done, the necessary degree of acidity can also be maintained in the cathode compartment.

Diaphragms. Clay diaphragms of our own make, consisting of beakers of the required size, were used. The material used for the diaphragms was a mixture of clay with Atterberg plasticity number 20-28 (60 – 70%), sand with grains < 0.01 mm (40 – 30%), and sawdust. The clay beakers were dried in air and fired in kilns; the fired wares were adequately microporous.

The clay diaphragms were serviceable for about a year. After a year they gradually disintegrated, usually from the top end.

Electrolytic tanks. It was found that ordinary birch or pine boards are quite suitable for the construction of electrolytic tanks (Fig. 1) up to 700 liters in capacity, provided that the moisture content of the wood does not exceed 8 – 10% and that the boards are free from knots. The tank joints are luted with water glass. The side walls of the tank are tightened by means of iron bolts. The assembled tanks are treated with steam until the moisture content of the wood has risen to 30 – 40%. Treatment of the tank walls with water is not recommended, as water leaches out the soluble water glass from the joints. After the steam treatment the joints do not leak even if the density of the electrolyte is 1.40. The use of lacquers, asphalt, or Mendeleev's grease for covering parts of the tank is not recommended, as these substances gradually enter the electrolyte and strongly contaminate the product.

The electrodes were round, made of carbon, 50 mm in diameter and 800 mm long. Two electrodes were contained in each diaphragm. The electrodes were used for two years without any sign of destruction, and were

* The adsorbent was peat from sphagnum moss, packed into barrels through which the brines were passed. After the brines had been passed through 10-12 such barrels the iodide concentration in the water fell from 30 to 1 mg/liter. The peat was ashed and leached.

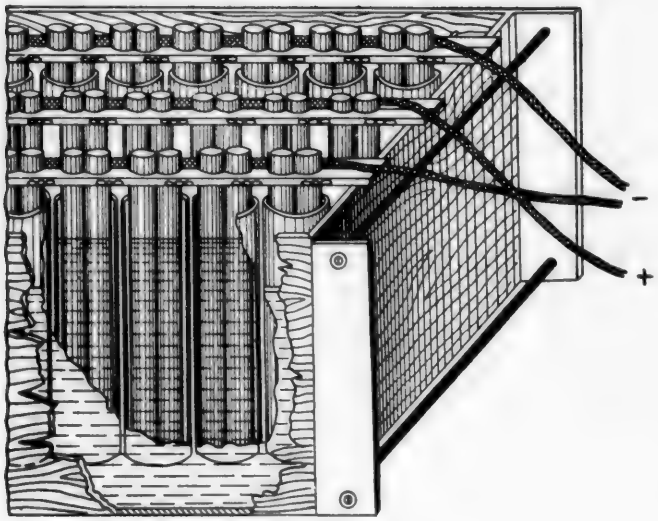

Fig. 1. Electrolytic tank.

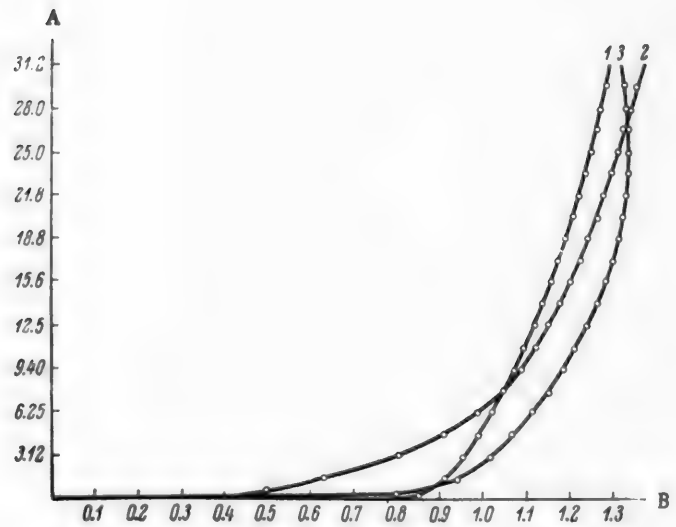

Fig. 2. Current density – voltage curves:
A) current density (ma/cm^2), B) voltage (v); composition of solutions (in g-equiv/liter): 1) $CaCl_2$ 7.28, KI 0.0714, HCl 0.10; 2) NaCl 2.32, KI 0.025, HCl 0.10; 3) KI 0.0512, HCl 0.10.

unchanged in appearance at the end of that time. This result is noteworthy, as it shows a radical difference between the behavior of amorphous-carbon and graphite electrodes in acid media, and in the electrolysis of sodium chloride brines in alkaline media. Ordinary domestic carbons, not impregnated, proved very resistant in our experiments; this shows that the existing concepts of the destruction mechanism of carbon and graphite electrodes during electrolysis of sodium chloride in aqueous solutions [9, 10] cannot be regarded as fully substantiated.

Electrode connections. The carbon electrodes were connected in pairs. The paired electrodes were held in wooden planks which were clamped by iron bolts. Copper conductors 50 mm in diameter were attached along

the wooden planks. Each electrode pair was connected to the copper conductor. The upper ends of the carbon electrodes were coppered.*

The central electrode, which acted as the anode, was immersed directly in the electrolyte, while the two side electrodes, the cathodes, were placed inside the clay diaphragms.

Two cathodes were used in order to attain a more complete and uniform utilization of the anode surface.

The electrolyte. The electrolyte was a solution of the composition given in Table 1, acidified with hydrochloric acid to prevent formation of free alkali in the cathode space. Technical hydrochloric acid was poured into the diaphragms in amounts equivalent to the iodine content of the electrolyte. The concentration of the hydrochloric acid was about 3%. The electrolyte was periodically stirred with a wooden spatula during the electrolysis. 10 – 15 minutes after the end of electrolysis the iodine settled on the floor of the tank; the electrolyte was then poured off and the product was scooped out in wooden ladles and dried by suction under vacuum in a ceramic vessel.

Selection of electrolysis conditions. For selection of the electrolysis conditions, we determined the liberation potentials of iodine with anodic polarization of carbon electrodes in the systems

$$CaCl_2 + KI + HCl \text{ and } NaCl + KI + HCl. \quad (2)$$

This investigation was performed in the Electrochemical Laboratory of the A. A. Zhdanov State University, Leningrad, in 1948. The conditions for obtaining the optimum iodine yields with the minimum expenditure of power were determined from the results. The electrolyte composition, anode material, and other electrolysis conditions were similar to those used in the industrial processes.

The polarization measurements were performed by the compensation method with a circuit as described by Izgaryshev [9].

The standard calomel reference electrode had a bridge immersed in a beaker containing KCl, which was connected by a second bridge to a beaker with a solution of KI + NaCl + HCl; this prevented iodine liberated during electrolysis from entering the standard electrode.

The anodes used for measurement of the liberation potential of iodine were carbon electrodes coated with paraffin wax at the top. The working anode area was 12.8 cm^2. The composition of the electrolyte was 403 g $CaCl_2$, 9.07 g KI, and 3.65 g HCl per liter.

Fig. 2 shows the polarization curves, which are somewhat similar to the usual anodic polarization curves described in the literature for other systems [11]. It is seen that none of the solution components is oxidized up to a potential of 0.5 v (0.25 v on the standard hydrogen scale). At 0.8 v (0.55 v on the standard hydrogen scale) noticeable oxidation occurs, as shown by the increase of the current strength required to maintain the potential. Appreciable liberation of iodine occurs at this stage, evidently mainly as the result of the direct anodic reaction [2], the reversible potential of which under standard conditions is 0.54 v [13]:

$$I' - e \rightarrow \frac{1}{2} I_2. \quad (2a)$$

As the anode polarization increases, the direct reaction of KI oxidation passes into the limiting diffusion current region owing to the low iodine concentration in solution, and proceeds further at a certain constant rate which depends on the diffusion conditions in the system. The explanation of the increase in the amount of iodine liberated with further increase of anode polarization is that iodine is liberated in relatively increasing amounts as the result of a secondary reaction of type (4), which is due to the appearance in the solution of chlorine liberated at the anode:

$$Cl' - e \rightarrow \frac{1}{2} Cl_2, \quad (3)$$

$$Cl + 2I' \rightarrow 2Cl' + I_2. \quad (4)$$

* Aluminum leads are quite unsuitable for connecting the electrodes, as they are rapidly attacked by the gaseous chlorine and iodine liberated from the electrolyte.

TABLE 1

Composition of Concentrated Brines

Density of brine	Contents of salts (g/liter)					
	$CaCl_2$	$MgCl_2$	$SrCl_2$	NaCl	Na_2S	KI
1.40	400.0	0.10	Traces	Traces	3.05	16.20
1.36	368.4	0.30	0.05	"	4.05	12.10
1.180	0.18	0.85	0.75	239.2	nil	0.45
1.10	0.45	0.91	0.85	1.38	"	0.25

TABLE 2

Current Efficiencies for Iodine

Anode area (cm^2)	Current strength (amps)	Iodine content (g/liter)	Electrolyte volume (liters)	Iodine content of electrolyte (kg)	Time theoretically required for electrolysis (hours)	Time actually taken for electrolysis (hours)	Current efficiency (%)
14220	284.4	8.5	450	3.82	2.84	3.54	80.0
15600	312.0	6.85	450	3.08	2.08	2.00	80.0
14800	286.0	5.4	500	2.70	2.00	2.52	79.5
23000	460.0	12.5	500	6.25	2.86	3.56	80.2
18400	368.0	14.8	500	7.40	4.24	5.32	80.00

The iodine yield continues to increase without appreciable increase in the liberation of molecular chlorine until the liberated chlorine has time to react in the solution with the iodine ions according to Reaction (4).

The polarization curves show that at a potential of 1.31 v (1.06 v on the standard hydrogen scale) the system already approaches the region of appreciable oxidation of Cl', although the reversible potential of Reaction (3), which is 1.56 v [12], is not yet reached. The current, which has the density 0.031 amp/cm^2 at this potential, is distributed under these conditions between the reactions of chlorine and iodide oxidation approximately in proportion to their concentrations in the solution at the anode surface. Violent and "useless" liberation of gaseous chlorine is observed.

It is clear from the foregoing that the problem is to select a current density at which, for a given electrolytic cell, the ratio of the I' and Cl' concentrations near the anode is such that all the chlorine liberated at the anode and dissolved in the electrolyte can be utilized in displacement of iodine by a reaction of type (4). It was found experimentally that this optimum current density for the conditions described is 0.016 – 0.020 amp/cm^2. It follows from the polarization curves that this current density is maintained in our system at an anode potential of 1.1 – 1.2 v (0.85 – 0.95 v on the standard hydrogen scale). Under these electrolysis conditions the maximum current efficiencies for iodine are obtained, while liberation of chlorine is quite slight.

The current efficiencies for iodine, obtained in the large-scale unit described above under the chosen electrolysis conditions, are presented in Table 2.

It follows from Table 2 that the current efficiency was close to 80% in all the experiments. From the data in Table 2 it can be calculated that under the chosen electrolysis conditions the energy consumption per kg of iodine is approximately 0.7 kw-hr.*

Oxidation of iodine to iodate in an acid medium. The elemental iodine liberated by electrolysis partially remains in solution and colors the electrolyte brown. According to Nekrasov [13] the solubility of iodine in water is 300 mg/liter.

If electrolysis is continued when oxidation of iodide is complete and the iodine has been precipitated to the bottom of the cell, the anode voltage being raised to 2.5 – 3.0 v and the current density to 0.03 – 0.035 amp/cm^2, the dissolved iodine begins to be oxidized to HIO_3. As the dissolved iodine is oxidized to HIO_3, more iodine is dissolved from the precipitate, and the process continues until all the iodine is oxidized to iodate. The solution becomes colorless when the oxidation is complete. Neither free iodine nor iodide ions can be detected in the colorless electrolyte by analysis, as all the iodine is present in the solution in the form of iodate. Thus, Izgaryshev's assertion [9] that iodates can be obtained only in an alkaline medium is quite erroneous.

The iodate solution can be used for oxidation of iodide ions to molecular iodine. This operation was performed as follows. Iodine was completely oxidized to HIO_3 in the cell. The iodate solution was poured into a tank, and calculated amounts of acid and KI solution were added. Molecular iodine was precipitated according to the equation

$$HIO_3 + 5HI = 3H_2O + 3I_2. \quad (5)$$

We used this simple method with great success for isolation of iodine from iodide solutions.

It may be pointed out that the oxidation of elemental iodine to HIO_3 during electrolysis in an acid medium has not been previously described in the literature. However, the reproducible results of hundreds of our experiments on the oxidation of iodine to HIO_3 by this method show without doubt that here we have a new method for the electrolytic oxidation of elemental iodine to iodate in an acid medium.

The mechanism of anodic oxidation of iodine to iodate is far from well understood at the present time. However, in the light both of modern and of earlier concepts of anodic processes for the production of oxidizing agents in the region of high anode potentials [11, 14, 15], it seems likely that the principal role in this reaction is played by active peroxide compounds formed at the anode, or by direct electrochemical oxidation of iodine at the anode surface. There is no doubt that detailed study of this anode process would be of considerable interest.

It must be added that the method described above for oxidation of iodine to iodates may have extensive practical applications in industry, as it is a simple method for obtaining a substance with powerful oxidizing properties.

SUMMARY

1. A simple method for electrochemical liberation of iodine by anodic oxidation of iodide ions has been developed. The method has the following distinctive characteristics.

a) Wooden electrolytic tanks are used; after iodine has been adsorbed on their walls, they operate without absorbing iodine.

b) Clay diaphragms are used to separate the anode and cathode compartments.

---

* The power consumption is estimated as follows. Theoretically 26.8 amp-hr is required for liberation of 1 g-equiv (127 g) of iodine, while in practice 33.6 amp-hr is required, as the current efficiency, according to Table 2, is 80%.

The measured optimum anode voltage is 1.2 v at current density 0.015 – 0.020 amp/cm^2. The total cell voltage at the same load is 2.5 v.

The power consumption for liberation of 1 g-equiv is $33.6 \times 2.5 = 83.5$ watt-hrs.

The power consumption for liberation of 1 kg of iodine is $\frac{83.5 \times 1000}{127} = 660$ watt-hrs $= 0.66$ kw-hrs.

c) Carbon electrodes without any impregnation are used (1 anode and 2 cathodes per cell).

d) Elemental iodine is liberated from solution by means of a current not exceeding 0.02 amp per cm^2 of anode surface. The anode voltage is about 1.2 v.

e) The cathode compartment is filled with hydrochloric acid in an amount equivalent to the amount of iodide to be oxidized. The electrolyte acidity is maintained at the required level by means of the hydrochloric acid.

f) This method can be used for isolation of iodine from solutions of chlorides, sulfides, and sulfates, and from oil-well brines.

g) The power consumption for liberation of 1 kg of iodine is about 0.7 kw-hr.

2. A new method for oxidation of elemental iodine to iodate in an acid medium has been developed. The iodate solution can be used for quantitative oxidation of iodide to elemental iodine.

3. No reagents except technical hydrochloric acid are required for either of the two electrochemical methods — the isolation of elemental iodine from iodide solutions, and production of iodates from iodine solutions.

LITERATURE CITED

[1] O. A. Magidson, J. Appl. Chem. 1 (1927).

[2] S. V. Konstantinov, Bull. Geol. Committee 5 (1925).

[3] S. V. Gorbachev and E. N. Vinogradov, J. Phys. Soc. 9, 5 — 6 (1927).

[4] O. Yu. Magidson, Author's Certif. 4561, June 6, 1954.

[5] A. A. Shmuk, Author's Certif. 40,333, August 14, 1933.

[6] L. Pisarzhevskii and S. Tel'nyi, J. Chem. Ind. 1, 13 (1924).

[7] V. P. Denisovich, J. Chem. Ind. 1 (1934).

[8] V. P. Denisovich, Iodine and Its Production [in Russian] (GONTI, People's Commissariat of the Heavy Industry, 1938).

[9] N. A. Izgaryshev, Electrochemistry and Its Technical Applications [in Russian] (1931).

[10] G. Grube, Principles of Theoretical and Practical Electrochemistry [in Russian] (Leningrad Chem. Sector, 1932).

[11] K. I. Rozental' and V. I. Veselovskii, J. Phys. Chem. 27, No. 8, 1163 (1953).

[12] W. M. Latimer, Oxidation States of the Elements and Their Potentials in Aqueous Solutions (Moscow, IL, 1954) [Russian translation].

[13] V. V. Nekrasov, Course of General Chemistry [in Russian] (Moscow, 1954).

[14] T. I. Borisova and V. I. Veselovskii, J. Phys. Chem. 27, No. 8, 1195 (1953); L. M. Elina, T. I. Borisova, and Ts. I. Zalkind, J. Phys. Chem. 28, 785 (1954); A. N. Frumkin et al., Kinetics of Electrode Processes [in Russian] (Moscow, 1952).

[15] H. J. Creighton, Principles of Electrochemistry (Leningrad, Chem. Theoret. Press, 1937) [Russian translation].

Received September 2, 1957

GRAPHITIZED ANODES IN THE ELECTROLYSIS OF AQUEOUS CHLORIDE SOLUTIONS

V. V. Stender and O. S. Ksenzhek

The Dnepropetrovsk Institute of Chemical Technology

The commonest anode material for electrolysis of chlorides, as in the production of chlorine and alkalies, is artificial graphite. The reason is that graphite conforms most closely to the requirements of industrial electrolysis with regard to anode materials, namely: it has high chemical resistance, low overvoltage in the electrode process, good conductivity, considerable mechanical strength, and is relatively cheap [1]. However, graphite is not an absolutely resistant anode material, and it is gradually destroyed in use. Thus, in chlorine production the service life of graphite anodes is about one year.

Graphite anodes are broken down by the chemical action of active oxygen formed at the anode during electrolysis, and by oxygen-containing oxidizing agents such as hypochlorous acid (chemical attack). As the result of chemical attack the individual graphite grains become separated from each other, and crumble away, leading to "mechanical" destruction of the anode. The proportion of this "mechanical" destruction in the total loss of anode weight during use may be from 10 – 20% [2] to 60 – 70% [3], according to the type of graphite and certain other factors.

The stability of anodes in electrolysis depends on the degree of graphitization of the carbon. Thus, it was observed by Foerster [4] that electrodes made from artificial graphite are broken down much less than charcoal electrodes under the same conditions. This result was confirmed by other authors [5]. The increase of stability with degree of graphitization is the result of growth of the carbon crystals, accompanied by increase in conductivity. This parallelism in the variations of stability and conductivity with graphitization of carbonaceous materials led some authors to consider conductivity to be a measure of graphite stability [6]. In some cases this view is justified; for example, in the combustion of coke [7] or electrodes in the electric arc [8]; up to a point it is valid for electrolysis.

The effects of technological process conditions in the chlorine cell on the destruction rate of graphite anodes have been repeatedly studied by numerous investigators [1 – 4]. The basic relationships have been established as the result of this work. It has been shown that the destruction rate of anodes is increased by increase of temperature, decrease of electrolyte concentration, and increase of alkali concentration. The destruction rate of graphite, relative to the quantity of electricity passed, falls somewhat with increase of current density. Graphite anodes are destroyed much more rapidly in the production of chlorates than of chlorine. Chemical destruction of graphite by hypochlorite plays an important part here [9].

Graphite electrodes are porous disperse bodies consisting of interconnected fine carbon crystals. In the varieties of graphite commonly used the solid material occupies about 70 – 80% of the volume; the rest of the volume consists of pores. The pore structure of graphite anodes plays a definite role in their destruction during electrolysis. This was noted by Sproesser [10], who considered that the adverse effect of electrolysis within the anode pores on anode stability is due to impoverishment of the electrolyte in the pores, so that oxygen is predominantly evolved there. Zhivotinskii, Lyubinskaya, and Stender [1] showed that electrolyte circulates continuously through the pores of a working graphite anode: the solution enters the electrode through the smaller pores, and emerges together with gas formed during electrolysis through the larger pores. As a result, the chloride concentration is only slightly lower in the pores of a working electrode than in the anode compartment of

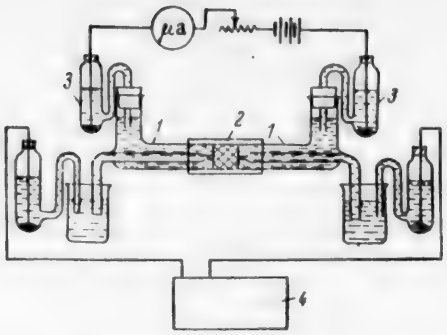

Fig. 1. Apparatus for determination of pore convolution:
1) vessel, 2) test specimen, 3) calomel electrode, 4) potentiometer.

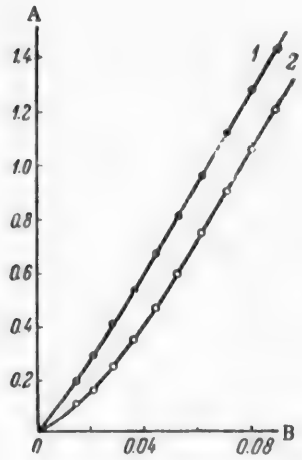

Fig. 2. Effects of frequency on capacitive 1) and active 2) resistance of a graphite electrode in a 5 M NaCl + 0.016 M HCl solution.
A) Resistance (ohms · cm^2),
B) frequency ($\omega^{-\frac{1}{2}}$).

the cell, and therefore the harmful effect of electrolysis within the pores on the stability of graphite anodes is not due to impoverishment of the electrolyte.

As long ago as 1934 one of us, jointly with Ioffe, Stroganov, and Zhivotinskii [1], gave the following explanation of the role of porosity in the destruction of anodes. The equilibrium potential of oxygen at a graphite electrode in the electrolysis of chloride solutions is lower (more negative) than the equilibrium potential of chlorine, but the overvoltage is higher for oxygen than for chlorine. As a result, simultaneous evolution of these gases is possible. The relative proportions of chlorine and oxygen depend on the electrode potential — at a high potential chlorine is predominantly liberated; at a low potential, close to the equilibrium potential of chlorine, the relative proportion of liberated oxygen increases, and finally, at potentials on the negative side of the chlorine potential, oxygen only is liberated. Direct measurements showed that the potential of a working graphite electrode falls rapidly from the surface to the interior.

The values of the potentials of a graphite anode at different distances from the external surface are given in Table 1. These results show that even within the limits of a surface layer 0.5-1mm thick the potential drops sharply to a value close to the equilibrium potential of chlorine. Thus, at a high potential and a correspondingly high current density the conditions in the outer layer of the electrode favor predominant liberation of chlorine. In the electrode pores further from the outer layer surface, where the process takes place at a very low current density, the relative proportion of the current consumed in liberation of oxygen and oxidation of graphite increases at the low potential, and may reach 100%.

The irregular distribution of potential and current within a graphite anode is the result of two causes — polarization of the outer electrode layers, in consequence of which the discharge process extends into the electrode to the inner surfaces of the pores, and resistance of the electrolyte in the pores, which limits the depth to which this process penetrates. The theory of porous-electrode processes, the main points of which are published elsewhere [11, 12] shows that the irregularity of current distribution within a porous electrode increases with increase of the inner surface of the electrode and with increase of polarization. Conversely, if an electrode process takes place at the electrode material with a high overvoltage, while the inner surface of the electrode is small and readily accessible to the current because of the large pore size and high conductivity of the electrolyte, the current is distributed more uniformly. These relationships are expressed by the following formula, which connects the value of the potential, within a porous electrode (φ_x), at a distance x from the outer surface, with the electrode structure, properties of the electrolyte and kinetics of the electrode process:

$$\varphi_x = 4b \operatorname{th}^{-1}\left[\exp\left(-x\sqrt{\frac{2i_0 S\rho}{b}}\right)\cdot \operatorname{th}\frac{\varphi_0}{4b}\right], \qquad (1)$$

TABLE 1

Potential of a Graphite Electrode at Various Distances from the Surface

Current density (amps/m²)	Potential at a distance of x mm from the external anode surface (in v)					
	$x = 0$	$x = 0.5$	$x = 1$	$x = 2$	$x = 7$	$x = 12$
100	1.403	1.361	1.323	—	—	—
200	1.445	1.370	1.326	1.325	1.322	1.322
400	1.474	1.379	1.334	1.336	1.331	1.329
600	1.497	1.388	1.343	1.343	1.340	1.334
800	1.515	1.394	1.352	1.352	1.350	1.343
1000	1.522	1.400	1.359	1.359	1.356	1.350
1250	1.548	1.413	1.370	1.367	1.363	1.358

where φ_0 is the polarization of the outer electrode surface, b is the constant in the Tafel equation, i_0 is the exchange current (in amp/cm²), S is the specific surface of the porous electrode (in cm²/cc), and ρ is the resistance of the electrolyte in the electrode pores, with the porosity and pore convolution taken into account.

Analysis of Equation (1) shows that the electrode process occurs at appreciable current density in an outer electrode layer the thickness of which is comparable to

$$x_a = n\sqrt{\frac{b}{2i_0 S\rho}}. \qquad (2)$$

The value of x_a, which we shall call "the acting electrode thickness", may vary over a very wide range in accordance with the properties of the electrode and electrolyte — from a few microns (for electrodes with a strongly developed surface, with high reversibility of the electrode process, and high electrolyte resistance in the pores) to several meters (if these values are small). In the former case, only the face of the electrode actually operates, while in the latter the internal surface is utilized uniformly. The value of the coefficient in Equation (2) decreases with increased polarization:

ψ_0 (mv) . .	150	200	300	400	500	600	700
n	4.3	4.0	3.5	2.8	2.1	1.4	0.8

Participation of the internal surface in the action of a porous electrode influences the form of the polarization curve.

Whereas with smooth electrodes the polarization curves for many processes can be represented more or less accurately by the Tafel equation, the relationship between polarization and current density for porous electrodes is more complex; in the simplest case it is represented by the formula

$$\varphi_0 = 2b\,\mathrm{arh}^{-1} I\sqrt{\frac{\rho}{8Sbi_0}}. \qquad (3)$$

The distinguishing feature of polarization curves for porous electrodes is that they lie lower (the polarization is less) than curves for the same processes on smooth electrodes, but their slope is roughly twice as great.

A certain difficulty arises in kinetic studies of electrode processes on graphite, due to the fact that graphite cannot be obtained in the form of nonporous monolithic specimens, or single crystals large enough for experimental purposes. It is therefore necessary to use porous electrodes, so that it is impossible to eliminate the influences of superposed macrokinetic factors which determine the participation of the internal electrode surface in the electrode process. It was shown in our investigations [11, 13] that the influence of macroscopic factors can be

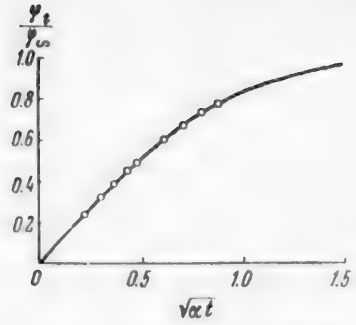

Fig. 3. Charge curve of graphite in $\varphi_t/\varphi_\infty - \sqrt{\alpha t}$ coordinates: continuous line represents the theoretical curve; circles correspond to experimental points for $\alpha = 9.7$.

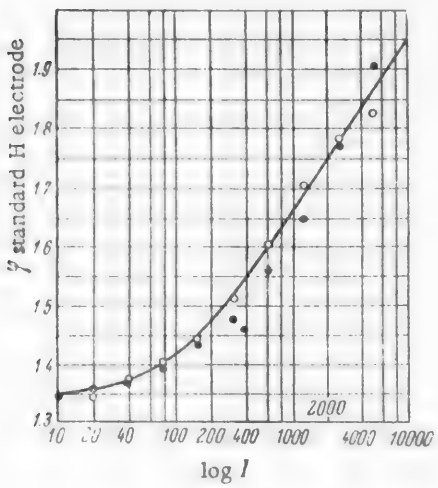

Fig. 4. Polarization curve for graphite in 5 M NaCl + 0.016 M HCl solution at 20°: continuous line is the calculated curve; black and white circles are experimental points for two specimens.

taken into account by the use of methods based on studies of nonequilibrium polarization processes of porous electrodes. Thus, the increase of potential of a porous electrode when the current is switched on is represented by the equation

$$\varphi_t = I\sqrt{\frac{\rho}{\alpha C}}\,\Phi(\sqrt{\alpha t}), \qquad (4)$$

where $\alpha = \frac{2i_0}{bC'}$; C' and C are the capacities of the double layer at 1 cm² of the true electrode surface and on all the true surface of 1 cc of a porous electrode respectively; C', C and S (the specific surface) are interrelated: $C = C'S$; i_0 is the exchange current (amps/cm²) $\Phi(Z) = \frac{2}{\sqrt{\pi}}\int_0^Z e^{-y^2}dy$ is the "error integral," and t is the time from the instant the polarization current J is switched on.

This equation can be used for determining such characteristics of a porous electrode as the exchange current and specific surface from its charge curve. The discharge curve of a porous electrode, i.e., the curve showing the decrease of potential after the polarizing current is switched off, can be used for the same purpose. The equation for the discharge curve is:

$$\varphi_t = \varphi_0 e^{-2\gamma t}\,[1 - \Phi(\sqrt{\alpha t})]. \qquad (5)$$

The specific surface of a porous electrode can also be determined by the method of alternating-current polarization. In the simplest case the specific surface is calculated from the formula

$$S = \frac{\rho}{\omega Z^2 C'}, \qquad (6)$$

where $Z = \sqrt{R^2 + \left(\frac{1}{\omega C}\right)^2}$ is the impedance of the porous electrode, ω is the angular frequency of the polarizing current, and R and $\frac{1}{\omega C}$ are the active and capacity resistance of the electrode respectively.

The foregoing principles and methods were used in our investigation of the action of graphite anodes in electrolysis of chloride solutions.

Method of Investigation of Graphitized Anodes

We had at our disposal 17 sorts of artificial graphite of different origin and structure, including Acheson anodes (51 × 51 mm), anodes made by the Dnepr Electrode Works (51 × 51 mm), samples of high-porosity graphite made by the Soyuzelektrod Trust (code marks SS, PT, and Ts), experimental samples differing in porosity, made by the Chelyabinsk Electrode Works (ChÉZ), and a series of experimental samples differing in porosity, made at the Dnepr Electrode Works (DKhTI – DÉZ) with the cooperation of the staff of the Electrochemical Department of the Dnepropetrovsk Institute of Chemical Technology [14]. The principal physical characteristics of all the electrodes were determined: the apparent and true densities, porosity, pore convolution, and specific surface.

TABLE 2

Characteristics of Graphite Electrodes

Electrode code mark	Porosity g (vol %)	Density d_a	Electrolyte resistance in pores ρ^* (in ohm/cm)	Specific capacity of internal surface, by alternating current	Specific capacity of internal surface, from charge curves (μF/cc)	Capacity of double layer on external surface (μF/cm²)	Specific surface S		External surface Sext (cm²/cm³)	α (sec^{-1})	Exchange current i_0 (amp/cm²)
							m²/cc	m²/g			
Acheson 51 × 51	31.0	1.52	255	$4.07 \cdot 10^5$	$4.26 \cdot 10^5$	506	1.13	0.74	14	9.7	$1.14 \cdot 10^{-5}$
DÉZ 51 × 51	25.0	1.65	400	$2.34 \cdot 10^5$	$2.32 \cdot 10^5$	555	0.65	0.395	15.4	4.95	$5.8 \cdot 10^{-6}$
CO-14	46	1.18	100	$8.3 \cdot 10^4$	$8.6 \cdot 10^4$	920	0.24	0.203	25.6	8.65	$1.0 \cdot 10^{-5}$
Ts-27	42	1.27	41	$6.6 \cdot 10^4$	$6.65 \cdot 10^4$	440	0.185	0.143	12.2	6.54	$7.65 \cdot 10^{-6}$
PT-6	46	1.18	46	$5.05 \cdot 10^4$	$5.25 \cdot 10^4$	286	0.14	0.122	8	9.2	$1.08 \cdot 10^{-5}$
CHÉZ thick	30	1.55	438	$6.6 \cdot 10^5$	$7.0 \cdot 10^5$	—	1.96	1.27	—	~8	$\sim 10^{-5}$
" 30%	54	1.01	525	$4.2 \cdot 10^5$	$4.6 \cdot 10^5$	—	1.28	1.27	—	~8	$\sim 10^{-5}$
" 40%	59.5	0.88	37	$4.1 \cdot 10^5$	$3.9 \cdot 10^5$	—	1.08	1.22	—	~8	$\sim 10^{-5}$
DKhTI-DÉZ-p1**	32.1	1.45	220	—	$14.7 \cdot 10^5$	—	4.1	2.83	—	~8	$\sim 10^{-5}$
" " -p2**	41.8	1.25	141	—	$8.2 \cdot 10^5$	—	2.3	1.84	—	~8	$\sim 10^{-5}$
" " -p3**	52.5	1.02	103	—	$3.9 \cdot 10^5$	—	1.1	1.00	—	~8	$\sim 10^{-5}$
" " -p4**	62.1	0.81	42.4	—	$1.9 \cdot 10^5$	—	0.53	0.65	—	~8	$\sim 10^{-5}$
" " -p5**	63.8	0.78	41.8	—	$1.5 \cdot 10^5$	—	0.42	0.56	—	~8	$\sim 10^{-5}$
" " -p6**	63.7	0.78	40.8	—	$3.0 \cdot 10^5$	—	0.83	1.06	—	~8	$\sim 10^{-5}$
" " -p7**	66.5	0.72	33.7	—	$2.6 \cdot 10^5$	—	0.72	1.00	—	~8	$\sim 10^{-5}$
" " -p8**	69.3	0.66	27.4	—	$1.4 \cdot 10^5$	—	0.39	0.59	—	~8	$\sim 10^{-5}$
" " -p9**	71.6	0.61	22.6	$1.08 \cdot 10^5$	$1.12 \cdot 10^5$	—	0.31	0.50	—	~8	$\sim 10^{-5}$

* Measured for electrodes impregnated with 5 M NaCl + 0.016 M HCl, with $\rho_{el} = 5.20$ ohms · cm

** Porous DKhTI – DÉZ electrodes made by mixing of a carbonaceous charge with NH_4Cl power; "p" indicates the use of petroleum coke; the numbers 1 through 9 indicate the porosity, which increases from p1 to p9.

In addition, the electrochemical properties of the graphites were studied — the polarization curves for chlorine liberation were plotted, and the exchange current and activation energy of the process were determined.

The apparent (d_a) and true (d_t) densities and volume porosity (g) were determined by the usual methods, described in detail in the literature [15 — 17].

Pore convolution was determined by a method based on measurement of the resistance of a porous electrode impregnated with electrolyte. This method has been used only for measurement of the convolution coefficient of pores in nonconductivity materials, such as asbestos diaphragms, etc. [15, 16, 18], but it can also be applied to conducting porous systems. Two fundamental conditions must be satisfied: 1) absence of chemical reaction between the electrolyte and the electrode material, and 2) "absolute" polarizability of the electrode over a certain potential range. If a porous body satisfying these conditions is placed in the path of a current in an electrolyte, then at low current strengths it is more "advantageous" for the current flow through the electrolyte in the pores rather than through the more conducting electrode, as the latter involves the surmounting of two potential differences, from the electrolyte to the electrode and back again.

The apparatus used for measurement of pore convolution is shown in Fig. 1. It consisted of two vessels, between which was clamped a cylindrical test electrode specimen, previously impregnated under vacuum with a solution of known conductivity. The external current was supplied with the aid of calomel electrodes, so that the composition of the electrolyte in the cell should remain unchanged during the passage of current. The potential drop which resulted when the current passed through the electrode pores was measured by means of a potentiometer.

The coefficient of pore convolution, which is the ratio of the mean pore length to the electrode thickness, was calculated from the formula

$$\beta = \sqrt{\frac{\rho}{\rho_{el}} \cdot g}, \qquad (7)$$

where β is the coefficient of pore convolution, ρ_{el} is the resistivity of the electrolyte impregnating the electrode (found experimentally), and g is the volume porosity (in fractions of unity).

The specific surface was determined by nonequilibrium polarization methods — from the charge curves and with the use of alternating current [11]. The method used for determination of specific surface is described more fully below.

Polarization curves were determined by the usual method. The measurement cell was fitted with a diaphragm separating the anode and cathode spaces. The anode compartment contained a stirrer which agitated the liquid near the anode surface very vigorously (at 5000 revolutions/minute).

The method used for studying nonequilibrium polarization of graphite electrodes is described in detail in an earlier paper [13].

In all cases the specimens were graphite cylinders about 1 cm in diameter and 5 — 6 cm long, subjected to previous anodic polarization for a total time of about 72 hours. The side surfaces of the specimens were insulated. The electrolyte in all cases was 5 M NaCl solution containing 0.016 M HCl.

Analysis of the experimental data is illustrated below for data on a sample of Acheson graphite, determined by nonequilibrium polarization methods.

The effects of frequency on the capacity and resistance of the electrode are shown in Fig. 2. The specific surface can be approximately calculated from these data by means of Equation (6). However, the fact that a certain part of the electrode is more accessible to the current than the inner pore surface is disregarded. The current reaches this (external) electrode surface directly from the electrolyte volume without entering the pores.

If this fact is taken into account somewhat more complicated formulas are obtained for the inner pore surface

$$S = \frac{2\rho R^2}{\omega Z^4 C'} \qquad (8)$$

and for the external surface

$$S_{ext} = \frac{1}{\omega Z^2 C'}\left(\frac{1}{\omega C} - R\right). \quad (9)$$

Calculation by Formula (8) gives $S = 1.13 \cdot 10^4 \pm 3\%$ cm^2/cc, where C' is taken to be 36 μF/cm^2. Calculation of the external surface by Formula (9) gives 14 cm^2/cm^2.

The data obtained in the determination of charge and discharge curves were analyzed as follows. The oscillogram was plotted point by point in a new coordinate system, $\sqrt{t}$ being taken along the abscissa axis, and the ratio φ_t/φ_∞ where φ_∞ is the steady polarization, along the ordinate axis. The oscillogram scale along the abscissa axis was varied so as to give the maximum correspondence of the experimental points with the plot of the function $\Phi(\sqrt{\alpha t})$ for the charge curves and of $e^{2\alpha t}[1 - \Phi(\sqrt{\alpha t})]$ for the discharge curves. This superposition of the experimental points on the theoretical curve for Acheson graphite charged at 6 ma/cm^2 is illustrated in Fig. 3. Agreement is obtained at $\alpha = 9.7$. The specific capacity of the double layer can then be determined. For example, the fifth point in Fig. 3 corresponds to time instant $t = 23.4 \cdot 10^{-3}$ second, polarization $\varphi_t = 23.6 \cdot 10^{-3}$ v, $\sqrt{\alpha t} = 0.476$, $\Phi(\sqrt{\alpha t}) = 0.499$, and hence Formula (4) gives $C = 0.426$ F/cm^2. Assuming that C' = 36 μF/cm^2, we have $S = 1.18 \cdot 10^4$ cm^2/cc, which is fairly close to the value found by the alternating-current polarization method.

The value found for α can be used for determining the exchange current for the discharge of chloride ions on graphite. For this, the coefficient b and the capacity of the double layer per unit graphite area must be known. Neither is known reliably, but it may be assumed that $b = 0.065$, which is about one half of the maximum slope of the polarization curve for Acheson graphite if the natural logarithm of I is taken. The above value of 36 μF/cm^2 was taken for the capacity, but it is possible that the actual value is somewhat lower, owing to the presence of adsorbed oxidation products on the graphite surface. On these assumptions we have, for the exchange current

$$i_0 = \frac{1}{2}(\alpha \cdot b \cdot C') = 0.5 \cdot 9.7 \cdot 0.065 \cdot 36 \cdot 10^{-6} = 1.14 \cdot 10^{-5} \text{ amp/cm}^2$$

The characteristics of the other electrodes were determined analogously.

DISCUSSION OF RESULTS

The principal results obtained for the graphite electrodes are given in Table 2.

It is seen in Table 2 that the value of α is roughly constant for all the kinds of graphite studied. Since α characterizes the electrochemical properties of the electrode material itself, irrespectively of porosity or other macrostructural factors, the fact that α is constant indicated that the true surface of different graphites is equivalent in the electrochemical sense. The observed fluctuations of α between 5 and 10 are not indicative of any significant differences in the kinetics of the electrode processes at the respective surfaces, and maybe attributed to surface contamination, for example by ash impurities.

The exchange current also remains roughly constant in the $10^{-5} - 5.10^{-6}$ amp/cm^2 range. The reliability of this value depends on the accuracy of the value of C' used for the capacity of the double layer per unit surface in the calculation. Since the surface of a working graphite anode cannot be regarded as quite free from contamination, for example by intermediate decomposition products of the graphite, the assumed value of 36 μF/cm^2 is probably rather too high. Comparison of the specific surfaces of DEZ and Acheson graphites, determined by adsorption methods [19], also leads to the conclusion that the actual value of C' is roughly half of the value taken, and is about 15 – 20 μF/cm^2. This gives $\sim 5 \times 10^{-6}$ amp/cm^2 for the most probable value of the exchange current in the discharge of chloride ions on graphite.

It is clear from Table 2 that when the specific capacity was determined by the alternating-current and the charge methods, the two methods gave results in good agreement. The specific surface was calculated from specific capacity on the assumption that C' = 36 μF/cm^2. If the more probable value of 18 μF/cm^2 is taken, the specific surfaces are double those given in the Table. For the dense Acheson and DEZ graphites these values are 1.5 and 0.8 m^2/g respectively, which are close to the values found by adsorption methods.

TABLE 3

Calculated Values of Actual Current Density, Polarization, and Acting Thickness for Two Kinds of Graphite

Over-all current density (amps/m²) and electrode characteristics	"Dense" DÉZ electrode			"Porous" ChÉZ electrode		
	Actual current density (amps/m²)	Polarization (mv)	Acting thickness (mm)	Actual current density (amps/m²)	Polarization (mv)	Acting thickness (mm)
300	9	265	1.3	0.5	90	4.3
1000	90	420	1.0	3.2	210	3.9
3000	700	560	0.5	25	340	2.9
10000	3600	700	0.2	315	500	1.6
Density		1.65			0.884	
Porosity (%)		25.0			59.5	
Resistivity (ohm · cm · 10^{-3})		0.8			7.2	
Electrolyte resistance in pores (ohm · cm)		460			37.0	
Specific surface (m²/cc)		1.3			2.16	

For the SS, Ts, and PT porous graphites the specific surface so determined is 0.4, 0.5, and 0.25 m^2/g respectively. Here we have porous graphites with an obviously polydisperse structure. These graphites consist of relatively large grains, the average sizes of which, by sieve analysis and direct microscopic measurements, are SS = 10 − 30 μ, Ts = 80 − 100 μ, PT ~ 300 μ. These grains, in their turn, have the porosity characteristic of ordinary "dense" graphites made from the appropriate materials. The concept of internal specific surface becomes more complex for porous graphites of this structure. We may consider either the surface formed by the large graphite grains, disregarding their internal surface, or the total internal surface which includes the internal surface of the fine pores in the individual grains.

The grain surface can be very roughly estimated from the grain size. This gives a value of the order of 0.02 − 0.2 m^2/g for the specific surface of the grains. The internal surface of the grains should be of the same order of magnitude as that of ordinary dense graphite (about $1 m^2/g$).

In measurements of the electrolyte resistance in pores by the method used in the present investigation the porosity structure also influences the results. Most of the current passes through the large pores, whereas the fine convoluted pores which have high resistance make a relatively small contribution to the total measured resistance. Substitution of values of ρ found by this method into formulas for determination of specific surface, such as (4) or (6), should give low results. However, it must be taken into account that the presence of large pores with low resistance allows the current to penetrate to a considerable depth into the electrodes, which compensates the above effect to a certain extent.

Calculations, which are not given in detail here, show that the following expression should be valid for a bidisperse porous electrode with two kinds of pores with resistance ρ_1 and ρ_2 and specific capacity C_1 and C_2 respectively:

$$\frac{C_{meas}}{C_{act}} = \frac{S_{meas}}{S_{act}} = \frac{(\sqrt{k} + \sqrt{n})^2}{(k+1)(n+1)}, \qquad (10)$$

where $k = \frac{\rho_2}{\rho_1}$ and $n = \frac{C_2}{C_1} = \frac{S_2}{S_1}$.

If we assume that for graphite SS $k = \frac{100}{250} = 0.4$ and $n = \frac{0.2}{1.0} = 0.2$, then the formula gives $\frac{S\ meas}{S\ act} = 0.7$, and hence the specific surface $S_{act} = \frac{0.4}{0.7} = 0.6\ m^2/g$. Similarly, for graphite PT we may assume $k = \frac{45}{250} = 0.18$ and $n = \frac{0.02}{1.0} = 0.02$ which gives $\frac{S\ meas}{S\ act} = 0.27$ and $S_{act} \approx 1\ m^2/g$.

It is obvious that this is only a very rough estimate. For more reliable conclusions regarding the role of the porosity structure it is necessary to know the pore size distribution function; this can be found by such methods as the mercury pressure [20] or gas flow [21] methods. On the other hand, certain inferences concerning the inner structure of porous electrodes can be drawn from their electrochemical behavior.

The situation is most complicated with porous graphites of the ChÉZ and DKhTI-ChÉZ types, made from materials containing an admisture of a volatile solid, NH_4Cl, as pore former [14]. Such graphites undoubtedly have pronounced polydispersity with a very wide range of pores. This is especially true for DKhTI-ChÉZ graphites, which were made with technical ammonium chloride ground in a mortar. ChÉZ graphites, made with sublimed NH_4Cl, are more homogeneous and apparently have a sharper maximum in the porosity spectrum. These graphites all had approximately the same specific surface per unit weight.

The measured specific surface of DKhTI-DÉZ graphite decreases, although not quite smoothly, with increase of porosity. This is due to increased irregularity of structure and to the appearance, in highly porous specimens, of relatively large cracks and channels, which decrease the apparent resistance of the electrolyte in the pores. Thus, the 2.2-fold increase of porosity from specimen p1 to p9 is accompanied by nearly a 10-fold decrease of resistance in the pores; this can be attributed only to enlargement and straightening of the pores. If the porosity increase was caused only by increase of the number of pores while their dimensions and shape remained unchanged, then the resistance of the electrolyte in the pores of DKhTI-DÉZ-p9 electrodes should be about 100 ohms·cm. The measured specific surface should then be approximately $0.5 \cdot \frac{100}{22.6} = 2.2\ m^2/g$, which is close to the value of 2.8 m^2/g for the dense DKhTI-DÉZ-p1 electrode.

The higher specific surface of DKhTI-DÉZ and ChÉZ electrodes is due to a lower degree of graphitization.

The external surface of the electrodes studied is relatively constant, between $10 - 30\ cm^2/cm^2$; if it is assumed that $C = 18\ \mu F/cm^2$, then it is $20 - 60\ cm^2/cm^2$. Accordingly, the distribution of current between the external and internal surfaces is such that under normal conditions the influence of the external surface may be disregarded.

The data obtained on the specific surface and structure of graphite electrodes and on the kinetics of chlorine evolution can be used for certain calculations which clearly demonstrate the relationship between the structure and operating conditions of graphite electrodes. Table 3 contains calculated values of the actual current density, the acting layer thickness, and polarization, for two kinds of graphite: "dense" DÉZ graphite and ChÉZ-40 graphite of higher porosity.

The table also contains the principal characteristics of the two types of graphite. The actual current density (maximum, near the external surface) was calculated by the formulas:

$$D = I^2 \frac{\rho}{2Sb} \tag{11}$$

(at high current densities, when $I > \sqrt{\frac{8Sbi_0}{\rho}}$)

and

$$D = I \sqrt{\frac{2i_0\rho}{Sb}} \tag{12}$$

(at current densities when $I < \sqrt{\frac{8Sbi_0}{\rho}}$).

The acting layer thickness was calculated by Formula (2), and polarization by Formula (3).

Table 3 shows that the actual current density is considerably less than the over-all value, especially for "porous" graphite. The actual value rises more rapidly with increase of the over-all current density, approximately in proportion to the square of the latter, and becomes comparable with it at some thousands of amperes per square meter. This situation is only reached at considerably higher current densities for the highly porous graphite.

The acting layer thickness for "dense" graphite at the current densities generally used in chlorine production is about 0.5 – 1.0 mm, and is consistent with the earlier data, presented in Table 1, obtained experimentally by one of us. The acting layer thickness for graphite of higher porosity is several times as large.

We attempted to calculate polarization curves for different kinds of graphite by means of Formula (3), and to compare the calculated and experimental curves. For the more homogeneous samples the agreement was quite satisfactory, especially in view of the poor reproducibility of polarization measurements with a material such as graphite. Fig. 4 shows the calculated polarization curve for Acheson graphite, together with the corresponding experimental points. The agreement between experimental and calculated data for less homogeneous graphites is somewhat less satisfactory.

All the results given in this paper were determined at 20 ± 1°. For conversion to other temperatures, it is possible to use the value for the activation energy of chlorine evolution, found to be 12,000 cal calculated in an earlier investigation [12] and the temperature coefficient of electrical conductivity. Calculation for 80°, which is the usual temperature in chlorine production, shows that the exchange current is increased approximately 36-fold, while the electrolyte resistance in the electrode pores decreases 3.2-fold at this temperature. The actual current density and electrode polarization diminish accordingly.

SUMMARY

1. Graphite electrodes were studied by methods based on nonequilibrium polarization. Data on the kinetics of chlorine evolution on graphite and information on the specific surfaces of different graphites were obtained as a result.

2. It is shown that the exchange current in chlorine evolution is virtually the same for different kinds of graphite, and is $5 \cdot 10^{-6}$ amp/cm² at 20°.

3. The specific surface is about 0.8 – 1.5 m²/g for well-graphitized samples, and 2.5 – 6 m²/g and over for less graphitized samples.

4. The actual current densities, acting electrode thicknesses, and polarizations were calculated for different conditions.

5. It is shown that differences in the electrochemical behavior of different kinds of graphite are largely determined by their structural characteristics.

LITERATURE CITED

[1] V. V. Stender, Electrochemical Production of Chlorine and Alkalies [in Russian] (Leningrad, ONTI, Chem. Theoret. Press, 1931).

[2] N. J. Johnson, Trans. Electroch. Soc., 86, 127 (1944).

[3] I. Ya. Sirak, J. Appl. Chem. 6, 808 (1933).

[4] F. Foerster, Electroch. wässriger Lösungen (1922).

[5] K. Arndt and W. Fehse, Z. Elektroch., 28, 376 (1922).

[6] M. S. Maksimenko, Principles of Electrothermics [in Russian] (Leningrad, ONTI, Chem. Theoret. Press, 1938).

[7] R. O. Davis and H. S. Auvil, Ind. Eng. Ch., 27, 1196 (1935).

[8] L. Ya. Markovskii, J. Tech. Phys. 6, 517 (1936).

[9] M. Janes, Trans. Electroch. Soc., 92, 23 (1947).

[10] L. Sproesser, Z. Elektroch., 7, 1012 (1901).

[11] O. S. Ksenzhek and V. V. Stender, Proc. Acad. Sci. USSR. 106, 487, (1956).*

[12] O. S. Ksenzhek and V. V. Stender, Proc. Acad. Sci. USSR. 107, 280, (1956).*

[13] O. S. Ksenzhek and V. V. Stender, J. Phys. Chem. 31, 117 (1957).

[14] O. S. Ksenzhek and A. B. Livshits, Trans. Dnepropetrovsk Inst. Chem. Technol. 5, (1956).

[15] V. V. Stender, Trans. Electroch. Soc., 67, 51 (1935).

[16] V. V. Stender, Diaphragms for Electrolysis of Aqueous Solutions [in Russian] (Moscow-Leningrad, Goskhimizdat, 1948).

[17] I. E. Bauslit, G. Z. Kir'yakov, and V. V. Stender, J. Appl. Chem. 18, 127 (1945).

[18] P. A. Rebinder (Editor), Electrokinetic Properties of Capillary Systems [in Russian] (Moscow – Leningrad, Izd. AN SSSR, 1956).

[19] R. H. Savage and C. Brown, J. Am. Chem. Soc. 70, 2362 (1948).

[20] H. L. Ritter and L. C. Dracke, Ind. Eng. Ch., Anal. Ed., 17, 787 (1945).

[21] I. P. Ishkin and M. G. Kaganer, J. Phys. Chem. 24, 943 (1950).

[22] O. S. Ksenzhek, Ukrain. Chem. J. 23, 328 (1957).

Received June 13, 1957

* Original Russian pagination. See C. B. Translation.

INFLUENCE OF ELECTROLYTE COMPOSITION ON THE DISTRIBUTION OF CURRENT INSIDE A GRAPHITE ANODE AND ON ITS INTERNAL WEAR*

B. M. Bulygin

The Ivanovo Institute of Chemical Technology

The breakdown of a graphite anode in the electrolysis of aqueous solution not only affects the outer layer of the electrode, but may penetrate deep into the electrode, causing "internal losses." The mechanism of graphite oxidation within the pores may differ substantially from the mechanism of external destruction which was considered in the preceding communication [1]. Internal oxidation should be less intensive than external, because of the low current density (low potential) in the pores [2]. According to Ksenzhek [3], the fraction of the current involved in "internal" discharge at current densities used in industry (750-1000 amps/cm^2) is 0.5 – 2% for DÉZ electrodes. Moreover, internal oxidation should not be accompanied by mechanical disintegration, as the conditions for the latter (high anodic potential and irregular combustion because of the high discharge rate) do not obtain in the inner pores. However, in prolonged operation under works conditions internal destruction can become considerable (up to 40% of the total losses), and this cannot be attributed only to the oxidizing action of the hydroxyl (water) ions discharging in the pores. It has been noted [4, 5] that purely chemical (i.e., independent of electrolysis in depth) oxidation of anode material by certain substances present in the electrolyte, mainly hypochlorous acid, is possible.

The purpose of our investigation was to determine the possibility of graphite destruction by "electrochemical" or "chemical" mechanisms in different electrolytes and to find whether various components of the solutions have any harmful effect with regard to internal wear.

The investigation consisted mainly of determination of anodic polarization curves for the anode surface, and measurements of the anode potential at various depths. The polarization curves in conjunction with the curves for distribution of potential at different depths were used to determine the current density at various distances from the acting anode surface (the internal current density, D_{int}). Since the electrolysis takes place at a porous surface, in order to obtain correct absolute values of D_{int} the external polarization data were first recalculated for "true" current densities by means of the formula proposed by Ksenzhek [3],

$$D_{true} = D_{app} \frac{\rho}{2 \cdot S \cdot b} \sqrt{D^2_{app} + \frac{8 \cdot S \cdot i_0 \cdot b}{\rho}},$$

which includes quantities characterizing the electrolyte and the electrode.

The electrolyte composition in the pores may differ from the composition of the external solution, and this may be the cause of the processes leading to internal destruction. Therefore a series of experiments was performed in which fresh electrolyte was forced into the pores to the point at which the internal potential, π_{int}, was measured. Comparison of the values obtained by the two methods makes it possible to draw definite conclusions concerning variations of the concentration and composition of certain electrolytes within the anode pores.

The anode gas and solution were also analyzed chemically in order to determine the quantitative effects of current distribution on the discharge of different ions and to compare the relative effectiveness of chemical and electrochemical oxidation.

* Communication II in the series of investigations of destruction of graphite anodes in aqueous electrolyte solutions.

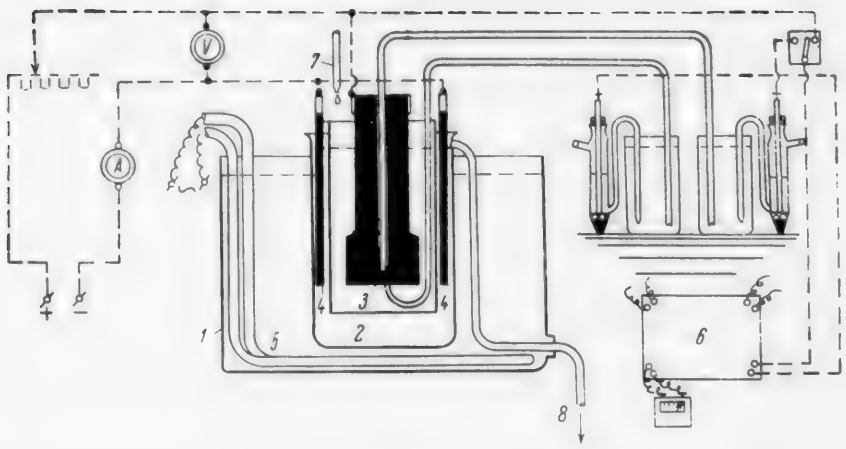

Fig. 1. Circuit of apparatus used for measurement of potentials within a graphite electrode: 1) thermostat, 2) electrolytic cell, 3) anode, 4) cathode, 5) electric heater, 6) P-4 potentiometer, 7) electrolyte inlet, 8) electrolyte outlet.

EXPERIMENTAL

The circuit of the apparatus used for determination of the polarization curves and measurement of potentials within the anodes is given in Fig. 1. The electrolytic cell was a bell-shaped bath. The anode, cut from DÉZ graphite in the shape of a circular plate with a rod, was placed in the bell. The bottom face of the anode, 3 cm^2 in area, was the working surface, the sides of the anode being insulated with polyvinyl chloride varnish. The capillary of a bridge for measurement of the internal potential was inserted in a hole drilled axially in the anode. Another bridge was introduced under the working surface of the electrode. Fresh electrolyte was introduced continuously into the anode compartment and withdrawn from the cathode compartment. The e.m.f. was measured to an accuracy of ±1 mv. The axial hole was deepened at intervals during the experiment, and the distance from the working surface of the anode to the point at which π_{int} was measured was gradually decreased from 25 to 0.5 mm.

Polarization curves and internal current densities were determined for the following groups of solutions: a) neutral NaCl solutions of various concentrations (Curves 1-3); b) solutions of pure acids and alkalies (Curves 4-7); c) alkaline hypochlorite solutions of different concentrations, with constant NaOH content, 10 g/liter (Curves 8 and 9); d) solutions containing 300 g of NaCl per liter with different HCl and NaOH contents (Curves 10-12); and e) solutions containing NaCl and NaClO in different proportions (Curves 13-15).

Polarization curves were plotted for the current density range 0.0003 – 0.3 amp/cm^2. The internal current density was determined for three values of external apparent current density – 0.075, 0.15 and 0.30 amp/cm^2. The temperature was maintained at 60 ± 1° deg in all the experiments.

The experimental results are plotted in Figs. 2-6. Figs. 2 and 3 show the curves for apparent polarization of the graphite anode in different solutions (the values of D_{app} are approximately 400 times the values of D_{true} at a given polarization). Curves for the distribution of potential at different depths in the anode are given in Figs. 4 and 5. Corresponding curves for the internal current density are given in Fig. 6.

DISCUSSION OF RESULTS

An exclusive process, adequately reversible over the entire current-density range, is observed only in solutions containing 50 g HCl per liter and strongly acid NaCl. All the other polarization curves are nonlinear. In alkaline electrolytes (pure NaOH and alkaline hypochlorite and sodium chloride solutions) the curves show an inflection at approximately +1.0 v, indicating that a qualitatively new process begins at higher current densities. Evidently at low polarizations only adsorption of atomic oxygen and accumulation of oxides on the graphite is possible. Beyond the infliction point, the curve corresponds to the liberation of CO, CO_2 and recombined

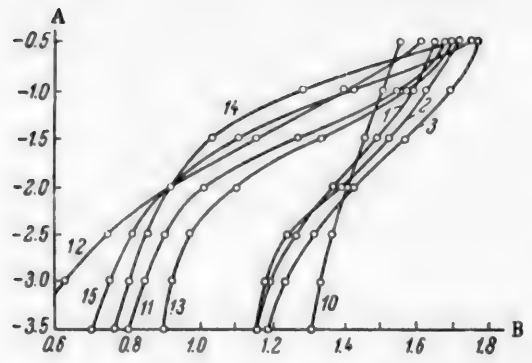

Fig. 2. Polarization curves for a graphite anode in different electrolytes:
A) log D_{app}, B) external potential $+\pi_{ext}$ (v); composition of solution (in g/liter): 1 – 300 NaCl, 2 – 150 NaCl, 3 – 50 NaCl, 10 – 300 NaCl + 20HCl, 11 – 300 NaCl + 10NaOH, 12 – 300NaCl + 50NaOH, 13 – 257NaCl + 6NaClO, 14 – 150NaCl + 20NaClO, 15 – 43NaCl + 34NaClO.

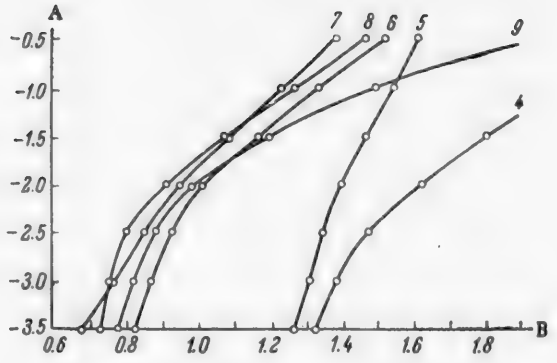

Fig. 3. Polarization curves for a graphite anode in different electrolytes:
A) log D_{app}, B) external potential $+\pi_{ext}$ (v); composition of solution (in g/liter): 4 – 5HCl, 5 – 50HCl, 6 – 10NaOH, 7 – 337NaOH, 8 – 40NaClO, 9 – 20 NaClO.

O_2 into the atmosphere. It is in this potential region that electrochemical destruction of graphite becomes possible.

The magnitude of the internal potential depends appreciably on the specific nature of the electrolyte. In solutions with exclusive discharge of chlorine (50 g HCl, and 300 g NaCl + 20 g HCl per liter) π_{int} is very close to the equilibrium potential of the chlorine electrode (+1.358 v), and the calculated D_{int} is very close to the exchange current ($i_0 \approx 10^{-6}$ amp/cm^2). Therefore there is virtually no discharge of chloride ions within pores more than 0.5 mm from the anode surface, while the fraction of the current involved in internal discharge is only 0.4% of the total current (at $D_{ext\ app} = 0.075$ amp/cm^2). Although the internal potential in solutions of pure alkali and strongly alkaline sodium chloride solution (300 g NaCl + 50 g NaOH per liter) is higher than the reversible oxygen potential, it is considerably lower than the actual potential of oxygen liberation (+1.0 v). Somewhat higher potentials (from +0.85 to +1.06 v) are observed in concentrated hypochlorite solutions, where discharge of hydroxyl ions may be accompanied by oxidation of hypochlorite ions. It follows from Fig. 6 that the current density in all these solutions is close to 10^{-7} amp/cm^2, and evidently electrolysis within the pores cannot cause any significant destruction of the anode. For all the above-named electrolytes supply of fresh electrolyte into the anode causes a small shift of potential in the negative direction; this indicates some degree of concentration polarization within the electrode. However, this cannot result in any significant differences in the distribution of the internal current density.

We now consider neutral NaCl solutions and their mixtures with hypochlorite. The course of the polarization curves (Fig. 2) suggests that the process at the external electrode surface in neutral NaCl solutions differs little from the process in acid solutions, while addition of hypochlorite to the solution gradually shifts the potential toward the values of π_{ext} for alkaline electrolytes. Therefore, if the external and internal discharge processes are assumed to be of the same type, considerable deviations of π_{int} and D_{int} from the values found for solutions containing 50 g of HCl or 20 and 40 g NaClO per liter cannot be expected. In reality, however, very high values of π_{int}, up to +1.45 v, are found for these solutions, while the internal current density is only 1/10 to 1/20 of the external true current density. The difference between these and all the electrolytes previously considered lies in the possibility of formation of a new product – hypochlorous acid – in them under certain conditions. Discharge of chlorine in the pores ($\pi_{int} > \pi_{Cl_2}$ in these solutions) leads to partial dissolution of chlorine in the electrolyte. The simultaneous discharge of hydroxyl ions acidifies the electrolyte somewhat. The weakly acid medium favors accumulation of HClO in the pores. In this case the potential is evidently established as the result of equilibrium in the reaction

$$HClO + H^+ + e \rightleftarrows {}^1/_2Cl_2 + H_2O$$

and its value depends on the pH of the electrolyte in the pores (π_0 = +1.63 v).

Hypochlorous acid is a powerful chemical oxidant. As it oxidizes the graphite, the equilibrium

$$ClO^- + HCl \rightleftarrows HClO + Cl^-$$

is shifted to the right and accumulation of HClO continues. Conditions necessary for existence and replacement of HClO can arise only in pores in which rapid removal of the products of electrochemical discharge is impossible. Such conditions do not obtain at the external surface, because of the high current density, and especially because of the free circulation of the solution.

This is confirmed by experiments with artificial supply of electrolyte into the pores. The greatest decrease of the value of π_{int}, reaching 0.25 v, is found in this case. As a result, the internal potential for the solution mixtures approaches the value of the equilibrium chlorine potential, and the formation of HClO is retarded. The calculated value of D_{int} decreases correspondingly.

TABLE 1

Composition of Anode Products in Electrolysis at Low Current Density D_a = 45 amps/m², t = 60° deg

	Solution (g/liter)											
	NaCl 300	NaCl 150	NaCl 50	HCl 5	H_2SO_4 5	NaOH 10	NaClO 40	NaCl 300 + NaOH 10	NaCl 300 + HCl 5	NaCl 257 + NaClO 6	NaCl 150 + NaClO 20	NaCl 43 + NaClO 34
Yield of CO_2 (g per amp-hr):												
in solution	0.160	0.123	0.148	—	—	0.385	0.186	0.246	—	1.290	0.644	0.443
in gas	0.096	0.118	0.115	0.449	0.336	—	0.005	—	—	?	?	?
total	0.256	0.241	0.263	0.149	0.336	0.385	0.191	0.246	—	>1.290	>0.644	>0.443
Current efficiency (%)												
Cl_2	31.0	28.4	19.0	21.5	—	—	—	—	100	?	?	?
CO_2	62.3	59.5	65.0	37.8	81.5	94.6	46.0	59.5	—	~300	~150	~110
O_2	6.7	12.1	16.0	40.7	18.5	5.4	54.0	40.5	—	?	?	?

Additions of either acid or alkali to a neutral saturated NaCl solution decrease the current density within the anode and interrupt the formation of HClO in the pores. Hypochlorite by itself is not a powerful oxidizing agent, and cannot react chemically with the anode material [1, 6].

The destructive action of electrolytes in which the formation and existence of HClO is possible was confirmed quantitatively by analysis of the anode gas and electrolyte. A method for compiling a balance of the anode products in studies of the destruction of graphite electrodes has been worked out by a number of authors [6 – 9]. The apparent external current density in our experiments was 0.0045 amp/cm² (as compared with 0.075 amp/cm² under production conditions), so that it was possible to bring the operating conditions of the external anode surface to those within the electrode. The anode gas and solution were analyzed for CO_2, Cl_2, O_2, Na_2CO_3 and NaClO.

The results of the experiments are presented in Table 1; it is seen that that in neutral and alkaline NaCl solutions, in which current is carried both by Cl^- and by OH^- ions, the amount of CO_2 formed is roughly constant (about 0.25 g per amp-hr). The anode gas always contains some oxygen. In an acid medium containing chloride

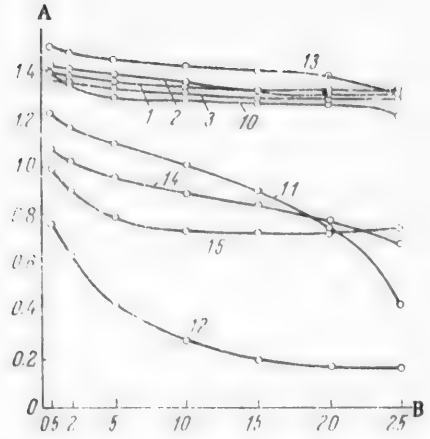

Fig. 4. Distribution of potential at different depths in a graphite anode, in various electrolytes:
A) internal potential $+\pi_{int}$ (v), B) thickness δ (mm);
composition of solution (g/liter: 1 – 300NaCl, 2 – 150NaCl, 3 – 50NaCl, 10 – 300NaCl + 20 HCl, 11 – 300NaCl + 10NaOH, 12 – 300NaCl + 50NaOH, 13 – 257NaCl + 6NaClO, 14 – 150 NaCl + 20NaClO, 15 – 43NaCl + 34NaClO.

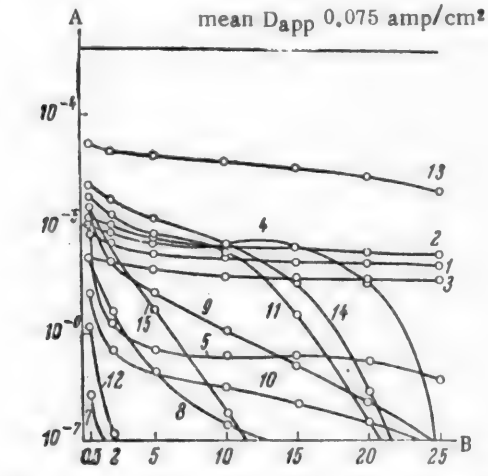

Fig. 6. Distribution of current density at different depths in a graphite anode, in various electrolytes: A) true current density (amp/cm²), B) thickness δ (mm); composition of solution (g/liter): 1 – 300 NaCl, 2 – 150NaCl, 3 – 50NaCl, 4 – 5HCl, 5 – 50 HCl, 7 – 337NaOH, 8 – 40NaClO, 9 – 20NaClO, 10 – 300NaCl + 20HCl, 11 – 300NaCl + 10NaOH, 12 – 300NaCl + 50NaOH, 13 – 257NaCl + 6NaClO, 14 – 150NaCl + 20NaClO, 15 – 43NaCl + 34NaClO.

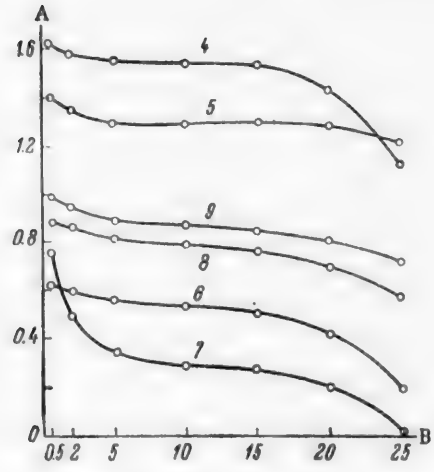

Fig. 5. Distribution of potential at different depths in a graphite anode, in various electrolytes:
A) internal potential $+\pi_{int}$ (v), B) thickness δ (mm);
composition of solution (g/liter): 5 – 50HCl, 4 – 5HCl, 6 – 10NaOH, 7 – 337NaOH, 8 – 40NaClO, 9 – 20NaClO.

ions all the current is expended in formation of Cl_2. Conversely, in absence of Cl^- ions (in NaOH and H_2SO_4 solutions) oxidation is increased 1.3 to 1.5-fold. Discharge of hypochlorite ions lowers the yield of CO_2 somewhat. The most interesting data are those on formation of CO_2 in mixed solutions of NaCl and NaClO, i.e., under conditions in which hypochlorous acid can be formed. Here the amount of CO_2 evolved is far greater than the amount theoretically possible as the result of primary discharge of oxygen. Decrease of the proportion of NaCl in the mixture (and corresponding increase of the proportions of NaClO and NaOH) naturally hinders chemical oxidation.

Good confirmation of the destructive action of the liberated HClO is provided by Table 2, which contains experimental data on the course of formation of hypochlorous acid. 1 N HCl was added at equal time intervals to an alkaline solution of NaClO (containing 40 g NaClO and 10 g NaOH per liter). At first, additions of acid have no effect on the gas composition. Only the alkali is neutralized at this stage. After a certain excess of acid has been added, displacement of hypochlorous acid from its salt begins. From this instant the contents of CO_2, and also of chlorine (by oxidation of excess HCl by the hypochlorous acid) in the gas begin to increase sharply.

TABLE 2

Composition of Anode Products During Neutralization of Alkaline NaClO Solution by 1 N Hydrochloric acid D_a = 45 amps/m², t = 60° deg

Time from start (min)	Amount of 1 N hydrochloric acid added (ml)	Composition of gas (%)			Carbonate content (g CO_2 per liter of solution)	NaClO concentration (g/liter)
		Cl_2	CO_2	O_2		
0	0	0	0	100	1.43	50.0
15	4	0	0	100	1.58	49.7
30	8	0	0	100	1.38	—
45	13	0	0	100	1.77	49.6
60	18	0	0	100	1.68	—
75	23	0	3	97	1.63	49.7
		0	13	87		
90	28	42	30	28	1.43	48.5
		42	36	22		
105	33	68	32	0	1.43	47.0
		60	34	6		
120	38	66	28	6	1.63	45.7
		71	25	4		

The sodium carbonate content of the solution remains unchanged, and therefore HCl is consumed exclusively in decomposition of hypochlorite, and a constant pH value becomes established in the solution by the buffering action of NaClO — HClO.

SUMMARY

1. The anode potential at depths greater than 0.5 mm in solutions containing Cl^- ions is close to the equilibrium potential of the system $2Cl^- \rightleftharpoons Cl_2 + 2e$, while in solutions in which hydroxyl ions are discharged this potential is less than the potential for the liberation of gaseous O_2 (about +1.0 v). The current density in deep pores is close to the exchange current, and therefore graphite is not destroyed as the result of internal discharge of ions.

2. Considerably higher internal potentials (up to +1.45 v) are found in solutions in which hypochlorous acid can form and exist in the anode pores (in neutral and weakly alkaline NaCl solutions, and especially their mixtures with hypochlorite). In such solutions the internal current density is only 15 to 20 of the external density, and therefore the formation of HClO by electrochemical oxidation $\frac{1}{2}Cl_2 + H_2O \rightarrow HClO + H^+ + e$ or by the displacement reaction $ClO^- + HCl \rightarrow HClO + Cl^-$ is very intensive.

3. Analytical data for the gas and electrolyte confirm the intensified destruction of graphite as the result of purely chemical oxidation by hypochlorous acid in the pores.

4. It is difficult to avoid internal destruction under industrial conditions for the electrolysis of weakly alkaline (0.15 — 0.20 g NaOH per liter) NaCl solutions. In such cases the best method of anode protection is efficient impregnation which prevents circulation of the electrolyte in the deep pores.

LITERATURE CITED

[1] B. M. Bulygin, J. Appl. Chem. 31, No. 12, 1832 (1958).*

[2] W. S. Joffe, Z. Elektroch., 42, 71 (1936).

[3] O. S. Ksenzhek, Author's Summary of Candidate's Dissertation [in Russian] (Dnepropetrovsk, 1956).

* Original Russian pagination. See C. B. Translation.

[4] M. Janes, Trans. Electroch. Soc., 92, 22 (1947).

[5] T. S. Filippov, Trans. Ukrainian State Inst. Appl. Chem. 1 (1936).

[6] I. Ya. Sirak, J. Appl. Chem. 6, 808 (1933).

[7] L. Sprösser, Z. Elektroch., 7, 971 (1901).

[8] T. S. Filippov and N. N. Nechiporenko, Trans. Ukrainian State Inst. Appl. Chem. 3, No. 1, 104 (1937).

[9] R. L. Murrey and M. S. Kicher, Trans. Electroch. Soc., 86, 83 (1944).

Received April 26, 1957

PRODUCTION OF IRON – NICKEL ALLOYS BY ELECTRODEPOSITION FROM CHLORIDE ELECTROLYTES

V. V. Sysoeva

During recent years there has been a considerable increase of interest in the production of coatings consisting of alloys of the iron group of metals (Fe – Ni, Fe – Co, Co – Ni), in relation to a number of practical problems in electrical engineering and communications [1, 2]. Moreover, it has been reported that iron – nickel alloys (Fe ≤40%) may be used as anticorrosion coatings [2].

However, despite a considerable number of studies of the electrodeposition of iron – nickel alloys [3 – 13], the results obtained have not been widely adopted in practice. Moreover, in the production of Permalloy-coated articles [1] the most suitable process has been found to be the application of alternating thin layers of iron and nickel, followed by heat treatment.

Sulfate [3 – 7, 9 – 13] and cyanide [8] electrolytes have been used for the formation of iron – nickel alloys.

The literature contains numerous bath recipes for the production of both iron and nickel from chloride electrolytes [3, 14 – 17], but, with only one exception, chloride electrolytes have not been used for the production of iron – nickel alloys. It is noted in one patent [18] that if cobalt salts are replaced by nickel in a chloride electrolyte ($FeCl_2$, $CoCl_2$, $CaCl_2$) Fe – Ni alloys can be produced.

It is clear from the foregoing literature data that no success has been achieved in the practical utilization of sulfate and other electrolytes for the electrodeposition of iron – nickel alloys; we used the indirect indication that nickel – iron alloys can be deposited from chloride electrolytes [18], and the well-known processes for production of iron [3, 14, 15] and nickel [3, 16, 17] coatings from chloride electrolytes, in an attempt to use chloride electrolytes for the formation of Fe – Ni alloy coatings with a wide range of component concentrations in the alloys.

The present communication is restricted to certain data which indicate the practical possibility of utilizing our proposed electrolyte.

In the development of electrolyte compositions suitable for practical use we also aimed at the maximum intensification of the process; electrolytes with a high total concentration of the components were therefore studied, and electrodeposition was also performed at elevated temperatures and very high current densities.

The electrolytic cells ranged in volume from 150 to 3000 ml, in accordance with the problem in hand. The electrolyte temperature was regulated thermostatically to within ±0.2°.

It is not necessary to give the circuit diagram of the apparatus in this paper, as a circuit of this type is given (with small modifications) in Kadaner's book [17].

Separate iron (Armco) and nickel (grade N-OOO) electrodes were used in the investigation; the total impurities in the electrodes did not exceed 0.03%.

The electrolytes were prepared from suitable salts in distilled water. Nickel chloride was prepared by solution of weighed quantities of once-crystallized chemically pure $NiCl_2$; for preparation of ferrous chloride, Armco iron was dissolved in HCl solution with addition of 70 g $FeCl_3$ per liter; the $FeCl_2$ concentration was determined by analysis and made up to 100 g/liter (calculated as the metal); the original $NiCl_2$ solution had the same concentration.

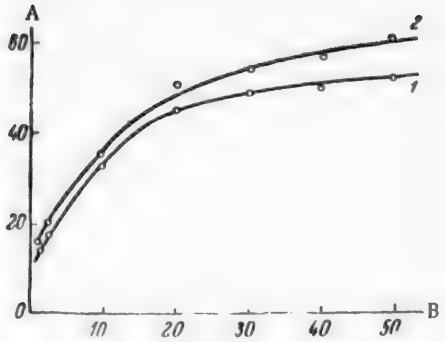

Fig. 1. Variation of the iron content of electrodeposited alloys with current density: electrolyte: $[Fe^{++}]$ 25 g/liter, $[Ni^{++}]$ 75 g/liter, citric acid 15 g/liter; pH = 3.0 ± 0.1. A) Iron content of deposit (%), B) current density D_c (amps/dm^2); temperature (°C): 1) 30, 2) 70.

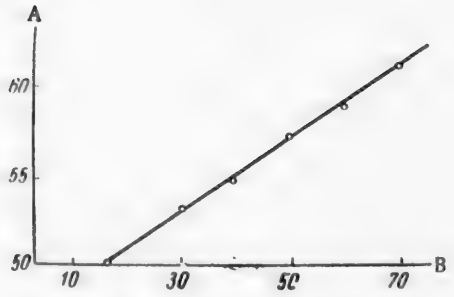

Fig. 2. Effect of electrolyte temperature on the composition of the alloy formed: electrolyte composition — see Fig. 1; D = 50 amps/dm^2; A) Fe content of deposit (%), B) temperature (°C).

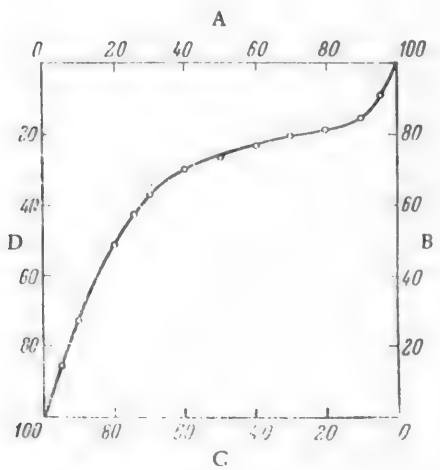

Fig. 3. Effect of the component ratio in the electrolyte on the composition of iron — nickel alloy coatings: electrolyte Σ$[Fe^{++}]$, $[Ni^{++}]$ 100 g/liter, citric acid 15 g/liter; pH = 3.0 ± 0.1; temperature 70° D_c = 40 amps/dm^2; A) Fe content of electrolyte (%) B) Fe content of deposit; C) Ni content of electrolyte (%); D) Ni content of deposit.

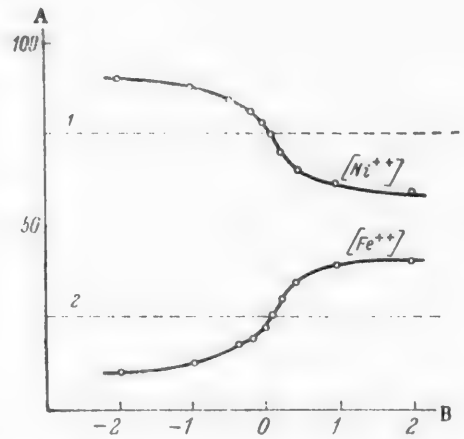

Fig. 4. Variations of electrolyte composition with the use of different ratios of current density at the iron and nickel anodes: electrolyte composition — see Fig. 1; volume 150 cc, temperature 70°, D = 40 amps/dm^2; Q = 8 amp-hrs; original electrolyte: 1) $[N^{++}]$, 2) $[Fe^{++}]$. A) Content of Σ$[Fe^{++}]$, $[Ni^{++}]$ (g/liter), B) values of $\lg \frac{D_{a_{Fe}}}{D_{a_{Ni}}}$.

The electrolytes were prepared from the original solutions taken in the desired proportions; thus the total concentration (calculated as the metals) was always 100 g/liter.

Systematic analysis of the electrolytes and of the deposits formed were performed during the experiments. The data on the compositions of the deposits and electrolytes are average values for triplicate determinations.

In view of the large amount of experimental data obtained, not all the results can be given here; we therefore confine ourselves to individual examples, which are typical in principle for all the cases studied; such data (selected) are presented in Figs. 1 — 4.

Fig. 1 shows variations of the iron content of the deposit with the cathode current density for an electrolyte containing 25 g of iron and 75 g of nickel (as the metals) per liter.

It is clear from the diagram that the composition of the deposit depends to a great extent on the current density and much less on the electrolyte temperature.

It should be noted that high-quality bright or semibright deposits are formed from an electrolyte of this composition at 70° and current densities of 30 – 50 amps/dm^2. To eliminate ferric iron [3], 15 g of citric acid per liter was added to the electrolyte, and the electrolyte pH was maintained in the 3.0 ± 0.1 range.

The use of high current densities not only results in rapid growth of the coatings, as is clear from Fig. 1, but is also more suitable from the point of view of uniform composition over the whole coated surface, as irregularities of the force field and therefore of D_c at different regions of the specimen lead to only slight variations in the composition of the deposit at high current densities.

Fig. 2 shows the effect of temperature on the composition of the deposit obtained from this electrolyte at $D_c = 50$ amps/dm^2; it is seen that in the temperature range studied the iron content increases linearly with the temperature, by about 2% per 10°.

Fig. 3 shows the effect of the iron – nickel ratio in the electrolyte on the composition of deposits from electrolytes containing: $\Sigma[Fe^{++}]$, $[Ni^{++}]$ 100 g/liter (as the metals), citric acid 15 g/liter, at pH = 3 ± 0.1.

It is seen that at low iron concentrations in the electrolyte the deposit formed is relatively richer in iron; as the iron concentration in the electrolyte increases, the relative enrichment of the deposit with iron progressively diminishes, and when the iron concentration in the electrolyte reaches 82.5 g/liter (with a total concentration of 100 g of metals per liter) the deposit becomes enriched with nickel, although to a relatively smaller extent than with iron at the corresponding electrolyte compositions (the data for electrolytes containing 90 g Fe^{++} + 10 g Ni^{++} per liter, and 90 g Ni^{++} + 10 g Fe^{++} per liter respectively may be compared). The absolute concentration of metal ions in the electrolyte has only a slight effect on the contents of the components in the deposit in the concentration range studied (from 60 to 110 g/liter); variations of the relative proportions of $[Fe^{++}]$ and $[Ni^{++}]$ have much more effect, except in the region from 60 to 25% Ni^{++} in the electrolyte, in which the variations of the deposit composition with the electrolyte composition are relatively small. It was therefore particularly important to maintain a constant component ratio in the electrolyte.

Experiments showed that in the range of deposit compositions from 10 to 90% Ni the current efficiency (cathodic) is virtually 100%, probably as the result of considerable depolarization of the electrode owing to formation of a solid solution; if one of the deposited metals is alloyed with less than 10% of the other, hydrogen begins to be liberated together with metal, and the current efficiency therefore falls somewhat. The current efficiency for pure nickel at 40 amps/dm^2 and 70° is 99%, and for iron under the same conditions, 98.6%.

Thus, at low contents of one of the metals in the alloy three kinds of ions are discharged simultaneously – the main metal, the alloying metal and hydrogen.

As the anodes do not become passive, the anodic current efficiencies both for iron and for nickel in electrolytes of the above-named compositions are 100%.

It follows from the foregoing that a very convenient method for maintaining constant electrolyte composition is the use of separate anodes. With 50% of Fe in the deposit, the current strengths at the iron and nickel anodes are in 1 : 1 ratio. If the ratio of the current strengths at the anode is varied, the composition of the electrolyte and therefore of the deposit changes; this is illustrated by the example in Fig. 4.

Thus, the following conditions may be recommended for the production of iron – nickel alloy coatings of any desired composition: 1) electrolyte containing $\Sigma[Fe^{++}]$, $[Ni^{++}]$ 100 g/liter (calculated as the metals, but in chloride form), citric acid 15 g/liter, pH = 3.0 ± 0.1; 2) operating conditions: $D_c = 40$ amps/dm^2, temperature 70° 3) anodic current densities at the iron and nickel anodes selected in accordance with the ratio of the metals in the alloy for the given electrolyte composition, as shown in Fig. 3.

Compact coatings are obtained by this method; in a number of instances (dependent on the composition) they are semibright or bright. Coatings up to 0.5 mm thick or more can be obtained.

In conclusion, the author thanks V. S. Daniel'-Bek for suggesting the subject of this investigation and for guidance, and O. K. Ritter for analytical determinations.

LITERATURE CITED

[1] F. Khol, Slaboproudy Obs, 16, 6, 323 (1955).

[2] U. S. Patent 1,920,964 (1933); R. M. Burns, U. S. Patent 1,837,355 (1931); A. F. Reilly, U. S. Patent 2,060,530 (1936).

[3] V. I. Lainer and N. T. Kudryavtsev, Principles of Electroplating, 2 [in Russian] (Moscow, Metallurgy Press, 1946).

[4] Toepfer, Z. Elektroch., 6, 342 (1899).

[5] R. Kreman, S. Suchy and Machy, Monatsh., 34, 1757 (1913); 35, 731 (1914).

[6] S. Glasstone and T. Symes, Trans. Farad. Soc., 23, 213 (1927); 24, 370 (1928).

[7] S. Glasstone, Trans. Farad. Soc., 19, 574 (1924).

[8] E. Stout and J. Card, Trans. Am. Electrochem. Soc. 58, 357 (1931).

[9] U. S. Patent 2,418,970 (1947).

[10] British Patent 589,561 (1947).

[11] DuRose, Pine, Steel, 114, 24, 124 (1944).

[12] Kaoru Aotani, J. Electrochem. Soc. Japan, 20, 88 (1952).

[13] T. A. Adilov and G. A. Tsyganov, Proc. Acad. Sci. Uzbek SSR, 12, 11 (1955).

[14] Plating and Finishing Guidebook, N. Y., (1943).

[15] N. T. Kudryavtsev, Electroplating Technology [in Russian] (1940).

[16] W. A. Wesley, W. W. Sellers and E. J. Roehl, Proc. Am. Electroplaters Soc., 36, 79 (1949).

[17] L. I. Kadaner, Latest Advances in Electroplating [in Russian] (Khar'kov University Press, 1951).

[18] U. S. Patent 2,507,400 (1950).

Received April 17, 1957

THE DISCHARGE MECHANISM OF A POWDERED-ZINC ELECTRODE

V. N. Flerov

The A. A. Zhdanov Polytechnic Institute, Gor'kii

During recent years the attention of investigators and users has been increasingly drawn to the group of alkali – zinc sources of current (copper – oxide cells, air-depolarization cells, mercury – oxide cells, and silver – zinc and nickel – zinc storage cells). The common feature of all these systems is the use of zinc as the negative electrode and of alkali solution as electrolyte.

Together with its well-known merits (ready availability, high negative potential, etc.), the solid zinc electrode has a number of disadvantages. These disadvantages hindered further increases in the specific capacity of alkali – zinc systems and the production of powerful storage batteries with the use of these electrodes. Among the most important defects is passivation of the electrode which occurs at high discharge rates or when the electrolyte is highly saturated with zincate. The onset of passivity could only be retarded by the use of optimum current densities [1, 2] or of special additives [3].

The problem of the zinc anode with low tendency to passivity was solved by the introduction of the powder electrode. Such electrodes were first suggested as long ago as 1936 [4, 5], and introduced industrially during the Second World War. Powdered-zinc electrodes are now used in silver – zinc storage batteries [6], mercury – oxide cells [7], and certain types of cells with air depolarization [8].

Despite the great practical importance of such electrodes, there are hardly any publications dealing with their action mechanism.

The purpose of the present investigation was to study the discharge characteristics of powdered-zinc electrodes in alkaline electrolytes.

EXPERIMENTAL

Powdered-zinc electrodes were made by two methods: 1) by briquetting of a mixture of 100 parts of zinc dust and 8 parts of K_2CO_3 solution, 1.10, under a pressure of 100 kg/cm^2; 2) briquetting of electrolytic zinc powder at 100 kg/cm^2 pressure for production of high-porosity electrodes ($p \approx 50\%$) and at ~ 3.5 tons/cm^2 for the production of low-porosity electrodes ($p \approx 18\%$).

Zinc powder was prepared by electrolysis of a zincate solution containing 5 N $NaOH_{total}$, 0.5 N Zn, at $D_{c,a} = 2.0$ amps/dm^2 and room temperature, with the use of zinc anodes and an iron zinc-coated cathode [9]. The spongy zinc deposit was washed free from alkali by repeated decantation in water saturated with CO_2. The filtered deposit was dried rapidly at 150-170° in air. The powder had bulk density 0.75 g/cc, and contained 96-97% of metallic zinc.

Solid zinc electrodes were cast from Ts-O grade zinc.

The zinc electrodes were discharged in pairs with inert (nickel) or with copper – oxide electrodes, made with a combustible binder.

Rectangular cells ~ 250 ml in capacity were used for experiments on passivation of zinc anodes in pure alkalies. The onset of passivity in such an anode, operating in a pair with an inert electrode, was indicated by an abrupt jump of potential, measured by means of the PPTVI potentiometer.

TABLE 1

Time for Passivation of Zinc Anodes in Pure Alkalies Temperature 20°

Type of zinc electrode	NaOH (1.9)	KOH (1.40)	
	passivation time (min) at different D_a		
	6 (amp /dm²)	8 (amp /dm²)	9 (amp /dm²)
Powdered ($p \approx 18\%$)	10	12	10
	11	10	9
Solid	32	34	11
	35	36	10.5

Cells of the copper – copper oxide type, each assembled from a zinc and two copper – oxide electrodes freely suspended in the vessel, were discharged until the zinc electrode was completely passive; the capacity was determined by means of a copper coulometer. The high-porosity zinc electrodes were wrapped in 2 layers of cellophane and assembled in cells, with more dense packing in organic glass vessels. The cellophane was previously washed free from glycerol and then treated with $MgCl_2$ solution. There was an excess of the active materials of the positive and negative electrodes, and a deficiency of the electrolyte, in all the cells.

The tests were performed in a thermostat with a mercury – toluene thermoregulator, regulated to within ±0.1°.

The methods used for determination of zinc and alkali in the electrolytes were described previously [10].

All the materials used were of chemically pure or reagent grade.

The porosity (packing density of the particles) has the greatest influence on the characteristics of a powdered-zinc electrode.

TABLE 2

Effects of Type of Zinc Electrode and Electrolyte on Cell Capacity t = +20° I = 80 ma, D_a = 0.53 amp/dm² (40 ml of electrolyte)

Cell No.	Type of zinc electrode	Electrolyte	Capacity (amp-hr)	Specific consumption of electrolyte (ml/amp-hr)	Maximum zinc concentration in electrolyte (g/liter)
1	Solid	9.5 N KOH	9.55*	4.19	199
2	The same		9.55*	4.19	196
3	Powder $p \approx 18\%$		5.82	6.88	151
4	Powder $p \approx 18\%$		5.82	6.88	153
5	Solid	5.8 N KOH	7.31	5.48	116
6	The same		7.09	5.65	120
7	Powder $p \approx 18\%$		3.54	11.3	88
8	The same		3.67	10.9	90
9	Solid	5 N NaOH	5.4	7.41	145
10	The same		5.5	7.28	148
11	Powder $p \approx 18\%$		3.10	12.9	90
12	The same		3.04	13.1	88

* Cells taken off discharge before passivation of zinc electrode.

A powdered-zinc electrode of low porosity becomes passive in pure alkalies much more rapidly than a solid electrode (Table 1). This effect is observed in alkalies of different concentrations and at different current densities; the time required for passivation becomes approximately the same for both types of electrode only at very high D_a.

The nature of the passive films differs on electrodes of the two different types. Whereas a dark gray film is formed on solid electrodes, powder anodes after passivation are coated with a white deposit with a dark gray film under it.

Low-porosity powder electrodes also become passive more rapidly when used in cells, i.e., during discharge at moderate current densities in an electrolyte with a gradually increasing zincate concentration (Table 2).

Powdered-zinc electrodes of high porosity ($p \approx 50\%$) have entirely different characteristics. Such electrodes do not become passive even at relatively high current densities, although they are wrapped in cellophane film which prevents diffusion of the electrolyte. Cells with such electrodes became inoperative only after most of the active material had been consumed. The specific electrolyte consumption is much lower in such cells than in cells with solid or powdered electrodes of low porosity, not wrapped in cellophane (Tables 2, 3). The latter types of electrodes, wrapped in cellophane, are useless in practice – they rapidly become passive when put on discharge (Table 3).

TABLE 3

Effect of Type of Zinc Electrode on Cell Capacity t = +20°, D_a = 0.65 amp/dm², 5 ml of electrolyte (zinc electrodes wrapped in 2 layers of cellophane)

Capacity	Type of zinc electrode									
	solid	powdered $p \sim 18\%$	power $p \sim 50\%$		from zinc dust $p \sim 40\%$		power $p \sim 50\%$		from zinc dust $p \sim 40\%$	
	5.8 N KOH						5 N NaOH			
Output capacity (amp-hr)	0.15	0.35	4.2	4.3	3.3	3.2	3.7	3.9	2.7	2.5
Specific electrolyte consumption (ml/amp-hr)	33.3	14.3	1.19	1.16	1.51	1.56	1.35	1.28	1.85	2.0

Note: Zinc-dust electrodes were charged until hydrogen began to evolve before being put on discharge.

The zincate concentration of the electrolyte does not reach such high values with the use of powdered-zinc anodes as in cells with solid electrodes (Table 2). In cells with powder electrodes (not wrapped in cellophane) the electrolyte became turbid and a ZnO precipitate appeared soon after the start of discharge. Because of the lower zincate concentration, an electrolyte obtained after discharge of powder electrodes shows very little aging effects, in contrast to electrolytes from cells with solid electrodes (Table 4).

If the powder electrodes are wrapped in cellophane, the decrease of the zinc concentration in the electrolyte is still greater (Table 5). Such electrolytes do not undergo aging even at elevated temperatures.

DISCUSSION OF RESULTS

It is seen that two of the defects found in solid zinc electrodes in zincate solutions can be eliminated almost completely by the use of high-porosity powdered-zinc electrodes. Powdered-zinc electrodes do not become passive even at high current densities. The electrolyte in which such an electrode is discharged is almost free from aging. Because of this last fact, the loss of active material from the zinc electrode of an alkaline storage cell by spontaneous precipitation of zinc oxide or hydroxide from the electrolyte can be avoided.

In our opinion the difference between the properties of powder and solid electrodes cannot be attributed merely to the lower actual current density on the powder electrode, which has the greater surface. If this was the case, the porosity of the electrode should not have such a pronounced influence on its behavior. The absence of any appreciable difference of polarization between solid and powder (unwrapped) electrodes, and the different maximum zincate concentrations in electrolytes after discharge of these electrodes, indicate that the influence of surface area is more complex.

TABLE 4

Aging of Zincate Electrolytes from Cells with Different Types of Zinc Electrodes, at t = +20°

Type of zinc electrode	Electrolyte	Zinc concentration (g/liter) after aging time (days)					
		0	1	3	7	15	30
Solid	KOH (9.5 N)	197	196	194	172	148	132
Powder	KOH (9.5 N)	152	152	152	151	149	141
Solid	KOH (5.8 N)	119	115	106.5	92.5	78.7	61.7
Powder	KOH (5.8 N)	88	88	88	88	88	88
Solid	NaOH (5 N)	146	117	100.5	88.1	80	73.5
Powder	NaOH (5 N)	88.5	88.5	88.5	87.2	84.3	81.2

We consider that these differences are due to differences in the character of the hydroxide film formed on the surface of the zinc electrode during discharge [3].

If the zincate concentration in the electrolyte is considerable, or if the current density is high, a permanent film of zinc hydroxide (or oxide) is formed on the surfaces both of powder and of solid zinc anodes. However, whereas the thickness of this film on a solid electrode increases relatively slowly, because part of it passes into solution in the form of zincate ions or colloidal particles [11], the situation is somewhat different with a powdered-zinc anode.

The hydroxide film on an individual zinc particle should behave similarly to the film on solid zinc so long as some unused metal remains in the particle (or, more accurately, while current can reach it). When the particle is fully discharged, a relatively large hydroxide film is left. The next zinc particle entering the discharge reaction begins to form its own hydroxide film. The hydroxide remaining after discharge of the previous particle undergoes fairly rapid aging, both because of its large size and because of its distance from the reaction zone. Aging can continue up to formation of ZnO, which partially remains on the electrode surface.

TABLE 5

Concentration of Zinc in Electrolytes of Nickel – Zinc Storage Cells

Electrolyte	KOH (1.20)	KOH (1.30)	KOH (1.40)	NaOH (1.19)
Zinc concentration (g/liter)	25	45	61	31

Note: Discharged cells used for several cycles were used for the analysis.

In our opinion, the constant renewal of the acting electrode surface is the most important cause of the more rapid formation of a ZnO film on the surface of a powdered-zinc anode.

If the porosity of such an electrode is low and the zinc particles are closely packed, then a continuous oxide film of low porosity is formed on its surface. The low porosity of this film is due not only to the close initial packing but also to the greater volume of the discharge products as compared with the original material. The more rapid aging of the hydroxide (or oxide) film on a powder electrode results in more rapid passivation (Tables 1 and 2).

In powdered-zinc electrodes of high porosity the anode film also ages more rapidly, but this film is no longer continuous. The products of discharge are formed in a loose state, owing to the highly porous packing of the active electrode material. Because of the porous character of the oxide film, such electrodes are much less prone to passivation than solid electrodes (Table 3).

In addition to porosity, particle size and surface area must undoubtedly have a strong influence. Electrodes with larger active particles, which have a smaller specific surface, are closer to solid electrodes in their properties. The observed decrease of the capacity of powdered-zinc electrodes in alkali – zinc cells with the number of service cycles is due, in our opinion, to the gradual growth of the particles of active material, which is mainly the consequence of aging processes.

If a high-porosity powder anode is regarded as an aggregate of microanodes, it is seen that the nature and concentration of the electrolyte should primarily influence the degree of utilization of the active material (Table 4). An electrolyte in which a porous hydroxide (or oxide) film is formed on the individual zinc particles should favor their more complete "conversion". An important role is also played, no doubt, by the degree of electronic conductivity of the ZnO formed, which is a semiconductor [12].

Accelerated aging of the solid discharge products, which form a film on the surface of the powder electrode, retards the conversion of zinc into the ionic state (Table 2). This is caused by the hindered access of electrolyte to the active forms of zinc hydroxide present within the depth of the anodic film. If the powder electrode is wrapped in cellophane, the zincate concentration in the outer electrolyte space is lowered still further because the colloidal phase cannot pass through the semipermeable cellophane. The decrease of zinc concentration leads to sharp retardation of electrolyte aging, as was reported earlier [10] (Tables 4, 5).

SUMMARY

1. The discharge characteristics of powdered-zinc electrodes of different porosities, and the properties of the zincate electrolytes formed in the discharge of these electrodes were studied; it was found that low-porosity powder electrodes become passive more rapidly than solid electrodes, whereas highly-porous electrodes wrapped in cellophane do not become passive even at relatively high current densities.

2. The maximum zincate concentration in the electrolyte is lower in the discharge of powder than of solid electrodes. The former solutions are almost free from aging effects.

3. The differences between the discharge characteristics of powdered and solid electrodes are attributed to constant renewal of the acting surface of a powdered electrode and to the more rapid aging of the hydroxide film formed on the electrode surface during discharge.

LITERATURE CITED

[1] Z. A. Iofa, S. Ya. Mirlina and N. B. Moiseeva, J. Appl. Chem. 22, 983 (1949).

[2] Z. A. Iofa, S. Ya. Mirlina, N. B. Moiseeva and E. E. Krymakova, Collected Papers on Air-Depolarized Alkaline Cells [in Russian] (Moscow – Leningrad, Gosenergoizdat, 1949) p. 26.

[3] V. N. Flerov, J. Appl. Chem. 30, No. 9, 1326 (1957).*

[4] Drumm, British Patent 365,125 (1932).

[5] H. G. Andre, French Patent 813,319 (1936).

[6] S. Eidensohn, J. Electroch. Soc., 99, 252 (1952).

[7] J. M. Booe, J. Electroch. Soc., 99, 197 (1952).

[8] E. A. Schumacher and G. W. Heise, J. Electroch.Soc., 99, 191 (1952).

[9] O. Kudra and E. Gitman, Electrolytic Production of Metal Powders [in Russian] (Kiev, Acad. Sci. USSR Press, 1952).

[10] V. N. Flerov, J. Appl. Chem. 29, 1779 (1956).*

[11] V. N. Flerov, J. Phys. Chem. 31, 49 (1957).

[12] A. F. Ioffe, Semiconductors in Modern Physics [in Russian] (Moscow – Leningrad, Izd. AN SSSR, 1954).

Received May 16, 1957

* Original Russian pagination. See C.B. Translation.

THE PROTECTIVE ACTION OF VOLATILE INHIBITORS AND ANTICORROSION GREASES AT TROPICAL TEMPERATURES AND HIGH HUMIDITIES*

B. E. Piskorskii and E. M. Il'ina

The use of volatile inhibitors has become very prominent in recent years for the prevention of corrosion, mainly of steel articles. These inhibitors vary greatly in composition; they are nearly all cyclic or aliphatic organic compounds. They are mostly salts of weak bases or organic acids, nitrite esters, or compounds containing nitro, nitroso, or amino groups. Their vapor pressures are generally low and the solubility in water is slight.

Among the numerous volatile inhibitors, dicyclohexylammonium nitrite (known by the trade name of Dichan) is most widely used abroad.

It was desired to compare the protective action of this inhibitor with that of liquid anticorrosion greases which are used with success at some of our factories, and also of certain other effective volatile inhibitors.

The experiments were performed under conditions approximating to those in tropical countries: ~ 98% relative humidity, and temperatures of 57-63°.

The following liquid anticorrosion greases were tested.

1) Vaseline oil with addition of 2% montanon barium soap [2]. Montanon is an artificial wax obtained by extraction from bituminous brown coals; it was saponified with barium hydroxide at about 200°, and the soap was dissolved in vaseline oil at 170-180° deg.

2) Chromate grease – vaseline oil containing 10% suspended potassium chromate and 2% ozokerite [2].

3) Thin grease: 10% gasoline solution of a melt of aluminum oleate and ozokerite [3].

The degree of corrosion was estimated visually on a six-mark scale [1]. Mark 1 means that the whole surface of the specimen is covered with rust; mark 6 means absence of rust. Marks 2, 3, 4, and 5 indicate the degree of rusting in decreasing order. This method gives a reliable picture for comparison of several specimens.

A second characteristic of the protective power of a grease or volatile inhibitor is the "protection coefficient" [2]. It is given by the formula

$$K_p = \frac{a - a_0}{1 - a_0},$$

where a is the ratio of the total marks of the protected specimens to the maximum total marks, i.e., to the marks if no corrosion took place; $a = \frac{Z_{act}}{Z_{max}}$; a_0 is the corresponding ratio for specimens not protected by grease or volatile inhibitor.

If the protection is complete $K_p = 1$, and if there is no protection at all $a = a_0$ and $K_p = 0$.

* Communication V in the series on the rusting of steel articles during production and storage [1 – 3].

Specimens of low-carbon steel strip were used for the corrosion tests in our investigations. The test specimens were suspended from glass hooks in desiccators containing water, in presence and in absence of volatile inhibitor. Some of the specimens were coated with anticorrosion greases in order to determine the effects of inhibitors on the protective powers of the greases.

TABLE 1

Comparative Corrosion Resistance Tests with Protection by Volatile Inhibitors and Liquid Greases (Steel strip specimens were tested (4 in each test) at relative humidity ~98%, temperature 57°, time 26 days; volatile inhibitor in powder form spread in a uniform layer over a porcelain plate 54 cm^2 in area; desiccator volume 1 liter)

Expt. No.	Composition of volatile inhibitor and grease	Average mark	Protection coefficient	Notes
I	Desiccator with dicyclohexylammonium nitrite (Dichan):			
	1) specimens without grease	3.25	0.42	
	2) thin grease	4.25	0.68	
	3) vaseline oil + 2% montanon barium soap	6	1	No corrosion
II	Desiccator with dicyclohexylammonium benzoate:			
	1) specimens without grease	2.0	0.14	
	2) thin grease	4.0	0.56	
	3) vaseline oil + 2% montanon barium soap	5.75	0.94	1 point on 60 cm^2 surface
III	Desiccator with urea:			
	1) specimens without grease	2.75	0.35	
	2) thin grease	4.25	0.68	
	3) vaseline oil + 2% montanon barium soap	6	1	No corrosion
IV	Desiccator with a mixture of urea and sodium nitrite (50%):			
	1) specimens without grease	3.0	0.37	
	2) thin grease	4.0	0.56	
	3) vaseline oil + 2% montanon barium soap	5.0	0.79	
V	Desiccator without volatile inhibitor:			
	1) specimens without grease	1.25	0	Specimens almost completely rusted
	2) thin grease	3.5	0.47	
	3) vaseline oil + 2% montanon barium soap	6	1	No corrosion

The amount of volatile inhibitor in each desiccator was such that its vapor concentration in the desiccator was constantly at a maximum. The desiccators were put in a thermostatically controlled chamber and opened at intervals to replenish the oxygen consumed in rusting. The experimental temperature was lowered twice to room level for short intervals in order to produce abundant dew.

The results of the tests are given in Tables 1 and 2.

It follows from the data in Table 2 that the volatile inhibitors tested, including Dichan, are considerably inferior in protective properties to the liquid anticorrosion greases. For example, a grease containing 2% of montanon barium soap protected the metal completely against corrosion in Experiments I, III, and V, while in Experiment II corrosion was insignificant (one point on 4 specimens, i.e., per 60 cm^2 of surface). The presence of inhibitor had no appreciable effect on this grease. The protective effect of the thin grease was increased considerably in presence of volatile inhibitors, especially Dichan (Experiments I, III, and V), but its protective effect was greater than that of the volatile inhibitors, although not to the same extent as the effect of the grease with montanon barium soap.

For investigation of the protective effect of liquid anticorrosion greases at tropical temperatures and high humidity in absence of volatile inhibitors, the steel strip specimens coated with the greases were exposed for 26 days at a higher temperature (63°) and ~ 98% relative humidity. The results of the tests are given in Table 2.

TABLE 2

Protective Effects of Liquid Anticorrosion Greases at 63° and ~ 98% Relative Humidity in Tests Lasting 26 Days; Steel Strip Specimens (4 per test) Were Tested

Grease No.	Grease	Average mark	K_p	Notes
1	Vaseline oil with 2% montanon barium soap	5.5	0.89	2 points on 60 cm² surface
2	Same grease + 4% ceresin	5.0	0.77	
3	Same grease + 10% ceresin	4.0	0.60	
4	Same grease + 10% lanolin	6	1	No corrosion
5	Thin grease	2.75	0.28	
6	Same grease + 5% lanolin	3.50	0.44	
7	Vaseline oil + 10% lanolin	3.75	0.50	
8	Pure vaseline oil	2.75	0.28	
9	Chromate grease	5.0	0.64	
10	Same grease + 5% lanolin	5.5	0.89	
11	Specimens without grease	1.5	0	Specimens almost completely rusted

It follows from Table 2 that at high humidities and tropical temperatures the liquid anticorrosion greases with additions of montanon barium soap, and chromate greases, have considerably higher protective effects then volatile inhibitors (Table 1).

Despite the more severe test conditions (63°), the grease with added montanon barium soap and chromate grease gave good results. Additions of lanolin increased the protective effects of all the anticorrosion greases tested; it is seen in the table that a grease with 2% montanon barium soap and 10% lanolin gave complete protection against corrosion (Table 2, No. 4).

Protection with volatile inhibitors alone was not very effective (Table 1).

Only the thin grease was influenced by the volatile inhibitor; its protective effect was intensified appreciably by 10% solution of aluminum oleate in gasoline.

It should be noted that our results are at variance with the findings of certain American workers [4, 5] who state that dicyclohexylammonium nitrite (Dichan) is superior to the best anticorrosion greases in its effect.

According to Baker [5], steel specimens tested at 66° in an atmosphere of about 98% relative humidity for 168 hours (7 days) in presence of Dichan or a mixture of sodium nitrite and urea were not corroded. Nevertheless, he recommends preliminary greasing of steel articles, followed by the use of a volatile inhibitor, for protection against corrosion. His claim that the protective power of the grease is increased in presence of volatile inhibitors is confirmed by our experiment, but only for the thin grease.

Wachter [4] performed prolonged open-air tests on steel specimens coated with various anticorrosion greases and wrapped in inhibitor paper. Parallel tests were performed in the same packing on ungreased specimens and greased specimens without volatile inhibitor. The outer packing consisted of waterproof paper sealed with wax at the corners. Wachter found that inhibitor paper impregnated with Dichan completely protected ungreased specimens from corrosion during 5-year tests. Greased specimens were slightly corroded in presence of Dichan; greased specimens without Dichan were appreciably corroded (85% of the total surface). Our accelerated tests under more severe conditions gave results which do not agree with these data.

SUMMARY

1. Tests showed that although the use of volatile inhibitors is very convenient, their protective action at high humidities and elevated temperatures is considerably inferior to the effect of the anticorrosion greases tested by us earlier.

2. Dichan, urea, and mixtures of urea with sodium nitrite increase appreciably the protective effect of thin grease but have no effect on the other liquid anticorrosion greases tested.

3. A grease containing 2% montanon barium soap and 10% lanolin gave complete protection against corrosion in 26-day tests at approximately 98% relative humidity and 63°.

LITERATURE CITED

[1] V. V. Skorcheletti and V. E. Piskorskii, J. Appl. Chem. 26, No. 7, 730 (1953).*

[2] V. V. Skorcheletti and V. E. Piskorskii, J. Appl. Chem. 27, No. 3, 314 (1954).*

[3] V. V. Skorcheletti, A. I. Bukhbinder and V. E. Piskorskii, J. Appl. Chem. 27, No. 4, 454 (1954).*

[4] A. Wachter, Corrosion 7, 9, 284 (1951).

[5] R. Baker, Ind. Eng. Ch., 46, 12, 2595 (1954).

Received March 28, 1958

* Original Russian pagination. See C. B. Translation.

STUDY OF THE PROTECTIVE ACTION OF MIXTURES OF CORROSION INHIBITORS IN NEUTRAL MEDIA

A. S. Afanas'ev and G. V. Zhuk

The Dnepropetrovsk State University

Inhibitors, which are substances which retard corrosion in neutral and almost neutral media, are used with success for prevention of corrosion. Such inhibitors are also effective against submerged corrosion. Several corrosion inhibitors of practical importance were studied by Rozenfel'd [1].

Inhibitors are often more effective when used jointly, but such combinations (mixtures) of inhibitors have been little studied from the quantitative aspect as yet. We have studied a number of mixtures of inhibitors of atmospheric corrosion, suitable for technical uses. The results of laboratory tests are given in this paper.

EXPERIMENTAL

The tests were performed on specimens of St 20 steel (20 × 50 × 0.3 mm with projection), carefully cleaned with No. 0 and No. 00 emery cloth and degreased by 3-fold washing with freshly distilled alcohol.

For the atmospheric corrosion (AC) tests, specimens covered with filter paper or moistened with the original solution (NaCl 0.030 g/liter, Na_2SO_4 0.070 g/liter, as used by Rozenfel'd [1]) with and without added inhibitor were suspended from stands in beakers with a little of the same solution on the bottom. The beakers were covered, but the air in them was renewed at intervals. The experimental procedure was described previously [2]. Parallel tests were performed with submerged corrosion (SC), similar specimens (not covered with filter paper) being completely immersed in the same solutions. The tests lasted up to 5650 hours at room temperature.

All the specimens were weighed to the nearest 0.1 mg before the experiments, and after complete removal of rust by cathodic etching in alkali [3]. Five specimens were taken for each experimental point. The external appearance of the specimens was observed and photographed during the tests.

The following inhibitors were added to the original solution: sodium nitrite ($NaNO_2$), sodium silicate ($Na_2SiO_3 \cdot 9H_2O$, $Na_2O : SiO_2 = 1.03 \pm 0.03$), sodium triphosphate ($Na_3PO_4 \cdot 12H_2O$), technical triethanolamine $N(CH_2CH_2OH)_3$, Emulsol B (GOST 1975-53), mixtures of sodium nitrite and silicate, mixtures of sodium nitrite and triethanolamine, and mixtures of Emulsol and sodium triphosphate and silicate. The concentrations are given later in this paper. The pH was determined by means of the LP-5 electronic potentiometer and a glass electrode. The determinations were accurate to within ± 0.1 pH unit.

The weight loss K was calculated in grams per 1 m^2 of apparent specimen area, and the protective effect (Z) was expressed in percentages [4]. The subscripts 0 i, and m to K and Z correspond to the original solution without inhibitor, inhibitor solution of a given concentration, and solutions of a mixture of the same inhibitor with other inhibitors.

The relative effect of inhibitor mixing was indicated by the magnitude and sign of the "mixing effect" (E, %). E is the relative increase or decrease of the protective (or stimulating) action of the component inhibitors resulting from the mixing of inhibitors, the concentrations being constant:

$$E = Z_m - Z_i = \frac{K_i - K_m}{K_0} \cdot 100.$$

If the protective effect of a particular inhibitor is intensified when it is mixed with another, so that the second "helps" the first, $E > 0$. If the protective effect is weakened, and the second inhibitor appears to "hinder" the first, $E < 0$.

The main inhibitor of a mixture was taken to be the inhibitor with the highest Z_i, and the others were subsidiary inhibitors.

The main mixing effect is $E_{main} = Z_m - Z_i$ of the main inhibitor. The subsidiary mixing effect is $E_{subs} = Z_m - Z_i$ of the subsidiary inhibitor.

TEST RESULTS

Original solution. Table 1 shows the course of corrosion of specimens in the original solution without inhibitors (pH = 5.9).

TABLE 1

Variations of the Weight Loss of St 20 Specimens (K in g/m^2) With Duration of Test in the Original Solution at Room Temperature

Test Conditions	Weight loss K (g/m^2) after test time (hours)						
	315	910	1450	2930	3930	5650	7215
AC	50.7	63.1	69.2	72.5	105.5	111.8	—
SC	16.1	38.0	45.7	135.3	153.3	227.6	242.6

Mixture of sodium nitrite and silicate. The test results are presented in Fig. 1 (AC) and 2 (SC). The inhibitor concentrations in the mixture (in g/liter) are shown at the bottom of the diagrams. The columns, drawn to scale, show the weight losses of the specimens (K in g/m^2) in a definite time in the original solution, in solutions of sodium nitrite, sodium silicate, and mixtures of these inhibitors in the concentrations shown. The absence of any particular column means that there is no appreciable corrosion in the corresponding solution. The same notation is used in all the diagrams. These diagrams show both the inhibiting and the stimulating effects of individual inhibitors (the latter effects are found mainly at low concentrations). The inhibitor mixtures studied had only a retarding effect on corrosion. The main inhibitor in this mixture is sodium nitrite. The "mixing effects" for different mixtures of these inhibitors are given in Table 2.

Mixture of sodium nitrite and triethanolamine. The test results are presented in Fig. 3 (AC) and 4 (SC). As in mixtures of sodium nitrite and silicate, the main inhibitor in this case is sodium nitrite.

It is clear from Fig. 3 that at certain concentrations both the individual inhibitors and their mixtures may have either inhibiting or stimulating effects on the atmospheric corrosion of steel. Fig. 4 (SC) shows that mixtures and individual inhibitors have only inhibiting effects (with the exception of nitrite alone, at concentrations up to 0.1 g/liter). The values of the "mixing effect" for different mixtures of sodium nitrite and triethanolamine are given in Table 3.

Mixtures of Emulsol, sodium silicate, and sodium triphosphate. The test results are presented in Fig. 5 (AC) and 6 (SC).

Fig. 5 (AC) shows that at lower inhibitor concentrations the individual inhibitors and their mixtures may have either inhibiting or stimulating effects (Fig. 5,a); at higher concentrations (Fig. 5,b) only inhibiting effects are found. Fig. 6 (SC) shows that only sodium silicate at certain concentrations can have either an inhibiting or a stimulating effect; the other inhibitors and their mixtures have only a protective effect on steel. The main inhibitor in these mixtures is Emulsol. The values of the mixing effect for different mixtures of Emulsol and sodium triphosphate are given in Table 4.

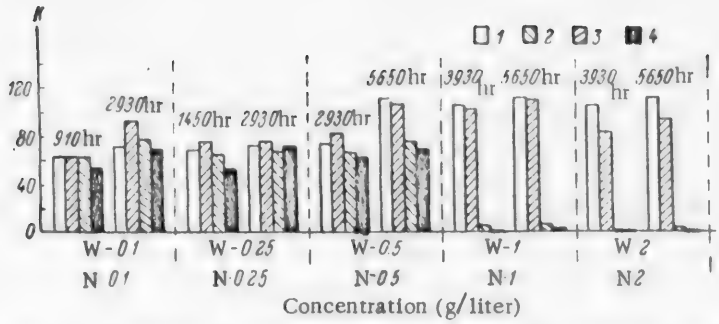

Fig. 1. Variation of atmospheric corrosion of St 20 specimens with the concentrations of sodium nitrite and silicate inhibitors in mixtures, and with duration of tests at room temperature.
Solutions: 1) original, 2) $NaNO_2$ (N), 3) Na_2SiO_3 (W), 4) mixture of Na_2SiO_3 and $NaNO_2$.

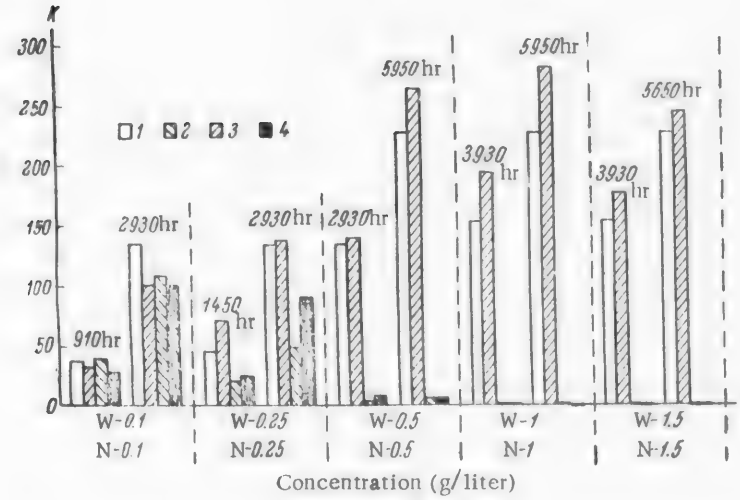

Fig. 2. Variation of submerged corrosion of St 20 specimens with the concentrations of sodium nitrite and silicate inhibitors in mixtures, and with duration of tests at room temperature.
Designations as in Fig. 1.

DISCUSSION OF RESULTS

The following conclusions may be drawn from the results of the investigation.

1) The solutions of mixtures of sodium nitrite and silicate studied, in contrast to solutions of these inhibitors taken separately, prevented the corrosion of steel in all cases (AC and SC). Solutions of each of the two inhibitors stimulate the corrosion of steel – sodium nitrite at concentrations up to 0.1 g/liter (AC and SC), and sodium silicate up to 0.5 g/liter (AC) and 0.1-0.5 g/liter (SC). Complete protection against corrosion ($Z_i \approx 100\%$) is given by sodium nitrite at concentrations above 2 g/liter (AC) and 1.5 g/liter (SC), and by sodium silicate above 25 g/liter (AC) and 10 g/liter (SC). For complete protection of steel against corrosion, the concentrations of these inhibitors in mixtures should be not less than 2 g/liter (AC) and 1.5 g/liter (SC).

It follows from the data in Table 2 that for mixtures of these inhibitors the main mixing effect (E_{NaNO_2})

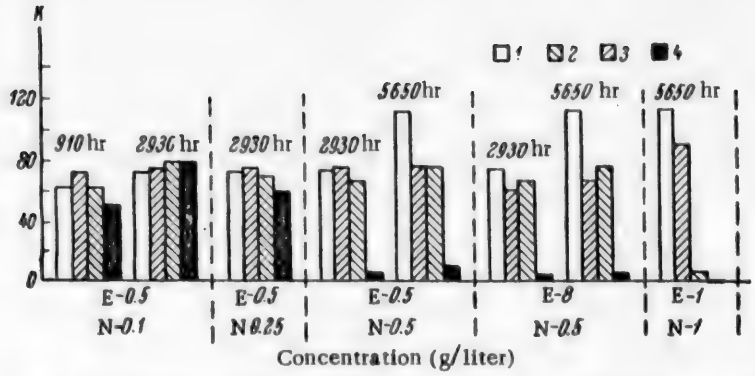

Fig. 3. Variation of atmospheric corrosion of St 20 specimens with the concentrations of sodium nitrite and triethanolamine inhibitors in mixtures, and with duration of tests at room temperature.
Solutions: 1) original, 2) $NaNO_2$(N), 3) triethanolamine (E), 4) mixtures of $NaNO_2$ and triethanolamine.

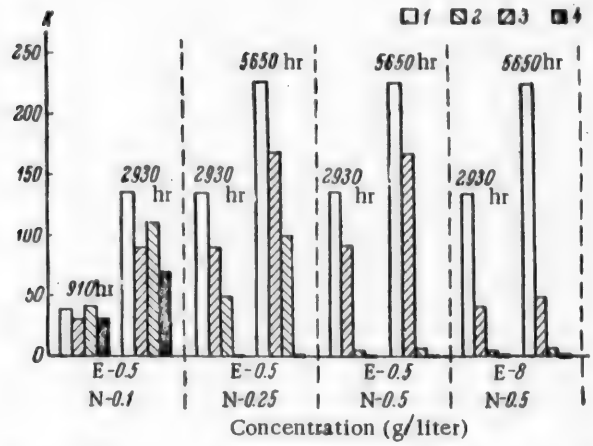

Fig. 4. Variation of submerged corrosion of St 20 specimens with the concentrations of sodium nitrite and triethanolamine inhibitors in mixtures, and with duration of tests at room temperature.
Designations as in Fig. 3.

is small, while the subsidiary effect is considerable. It is therefore useful to add nitrite to sodium silicate used in practice as a corrosion inhibitor.

It has already been noted that if sodium nitrite and silicate are mixed, the stimulating effects of low concentrations of these inhibitors are completely eliminated. It is known that sodium silicate is an especially effective inhibitor for aluminum and its alloys, even in strongly alkaline solutions [1]. Our experience with the use of these inhibitors for protection of machine parts and equipment under factory conditions shows that sodium silicate acts as an inhibitor for aluminum and its alloys, and for other nonferrous metals and alloys, in nitrite solutions. Therefore in a number of practical cases sodium silicate should also be added to solutions containing sodium nitrite, for example, to wash liquors and to cooling and lubricating fluids. Since sodium silicate has a high detergent effect, its addition to wash liquors should be especially useful.

TABLE 2

Mixing Effects (E) of Mixtures of Sodium Nitrite and Silicate for Different Corrosion Times of St 20 Specimens at Room Temperature

Inhibitor	concentration (g/liter)	pH	test conditions	Mixing effect (E, %) for corrosion time (hours)									
				910		1450		2930		3930		5650	
				main E_{NaNO_2}	subsidiary $E_{Na_2SiO_3}$	main E_{NaNO_2}	subsidiary $E_{Na_2SiO_3}$	main E_{NaNO_2}	subsidiary $E_{Na_2SiO_3}$	main E_{NaNO_2}	subsidiary $E_{Na_2SiO_3}$	main E_{NaNO_2}	subsidiary $E_{Na_2SiO_3}$
$NaNO_2$	0.1	9.6	AC	+ 5	+15	—	—	+13	+35	—	—	—	—
Na_2SiO_3	0.1		SC	+32	+12	—	—	+ 6	− 1	—	—	—	—
$NaNO_2$	0.25	10.5	AC	—	—	+18	+32	− 7	+ 5	—	—	—	—
Na_2SiO_3	0.25		SC	—	—	− 9	+98	−31	+34	—	—	—	—
$NaNO_2$	0.5	10.9	AC	—	—	—	—	+ 6	+27	—	—	+6	+ 34
Na_2SiO_3	0.5		SC	—	—	—	—	− 2	+98	—	—	0	+107
$NaNO_2$	1	11.2	AC	—	—	—	—	—	—	+3	+ 95	+2	+ 95
Na_2SiO_3	1		SC	—	—	—	—	—	—	0	+125	+1	+124
$NaNO_2$	1.5	11.2	AC	—	—	—	—	—	—	0	+ 80	0	+ 77
Na_2SiO_3	1.5		SC	0	—	0	—	0	—	0	+115	0	+108
$NaNO_2$	2	11.4	AC	0	—	0	—	0	—	0	+ 78	+2	+83
Na_2SiO_3	2		SC	0	—	0	—	0	—	0	+ 43	0	—

TABLE 3

Mixing Effects (E) of Mixtures of Sodium Nitrite and Triethanolamine for Different Corrosion Times of St 20 Specimens at Room Temperature

Inhibitor	concentration (g/liter)	pH	test conditions	Mixing effect (E, %) for corrosion time (hours)									
				910		1450		2930		3950		5650	
				main E_{NaNO_2}	subsidiary $E_{triethanolamine}$	main E_{NaNO_2}	subsidiary $E_{triethanolamine}$	main E_{NaNO_2}	subsidiary $E_{triethanolamine}$	main E_{NaNO_2}	subsidiary $E_{triethanolamine}$	main E_{NaNO_2}	subsidiary $E_{triethanolamine}$
$NaNO_2$	0.1	9.3	AC	+22	+36	—	—	0	− 5	—	—	—	—
triethanolamine	0.5		SC	+26	+ 2	—	—	+30	+15	—	—	—	—
$NaNO_2$	0.25	9.4	AC	—	—	+50	—	+11	+21	—	—	—	—
triethanolamine	0.5		SC	—	+82	+45	—	+36	+66	—	—	—	+74
$NaNO_2$	0.5	9.4	AC	—	—	—	—	+84	+95	—	—	+60	+60
triethanolamine	0.5		SC	—	—	—	—	+ 4	+66	—	—	+ 4	+74
$NaNO_2$	0.5	10.4	AC	—	—	—	—	+86	+74	—	—	+63	+54
triethanolamine	8		SC	—	—	—	—	+ 4	+30	—	—	+ 4	+20
$NaNO_2$	1	9.7	AC	—	—	—	+125	—	—	+4	—	+ 4	+79
triethanolamine	1		SC	—	—	—	+119	—	—	+1	—	+ 1	+84

TABLE 4

Mixing Effects (E) of Mixtures of Emulsol and Sodium Silicate and Triphosphate for Different Corrosion Times of St 20 Specimens at Room Temperature

Inhibitor	Concentration (g/liter)	pH	Test conditions	Mixing effect (E, %) for corrosion time (hours)											
				1450			2930			3930			5650		
				main	subsidiary		main	subsidiary		main	subsidiary		main	subsidiary	
				$E_{Emulsol}$	$E_{Na_2SiO_3}$	$E_{Na_3PO_4}$	$E_{Emulsol}$	$E_{Na_2SiO_3}$	$E_{Na_3PO_4}$	$E_{Emulsol}$	$E_{Na_2SiO_3}$	$E_{Na_3PO_4}$	$E_{Emulsol}$	$E_{Na_2SiO_3}$	$E_{Na_3PO_4}$
Emulsol	1	10.7	AC	+15	—	+39	+9	+29	+22	—	—	—	—	—	—
Na_2SiO_3	0.1		SC	−50	—	+36	0	+36	+50	—	—	—	—	—	—
Na_3PO_4	0.25														
Emulsol	2	10.7	AC	− 1	—	+39	+17	+21	+14	—	—	—	—	—	—
Na_2SiO_3	0.1		SC	−62	—	+61	−29	+41	+55	—	—	—	—	—	—
Na_3PO_4	0.25														
Emulsol	5	11.1	AC	—	—	—	− 6	+ 7	+17	−16	—	+ 1	—	—	—
Na_2SiO_3	0.25		SC	—	—	—	−26	+74	+54	−32	—	+65	—	—	—
Na_3PO_4	0.5														
Emulsol	10	11.5	AC	—	—	—	−35	−29	− 1	—	—	—	−22	+ 3	+ 8
Na_2SiO_3	0.5		SC	—	—	—	− 6	+96	+79	—	—	—	−14	+96	+81
Na_3PO_4	1														
Emulsol	25	11.8	AC	—	—	—	—	—	—	−26	−2	−24	−25	+4	−14
Na_2SiO_3	1		SC	—	—	—	—	—	—	+ 0.2	+126	+72	+ 1	+124	+56
Na_3PO_4	2														
Emulsol	50	11.3	AC	—	—	—	—	—	—	−10	+47	+60	−35	+12	+19
Na_2SiO_3	2														
Na_3PO_4	4														
Emulsol	100	11.2	AC	—	—	—	—	—	—	0	+65	+78	+6	+70	+77
Na_2SiO_3	2														
Na_3PO_4	4														
Emulsol	200	11.0	AC	—	—	—	—	—	—	+19	+78	+91	+21	+83	+90
Na_2SiO_3	2														
Na_3PO_4	4														

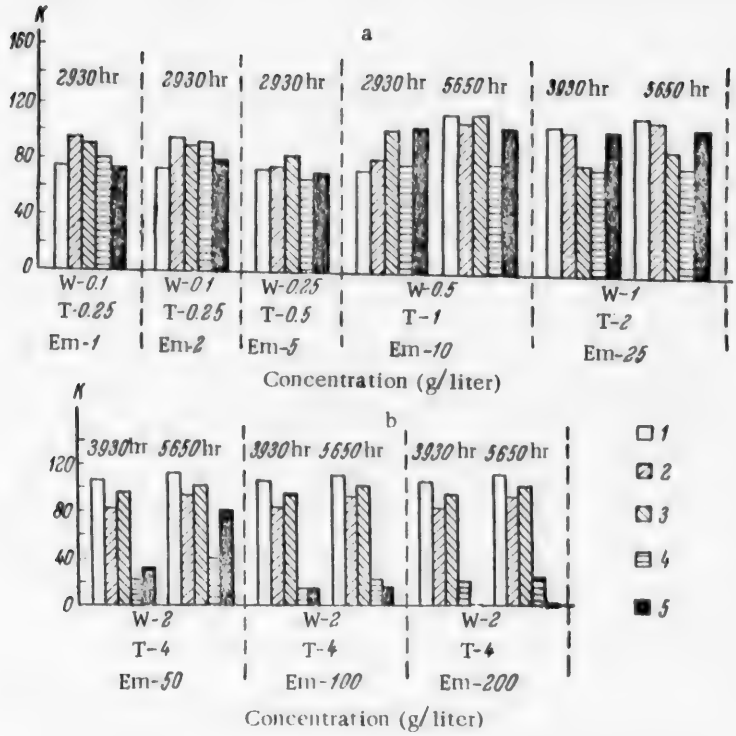

Fig. 5. Variation of atmospheric corrosion of St 20 specimens with the concentrations of Emulsol, sodium silicate, and sodium triphosphate inhibitors in mixtures, and with duration of tests at room temperature. Solutions: 1) original; 2) Na_2SiO_3 (W); 3) Na_3PO_4 (T); 4) Emulsol (Em); 5) mixtures of Na_2SiO_3, Na_3PO_4 and Emulsol.

2) Mixed solutions of sodium nitrite and triethanolamine are also very effective in protecting steel against corrosion. Complete protection ($Z_i \approx 100\%$) is obtained with only 1 g each of sodium nitrite and triethanolamine per liter in AC, and 0.25 g/liter of sodium nitrite and 0.5 g/liter of triethanolamine in SC. For complete protection of steel by these inhibitors taken individually, more than 2 g/liter (AC) or 1.5 g/liter (SC) of sodium nitrite, and more than 16 g/liter (AC) or 32 g/liter (SC) of triethanolamine is required.

Consequently, mixtures of sodium nitrite and triethanolamine are very suitable for the prevention of corrosion (AC and SC) of steel. Such mixtures have considerably greater protective powers than either of the inhibitors separately.

Mixtures of sodium nitrite and triethanolamine give high positive values of the main (E_{NaNO_2} in AC) and subsidiary ($E_{triethanolamine}$ in AC and SC) mixing effects. The low value of the main mixing effect (E_{NaNO_2}) with 1 g/liter of sodium nitrite in AC, and over 0.5 g/liter in SC is due to the high effectiveness of this inhibitor individually in solutions of the same concentrations. However, even in this case, owing to the additional protective effect which results from the mixing of these inhibitors, complete protection of the metal is ensured even if the medium should accidentally become more corrosive.

3) Mixed solutions of Emulsol, sodium silicate, and sodium triphosphate are ineffective up to considerable concentrations (Fig. 5). Steel is completely protected against corrosion by the following mixed inhibitor solutions: Emulsol 200 g/liter in AC and 25 g/liter in SC, sodium silicate 2 g/liter in AC and 1 g/liter in SC, and sodium triphosphate 4 g/liter in AC and 2 g/liter in SC; and higher concentrations. These inhibitors, taken separately in the same concentrations, do not give complete protection to steel under the same corrosion conditions. Even higher concentrations are ineffective (for example, 500 g/liter of Emulsol, 25 g/liter of sodium silicate, or

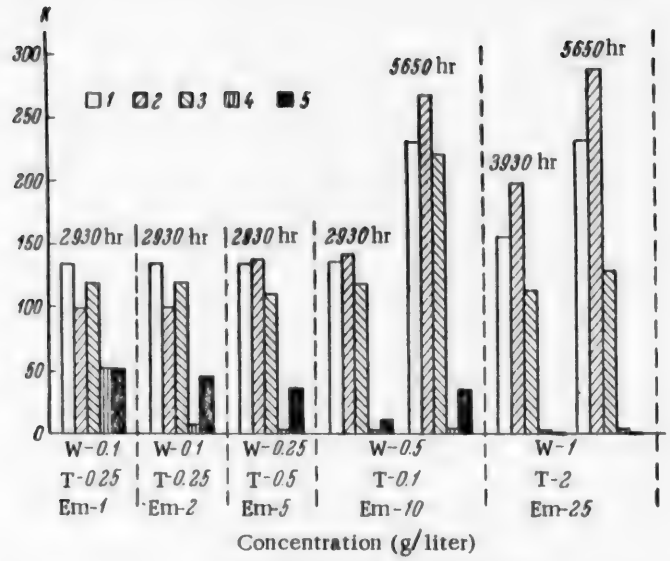

Fig. 6. Variation of submerged corrosion of St 20 specimens with the concentrations of Emulsol, sodium silicate, and sodium triphosphate inhibitors in mixtures, and with duration of tests at room temperature.
Solutions: 1) original; 2) Na_2SiO_3 (W); 3) Na_3PO_4 (T); 4) Emulsol (Em); 5) mixtures of Emulsol, Na_2SiO_3, and Na_3PO_4.

12 g/liter of sodium triphosphate, in AC). Therefore, despite the small positive main mixing effect ($E_{Emulsol}$), Emulsol should be used in mixtures with sodium silicate and triphosphate for complete protection of steel against corrosion (AC and SC). The considerable positive subsidiary mixing effects ($E_{Na_2SiO_3}$ and $E_{Na_3PO_4}$) make it advisable to add Emulsol to solutions of sodium silicate and triphosphate to ensure more effective protection (for example, to wash liquors of high detergent power, and solutions used for other purposes).

SUMMARY

1. The effects of inhibitors (sodium nitrite, sodium silicate, triethanolamine, sodium triphosphate, and Emulsol) and their mixtures in various concentrations on the atmospheric and submerged corrosion of steel (St 20) were studied; the minimum concentrations giving complete protection were determined for each inhibitor individually and for mixtures.

2. It is shown quantitatively that mixtures of these inhibitors are much more effective than the inhibitors taken individually in the same concentrations.

LITERATURE CITED

[1] I. L. Rozenfel'd, Corrosion Inhibitors in Neutral Media [in Russian] (Moscow, Izd. AN SSSR, 1953).

[2] G. V. Zhuk and A. S. Afanas'ev, Methods for Laboratory Testing of Atmospheric-Corrosion Inhibitors, 4 [in Russian] (VINTI Izd. AN SSSR, p. 17, 1958).

[3] A. S. Afanas'ev, Sci. Trans Dnepropetrovsk Metallurgical Inst. 25, 3 (1951); Ind. Lab. 2, 217 (1957).

[4] S. A. Balezin, Metal Corrosion and Its Prevention (Inhibitors of Acid Corrosion) [in Russian] ("Knowledge" Press, 1953).

Received June 10, 1957

SULFONATED ION-EXCHANGE RESINS BASED ON POLYVINYL CHLORIDE AND OTHER VINYL POLYMERS

A. A Vasil'ev and A. A. Vansheidt

Institute of High-Molecular Compounds, Academy of Sciences USSR

It is known that sulfonated ion-exchange resins are generally made from compounds of the aromatic series; for example, by sulfonation of phenol with subsequent condensation of the phenolsulfonic acids with formaldehyde, or by introduction of sulfo groups into the cross-linked styrene – divinylbenzene copolymer. Literature data on aliphatic sulfonated ion exchangers are still very scanty [1], although aliphatic compounds and their polymers are worthy of special attention as starting materials for the synthesis of ion-exchange resins of high exchange capacity. In particular, little use has been made as yet of aliphatic vinyl polymers for the production of sulfonated ion exchangers, although such compounds as polyvinyl chloride, polyvinyl acetate and others have long been readily available materials. It was therefore desired to determine the extent to which these plastics can be used for the synthesis of sulfonated ion-exchange resins.

Our investigations showed that sulfonation of many aliphatic polyvinyl compounds by means of oleum or chlorosulfonic acid under certain conditions yields space polymers, which swell but do not dissolve in organic solvents, water, and aqueous alkalies, and which contain considerable amounts of sulfur in the form of sulfo groups, easily determined quantitatively by alkali titration Thus, these final sulfonation products are typical strongly acid ion-exchange resins of considerable exchange capacity, which depends on the nature of the original polymers and the sulfonation conditions.*

Sulfonated Cation Exchangers Based on Polyvinyl Chloride (SVC Resins)

The starting materials in our experiments were samples of powdered polyvinyl chloride of different brands (PB, PF, M, and Igelat F), and shredded PVC film. The sulfonation was effected by means of 2-5 parts of 8-20% oleum or 92% chlorosulfonic acid per 1 part of polyvinyl chloride.

When polyvinyl chloride was heated with the sulfonating agents, HCl was evolved; this process began at about 95° with oleum, and at about 65° with chlorosulfonic acid. On further increase of temperature the polyvinyl chloride swelled rapidly and was converted into a black insoluble product without previous solution of the original polymer. In the case of oleum the heating was stopped at about 180° and in the case of chlorosulfonic acid, at 100°. The product formed in the latter case contained SO_2Cl groups in addition to SO_3H groups; the former were saponified by the action of water, 5% caustic alkali, or concentrated sulfuric acid on a water bath. The total time required for production of the resin (including saponification) under laboratory conditions did not exceed 2-3 hours. The material was then washed with water, shredded if necessary, sifted, and dried at room temperature. The yield of cation exchanger reached 75% on the original polyvinyl chloride. The exchange capacity of the resins (which depended on the starting material, and the nature and amount of sulfonating agent) was 2-4 meq/g or over, and the swelling coefficient was 1.2-1.5. When chlorosulfonic acid was used, the reaction proceeded at a higher rate despite the lower temperature, and the exchange capacity of the resins was considerably higher than those obtained with the use of oleum (Table 2). Therefore most of the experiments on the synthesis of SVC cation exchangers were performed with the use of chlorosulfonic acid.

* V. S. Matrosova and T. V. Gerasimyuk took part in the experimental work.

TABLE 1

Composition and Properties of SVC Resins Made from Different Brands of Polyvinyl Chloride

Polyvinyl chloride resin brand	Swelling coefficient	Sulfur content (%)		Exchange capacity (meq/g)	Chlorine content (%)
		total S	in SO_3H groups, S_{act}		
PB-1 . . .	—	7.15	5.77	1.80	26.15
PB-2 . . .	—	7.01	6.45	2.01	23.27
PB-4 . . .	—	7.22	6.10	1.91	26.14
M	1.2	—	5.70	1.78	—
PF-1 . . .	1.1	—	5.65	1.77	—
PF-4 . . .	1.1	—	5.62	1.76	—
PF-3 . . .	1.3	—	6.53	2.04	—

SVC resins were obtained in the form of particles of different sizes, from 0.1 to 2 mm, according to the form of the original polyvinyl chloride. Granular ion exchangers were made both from sulfonated PVC film by crushing, and from powdered polyvinyl chloride. The latter was first swollen in a mixture of chlorosulfonic acid and dichloroethane for 0.5-1 hour. The mixture was then heated in the usual way. After the sulfonation and dehydrochlorination reactions and removal of dichloroethane the product was not a powder, but consisted of grains of high mechanical strength.

The dynamic exchange capacity of the resins "to breakthrough" was 700-850 meq/liter (at a linear filtration velocity of 2.5-5.0 m/hour through a layer 25 cm high). SVC resins had good chemical resistance. Their properties (exchange capacity, swelling coefficient) were unchanged after treatment with 0.1 N solutions of caustic alkali or HNO_3 for 20 minutes on a boiling water bath.

Experiments on the synthesis of SVC resins from polyvinyl chloride resins of different brands showed that cation exchangers of almost the same properties are obtained under the same experimental conditions, with chlorosulfonic acid and resin taken in 2:1 ratio (Table 1).

The effects of the ratio of sulfonating agent to resin on the properties of SVC resins are given in Table 2. The advantages of using chlorosulfonic acid rather than oleum are evident.

The shredded PVC film was sulfonated under the same conditions as the polyvinyl chloride resins, the same effects were observed during the process, but the cation exchangers obtained had exchange capacities of about 2/3 of those formed from the resins. It is possible that the sulfonation of a partially cross-linked polymer such as the PVC film proceeds with greater difficulty than sulfonation of resins which had been previously subjected to high temperatures. The exchange capacity of resins based on PVC film could be increased by preliminary swelling of the material in dichloroethane (2-4 parts per 1 part of the material) for 1 hour (approximately).

The effect of sulfonation temperature on the properties of SVC cation exchangers is shown in Table 3. At room temperature chlorosulfonic acid does not sulfonate polyvinyl chloride. On the other hand, sulfonation at temperatures above 80-90° and increase of the heating time of the insoluble product did not increase its exchange capacity, while the latter decreased appreciably if temperatures up to 150° were used. The effect of sulfonation temperature on the properties of SVC resins is shown in Table 3, which contains data on specimens made from chlorosulfonic acid and polyvinyl chloride taken in 5:1 ratio. If the results given in Table 2 are also taken into consideration, it seems that the optimum ratio of sulfonating agent to resin, with the use of chlorosulfonic acid, is 4:1 or 5:1. The use of more than 5 parts of chlorosulfonic acid per 1 part of resin did not increase the exchange capacity of the cation exchangers further.

TABLE 2

Effect of Relative Proportions of Sulfonating Agent and Resin on the Properties of SVC Cation Exchangers

Starting materials		Amount of sulfonating agent		Swelling coefficient	S_{act} (%)	Exchange capacity (meq/g)	Chlorine content (%)
polyvinyl chloride	sulfonating agent	weight parts per 1 part of resin	moles per monomer unit				
PB-4 powdered resin	19.6% oleum	1.7	1.1	1.0	1.34	0.42	—
		3.35	2.2	1.1	4.00	1.25	—
		6.7	4.4	1.2	7.90	2.47	—
	92% chlorosulfonic acid	2	1	—	6.66	2.08	28.40
		4	2	1.5	10.91	3.41	15.15
		8	4	1.5	11.07	3.46	15.45
PVC film 0.5 mm thick		2	1	1.1	3.55	1.11	—
		4	2	1.2	6.86	2.14	—
		8	4	1.3	9.15	2.85	—

TABLE 3

Effect of Sulfonation Temperature on Properties of SVC Resins*

Sample No.	Sulfonation conditions		Resin properties		
	temperature (°C)	time (min)	swelling coefficient	S_{act} (%)	exchange capacity (meq/g)
1	20	48 × 60	1.0	0.00	0.00
2	20→100	30	1.4	13.34	4.17
3	20→100	20	1.7	13.28	4.15
	100→105	60			
4	20→150	50	—	10.66	3.33

* The cation exchangers were saponified by means of 10% NaOH solution at 70° deg for 2 hours.

Sample 2 was heated with uniform rise of temperature from 20 to 100° during 30 minutes; sample 3 was heated similarly, but in two stages: during 20 minutes from 20 to 100°, and then during 60 minutes from 100 to 105°.

The effects of saponification conditions on the exchange capacity of cation exchangers based on polyvinyl chloride are shown in Table 4. Almost the same results are obtained by any of the methods given.

The formation mechanism of sulfonated polyvinyl chloride resins cannot be regarded as fully understood; however, certain conclusions concerning the structure of these resins can be drawn from the following data.

According to Boyer [3], degradation of polyvinylidene chloride and its copolymers is accompanied by loss of HCl with formation of polyene chains of conjugated double bonds; this incidentally accounts for the appearance of color in degraded polymers. It is quite probable that similar processes take place in the sulfonation of polyvinyl chloride, as this is accompanied by considerable liberation of HCl with formation of dark cross-linked polymers. It is interesting to note that dehydrochlorination of polyvinyl chloride resin in presence of chlorosulfonic

TABLE 4

Effects of Saponification Conditions on the Exchange Capacity of SVC Resins

Saponification conditions*			S_{act} (%)	Exchange capacity (meq/g)
reagent	temperature (°C)	time (hours)		
KOH 10%	70	1	5.82	1.82
H_2SO_4, 92%**	70	1	5.75	1.80
H_2O (additional)	80	1		
H_2O	90	1	10.61	3.32
NaOH 10%	90	1	10.10	3.15
H_2O	90	0.5	5.92	1.85
H_2O	90	1	5.54	1.73

* The saponification reagents were used in considerable excess (about 20 weight parts to 1 part of resin).

** In saponification by means of sulfuric acid, the intermediate product $RSO_2 \cdot SO_3H$ may be formed; this decomposes into RSO_3H and H_2SO_4 during subsequent treatment with water [2].

acid occurs at temperatures about 100° below the temperature of the thermal degradation of polyvinyl chloride.

It is clear from Tables 1 and 2 that SVC resins contain considerable amounts of chlorine; this indicates that they contain unchanged polyvinyl chloride units ($-CH_2-CHCl-$).

A large excess of chlorosulfonic acid is needed in all cases for the formation of sulfonyl chlorides in good yields. If the excess of chlorosulfonic acid is relatively small, a mixture of sulfonyl chlorides and sulfonic acids [4] is formed.

$$RH + HOSO_2Cl = RSO_2Cl + H_2O \quad (1)$$

$$RSO_2Cl + H_2O = RSO_2OH + H_2O \quad (2)$$

Under our usual synthesis conditions, with 4 parts of chlorosulfonic acid per 1 part of resin, products containing sulfo groups together with sulfonyl chloride groups were also obtained. The contents of the latter could be estimated from the nitrogen contents of sulfonamides formed by the action of ammonia on unsaponified resins washed free from excess of mineral acid with ice-cold water (see, for example, Table 5).

Thus, about $\frac{1}{2}$ of the sulfur in unsaponified resins is present in the form of SO_2Cl groups, which are converted into sulfo groups after saponification, and the process of SVC resin formation can be represented by the following general scheme:

$$(CH_2CHCl)_n \xrightarrow[-HCl]{SO_2HCl} A\begin{matrix} Cl \\ SO_3H \\ SO_2Cl \end{matrix} \xrightarrow[-HCl]{H_2O} A\begin{matrix} Cl \\ SO_3H \end{matrix},$$

where A is a polymeric hydrocarbon residue.

In the light of all the foregoing considerations, the structure of SVC cation-exchange resins can be represented in general form as

$$(-CH_2-CHCl-)_w(-CH=CH-)_x\left(-\underset{|}{\overset{|}{C}}H-CH-\right)_y\left(-\underset{SO_3H}{\overset{|}{C}}=CH-\right)_z$$

TABLE 5

Sulfur Contents of Sulfonic and Sulfonamide Groups of Amidated SVC Resins

Sulfur and nitrogen contents of amidated resins (%)		Sulfur contents in sulfonamide groups calculated from percentage nitrogen contents (%)
S	N	
12.05	2.86	6.55
11.95	2.99	6.85

TABLE 6

Contents of SO_3H Groups and Chlorine in SVC Resins

Resin no.	Contents in resins (%)			
	S_{act}	SO_3H	Cl	Cl (% of initial chlorine content)
1	6.94	17.5	29.00	40.5
2	11.07	27.9	15.45	20.3

The contents of different types of units in SVC resins can be approximately calculated from the results of chlorine and sulfur determinations for these resins; this is illustrated by the examples given in Tables 6 and 7.*

Cation Exchangers Based on Various Vinyl Polymers

When polyvinyl acetate is sulfonated, acetic acid is liberated, in the same way as hydrogen chloride is liberated in the sulfonation of polyvinyl chloride, and the reaction ends with the formation of an insoluble sulfonating resin of low swelling power.

Sulfonation of vinyl chloride – vinyl acetate copolymers is accompanied by liberation of hydrogen chloride together with acetic acid.

In addition to polyvinyl acetate and vinyl acetate – vinyl chloride copolymer, the following were sulfonated: polyethylene, copolymers of vinyl chloride with methyl acrylate and butyl maleate, and polyvinyl alcohol.

The sulfonation reactions were very similar for all these polymers (with the exception of polyvinyl alcohol). The action of chlorosulfonic acid on vinyl polymers at moderate temperatures (not over 100°) resulted in the liberation of gaseous products, with eventual formation of insoluble sulfonated resins of exchange capacities of the order of 2-4 meq/g and low swelling (1.3-1.6).

TABLE 7

Contents of Different Units in SVC Resins, Based on the Results of Sulfur and Chlorine Determinations

Resin No.	Monomer units in resin chains				
	formula	molecular weight of unit	content of unit in resin		no. of monomer units per one $-CH=CSO_3H-$ unit
			in %	in molar %	
1 2	$CH=CSO_3H$ |	106.1	22.9, 36.6	10.6, 15.8	1.00, 1.00
1 2	| CH_2-CHCl |	62.5	51.0, 27.1	40.1, 36.4	3.78, 1.26
1 2	| $CH=CH$ |	26.0	21.1, 36.4	49.3, 64.3	4.65, 4.07

* It was assumed in the calculations that the resins do not contain "inactive" sulfur (sulfur not in sulfo groups).

TABLE 8

Properties of Sulfonated Cation Exchangers Made From Various Vinyl Polymers

Polymer	Amount of chlorosulfonic acid, wt. parts per 1 part polymer	Exchange capacity (meq/g)	Swelling coefficient
Polyvinyl acetate	4	3.21	1.4
Polyethylene	8.3	1.96	1.3
Polyethylene	13.3	2.30	–
Copolymers:			
Vinyl chloride 83.5% + vinyl acetate 16.5%	4	3.36	1.6
Vinyl chloride 83.5% + vinyl acetate 16.5%	2	2.93	1.5
Vinyl chloride 87% + methyl acrylate 13%	8	3.12	1.7
Vinyl chloride 52.5% + methyl acrylate 47.5%	8	2.99	–
Vinyl chloride 89.5% + monobutyl maleate 10.5%	4	3.19	1.6

Sulfonation of copolymers of vinyl chloride with esters of unsaturated acids is of special interest, as it is possible in this way to obtain cation-exchange resins containing carboxyl groups, formed by saponification of some of the ester groups, in addition to sulfo groups.

The preliminary experiments on sulfonation of vinyl polymers were performed with the use of 92% chlorosulfonic acid (4-8 parts by weight to 1 part of polymer). The heating was stopped when the temperature in the reaction flask reached 110° deg. The sulfonation products were saponified by means of 10% caustic potash solution under reflux on a boiling water bath for 1 hour.

TABLE 9

Results of Determinations of the Exchange Capacity of Cation Exchangers Based on Vinyl Chloride – Methyl Acrylate Copolymers

Copolymer composition (%)		Exchange capacity from results of titration with	
vinyl chloride	methyl acrylate	NaCl and methyl orange	CH_3COONa and phenolphthalein
87.0	13.0	3.12	3.27
52.5	47.5	2.99	3.95

The results of tests on sulfonated cation exchangers made from various vinyl polymers are given in Tables 8 and 9.

All the cation exchangers, like the starting polymers, were powders.

The data in Table 7 confirm the considerable content of carboxyl groups in the second of the sulfonated copolymers.

The behavior of polyvinyl alcohol in sulfonation differed in certain respects from that of the other vinyl polymers.

When polyvinyl alcohol reacts with sulfuric acid, the latter is expended mainly in the formation of esters,

which have been described in the literature as intermediate products in the production of polyvinyl nitrates [5]. It is known that when polyvinyl alcohol is heated above 160° it can form infusible and insoluble products [6], the formation of which occurs more rapidly and at lower temperatures in presence of traces of acids and other condensation agents.

In our experiments on the sulfonation of polyvinyl alcohol by concentrated sulfuric acid the insoluble product was formed at 87-90°.

Chlorosulfonic acid and oleum proved unsuitable for sulfonation of polyvinyl alcohol. The properties of the cation exchangers were no better than those of resins obtained with the use of sulfuric acid, while the reaction was violently exothermic. For saponification of the esters, the sulfonated polyvinyl alcohol was ground and heated on a water bath with 5% alkali solution; this was followed by regeneration of the product, washing with water, and drying at room temperature.

Cation exchangers based on polyvinyl alcohol had low exchange capacity (1.0-1.2 meq/g) and low swelling coefficients (1.1-1.5).

The methods used for testing the resins were described in our previous paper [7].

SUMMARY

1. Ion-exchange resins can be synthesized by sulfonation of various vinyl polymers: polyvinyl chloride, polyvinyl acetate, copolymers of vinyl chloride with various unsaturated compounds, polyethylene, and polyvinyl alcohol.

2. Sulfonated resins based on polyvinyl chloride (SVC resins) have exchange capacities of 2-4 meq/g, swelling coefficients of 1.1-1.5, and good resistance to alkalies and nitric acid. The properties of cation exchangers based on other vinyl polymers, except polyvinyl alcohol, are similar to those of SVC resins.

LITERATURE CITED

[1] E. E. Gilbert and E. P. Jones, Ind. Eng. Ch., 43, 2022 (1951); R. Oda and H. Shimizu, Chem. High Polymers (Japan), 4, 2706 (1951).

[2] Nölting, Ber., 8, 597 (1875).

[3] R. F. Boyer, J. Phys. Coll. Chem., 51, 1, 3 (1947).

[4] V. V. Kozlov, J. Appl. Chem. 20, 887 (1947).

[5] German Patent 537,303, Cl. 12; Chem. Zentr. 1153 (1932).

[6] I. Jones, in the book "High Polymers", 4 (1945) [Russian Translation].

[7] A. A. Vasil'ev and A. A. Vansheidt, J. Appl. Chem. 31, No. 7, 1075 (1958).*

Received April 8, 1958

* Original Russian pagination. See C. B. Translation.

ACID CONDENSATION OF LIGNIN

D. Tishchenko

The technology of the sulfite process for the production of cellulose from wood has been developed empirically; it has been found that the chips are successfully delignified by the cooking liquor (aqueous solution of sulfurous acid and bisulfite) only if definite conditions are maintained during soaking of the chips (at about 100°), precooking (110-115°), and cooking (135-145°). Rapid heating of the chips with the cooking liquor to 135-145° results in the so-called "black cook", when lignin is sulfonated but not dissolved. This gave rise to the concept of "condensation" or "inactivation" of lignin.

It was subsequently found that wood cannot be cooked by the sulfite process at the normal rate if it has been pretreated with hot water, or solutions of acids or alkalies, or if phenols, especially polyhydric, are added to the cooking liquor; that the unsuitability of the wood of various pines, Douglas fir, and floated unstripped spruce is due to the presence of polyhydric phenols and their derivatives in these woods and bark; that all lignin preparations isolated by acid treatment of wood, under apparently mild conditions, cannot be cooked by the sulfite process (cannot dissolve in the cooking liquor) at the normal rate; and that only periodate lignin, isolated by treatment of wood with sodium periodate (at pH 5-7), can be dissolved normally in this way.

These and numerous other observations have not been coordinated from a single viewpoint whereby it is possible to establish a relationship between modern concepts of lignin structure and the observed "condensation" or "inactivation" effects. There is no doubt that the establishment of such relationships is most desirable from the theoretical and practical aspects. Such relationships may be deduced and established by analogy with the chemistry and technology of phenol – aldehyde resins.

It is known that phenols react with aldehydes in presence of alkalies or acids, ultimately yielding polycondensation products (resoles, novolacs, resites). If this reaction is effected in alkaline solutions without heat, the primary reaction products, alkylol phenols, can be isolated.

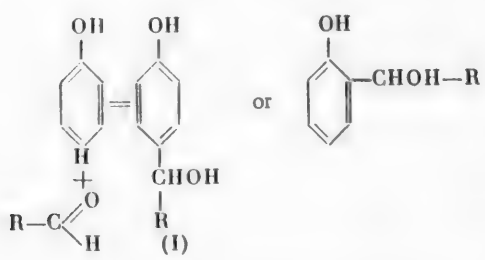

In the case of formaldehyde, the primary product is methylolphenol or hydroxybenzyl alcohol; in all other cases, homologs of hydroxybenzyl alcohol are obtained [1].

These alkylol phenols condense rapidly in acid solution, with liberation of heat, to yield linear polycondensation products.

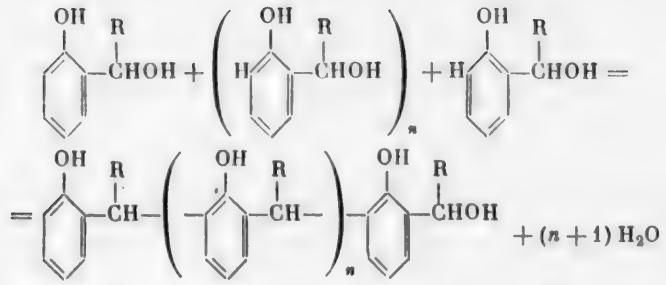

To bring this polycondensation about in alkaline solutions, it is usually necessary to heat them to 80-100°, except in the case of the most reactive phenols (such as resorcinol; see below). In acid solutions the condensation of phenols with aldehydes is usually so rapid that it cannot be stopped at the alkyl phenol stage; polycondensation products (novolacs) are formed at once. It must be pointed out that the condensation of phenols with aldehydes proceeds at the minimum rate at pH=4.2, i.e., in a weakly acid medium [1].

The number of aldehyde groups adding on to a particular phenol with formation of alkylol groups is equal to the number of unsubstituted carbon atoms in the benzene ring, activated by the phenolic hydroxyl (the ortho and para positions relative to the hydroxyl). Thus, p-cresol readily yields a dimethylol derivative, which easily condenses in an acid medium with two molecules of a phenol or novolac of definite structure to give the corresponding novolac, for example [2].

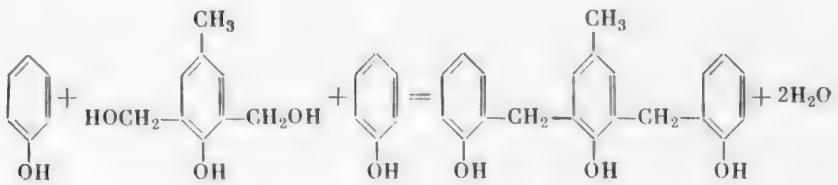

We showed earlier [3] that if one of the components of this reaction (phenol, novolac, or alkylol phenol) contains a sulfo group, condensation does not occur; the sulfo group prevents condensation, and this is of special significance in consideration of the problem of lignin condensation.

Any phenol with not less than two free ortho – para positions can bind two or more molecules of an alkylol phenol, for example

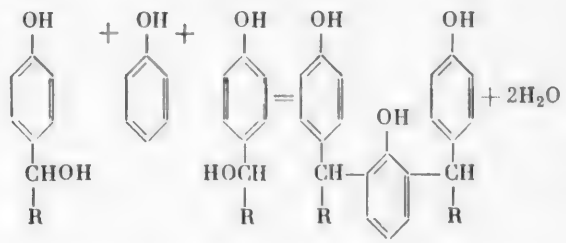

The rate of reaction of any particular phenol with aldehydes or alkylol phenols depends on the structure of the phenol. It is highest for polyhydric phenols of the meta series (resorcinol, phloroglucinol, etc.), as in such cases the hydroxyls simultaneously activate the same positions of the benzene rings (the activated positions are marked by crosses).

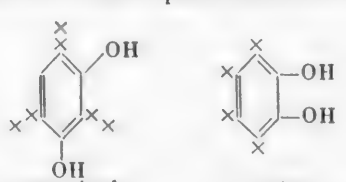

resorcinol

catechol
(ortho series)

All the foregoing considerations apply to the reactions of phenols with aldehydes or of alkylol phenols with phenols. The quantitative determination of phenolic hydroxyls in lignins involves considerable difficulties.

Different determination methods give different results. However, it may be stated with confidence that far from every phenylpropane structural unit in conifer lignin contains a phenolic hydroxyl (II):

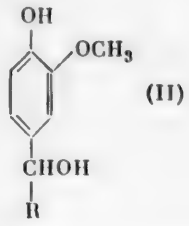

(II)

At the same time, nearly every formula proposed for the structure of conifer lignin includes considerable numbers of groups of fully etherified catechol derivatives (III, IV).

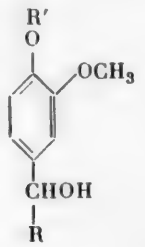

(III) or

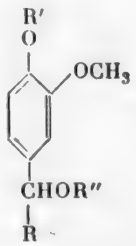

(IV)

We know from the chemistry of phenolic resins that not only phenols but also their ethers react with aldehydes to form resins. For example, phenol ethers condense with formaldehyde when heated with aqueous formic acid [4]; phenoxyacetic acid and its homologs condense with formaldehyde even without catalysts when heated above 100° (their own acidity is sufficient) [5]; finally, benzhydrol and other aromatic alcohols (homologs of benzyl alcohol) readily condense with phenol ethers in presence of acids [6]. In the light of these facts, the reactivity of (III) and (IV) structural units in addition to (II) should be taken into account in consideration of "condensation" and "inactivation" of lignin.

Finally, it should be noted that under constant conditions the solubility of substances in a polymer-homolog series decreases with increasing molecular weight.

Levoglucosan $C_6H_7O_2(OH)_3$ and cellulose $[C_6H_7O_2(OH)_3]_n$ have equal relative hydroxyl-group contents, but the former is readily soluble in water and alcohol, while the latter is insoluble. Phenolsulfonic acids are readily soluble in water, whereas sulfonated phenolic resins are insoluble, and are used as ion-exchange resins. The higher the molecular weight of a substance, the more lyophilic groups must be introduced into it to make it soluble.

If all the above facts are taken into account, "condensation" and "inactivation" of lignin can be considered from a unified standpoint and correlated with modern concepts of lignin structure.

The chemistry of sulfite cooking of wood has been greatly clarified during the past twelve years, mainly by the work of Swedish chemists [7]. Experiments on sulfonation of model substances by solutions of sulfurous acid and its salts showed that substances containing the group (II) (see above) are sulfonated very rapidly and over a wide pH range (1.2-7.0 and over), those containing group (III) are sulfonated much more slowly, but in the same pH range, while those containing group (IV) are sulfonated only at low pH (not over 2-2.5), i.e., after hydrolysis of ethers of substituted benzyl alcohol. In all cases the sulfo group enters the position of the hydroxyl in the substituted benzyl alcohol. However, groups (II) and (III) are alkylol phenols, while (IV) is converted into an alkylol phenol after hydrolysis of the ether group. Alkylol phenols can condense rapidly with phenols and their ethers in an acid medium, and slowly in an alkaline medium. Therefore, there must be two competing reactions involving benzyl alcohol hydroxyls in the sulfite cooking of wood: 1) sulfonation, 2) condensation of lignin molecules, with doubling, trebling, etc., of its molecular weight.

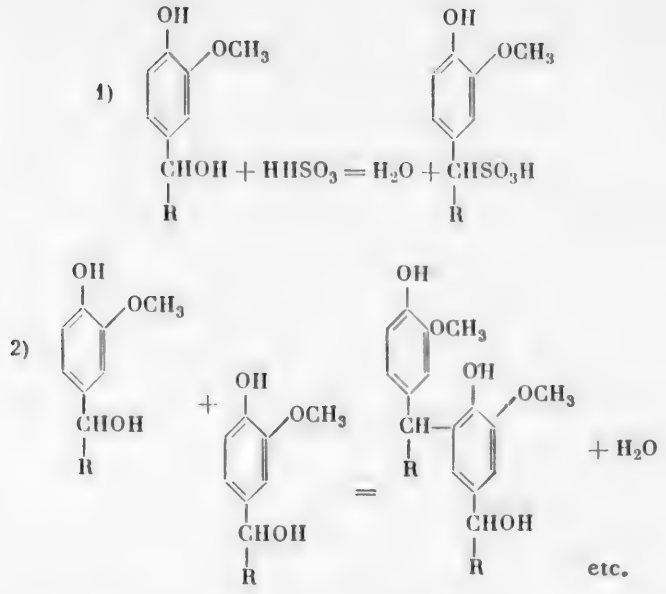

The first reaction is possible only in presence of sulfurous acid or its salts, while the second can take place in presence of any acid (or alkali, but under harsher conditions). Therefore pretreatment of wood with acids or alkalies should condense lignin, increase its average molecular weight, and hinder subsequent sulfite cooking, i.e., extraction of lignin as lignosulfonic acids in the cooking liquor. This conclusion is confirmed by abundant experimental data. It is known that pretreatment of spruce wood with water or with 1% sulfurous acid at 100-130°, or with 5 or 25% hydrochloric acid at 30°, "deactivates" lignin for subsequent sulfite cooking [8]; however, if wood is heated in running water (when the formic and acetic acids formed are washed out) lignin is not deactivated; it was found by the use of buffer solutions that heating at pH=4.6 had the least influence on the subsequent sulfite cooking (compare this with the minimum condensation rate of alkylol phenols with phenols at pH=4.2 [1]); similar heating of wood in nitrogen or in toluene does not have an adverse effect on sulfite cooking [9]; the more "inactivated" the lignin, the more sulfo groups must be introduced to make the lignin sulfonic acids soluble in the cooking liquor [10]; preliminary heating of wood with hydrochloric acid (pH=2.2) sharply retards subsequent sulfite cooking, and 60% of the lignin sulfonates does not dissolve but remains in the chips [11]. Similar results were obtained in sulfite cooking of different lignins: periodate lignin, not subjected to the action of acids or alkalies during isolation from wood, cooks normally; the same lignin behaves differently after preliminary heating with buffer solutions at 100°: the least effect was produced by heating at pH=4.5 (92% was dissolved, see [1]), and the greatest, at pH=2.2 (sulfite cooking greatly retarded) [12]; lignins isolated from wood in presence of acids do not dissolve in sulfite at the normal rate: lignin isolated from spruce meal by 30 minutes of treatment with 42% HCl at 0° dissolved completely in 20 hours at 135° in a cooking liquor which contained 5% SO_2 and 1% Na_2O, whereas lignin treated with hydrochloric acid for 36 hours was only 28% dissolved in 24 hours [13]. Condensation of lignin by alkali solutions takes place under much harsher conditions: heating of spruce wood with 10% sodium carbonate solution at 160°, or exposure to 10% ammonia solution for 6 days at room temperature, gave residues containing 14.2 and 6.4% lignin respectively after sulfite cooking [14]; other workers report that wood lignin is deactivated by alkali solutions only at temperatures above 50° [11, 15].

Several workers have shown that preliminary introduction of 1 sulfo group per 4 structural units (1 sulfur atom per 40 carbon atoms) into wood lignin virtually prevents the condensation of lignin in acid media, and eliminates "black cook" [16]. This very remarkable effect has not as yet been correlated with modern views on the chemical nature and reactivity of lignin.

This effect also becomes understandable when considered in the light of the similarity between the chemistry of lignin condensation processes and the chemistry of condensation of phenols with aldehydes and alkylol phenols. As stated earlier, we have shown [3] that introduction of sulfo groups into phenols, novolacs, or alkylol phenols prevents mutual condensation of these substances. Hence it follows that the "condensation" and "inactivation" of wood lignin as the result of various treatments, as described above, and the prevention of acid con-

densation of lignin by the preliminary introduction of small amounts of sulfo groups, can be explained satisfactorily by analogy with the chemistry of phenol – aldehyde condensation products.

All the foregoing is valid only if, as in the condensation of aldehydes with phenols, the alcoholic hydroxyls in the α-position relative to the benzene ring are responsible for condensation of lignin. Studies of model substances show that compounds with alcoholic hydroxyls in the α-position condense with themselves in presence of acids; if the hydroxyl is in some other position, they do not condense. For example, pinoresinol, which is an ether of substituted benzyl alcohol, can undergo "sulfite cooking" at pH>4, with preliminary hydrolysis of the ether bond, while at pH<4 it is resinified (undergoing condensation with itself) [17].

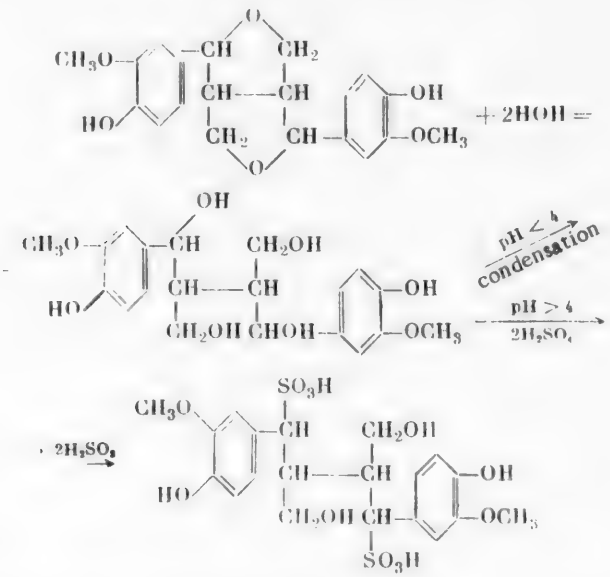

The guaiacyl ether of veratrylglyceraldehyde (with an alcoholic hydroxyl in the γ position) does not condense by the action of acids.

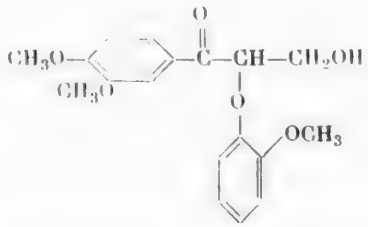

It must be pointed out that 1-alkylol phenols, in contrast to methylolphenols $HO-C_6H_4-CH_2OH$, are less sensitive to the action of acids, and, moreover, their molecular weight is no more than trebled by condensation under acid conditions. Thus, the condensation of higher aldehydes with phenols, even in an acid medium, gave the corresponding alkylol phenols in good yields in a number of cases [18].

Lignin contains alkylol phenol structural units, and these are therefore relatively stable to the action of acids. This explains Richter's observation [19] that chips infused for two weeks in 10% SO_2 solution (in absence of bases) can be subsequently delignified when heated with the same solution at 125°; the relatively low acid activity of sulfurous acid does not cause acid condensation of the alkylol phenol structural units in lignin in the cold, but lignin is sulfonated (although slowly) at the α-benzyl alcohol hydroxyls; the introduced sulfo groups protect the lignin against acid condensation at the higher cooking temperature (see above), and no base is required.

The role of the base in the ordinary sulfite process can be examined in the same light: metal bisulfite buffers the cooking liquor and lowers its active acidity, so that condensation of alkylol phenol groups in lignin is inhibited but sulfonation is not prevented; after introduction of a small number of sulfo groups the lignin is protected by them against condensation, and the cooking temperature can be raised to the final level. In accordance with these views, "black cook" is the result of the action of acid on lignin which has not been protected by preliminary sulfonation, with doubling or trebling of its molecular weight; the high-molecular lignin cannot dissolve rapidly enough in the cooking acid even after introduction of a large number of sulfo groups. It is immaterial whether the lignin is condensed by preliminary treatment of the wood with some other acid and the wood is then used for sulfite cooking, or whether in the sulfite cooking of fresh wood the temperature is raised rapidly to a point at which the condensation and sulfonation rates become comparable.

It has been known for a fairly long time that phenol retards sulfite cooking [20]. Pine wood cannot be cooked by the usual sulfite process; the reason is the presence of pinosilvyn (styrylresorcinol) in the wood; cooking is normal if pinosilvyn is removed by extraction of the chips with acetone [21, 22]. The wood of Douglas fir contains pentahydroxyflavanone, another derivative of resorcinol, and therefore it cannot be cooked by the normal sulfite process [23]. Studies of the effect of added phenols in cooking liquor showed that dihydric phenols of the meta series (orcinol, resorcinol, pinosilvyn) have the greatest retarding effect on sulfite cooking, while the effects of dihydric ortho (catechol) and para (hydroquinone), and of monohydric phenols are weaker. Addition of only 1% of resorcinol to spruce chips greatly hinders the solution of lignin sulfonates in ordinary sulfite cooking, although the sulfur content of these sulfonates is normal [24]. Therefore addition of small amounts of resorcinol does not prevent sulfonation of lignin, but lowers the solubility of lignin sulfonates. On the other hand, addition of up to 3.3 wt.% of resorcinolsulfonic acid (calculated as resorcinol) to the cooking liquor has no effect on sulfite cooking [25], and addition of 3% of resorcinol on the weight of spruce chips during preliminary bisulfite cooking (pH = 4.5) has no adverse effect during subsequent cooking with the cooking liquor [24]. A two-stage process for cooking of pine wood: 1) sulfite – bisulfite (pH ~ 5), and 2) normal, which makes it possible to treat pine wood by the sulfite process, was proposed long ago [26]. Lignosulfonic acids give an insoluble precipitate when heated with phloroglucinol [27]. Hardly any explanations of these effects have been put forward.

Erdtmann [24] wrote that "it is difficult to answer" all these questions, and merely added "the formation of three-dimensional molecules comparable with phenolic resins may be postulated," without explaining how they may be formed, and why they should be three-dimensional.

It is known that dihydric phenols of the meta series react most rapidly with aldehydes, yielding alkylol phenols or polycondensation products, in accordance to the molar proportions of the reagents. The cause of this is discussed above. It also explains the above sequence of the rates at which different phenols inactivate lignin. It was also shown above that every phenol can react with two molecules of any alkylol phenol with formation of a linear molecule of more than doubled molecular weight. Since the condensation rate of phenols with alkylol phenols is lowest at pH = 4.2 [1], sulfite – bisulfite cooking of pine wood (containing pinosylvin), or of spruce with added resorcinol, at approximately this pH does not favor condensation of the alkylol phenol structural units in lignin, but does not prevent sulfonation in these units; the entry of even a few sulfo groups into the lignin molecule protects it against subsequent condensation with resorcinol or pinosylvin during subsequent normal sulfite cooking under acid conditions. This explanation also accounts for the absence of difficulties in sulfite cooking on addition of large amounts of resorcinolsulfonic acid; sulfonic acids do not usually condense with alkylol phenols [3]. The adverse effect of small amounts of resorcinol on cooking is explained by cross linking of lignin molecules by resorcinol with at least a 2-fold increase of molecular weight, leading to a decrease in the solubility of the sulfonic acids under otherwise equal conditions.

The condensation of lignosulfonic acids with phloroglucinol, which is contrary to the general rule that alkylol phenolsulfonic acids (in this case lignin) cannot be condensed with phenols, is explained by the exceptional properties of phloroglucinol. In this compound every hydrogen of the benzene ring is in ortho and para positions to each of the three hydroxyls, and is therefore triply activated; this is not the case for any other phenols studied in this respect.

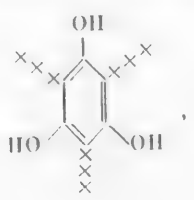

Finally, preliminary cooking of chips with excess formaldehyde in presence of 0.01 N sulfuric acid, or addition of large amounts of formaldehyde to the cooking liquor, results in "black cooking" of spruce wood [28], while addition of small amounts of formaldehyde to the cooking liquor increases the yield of cooked cellulose from 36 to 42% in sulfite cooking of pine wood [29]. In the former case formaldehyde, being the most reactive aldehyde with regard to condensation with phenols, cross links the II groups of lignin in the ortho position to the phenolic hydroxyl, which at least doubles the molecular weight of the lignin and lowers the solubility of the corresponding lignosulfonic acids and their salts.

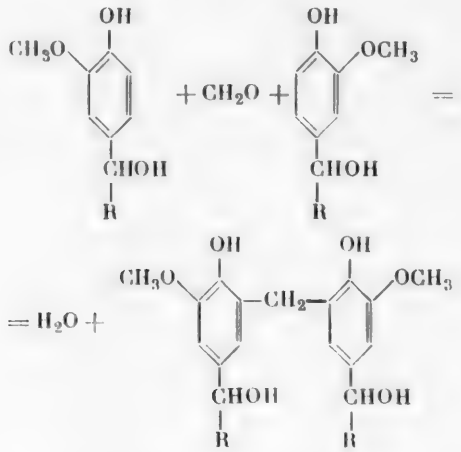

Spruce wood yields up to 30% vanillin, calculated on the lignin, when oxidized by nitrobenzene in an alkaline medium [30], while similar oxidation of model substances gives high yields of vanillin only if the substances are 3-methoxy-4-hydroxyphenyl derivatives with a carbon side chain in the first position and have either a hydroxyl group or a double bond at the first carbon of the chain [31]; it follows that in spruce lignin about 40% of the structural units should have phenolic hydroxyls in position 4 in the benzene ring, and in such cases repeated cross linking of lignin molecules is possible, with multiple increases of the average molecular weight. The explanation of the favorable influence of small amounts of formaldehyde on the cellulose yield in the sulfite cooking of pine wood is that pinosylvin (substituted resorcinol) rapidly condenses with formaldehyde to give a polycondensation product, and this prevents the cross linking of the lignin molecules, with increase of their average molecular weight, by the pinosylvin molecules.

The interpretation of "condensation" and "inactivation" of lignin presented in this paper is not the generally accepted one. Apart from the views put forward by Erdtmann [24], two other hypotheses may be noted. Lindgren [32] suggests that phenol condenses with α-benzyl alcohol hydroxyls of lignin as follows:

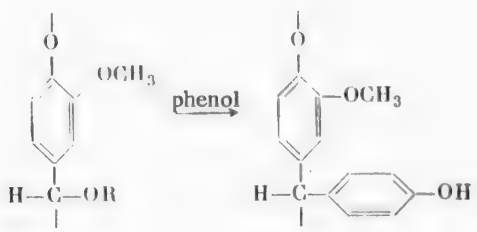

Harris and Bergstrom [33], who studied the hydrogenation products of lignin, found compounds with substituent groups in position 5 of the six-membered ring, and therefore concluded that the condensation of lignin takes place at that position.

It is difficult to agree with Erdtmann's view that condensed lignin is a three-dimensional polycondensation product. No three-dimensional polycondensation products are soluble in the various solvents. The introduction

of lyophilic groups does not change the situation: sulfonated phenolic resins are insoluble in water, and are ion-exchange resins; the same applies to sulfonated coals. It is known (see above) that "condensed" lignin can be sulfonated up to a normal sulfur content, and that the lignosulfonic acids so formed dissolve in the cooking liquor, although slowly [10, 13].

Lindgren's scheme is also inconsistent with the facts. One per cent of resorcinol on the weight of wood is enough to retard sulfite cooking sharply; in our interpretation, this is accounted for by cross linking of the lignin macromolecules by resorcinol, with doubling, trebling, etc. of the molecular weight of lignin and all the consequences of this. According to Lindgren, sulfite cooking can be inhibited by phenols only if a very considerable number of α-alcohol or α-ether groups reacts with a phenol; the amount of phenol needed for this must be comparable with the weight of lignin, and this is not in fact the case.

We agree with the hypothesis of Harris and Bergstrom, as in the structural unit of type II only the fifth position (the ortho position with respect to the phenolic hydroxyl) should be capable of condensation.

These authors did not attach a wide significance to their views, and did not attempt to correlate the chemistry of lignin with the chemistry of phenol – aldehyde resins.

In our opinion such correlation is justified, and can lead to many conclusions of theoretical and practical importance.

LITERATURE CITED

[1] K. Jong, Rec. trav. chim., 72, 497 (1953).

[2] M. Koebner, Z. ang. Ch., 46, 118, 251 (1933).

[3] D. Tishchenko and I. Uvarov, J. Appl. Chem. 30, 105 (1957).*

[4] German Patents 406,152, 406,999, 407,000.

[5] German Patents 364,040, 371,149.

[6] Szeki, C. A., 20, 2849 (1926); B. Lingdren, Svensk Papperstidning, 55, 78 (1952).

[7] See reviews, e.g. in: B. Leopold, Pulp and Paper Magazine of Canada, 55, 184 (1954); B. Harris, Forest Products Journal 5, 26 (1955).

[8] G. Richter, Tappi, 37, 263 (1954).

[9] A. Corey and O. Maass, Canadian Journal of Research, 13, Sect. B, 289 (1955).

[10] E. Hägglund, Bioch. Z., 202, 439 (1928).

[11] H. Erdtmann, Svensk Papperstidning, 43, 255 (1940).

[12] W. Cabot and C. Purvis, Pulp and Paper Magazine of Canada, 37, 151 (1956).

[13] E. Hägglund, Chemistry of Wood (1951).

[14] R. Hilpert, Cellulosechemie, 17, 28 (1936).

[15] See, e.g., N. A. Rozenberger, Trans. Central Sci. Res. Inst. Paper 40 (1953); E. Bennet, Soil Sci. 68, 399 (1949).

[16] E. Hägglund, Papierfabrikant, 226 (1938); J. Hedlund, Svensk Papperstidning, 50, 109 (1947); G. Richter, Pulp and Paper, 22, 48 (1948); N. A. Rozenberger, Trans. Central Sci. Res. Inst. Paper 40 (1953).

[17] B. Lindgren, Acta Chem. Scand., 6, 91 (1952).

[18] J. Scheiber, p. 339 and 446 (1949).**

[19] G. Richter, Tappi, 37, 263.

* Original Russian pagination. See C. B. Translation.

** As in original – Publisher's note.

[20] J. Goodwin, Paper Industry, 8, 617 (1928).

[21] E. Hägglund, Svensk Papperstidning, special issue, 37, 39 (1936).

[22] H. Erdtmann, ibid, 42, 344 (1939).

[23] R. Pew, Tappi, 32, 39 (1949).

[24] H. Erdtmann, Svensk Papperstidning, 43, 255 (1940).

[25] K. Mori, C. A., 48, 13, 218 (1954).

[26] British Patent 5365 (1882); German Patent 375,053 (1923).

[27] T. Hata, C. A., 47, 10 846 (1953).

[28] E. Adler, Svensk Papperstidning, 54, 477 (1954).

[29] J. Hachihama, C. A., 48, 11 055 (1954).

[30] B. Leopold, Acta Chem. Scand., 6, 38 – 49 (1952).

[31] H. Erdtmann, ibid, 3, 1358 (1949).

[32] B. Lindgren, Svensk Papperstidning, 55, 78 (1952).

[33] E. Harris, Bergstrom, Ind. Eng. Ch., 41, 2093 (1949).

Received May 22, 1957

METHODS FOR THE SEPARATION OF LIGNOSULFONIC AND CARBOHYDRATE SULFONIC ACIDS*

M. N. Tsypkina and I. M. Balashova

Central Scientific Research Institute of Paper

The liquors formed in sulfite cooking of cellulose are very complex in composition. In addition to dissolved mono- and polysaccharides and such of their degradation products as furfural, aldonic acids, carbohydrate sulfonic acids of different molecular weights and probably of different structures, the liquors contain lignosulfonic acids among their principal components. These acids vary greatly in molecular weight and composition. According to available data, the molecular weight of lignosulfonates varies from 300-400 to 20,000 [1]. In accordance with the cooking conditions, the acid constituents of lignosulfonates contain both sulfo groups of different strengths (with $K = 10^{-1}$, 10^{-2}, and 10^{-3}) [2], and strongly acid COOH groups [3].

For investigation of the reactions of lignin in sulfite cooking, it is necessary to extract the lignosulfonic acids formed during cooking from the liquor and to study them. All the methods proposed up to now for isolation of lignosulfonates are based on salting out or dehydration, and not on chemical reactions, and the degree of precipitation of the low-molecular lignosulfonate fractions depends on the nature of the precipitant.

A particularly important fact is that in such precipitation it is impossible to avoid, by any technical methods, the coprecipitation of carbohydrate sulfonic acids of fairly high molecular weight together with the lignosulfonates.

For separation of lignosulfonates and carbohydrate sulfonates it is necessary to have a range of specific precipitants, each of which reacts chemically with only one of these acids. For this purpose we made use of the fact, discovered by Yatsimirskii [4], that complex compounds with anions of aromatic sulfonic acids in the outer sphere are sparingly soluble.

Carbohydrate sulfonic acids are not aromatic, and therefore should not be precipitated by complex salts. The sulfo group in lignosulfonic acids is in the side chain and not in the aromatic nucleus. Moreover, they contain the hydrophilic – OH and – COOH groups which, according to Yatsimirskii, increase the solubility of the complex compound formed; therefore it was necessary to carry out special tests to confirm that lignosulfonates are precipitated by complex salts. Sulfite liquors from the cooking of spruce wood, and periodate lignin containing 89.15% of Klason's lignin, were used for these tests. The precipitation of sulfonic acids from liquors obtained in the sulfite cooking of holocellulose containing 0.2% lignin, and in the cooking of glucose with sulfite – bisulfite solution, was studied for comparison.

The precipitants used were saturated solutions of hexamminecobaltichloride $[Co(NH_3)_6]Cl_3$ and hexamminecobaltinitrate $[Co(NH_3)_6](NO_3)_3$, added in excess. The precipitates were centrifuged and washed with water to a negative reaction for chloride or NO_3^- respectively. The results are given in Table 1.

---

* Communication III on the chemistry of the sulfite process. Communication II was published in the Scientific Transactions of the Institute of Paper, No. 42 (1957).

E. I. Kosilova, M. N. Atapina, and Z. P. Lampsakova took part in the work.

TABLE 1

Precipitation of Lignosulfonic Acids and Carbohydrate Sulfonic Acids by Complex Salts

Cooking conditions, and characteristics	Material cooked			
	spruce wood	periodate lignin from spruce	holocellulose	glucose
	Cooking acid			
Cooking liquor	total SO_2 — —7.0 % $(NH_4)_2O$— —0.64%	total SO_2— —6.8% CaO—1.0 %	total SO_2— —6.8% CaO—1.0%	Sulfite — bisulfite solution, pH=6.6, total SO_2—10.64%
Cooking conditions	Heating up to 135°, 3.5 hours; cooking at 135°, 1.5 hours	Heating up to 140°, 5.5 hours; cooking at 140°, 4 hours		Heating up to 135° 1 hour; cooking at 135°; 6 hours
Nature of sulfonic acids formed	Mixture of lignosulfonic and carbohydrate sulfonic acids	Lignosulfonic acids, with a small mixture of carbohydrate sulfonic acids	Carbohydrate sulfonic acids	Glucosesulfonic acid
Dense residue from liquor (% on ash-free substance)	11.85	0.34	3.86	3.48
Firmly bound sulfur (% on organic matter)	5.77	5.18	5.07	6.59
Methoxyl content (% on organic matter)	10.92	13.58	1.61	nil
S : OCH_3 in organic matter of liquor	1 : 1.95	1 : 2.70	1 : 0.33	—
Precipitant	Hexamminecobaltichloride			
Amount of firmly-bound sulfur precipitated (% of initial content)	67.7	100	nil	nil
Amount of methoxyl precipitated (% of initial content)	83.0	90.9	nil	nil
S : OCH_3 in precipitate	1 : 2.38	1 : 2.43	—	—

As was to be expected, neither the carbohydrate sulfonic acids formed in the cooking of holocellulose nor glucosesulfonic acid are precipitated by the complex salts. Lignosulfonic acids formed by the cooking of periodate lignin are precipitated almost quantitatively by complex salts. The degree of precipitation of methoxyls and firmly-bound sulfur from sulfite liquors was 67.7 and 83.0% respectively. The unprecipitated portions of these are probably combined with the carbohydrate components of the liquor. Thus, hexamminecobaltichloride can be used for quantitative precipitation of lignosulfonic acids and separation of the latter from carbohydrate sulfonic acids.

TABLE 2

Influence of Various Factors on Precipitation of Lignosulfonates by Complex Salts

Type of liquor	pH of liquor	Dense residue (ashless) (%)	Amount of lignosulfonates precipitated (% of dense liquor residue)
Sulfite liquor, hardness 92° B	1.69	10.13	71.70
Same liquor after cation exchange	0.99	6.48	72.50
Same liquor, boiled 1.5 hours with hydrochloric acid (0.5% HCl solution)	Not determined	6.20	71.00
Sulfite liquor, hardness 46° B	1.25	9.82	70.12
Same liquor after addition of NaOH	1.50	Not determined	71.35
The same	2.50		70.00
Same liquor after cation exchange and conversion of lignosulfonates into barium salts	6.50	9.30	71.30

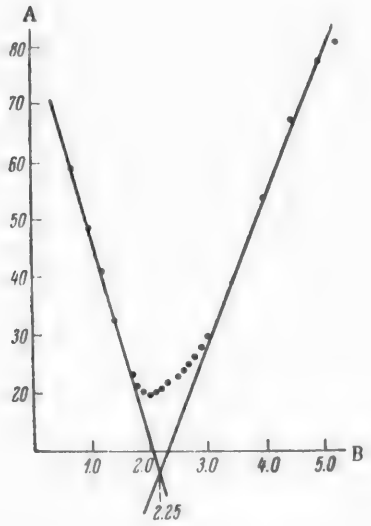

Conductometric titration of acids from lignosulfonate sample (30 ml of sample + 20 ml of water) with caustic soda: A) conductivity; B) ml of 0.1000 N NaOH.

It was found in separate experiments that hexamminecobaltinitrate acts similarly. The reaction taking place in the precipitation of lignosulfonates can be represented as follows:

$$3LignSO_3Me + [Co(NH_3)_6]Cl_3 \rightarrow [Co(NH_3)_6](LignSO_3)_3 + 3MeCl.$$

In the usual precipitation of lignosulfonates by means of aromatic amines, alcohols, etc., it has been found that salts are precipitated very much better than the free lignosulfonic acids; the barium salts are precipitated most completely. The precipitation of lignosulfonates, especially by alcohols, is largely determined by their concentration in solution. Finally, the degree of precipitation of lignosulfonates from sulfite liquors varies with the degree of cooking, which influences their molecular dimensions.

Table 2 shows the effects of all these factors, and of the pH of the medium (in the pH range from 1.0 to 6.5), on the precipitation of lignosulfonates by complex salts.

It is clear from Table 2 that none of the factors tested has any appreciable influence on the precipitation of lignosulfonates by complex salts.

The precipitates with complex salts were treated with 0.1 and 1 N caustic soda solutions to isolate lignosulfonates. The precipitate is dissolved completely in 15 minutes, 0.40 g NaOH per g of precipitate being consumed, irrespectively of the normality of the caustic soda solution. With a lower consumption of NaOH the precipitate dissolves more slowly. If the alkaline solution formed is passed through a cation exchanger in the H form, it can be freed both from the cations bound with the lignosulfonates and from excess alkali.

The diagram shows the curve obtained by conductometric titration, with 0.1 N caustic soda solution, of a sample of lignosulfonic acids isolated from sulfite liquor by means of hexamminecobaltichloride and then freed

from cations as described above. The sulfonic sulfur in the sample, calculated from the titration curve, was found to be 6.86% of the dense residue.

SUMMARY

1. The complex salts $[Co(NH_3)_6]Cl_3$ and $[Co(NH_3)_6](NO_3)_3$ can be used for complete isolation of lignosulfonates from solution, and for separation of lignosulfonates from carbohydrate sulfonic acids present with them in sulfite liquors.

2. Precipitation of lignosulfonic acids by complex salts is not influenced by the degree of cooking of the pulp, the solution pH (in the range from 0.1 to 6.5), or the nature of the cations in the lignosulfonates. Free lignosulfonic acids are precipitated as completely as their salts.

3. The free acids can be isolated from the complex precipitates, containing the lignosulfonate anion in the external sphere, by solution of the precipitates in alkali and removal for cations by means of a cation-exchanger in the H form.

It is our pleasant duty to thank Professor K. B. Yatsimirskii for advice in this investigation.

LITERATURE CITED

[1] K. Schwabe and L. Hasner, Cellulosech., 20, 61 (1942); cited through N. I. Nikitin, Chemistry of Wood [in Russian] (Moscow – Leningrad, Izd. AN SSSR, 1951) p. 502.

[2] M. N. Tsypkina, Z. V. Sevast'yanova and M. A. Vishnyakova, Trans. Leningrad Academy of Wood Technology 75, 41 (1956).

[3] M. N. Tsypkina, L. G. Zhigirzhi and Z. V. Sevast'yanova, Sci. Trans. Central Sci. Res. Inst. Paper 425 (1957).

[4] K. B. Yatsimirskii, K. E. Prik, E. P. Skvirskaya and V. V. Starostin, J. Gen. Chem. 21, No. 3, 486 (1951).*

Received May 16, 1957

* Original Russian pagination. See C. B. Translation.

DETERMINATION OF THE PERCENTAGES OF 1 − 4, 3 − 4, AND 1 − 2 UNITS IN SYNTHETIC ISOPRENE RUBBERS FROM THE CURVES FOR THEIR RATES OF OXIDATION BY BENZOYL HYDROPEROXIDE

N. G. Kasatkina

Ethylenic compounds of different degrees of substitution are oxidized by benzoyl hydroperoxides at different rates. Tetrasubstituted ethylenes are oxidized at the highest rate, and monosubstituted at the lowest [1]. The relative contents of double bonds in unsaturated compounds can be estimated from the kinetic curves for their oxidation by benzoyl hydroperoxide [2]. The reaction of benzoyl hydroperoxide with unsaturated compounds has been used for determination of relative contents of bonds formed by 1 − 4 and 1 − 2 addition in divinyl rubbers [3, 4].

Synthetic isoprene rubbers containing the units (I), (II), and (III) were studied in the present investigation:

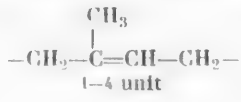
1–4 unit (I)

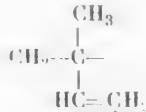
1–2 unit (II)

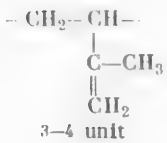
3–4 unit (III)

The double bond in unit (I) corresponds to the double bond in trisubstituted ethylene; in unit (II), to the double bond in monosubstituted ethylene; and in unit (III), to the double bond in disubstituted asymmetric ethylene. These three types of double bond present in the molecule of synthetic isoprene rubber should be oxidized at different rates.

Curves for the rates of oxidation of unsaturated compounds and their mixtures by benzoyl hydroperoxide may be interpreted by various methods, such as the use of calibration graphs, graphical extrapolation, etc. Our chosen method was by comparison of the kinetic curve for the oxidation of rubber by benzoyl hydroperoxide with curves for the oxidation rates of model compounds containing double bonds of the same type as are present in the rubber.

Limonene 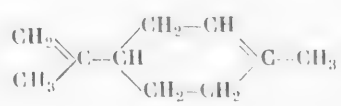

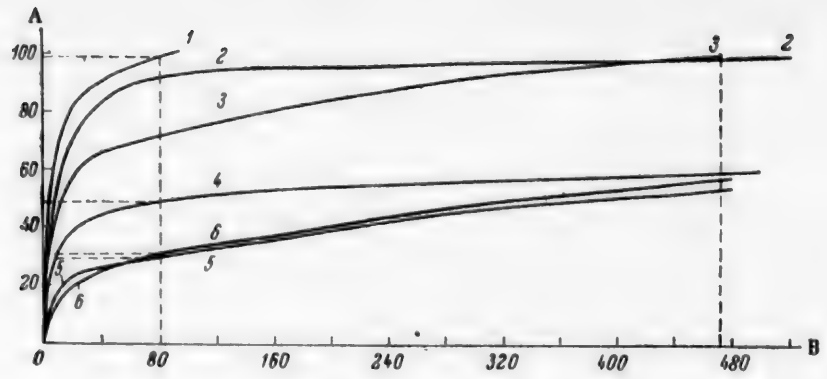

Curves for the rate of oxidation of benzoyl hydroperoxide:
A) amount of substance oxidized (%), B) time (minutes); 1) gutta-percha, 2) No. 1, 3) limonene, 4) No. 4, 5) No. 3, 6) No. 2.

TABLE 1

Results of Determinations of the Contents of Different Units in Synthetic Isoprene Rubbers

Rubber sample No.	Number of units determined by titration with benzoyl peroxide (%)			Total contents of 3 — 4 and 1 — 2 units, determined by infrared spectroscopy (%)
	1 — 4	3 — 4	1 — 2	
1	91	7	2	9
2	29	29	40	—
3	28	26	45	70
4	48	12	31	45

TABLE 2

Elementary Analysis of Rubbers

Rubber sample No.	Carbon	Hydrogen
	Found (%)	
1	88.22	11.65
2	88.18	11.54
3	88.23	11.59
4	87.85	11.76
Gutta-percha	88.20	11.63
	Calculated for C_5H_8 (%)	
	88.24	11.76

contains double bonds similar to the bonds in (I) and (III) units of isoprene rubber [the double bond in the limonene ring corresponds to the double bond of unit (I), and the double bond in the side chain corresponds to the double bond of unit (III)]. This hydrocarbon was used as the model compound for determination of the total amount of 1 — 4 and 3 — 4 units in isoprene rubbers. The second model compound used for determination of (I) units in isoprene rubber was gutta-percha, which contains 98% of 1 — 4 units. The double bond in gutta-percha is of the type in trisubstituted ethylene.

Curves for the oxidation rates of different isoprene rubbers were plotted.* Kinetic curves for the oxidation of limonene and gutta-percha under the same conditions, i.e., at the same concentration ratios of unsaturated compound to benzoyl hydroperoxide, were also determined. The oxidation-rate curves for the rubbers, limonene, and gutta-percha were plotted on the same graph, with the time taken along the abscissa axis, and the amount of substance oxidized (%) taken along the ordinate axis. The time required for oxidation of all the double bonds in gutta-percha corresponds to the time required for oxidation of all the double bonds in 1-4 units of isoprene rubber. The time needed for oxidation of all the double bonds in limonene corresponds to the time of oxidation of the double bonds in 1-4 and 3-4 units of isoprene rubber.

* We thank D. P. Feringer for supplying us with rubbers characterized by their infrared spectra.

Ordinates are drawn from the points corresponding to the oxidation times of gutta-percha and limonene to their points of intersection with the curve for the oxidation rate of the rubber, and then to the abscissa axis. The intercepts of the ordinates from the absicssa axis to the points of intersection on the curve for the oxidation rate of the rubber give the percentage of 1 – 4 units and the total percentage of 1 – 4 and 3 – 4 units respectively.

If the total unsaturation of the rubber is known, subtraction of the total percentage of 1 – 4 and 3 – 4 units from it gives the percentage of 1 – 2 units.

Curves were plotted for the oxidation rates of four samples of synthetic isoprene rubber, and of the model compounds: limonene and gutta-percha (Table 1; diagram; samples Nos. 1, 2, 3, and 4).

The aggregate contents of 3 – 4 and 1 – 2 units in rubber Nos. 1, 3, and 4 were estimated by infrared spectroscopy.

These data almost coincide with the results found by titration with benzoyl hydroperoxide.

The proposed titration method with the use of benzoyl hydroperoxide is very convenient, as it does not involve the use of complicated apparatus, and can be used for fairly rapid determination of the percentage contents of 1 – 4, 3 – 4, and 1 – 2 units in synthetic rubbers.

EXPERIMENTAL

The rubbers were purified by twofold precipitation by ethyl alcohol from benzene solution. All the operations were performed in oxygen-free nitrogen. The rubbers were dried to constant weight under 2 mm residual pressure, and analyzed by combustion with copper oxide. The results of elementary analysis of the rubbers are given in Table 2.

Total unsaturation was found from the amount of iodine bromide added at the double bonds [5-7]. The results of unsaturation determinations on the synthetic isoprene rubbers are given below:

Rubber sample No.	1	2	3	4
Unsaturation (%)	100	98.3	98.8	91.1

The rates of oxidation of rubbers and model compounds by benzoyl hydroperoxide were determined as follows: to 100 ml of 0.02 M solution of rubber or model compound in chloroform an equal volume of 0.11 N solution of benzoyl hydroperoxide in the same solvent was added, and 5 ml samples were taken at definite time intervals for iodometric determination of the converted double bonds. Parallel 2.5 ml samples of benzoyl hydroperoxide solutions were taken (blank experiment). The oxidation was performed in a thermostat at 0°. Benzoyl hydroperoxide was prepared from benzoyl peroxide (m.p. 103 – 104°) by the action of sodium methylate with subsequent decomposition of the hydroperoxide salt by sulfuric acid.

SUMMARY

1. Conditions have been found for simple and rapid determination of the percentage contents of 1 – 4, 3 – 4, and 1 – 2 units in synthetic isoprene rubbers from the curves for the rates of their oxidation by benzoyl hydroperoxide.

2. The contents of 1 – 4, 3 – 4, and 1 – 2 units in synthetic isoprene rubbers were determined by comparison of the curves for the rates of their oxidation by benzoyl hydroperoxide with oxidation curves for model compounds – limonene and gutta-percha.

LITERATURE CITED

[1] N. A. Prilezhaev, J. Russ. Phys-Chem. Soc. 42, 1387 (1910); 43, 609 (1911); 44, 613 (1912).

[2] H. Meerwein, J. pr. Ch., 113, 9 (1926).

[3] J. Kolthoff and T. Lee, J. Polymer Sci., II, 206 (1947).

[4] A. Saffer and B. Johnson, Ind. Eng. Chem., 40, 538 (1948).

[5] A. Kemp, Ind. Eng. Chem., 19, 531 (1927).

[6] A. Gorgas, Kautschuk, 4, 253 (1928).

[7] A. A. Vasil'ev, J. Gen. Chem. 17, 923 (1947).

Received June 29, 1957

OXIDATION OF PARAFFIN, INITIATED BY CHLORINE AT THE FIRST REACTION STAGE

I. V. Berezin, G. Vagner, and N. M. Émanuél'

It is known that the oxidation of paraffin by atmospheric oxygen is the basis of the industrial process for production of synthetic fatty acids used in detergent manufacture, and as raw materials for the production of higher aliphatic alcohols, plasticizers, etc. The best catalyst for the technical oxidation process at the present time is potassium permanganate, with the aid of which the reaction can be conducted at an acceptable rate to give acids of the required composition. However, the use of this catalyst results in the formation of the so-called catalyst sludge during the reaction; this contaminates the reactors and makes it impossible to perform the oxidation as a continuous process, which would make possible considerable intensification of the production of synthetic fatty acids. In this connection recent work on the oxidation of liquid hydrocarbons by gaseous catalysts is of definite interest. This method for stimulation of liquid-phase chain oxidation reactions by addition of certain catalytic gases (NO_2, HBr, O_3 etc.) to the air during a brief initial period has been termed gaseous initiation [1].

The literature contains some instances of gas initiation of hydrocarbon oxidation; for example, by chlorine [2]. However, in these cases gas initiation was used during the entire reaction; it has been found [1] that this is not only superfluous, but gives worse results than brief initiation during the first period.

An important advantage of gaseous initiation is absence of catalyst sludge and of consequent contamination of the reactor. This suggests that the oxidation process might be made continuous with the use of this initiation technique.

The purpose of the present investigation was to determine the principal characteristics of primary initiation by means of chlorine addition in the oxidation of brown-coal "Koepsen" paraffin (from the German Democratic Republic). Since the principle oxidation products are fatty acids, attention was devoted mainly to the kinetics of their formation and accumulation.

The theoretical principles of primary gas initiation were considered in a paper by one of us [1]. This paper was based on the view that processes of hydrocarbon oxidation belong by their mechanism to the class of chain reactions with degenerate branching, the theory of which was put forward by Semenov [3]. The increase in the number of free valences in reactions with degenerate branching is the consequence of the comparatively rare instances of decomposition of intermediate products into free radicals. Because of this, the course of the reaction as a whole depends on the formation rate of active centers during the initial period, when the rate of branching is still low. According to the paper cited [1], the mechanism of chain reactions includes at least two consecutive macroscopic stages – combinations of elementary processes leading to the formation of the final products or of stable intermediate substances. The course of the process as a whole can be influenced by action on these macroscopic stages, or by artificial creation of such stages. Gas initiation is such an artificially-created macroscopic stage, the purpose of which is to stimulate the branched chain reaction. In the first approximation, the action of this macroscopic stage of primary gas initiation consists of increasing of the rate of chain initiation.

EXPERIMENTAL

The apparatus used for experiments on the kinetics of paraffin oxidation is shown schematically in Fig. 1. The oxidation cell 1 with a sampling pipet 2 was contained in a thermostat 3. Air and chlorine passed into the

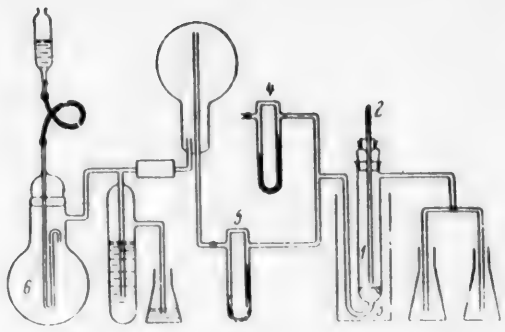

Fig. 1. Apparatus for chlorine-initiated oxidation of paraffin.

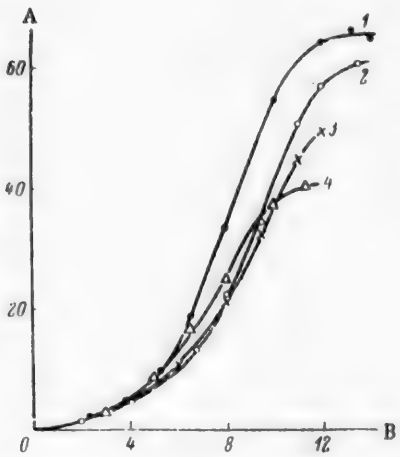

Fig. 2. Effects of paraffin charge in the reactor and air rate on the kinetics of acid accumulation; temperature 135°, initiation period 15 minutes with 15% chlorine content:
A) acid number, B) time (hours); air rate (liters/hour): 1) 11 per 40 g, 2) 11 per 30 g, 3) 8 per 30 g, 4) 15 per 30 g.

reactor through the flow meters 4 and 5. Chlorine was made by oxidation of hydrogen chloride by permanganate in the continuous generator 6.

Of the oxygen-containing compounds, only acids were determined; this was done by titration with 0.05 N alcoholic KOH. The acid contents of the oxidation products were expressed, in accordance with works practice, in terms of acid numbers, i.e., in mg KOH required for neutralization of the acids present in 1 g of a sample.

The oxidation of paraffin depends considerably on the air rate, temperature, and the kind of catalyst (initiator). The rate of air supply per unit weight of the material being oxidized is an important parameter. The air rate was therefore specially chosen to give the maximum rate of acid formation (at a given paraffin charge in the oxidation cell).

The experiments on paraffin oxidation were performed at 135°. The reaction was initiated during the first 15 minutes with 15% of chlorine in the air. The course of the kinetic curves showing accumulation of acids at different air rates is shown in Fig. 2. It follows from Fig. 2 that the optimum air rate w is 11 liters/hour per 40 g. In the following series of experiments the effect of the initiation time on the kinetics of acid formation was investigated. The experiments were performed at 135°, w = 11 liters/40 g, and 15% Cl_2 in the air. The results of these experiments are given in Fig. 3. It is seen that 3 minutes of initiation results in a high yield of acids, but with a quite appreciable induction period (6.5 hours).

With initiation periods of 10 and 7.5 minutes (i.e., intermediate between 15 and 3 minutes) the process of acid accumulation is worsened appreciably. The kinetic curves for acid formation have maxima at acid numbers of about 50. Thus, in this series of experiments the best results were obtained with initiation for 15 minutes.

A similar effect was observed in experiments with initiation of constant duration (15 minutes), but with different percentage contents of Cl_2 in the air. As before, the temperature and air rate in these experiments were maintained at 135° and 11 liters/40 g respectively.

Fig. 4. shows kinetic curves for acid formation with the process initiated by chlorine, with chlorine contents from 15 to 1.5% by volume in the air. It is seen in Fig. 4 that the kinetic curves for acid formation at 1.5 and 15% are fairly close to each other. The results are less good at intermediate chlorine contents in the air. (The maximum yield was obtained roughly at acid number 40). There is some resemblance to the experiments the results of which are given in Fig. 3, but with the difference that in this case the difference between the induction period is not so great.

All the oxidation products in the experiments represented in Figs. 3 and 4 were dark in color at the end of the reaction, owing to the formation of appreciable amounts of ether acids and hydroxy acids [4]. This is particularly the case in the experiments the kinetic curves of which have maxima at acid numbers 40-50. In experiments with additional initiation of the reactions at the saturation points of the kinetic curves better results or higher yield were not obtained.

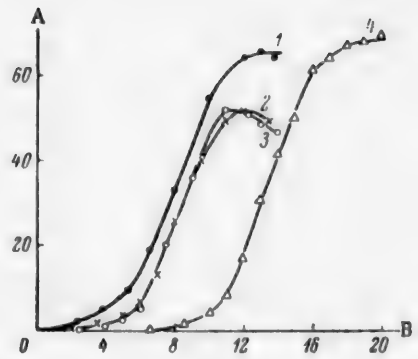

Fig. 3. Effect of initiation time on the kinetics of acid formation (with 15% Cl_2 in air); temperature 135°;
A) acid number, B) time (hours); initiation time (minutes): 1 — 15, 2 — 10, 3 — 7.5, 4 — 3.

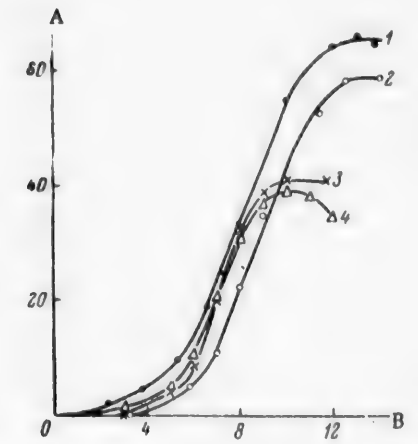

Fig. 4. Effect of chlorine content in air on the kinetics of acid formation at constant initiation time (15 minutes); temperature 135°:
A) acid number B) time (hours); chlorine content (%): 1 — 15, 2 — 1.5, 3 — 4, 4 — 7.5.

The results obtained in oxidation of paraffin at 125° are given in Fig. 5. The air rate was 11 liters/40 g as before. Initiation was continued for 15 minutes with 15% Cl_2 in the air. It is clear from Fig. 5 that the reaction develops sluggishly after a 7-hour induction period. Although the color of the oxidation product after 24 hours of oxidation was good, the acid content did not increase with further oxidation, but remained constant at a level corresponding to acid number 28.

A series of experiments was performed in order to determine the influence of a variable-temperature regime on the oxidation kinetics. At the initial stage of the reaction the temperature was maintained at 135°, and after some time it was lowered to 125° (Fig. 5). This diagram shows the kinetic curve for acid formation when the process was conducted for 5 hours at 135°, the temperature then being lowered (during 1 hour) to 125°. When the reaction was initiated with 15% of chlorine in the air during the first 15 minutes, at an air rate of 11 liters/40 g, it proceeded during the first 5 hours in accordance with the kinetics of the process at 135°, and then continued at a rate characteristic of the process at 125°, i.e., the induction period was shortened, and in 16 hours the reaction reached a limit which was somewhat higher than in oxidation at 125°.

The same diagram shows the results of an experiment in which a temperature of 135° was maintained only during 15 minutes of initiation, and it was then lowered to 125° during 10 minutes. In comparison with the reaction performed at 125° throughout, the induction period was considerably shortened, while the ultimate acid yield rose to acid number 36.

Whereas the induction periods were considerably shortened in experiments in which the initial stage of the reaction took place at 135°, and the reaction then proceeded at 125°, in the experiments in which the temperature at the start of the reaction was 145° and was then lowered to 135° there were no induction periods at all (Fig. 6). This diagram shows the results of an experiment in which the temperature was maintained at 145° during the first 3 hours, and then dropped rapidly to 135°. The reaction was initiated with 15% chlorine for 15 minutes at an air rate of 11 liters/40 g (Fig. 6, Curve 4). The process develops very rapidly at first, but the acid yield reaches a certain limit (acid number 16) just as rapidly, where it stops. Another experiment performed under milder initiation conditions, with 15% Cl_2 for two minutes, followed by 2 hours 15 minutes at 145°, and then continued to the end at 135°(Fig. 6, Curve 2). The kinetic curve for acid formation rose sharply in this experiment also, reaching the limiting acid number of 33 in 5 hours. The last in the series with variable temperature regimes was an experiment with even milder initiation conditions. For 4 hours the oxidation temperature was kept at 145°, and it was then lowered to 135°. The initiation was effected with 1.5% chlorine in the air for only 4 minutes (Fig. 6, Curve 3). There was virtually no induction period in this instance, and the process was slower, although the acid number was higher (38) than in the preceding experiment. The results of initiation with 15% Cl_2 for 15 minutes at 135° are shown in Fig. 6 (Curve 1).

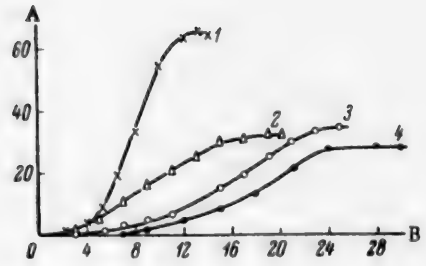

Fig. 5. Effect of temperature on the kinetics of acid formation; initiation conditions: 15 minutes with 15% Cl_2 in air; A) acid number, B) time (hours); curves:
1) at 135°; 2) 135° for 5 hours, then at 125°; 3) 135° for 15 minutes, then at 125°; 4) at 125°.

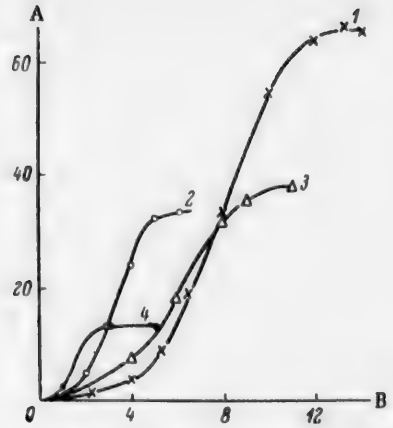

Fig. 6. Kinetics of acid accumulation under different initiation conditions:
A) acid number, B) time (hours); the curve numbers are explained in the text.

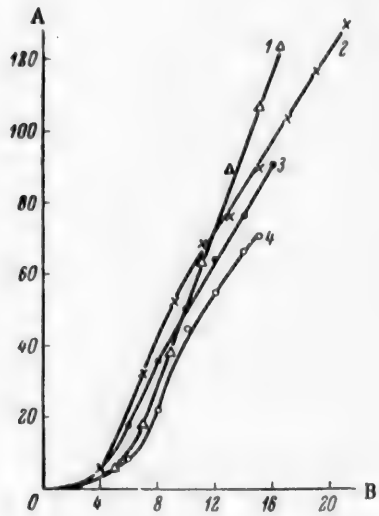

Fig. 7. Effect of chlorine content in the air on the kinetics of acid formation in oxidation of Groznyi paraffin; temperature 135°, initiation time 15 minutes; A) acid number, B) time (hours); chlorine contents (%):
1) 7.5; 2) 12; 3) 15; 4) 1.5.

In order to introduce another material into the investigation range and at the same time to check whether the low yields in experiments with Koepsen paraffin are due to side processes which develop independently of the initiation conditions, experiments on gas initiation with chlorine were also performed with paraffin obtained from petroleum.

The results of these experiments, with different percentage contents of chlorine in the air, are plotted in Fig. 7. In these experiments oxidation was characterized by a rapid increase of the acid numbers. In none of the instances given did the accumulation of acids reach a limit, although the acid numbers reached were rather high (up to 130). The oxidation products did not darken during the reaction, but remained quite light. The only difficulty in reaching even higher degrees of oxidation was the considerable foaming toward the end of the experiments.

The results obtained with gas initiation of the oxidation of Groznyi paraffin showed convincingly that the low limiting acid concentrations (acid numbers from 40 to 70) obtained in the oxidation of Koepsen paraffin are due not to the initiation regime but to the nature of the Koepsen paraffin itself. Since paraffin derived from brown coal may contain aromatic compounds, which might have an adverse effect on the oxidation process, an attempt was made to separate such compounds from the paraffin. The paraffin was passed through an externally-heated column filled with silica gel. The paraffin so treated with oxidized at 135° at an air rate of 5 liter/hour per 15 g of charge. The initiation was performed for 15 minutes with 7.5% Cl_2. Under these conditions the worst results were obtained in the oxidation of unpurified paraffin. As is clear from Fig. 8, the oxidation kinetics of the paraffin changed sharply after purification. Whereas the kinetic curve for the oxidation of unpurified paraffin has a maximum at an acid number of about 40, the corresponding curve for the oxidation of paraffin purified by passage through silica gel ascends steeply without any tendency to pass through a maximum.

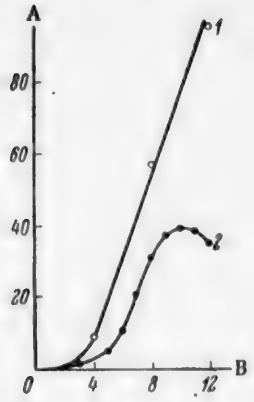

Fig. 8. Comparison of the kinetics of acid accumulation in the oxidation of purified (1) and unpurified (2) Koepsen paraffin; temperature 135° initiation with 7.5% Cl_2 for 15 minutes; A) acid number, B) time (hours).

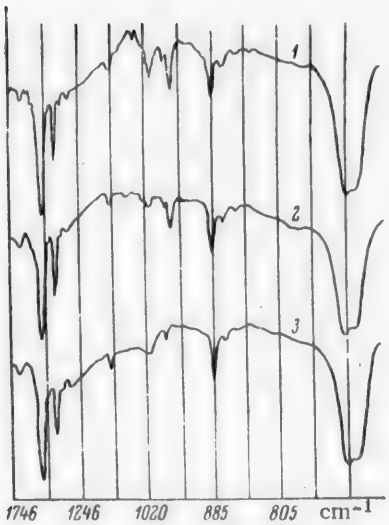

Fig. 9. Infrared spectra of paraffins: 1) unpurified Koepsen paraffin, 2) purified Koepsen paraffin, 3) Groznyi paraffin.

The infrared spectrum of unpurified Koepsen paraffin was studied in order to determine the nature of the supposed contamination. For comparison, the spectra of purified Koepsen paraffin and Groznyi paraffin were obtained; these are also shown in Fig. 9. Comparison of the spectra shows that Koepsen paraffin contains admixtures of a substance giving fairly intense absorption bands at 1014, 989, and 969 cm^{-1}. These substances are effectively adsorbed by silica gel. The nature of the contamination was not studied in greater detail.

DISCUSSION OF RESULTS

The results of these experiments indicate first, that addition of chlorine to air during a brief initial reaction stage has a strong initiating effect on the oxidation of paraffin. This effect primarily consists of a considerable shortening of the induction period (without initiation, $\tau > 100$ hours). The length of the induction period greatly depends on the duration of the initiation, i.e., on the time during which chlorine is blown through, and depends little on the chlorine concentration in the air at a given temperature.

With regard to the rate of the oxidation process, the experimental results show that the maximum rate of acid accumulation remains the same with variations of the initiation time and chlorine concentration, and depends only on the temperature and the air rate.

In oxidation of Koepsen paraffin the extent of the process, i.e., the limiting acid number, depends on the amount of chlorine supplied; however, the acid number does not exceed 70 under any initiation conditions.

The results obtained with the use of higher temperatures during initiation and the early stages of the reaction, with continuation of the reaction at a lower temperature, show that the maximum rate of acid accumulation is determined by the temperature conditions in the second reaction stage. The maximum acid concentration in oxidized paraffin attained under a variable-temperature regime is determined by the initiation conditions. This is especially true of the processes initiated at 145°, with the subsequent reaction performed at 135°. In such reactions the ultimate acid yields decrease with the use of large amounts of chlorine.

The acid contents reach much higher values in the oxidation of Groznyi paraffin than in the oxidation of Koepsen paraffin. The kinetic curves for the accumulation of acids in Grozyni paraffin show no tendency to bend or pass through maxima. This indicates that the maxima at acid numbers from 40 to 70 on the kinetic curves for the oxidation of Koepsen paraffin are caused by the chemical composition of this paraffin.

Analysis by infrared spectroscopy shows that Koepsen paraffin differs from the Groznyi product in containing considerable admixtures of a substance which gives intense absorption bands at 1014, 989, and 969 cm^{-1}, and which is readily adsorbed by silica gel.

It is known that unsaturated and aromatic compounds are particularly well adsorbed by silica gel. However, as the iodine number of Koepsen paraffin is low (5 by the Kaufmann method), it may be concluded that the adsorbed substance, which gives these absorption bands in the infrared spectrum, is a substance of aromatic character.

If Koepsen paraffin is oxidized after removal of the aromatic substances by passage through silica gel, the kinetics of acid accumulation changes sharply, the acids accumulate more rapidly, and the kinetic curves no longer show any tendency to pass through maxima. This experimental effect indicates that the maxima on the kinetic curves for acid accumulation in the oxidation of unpurified Koepsen paraffin and the accompanying resinification of the oxidation products are caused by the presence of substances of an aromatic character. Therefore the yield and quality of fatty acids can be greatly improved by preliminary treatment of difficultly-oxidized paraffins by silica gel.

SUMMARY

1. Gas oxidation by chlorine greatly stimulates the oxidation of paraffin; the initiation takes place during a brief period at the beginning of the process.

2. Kinetic curves showing the accumulation of acids in chlorine-initiated paraffin oxidation were plotted, and it was found that the low maxima on the kinetic curves and the resinification of the oxidation products formed from Koepsen paraffin are caused by the presence of substances of an aromatic nature in this paraffin.

3. Experiments with a new initiator (chlorine) and a new raw material for oxidation (paraffin) confirmed the widespread initiating action of gaseous initiators.

LITERATURE CITED

[1] N. M. Emanuel', J. Phys. Chem. 30, 847 (1956).

[2] M. S. Malinovskii, N. I. Zemlyanskii, and L. K. Klimovskaya, J. Appl. Chem. 27, 1028 (1954).*

[3] N. I. Semenov, Chain Reactions [in Russian] (Goskhimizdat, 1934).

[4] V. K. Tsyskovskii, Production of Synthetic Fatty Acids by Oxidation of Kerosene Fractions [in Russian] (Moscow – Leningrad, 1954).

Received December 20, 1956

* Original Russian pagination. See C. B. Translation.

EFFECT OF ESTERS OF UNSATURATED PHOSPHONIC ACIDS ON THE ANTIOXIDANT PROPERTIES OF MINERAL OIL

K. K. Papok, K. N. Anisimov, B. S. Kuseva, and N. E. Kolobova

Institute of Heteroorganic Compounds, Academy of Sciences USSR

The experience of a number of years has demonstrated the possibility of wide utilization of various organophosphorus compounds for improving the properties of lubricating oils. During the period 1912-1950 more than 500 patents relating to the use of organophosphorus compounds as additives have been issued [1]. A considerable number of investigations on the use of esters and thioesters of phosphorous and phosphoric acids as lubricant additives has been published. It should be noted that among the organophosphorus compounds many derivatives of the acids of phosphorus have been discovered, which have so far been investigated and used very little as additives for oils. In view of this we studied a series of new compounds, namely: esters, amides, and thioesters of unsaturated phosphonic and thiophosphonic acids.

Compounds of the following types were synthesized for the investigation:

$$ROCH=CHPO(OR)_2,\quad ROCH=CHPO(NR_2)_2,\quad ROCH=CHPO(SR)_2$$

$$RCH=CHPO(OR)_2,\quad RCH=CHPO(NR_2)_2,\quad RCH=CHPO(SR)_2$$

$$ROCH=CHPS(SR)_2,\quad ROCH=CHPS(OR)_2 \text{ etc.}$$

where $R = CH_3$, C_4H_9, C_5H_{11}, C_7H_{15}, $CH_3OCH_2-CH_2$, $C_2H_5OCH_2-CH_2$, $C_4H_9OCH_2-CH_2$, C_6H_5.

In the present communication we consider the effects of diesters of unsaturated phosphonic acids on the antioxidant properties of MS-20 mineral oil.

The diesters of unsaturated phosphonic acids were prepared by the action of acid dichlorides of unsaturated phosphonic acids on the corresponding alcohols in presence of tertiary amines in benzene or ligroine [2]. The n-butyl and n-hexyl esters of β-ethoxyethoxyvinylphosphonic acid are described here for the first time.

All the esters are colorless liquids, readily soluble in organic solvents and insoluble in water; they do not decompose on prolonged keeping. Some of these compounds, such as the n-butyl and n-hexyl esters of β-ethoxyethoxyvinylphosphonic acid, freeze at temperatures such as −50 and −70° deg.

The antioxidant properties of oils containing these compounds were evaluated from their stability to thermal oxidation (T) (GOST 4953-49), volatility (E), working fraction (WF), and lacquer formation (L) (GOST 5737-53). The results of this investigation are presented in four tables, which give the physical and engine properties of each compound.

The data in the tables are presented in such a way as to reveal a certain connection between the engine properties of the oil and the structure of the compounds used as additives. The right-hand side of the formula of each compound contains similar ester groups: ethyl in Table 1, allyl in Table 2, butyl in Table 3, and hexyl in Table 4, while the left-hand sides contain various unsaturated organic radicals.

Table 1 gives data on diethyl esters of β-ethoxyvinylphosphonic, β-butoxyvinylphosphonic, β-hexyloxyvinylphosphonic, β-ethoxyethoxylvinylphosphonic, β-phenylvinylphosphonic, and indenylphosphonic acids.

TABLE 1

Effect of Diethyl Esters of Unsaturated Phosphonic Acids on the Antioxidant Properties of MS-20 Oil

Code mark	Formula of compound	Name of compound	Boiling point (°C/mm Hg)	n_D^{20}	d_4^{20}	Laboratory evaluation of engine properties of MS-20 oil + 2% additions (in %)			Thermo-oxidative stability by Papok method at 250 °C (min)
						E	WF	L	
		MS-20 oil				61	19	20	23
AP-52	$C_2H_5OCH{=}CHPO(OC_2H_5)_2$	Diethyl ester of β-ethoxy-vinylphosphonic acid	95/2	1.4476	1.0710	58	35	7	31
AP-41	$n\text{-}C_4H_9OCH{=}CHPO(OC_2H_5)_2$	Diethyl ester of β-butoxy-vinylphosphonic acid	129/3	1.4460	1.0360	65	21	14	24
AP-42	$n\text{-}C_6H_{13}OCH{=}CHPO(OC_2H_5)_2$	Diethyl ester of β-hexyloxy-vinylphosphonic acid	140/2	1.4495	1.0110	61	29	10	24
AP-43	$C_2H_5OCH_2{-}CH_2OCH{=}CHPO(OC_2H_5)_2$	Diethyl ester of β-ethoxy-ethoxyvinylphosphonic acid	153/2	1.4512	1.0812	64	24	12	24
AP-53	$C_6H_5CH{=}CHPO(OC_2H_5)_2$	Diethyl ester of β-phenyl-vinylphosphonic acid	138/2	1.5325	1.1082	58	34	8	31
AP-12	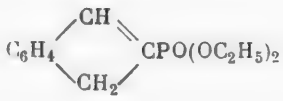	Diethyl ester of indenyl-phosphonic acid	150/1	1.5398	1.1410	59	37	4	59

TABLE 2

Effect of Diallyl Esters of Unsaturated Phosphonic Acids on the Antioxidant Properties of MS-20 Oil

Code mark	Formula of compound	Name of compound	Boiling point (°C/mm Hg)	n_D^{20}	d_4^{20}	Laboratory evaluation of engine properties of MS-20 oil + 2% additions (%)			Thermo-oxidative stability by the Papok method at 250 °C (min)
						E	WF	L	
		MS-20 oil				61	19	20	23
AP-44	$C_2H_5OCH{=}CHPO(OC_3H_5)_2$	Diallyl ester of β-ethoxy-vinylphosphonic acid	112/1	1.4698	1.0792	62	20	18	24
AP-54	$n\text{-}C_4H_9OCH{=}CHPO(OC_3H_5)_2$	Diallyl ester of β-butoxy-vinylphosphonic acid	139.5/2	1.4651	1.0442	58	34	8	32
AP-14	$n\text{-}C_6H_{13}OCH{=}CHPO(OC_3H_5)_2$	Diallyl ester of β-hexyloxy-vinylphosphonic acid	151/1	1.4650	1.0178	58	39	3	47
AP-45	$C_2H_5OCH_2{-}CH_2OCH{=}CHPO(OC_3H_5)_2$	Diallyl ester of β-ethoxy-ethoxyvinylphosphonic acid	138.5/2	1.4702	1.0854	64	19	17	35
AP-15	$C_6H_5OCH{=}CHPO(OC_3H_5)_2$	Diallyl ester of β-phenoxy-vinylphosphonic acid	153/2	1.5220	1.1330	58	40	2	54
AP-16	$C_6H_5CH{=}CHPO(OC_3H_5)_2$	Diallyl ester of β-phenyl-vinylphosphonic acid	159/2	1.5445	1.1076	55	43	2	54
AP-13	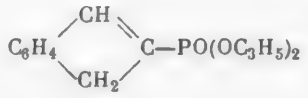	Diallyl ester of indenyl-phosphonic acid	169/1	1.5514	1.1354	58	41	1	75

TABLE 3

Effect of Dibutyl Esters of Unsaturated Phosphonic Acids on the Antioxidant Properties of MS-20 Oil

Code mark	Formula of compound	Name of compound	Boiling point (°C/mm Hg)	n_D^{20}	d_4^{20}	Laboratory evaluation of engine properties of MS-20 oil + 2% additions (%)			Thermo-oxidative stability by the Papok method at 250 °C (min)
						E	WF	L	
		MS-20 oil				61	19	20	23
AP-46	$C_2H_5OCH=CHPO(OC_4H_9\text{-}n)_2$	Dibutyl ester of β-ethoxyvinylphosphonic acid	144/5	1.4492	1.0069	60	25	15	30
AP-47	$n\text{-}C_3H_7OCH=CHPO(OC_4H_9\text{-}n)_2$	Dibutyl ester of β-propoxyvinylphosphonic acid	139/2	1.4485	0.9969	57	30	13	31
AP-48	$n\text{-}C_4H_9OCH=CHPO(OC_4H_9\text{-}n)_2$	Dibutyl ester of β-butoxyvinylphosphonic acid	144/1	1.4491	0.9879	58	29	13	31
AP-49	$n\text{-}C_6H_{13}OCH=CHPO(OC_4H_9\text{-}n)_2$	Dibutyl ester of β-hexyloxyvinylphosphonic acid	156/1	1.4495	0.9723	61	27	12	29
AP-50	$C_2H_5OCH_2—CH_2OCH=CHPO(OC_4H_9\text{-}n)_2$	Dibutyl ester of β-ethoxyethoxyvinylphosphonic acid	150/2	1.4510	1.0238	59	32	9	30
AP-57	$C_6H_5CH=CHPO(OC_4H_9\text{-}n)_2$	Dibutyl ester of β-phenylvinylphosphonic acid	$\frac{172—173}{2}$	1.5153	1.0403	57	38	5	32
AP-24	$C_2H_5OCH_2—CH_2OCH=CHPO(OCH_2—CH_2OC_2H_5)_2$	Diethoxyethyl ester of β-ethoxyethoxyvinylphosphonic acid	180/1	1.4565	1.0917	52	44	4	35
AP-23	$C_6H_5CH=CHPO(OCH_2—CH_2—OC_2H_5)_2$	Diethoxyethyl ester of β-phenylvinylphosphonic acid	187/2	1.5179	1.1114	55	40	5	45

TABLE 4

Effect of Dihexyl Esters of Unsaturated Phosphonic Acids on the Antioxidant Properties of MS-20 Oil

Code mark	Formula of compound	Name of compound	Boiling point (°C/mm Hg)	n_D^{20}	d_4^{20}	Laboratory evaluation of engine properties of MS-20 oil + 2% additions (%)			Thermo-oxidative stability by the Papok method at 250 °C (min)
						E	WF	L	
		MS-20 oil				61	19	20	23
AP-55	$C_2H_5OCH{=}CHPO(OC_6H_{13}\text{-n})_2$	Dihexyl ester of β-ethoxyvinylphosphonic acid	157—158/2	1.4511	0.9710	59	37	4	44
AP-56	n-$C_4H_9OCH{=}CHPO(OC_6H_{13}\text{-n})_2$	Dihexyl ester of β-butoxyvinylphosphonic acid	164—165/2	1.4518	0.9635	57	39	4	46
AP-1	n-$C_6H_{13}OCH{=}CHPO(OC_6H_{13}\text{-n})_2$	Dihexyl ester of β-n-hexyloxyvinylphosphonic acid	190/2	1.4528	0.9515	54	44	2	56
AP-60	$C_2H_5OCH_2{-}CH_2OCH{=}CHPO(OC_6H_{13}\text{-n})_2$	Dihexyl ester of β-ethoxyethoxyvinylphosphonic acid	216/1	1.4540	0.9874	57	41	2	38
AP-11	n-$C_4H_9OCH_2{-}CH_2{-}OCH{=}CHPO(OC_6H_{13}\text{-n})_2$	Dihexyl ester of n-butoxyethoxyvinylphosphonic acid	202/2	1.4550	0.9794	54	45	1	78
AP-2	$C_6H_5OCH{=}CHPO(OC_6H_{13}\text{-n})_2$	Dihexyl ester of β-phenoxyvinylphosphonic acid	204/1	1.4925	1.0237	58	38	4	57
AP-13	$C_6H_5CH{=}CHPO(OC_6H_{13}\text{-n})_2$	Dihexyl ester of β-phenylvinylphosphonic acid	187.5/2	1.5500	1.054	56	44	0	58
AP-6	$C_6H_5CH{=}CHPO(OC_7H_{15})_2$	n-Diheptyl ester of β-phenylvinylphosphonic acid	213/1	1.5020	0.9888	55	43	2	75

Introduction of 2% of any of the first five esters of unsaturated phosphonic acids into MS-20 oil resulted in a small decrease of the amount of lacquer, an increase of the working fraction, and a slight increase of thermooxidative stability (from 1 to 8 minutes). In contrast to these esters, the diethyl ester of indenylphosphonic acid decreased the lacquer formation in the oil from 20 to 4%, and raised the thermooxidative stability by 36 minutes.

Among the allyl esters of the same unsaturated phosphonic acids there were some compounds more effective than diethyl esters (Table 2). The following effects were observed. The thermooxidative stability increases and lacquer formation diminishes with increase of the hydrocarbon radical length (AP-44, AP-54, and AP-14). Introduction of an ethoxy group ($-CH_2-CH_2O-$) into the diallyl ester of β-ethoxyvinylphosphonic acid raised the thermooxidative stability from 24 to 35 minutes, but had no effect on the amount of lacquer (AP-44, AP-45). The antioxidant properties are improved by the presence of phenyl or indenyl groups in the diallyl esters. The most active diallyl esters, greatly diminishing lacquer formation and increasing the thermooxidative stability, were the esters of β-phenoxyvinylphosphonic, β-phenylvinylphosphonic, and indenylphosphinic acids (AP-15, AP-16, and AP-13), which increased the thermooxidative stability to 54-75 minutes, and lowered lacquer formation to 1-2%. In contrast to the diallyl esters, the thermooxidative stability and lacquer formation of the dibutyl esters do not change with increase of the hydrocarbon radical (Table 3, AP-46, AP-47, AP-48, AP-49). Similarly, introduction of the $-CH_2-CH_2O$ group did not affect the antioxidant properties of the dibutyl esters (AP-46, AP-50). All the investigated compounds of this class increased the thermooxidative stability of the oil by only 7-12 minutes, apart from the dibutyl and diethoxyethyl esters of phenylvinylphosphonic acid (AP-23, AP-57), which doubled the thermooxidative stability and lowered lacquer formation to 5%; this effect is caused by the introduction of the phenyl radical.

Of all the esters studied, the dihexyl esters have better antioxidant properties than the diethyl, diallyl, and dibutyl esters of unsaturated phosphonic acids (Table 4). The thermooxidative properties improve with increase of hydrocarbon-radical length in the series AP-55, AP-56, and AP-1, and also AP-60 and AP-11. The most active compounds, which sharply lower lacquer formation, and increase the working fraction and the thermooxidative stability, are the n-dihexyl ester of β-n-butoxyethoxyvinylphosphonic acid and the n-diheptyl ester of β-phenylvinylphosphonic acid (AP-11, AP-6). Comparison of the diethyl and diallyl esters of phenylvinylphosphonic and indenylphosphonic acids shows that the esters of indenylphosphonic acid (AP-53, AP-12, AP-16, and AP-13) are the most effective antioxidants.

TABLE 5

Effect of Chain Length of the Ester Radical on the Antioxidant Properties of the Compounds

Compounds	Thermooxidative stability by the Papok method at 250 °C (min)
MS-20 oil + 2% of	23
n-$C_4H_9OCH{=}CHPO(OC_2H_5)_2$	24
n-$C_4H_9OCH{=}CHPO(OC_3H_5)_2$	32
n-$C_4H_9OCH{=}CHPO(OC_4H_9\text{-}n)_2$	31
n-$C_4H_9OCH{=}CHPO(OC_6H_{13}\text{-}n)_2$	46
$C_6H_5CH{=}CHPO(OC_2H_5)_2$	31
$C_6H_5CH{=}CHPO(OC_3H_5)_2$	54
$C_6H_5CH{=}CHPO(OC_4H_9\text{-}n)_2$	46
$C_6H_5CH{=}CHPO(OC_6H_{13}\text{-}n)_2$	58
$C_6H_5CH{=}CHPO(OC_7H_{15}\text{-}n)_2$	75
n-$C_6H_{13}OCH{=}CHPO(OC_2H_5)_2$	24
n-$C_6H_{13}OCH{=}CHPO(OC_3H_5)_2$	47
n-$C_6H_{13}OCH{=}CHPO(OC_4H_9\text{-}n)_2$	29
n-$C_6H_{13}OCH{=}CHPO(OC_6H_{13}\text{-}n)_2$	56

The antioxidant properties of a number of these compounds depend on the chain length of the ester radical. For example, the thermooxidative stability of esters of β-butoxyvinylphosphonic, β-phenylvinylphosphonic, and

β-hexyloxyvinylphosphonic acids increases with increasing chain length of the ester radical; exceptions are the dibutyl esters of β-alkoxy (phenoxy) vinylphosphonic acids, which have even worse antioxidant properties than the diallyl esters (Table 5).

SUMMARY

1. The antioxidant properties of esters of unsaturated phosphonic acids increase: a) on introduction of a phenyl group in diethyl, diallyl, and dihexyl esters; b) in presence of an indenyl group in diethyl and diallyl esters; c) with increasing length of the hydrocarbon chain (from C_2 to C_6) in diallyl and dihexyl esters, and d) with increase in the length of the ester radical (from C_2 to C_6) in esters of β-butoxyvinylphosphonic, β-phenylvinylphosphonic, and β-hexyloxyvinylphosphonic acids.

2. Of the compounds studied, the dihexyl esters of unsaturated phosphonic acids have the best antioxidant properties.

LITERATURE CITED

[1] Petroleum Processing, 7, 1780 (1952).

[2] K. N. Anisimov, N. E. Kolobova and A. N. Nesmeyanov, Bull. Acad. Sci. USSR Div. Chem. Sci. 2, 241; 3, 432; 5, 827 (1955);* 1, 16 (1956).*

Received May 23, 1957

* Original Russian pagination. See C. B. Translation.

FOAM HYDROGENATION OF FATS

S. Yu. Elovich, G. M. Zhabrova, P. G. Krivenkova,

and T. D. Semenovskaya

Catalytic hydrogenation of fats is a complex heterogeneous reaction of great applied significance and considerable scientific interest.

The reaction is usually effected with the aid of a metallic catalyst, generally pure nickel or nickel with metallic additives, finely distributed in the liquid phase. Hydrogen is introduced into this medium, and adds on at different rates to triglyceride radicals of different degrees of saturation. As is known, hydrogenation of fats can be represented by a scheme of concurrent and consecutive reactions. The process is accompanied by migration of double bonds, leading to isomerization of the corresponding radicals. In this paper we do not consider isomerization processes, but concentrate on the laws governing the addition of hydrogen to double bonds.

It is known [1] that a consequence of the complexity and heterogeneity of the reactions of fat hydrogenation is that the factors which determine the rate at which the molecules are transported to the catalyst also determine to a definite extent the selectivity of the hydrogenation process. Since hydrogen must dissolve in the oil and then diffuse through a definite layer of the latter in its approach to the catalyst particle, in practice the process is most often controlled by diffusion, and the selectivity of the hydrogenation process is at a maximum in this region. Intensified supply of hydrogen in the region controlled by hydrogen diffusion raises the reaction rate, but does not affect selectivity.

When agitation becomes sufficiently intensive, difficulties arise in the access of triglycerides to the catalyst particles, and the selectivity of hydrogenation then diminishes under certain conditions. This is especially noticeable in hydrogenation under pressure. These effects have been considered in detail in a series of papers by Elovich, Zhabrova, and others, published during the last 20 years.

Electron microscope investigations of industrial nickel catalysts, carried out by Elovich and Tret'yakov [2], showed that the diameters of the catalyst particles are in the 1-10 μ range. Evaluation of the hydrodynamic agitation conditions when hydrogen is bubbled through oil, based on Levich's work [3], led to the following relationship, derived by the above-named authors:

$$\frac{V}{M} \cdot \frac{\left(\frac{\delta}{a}\right)^{2/3}}{D^{1/4}L^{1/4}} = K\Delta c, \tag{1}$$

where

$$K = \frac{\left(\frac{\rho_0' - \rho}{\rho_0}\right)^{2/3} \cdot k_f^{1/6} \nu^{1/6}}{\frac{3}{4}\pi D^{1/2}\left(\frac{\rho_0}{\rho}\right)^{1/2}\beta Pr^{2/3}}. \tag{2}$$

In these equations D is the diffusion coefficient of hydrogen in the oil, M is the weight of catalyst per unit volume of oil, δ is the diameter of the catalyst particles, a is the diameter of the hydrogen bubbles, U is the maximum liquid velocity in turbulent flow over the catalyst. L is the reactor diameter, Δ c is the drop of tri-

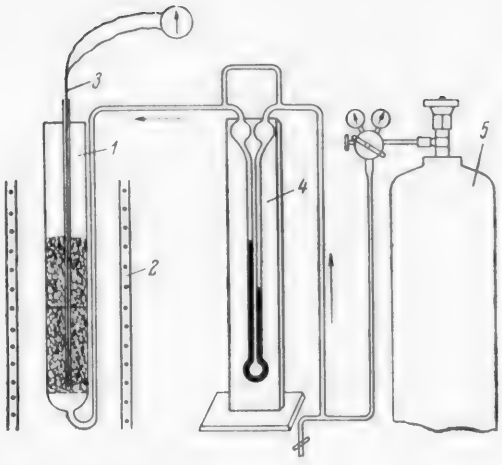

Fig. 1. Diagram of apparatus:
1) reaction vessel, 2) electric furnace, 3) thermocouple, 4) flow meter, 5) hydrogen cylinder.

glyceride concentration at the catalyst surface, ρ_0 is the density of the gas, ρ is the density of the liquid, ν is the kinematic viscosity, C_0 is the gas concentration in a bubble, ρ_0' is the density of a catalyst particle, k_f is the coefficient of liquid resistance to the motion of a catalyst particle, β is a factor which takes into account the shape of the catalyst particles, Pr is the Prandtl number, and V is the volume of hydrogen per 1 cc of oil per second.

It follows from the above equation that at constant U and L the ratio $\frac{\delta}{a}$ is of primary practical significance for increasing the diffusion flow of glycerides. The smaller the ratio of the gas bubble diameter to the catalyst particle diameter, the greater is the diffusion flow. Since the particle size of the catalyst, as already mentioned, is small, this condition poses extremely difficult technical problems; therefore the use of other effective agitation methods is of considerable interest.

We used the method of foam hydrogenation [1, 4], which gives quite good results. Methods of foam agitation have recently been developed by a number of workers. Extensive data on this subject are presented in the book by Pozin, Mukhlenov, Tumarkina, and Tarat [5]. We used porous partitions in Schott filters of different numbers for foam formation. As is known, in No. 2 Schott filters the pore diameter is $< 40-50\ \mu$, and in No. 3 filters it is $< 20-30\ \mu$ [6].

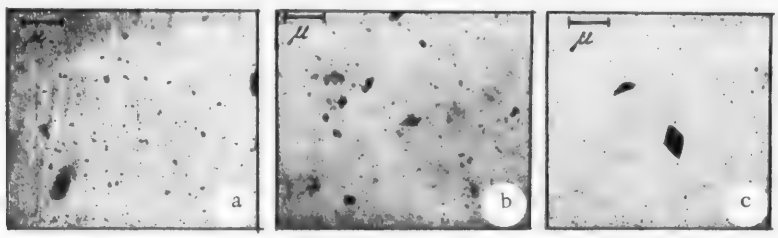

Fig. 2. Electron micrographs of nickel formate catalyst, under magnification of 7000:
a) before hydrogenation, b) after hydrogenation, c) catalyst particles with a distinct crystalline structure.

The experiments were performed as follows. The reaction vessel consisted of a tube of molybdenum glass with a Schott filter sealed in its lower end. A stream of hydrogen was passed through the Schott filter from below (Fig. 1). 50 – 100 g of oil was put into the reaction vessel and heated to the required temperature with a continuous flow of hydrogen (Fig. 1). The required quantity of catalyst (nickel in hydrogenated oil) was then added to the heated oil, and the temperature was raised to the required level in 2-3 minutes. The temperature was maintained constant to within ±2° by the regulation of the furnace voltage. Samples were taken during hydrogenation by means of a glass pipet, the times being noted with the aid of a seconds clock. Nickel was removed from the samples, and their iodine numbers were determined. Hydrogen numbers were also determined in some cases. The thiocyanate numbers were determined in one experiment. Cottonseed and sunflower oils were hydrogenated. The catalyst was nickel, made by decomposition of nickel formate in cottonseed oil. The decomposition was performed in a glass test tube at 240°, in a stream of hydrogen passed at 12 – 13 liters/minute. The oil was previously heated to 200° in a current of hydrogen, and the nickel formate was then added. The temperature was then raised to 240°. The decomposition was continued for 1 hour, after which the thick black mass was poured

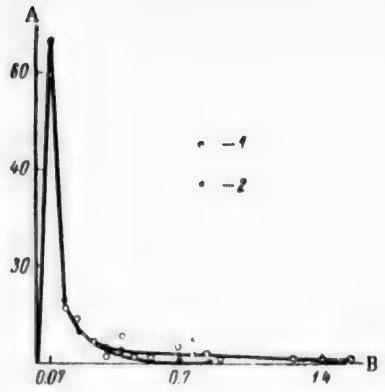

Fig. 3. Particle-size distribution of catalysts:
A) number of particles (%), B) particle size (μ); catalyst: 1) before reaction, 2) after reaction.

out into a porcelain basin, where it was stirred and allowed to solidify. The product was ground in a mortar and analyzed for nickel. The nickel content of our catalyst sample was 5.82%.

The electron microscopy was performed by I. I. Tret'yankov and I. A. Bespalova, to whom we offer our thanks. The specimens for electron microscopy were prepared as follows [2].

The hydrogenated oil samples were warmed and stirred thoroughly. 1 ml samples were withdrawn with a pipet and mixed with 10 ml of dichloroethane.

The solid phase was centrifuged off and shaken with a fresh portion of dichloroethane. This washing was repeated 3 times, after which the catalyst was shaken first with 1 ml of amyl acetate, and then with 1 ml of a solution of collodion in amyl acetate. A drop of this suspension was spread on the surface of distilled water in a crystallizing dish. After evaporation of the amyl acetate a very thin collodion film containing embedded catalyst particles remained on the water surface. Pieces of this film were caught on gauze circles, dried and examined under the electron microscope.

Electron micrographs of the catalyst under magnification of 7000 are given in Table 2. There is little difference between the catalyst before (Fig. 2,a) and after (Fig.2,b) the reaction. It is clear that a single hydrogenation, lasting 2-3 hours, results in a relatively small increase of particle size in the micron range. Fig. 2,c shows well-defined crystalline nickel particles free from pores. Such particles can be formed only by growth of smaller crystals. The particle-size distribution was calculated. The particle-size distribution curves for the catalyst before and after use are given in Fig. 3. It seems that the distribution changes little. The commonest particle size is in the ~0.1 μ region. Works catalysts are approximately 10 times as coarse [2].

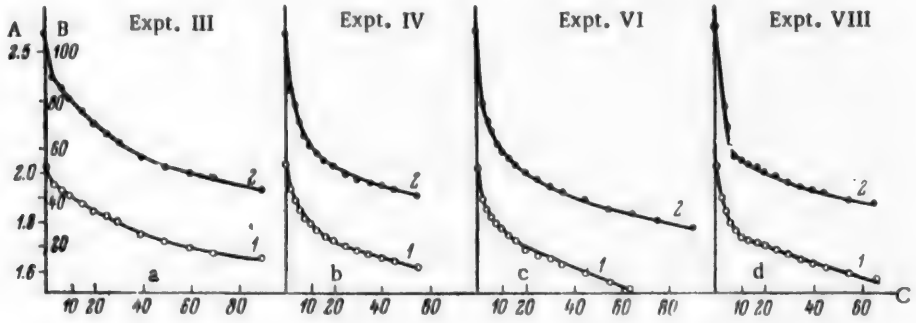

Fig. 4. Kinetic curves for the hydrogenation of cottonseed oil; amount of oil 50 g, nickel content 0.175%, hydrogen rate 1.15 liters/minute:
A) log iodine number (1), B) iodine number (2), C) time (minutes); hydrogen supplied through: a) orifice 1 mm in diameter; b) No. 2 Schott, c) No. 3 Schott (100 g of oil), d) No. 3 Schott (50 g of oil).

The principal experimental results are given in Table 1.

The cottonseed oil used contained 47.8% linoleic radicals, 29.5% oleic radicals, and 22.7% saturated radicals.

The volume of the foam increased when hydrogen was passed. At a relatively low rate (1.15 liters/minute) of hydrogen passed through the oil the volume of the foamed oil during the reaction increased 1.5 to 2 fold in comparison to the initial volume of the oil. When the hydrogen rate was increased to 2.4 liters/minute, the

TABLE 1

Results of Experiments With Cottonseed Oil Hydrogen Rate 1.15 Liters/Minute

Expt. No.	Hydrogen supply conditions	Increase of oil volume in foam (%)	Nickel content in oil (%)	Amount of oil (g)	Temperature (°C)	Duration of experiment (min)
III	One orifice of 1 mm		0.175	50	218	85
IV	Schott No. 2	210	0.175	50	198	55
VI	Schott No. 3	140	0.175	100	219	90
VIII	Schott No. 3	180	0.175	50	217	65
X	Schott No. 3	180	0.035	50	213	170

TABLE 2

Composition of Samples in Hydrogenation of Cottonseed Oil (Experiment X)

Sample No.	Time from start of reaction (min)	Iodine number	Thiocyanate number	Composition of sample (%)		
				linoleic radicals	oleic radicals	saturated radicals
Original	0	108.2	66.8	47.8	29.5	22.7
5	20	102.6	65.4	43.0	32.8	24.2
6	25	102.1	67.2	40.8	33.9	25.3
8	40	98.8	67.6	36.0	42.3	21.7
11	75	91.8	65.3	30.6	45.2	24.2
13	100	88.5	65.7	26.4	49.9	23.7
15	120	86.0	66.0	23.1	53.5	23.4
18	170	79.0	65.2	15.9	59.8	24.3

volume of the foam was 500% of the initial volume. It was then difficult to regulate the reaction conditions, so that all the experiments were performed at the lower hydrogen rate.

Kinetic data for cottonseed oil are plotted in ordinary and logarithmic coordinates in Figs. 4 and 5. It is seen that the iodine values fall very rapidly during foam hydrogenation. After 5-10 minutes nearly all the linoleic glycerides are reduced to oleic. An experiment (Fig. 5) was performed with a small amount of catalyst, so that it was possible to follow the course of conversion of linoleic radicals during hydrogenation. The amount of catalyst was diminished 5-fold, and was 0.035%. The experiment lasted 170 minutes, and the iodine number fell from 108.2 to 83. The thiocyanate numbers of several samples were determined. Table 2 contains the analytical data and the calculated contents of oleic, linoleic, and saturated radicals. The results show that the oleic radicals did not undergo any appreciable saturation during the experiment.

The data for Experiment X can be used to calculate the selectivity coefficient of the hydrogenation reaction. We showed earlier [7] that the oleic acid content in relation to the content of linoleic radicals during hydrogenation can be represented by the equation:

$$[Ol] = \frac{(Ol_0 + L_0 - kL_0)[L]^k}{L_0^k(1-k)} - \frac{L}{1-k}. \quad (3)$$

Since we have only the initial part of the curve (up to the oleic acid maximum) in our experiment, we use the fact that at the start of the experiment

$$\frac{d[Ol]}{d[L]} = \frac{kL_0}{Ol_0} - 1. \quad (4)$$

Here [Ol] and [L] are the molar concentrations of oleic and linoleic radicals at a given instant; Ol_0 and L_0 are their initial concentrations; k is the selectivity coefficient which is roughly the ratio of the hydrogenation rates of oleic and linoleic radicals.

The data of Table 2 are presented graphically in Fig. 6. The initial slope of the curve (at the point O) is i.e. $\frac{d[Ol]}{d[L]} = 1.025$.

Hence the selectivity coefficient is 0.04.

Therefore we are dealing with a fairly selective process. It is possible that the value is even lower, as determination of the selectivity coefficient from the initial slope cannot be very accurate.

Thus, examination of the data for Sample No. 6 (Table 2) leads to the conclusion that at first only linoleic acid is hydrogenated. The form of the curves indicates that in other instances of foam hydrogenation we have a similar process. From this we may conclude that in our experiments two periods may be distinguished in the course of the reaction. In the initial period, for 5-10 minutes, virtually the linoleic radicals alone are hydrogenated; during the second and final period only the oleic radicals are saturated.

Fig. 5 (Curve 1) indicates that the reaction order in the first period is close to unity. The final period also conforms to the first order. This follows from Fig. 4,c, as the slope of the end of the logarithmic plot remains almost unchanged.

Therefore the rate constants for the hydrogenation of cottonseed oil components can be calculated from the initial and final regions of all the kinetic curves shown in the diagrams (Table 3).

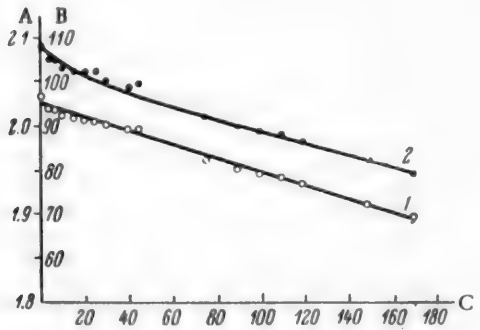

Fig. 5. Kinetic curve for hydrogenation of cottonseed oil with 0.035% catalyst; amount of oil 50 g, hydrogen rate 1.15 liters/minute (Experiment X):
A) log iodine number (1), B) iodine number (2), C) time (minutes).

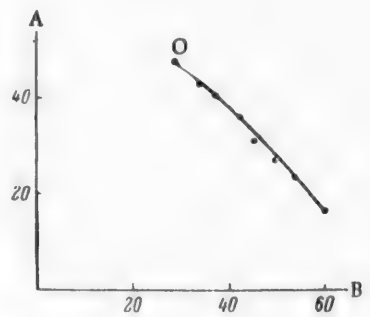

Fig. 6. Selectivity curve for hydrogenation of cottonseed oil (Experiment X); Point O represents the original oil composition:
A) linoleic acid content (%), B) oleic acid content (%).

The data in Table 3 show that the selectivity is high in foam hydrogenation. The selectivity differences between individual experiments are not large. In any event, our calculation method cannot be very accurate. Evidently we are concerned here with the maximum possible selectivity. In experiments in which the nickel content was 0.175% the absolute hydrogenation rates of linoleic and oleic radicals differ somewhat.

TABLE 3

Rate Constants for Hydrogenation of Oleic and Linoleic Radicals in Cottonseed Oil

Expt. No.	Hydrogen supply conditions	Amount of		kL	kOl	$\frac{kOl}{kL}$
		oil (g)	catalyst (%)			
III	Narrow orifice	50	0.175	0.0535	0.0038	0.071
IV	Schott No. 2	50	0.175	0.113	0.0062	0.0548
VI	Schott No. 3	100	0.175	0.27	0.0085	0.035
VIII	Schott No. 3	50	0.175	0.113	0.0062	0.055
X	Schott No. 3	50	0.035	0.045	0.0018	0.04

The constants are lower for Experiment III than for the other experiments. In this experiment hydrogen was bubbled through a single orifice (d ~ 1 mm). Evidently the mixing of the different phases of the system was least effective in this case. Comparison of Experiments IV and VIII, in which Schott filters of different porosities were used but all the other conditions were the same, shows that doubling of the porosity has no effect. The explanation is that because of the very efficient agitation in the foam the reaction took place in the kinetic region for all the components.

As there were some variations of the experimental temperatures, there should be some variability in the results. However, since the experimental temperatures lie in the region where the rate of the hydrogenation reaction depends little on the temperature, our conclusions are justified. It is known that the temperature coefficient undergoes inversion [8] in the hydrogenation of organic compounds. In the case of fats this occurs at 200-220°.

For comparison, we may consider data on the hydrogenation of sunflower oil with the aid of a wide tube (d ~ 6 mm) for the hydrogen supply. The hydrogenation curve is given in the monograph by Elovich and Zhabrova [1].

In this case the selectivity coefficient is unity according to our calculations, i.e., the reaction proceeds nonselectively.

Thus, by means of the foam regime it is easily possible to conduct hydrogenation very selectively; the reaction evidently takes place in the kinetic region. It is very important to establish the relationship between the hydrodynamics of the foam regime and the selectivity of the hydrogenation process. This problem is not considered in the present investigation.

SUMMARY

1. If cottonseed oil is hydrogenated in the foam formed by the passage of hydrogen through a Schott filter, the reaction proceeds very selectively. The ratio of the hydrogenation rates of oleic and linoleic radicals is 0.01 – 0.04.

2. Analysis of the experimental data indicates that the process, carried out under foam conditions, took place in the kinetic region with respect to all the components of the heterogeneous reaction of catalytic hydrogenation.

3. Examination of the nickel catalyst, made from nickel formate, under the electron microscope indicates that the predominant particle size is 0.1 – 0.2 μ.

LITERATURE CITED

[1] S. Yu. Elovich and G. M. Zhabrova, Theoretical Principles of Fat Hydrogenation [in Russian] (Izd. AN SSSR, 1948) pp. 135-185; S. Yu. Elovich and G. M. Zhabrova, Oil and Fat Ind. 5-6, 24 (1940).

[2] S. Yu. Elovich and I. I. Tret'yakov, Proc. Conference on Catalytic Hydrogenation and Oxidation [in Russian] (Acad. Sci. Kazakh SSR Press, 1955) pp. 218-232.

[3] V. G. Levich, Chemical Hydrodynamics [In Russian] (Moscow, 1952).

[4] S. Yu. Elovich and G. M. Zhabrova, Authors' Certif. No. 80342 (1949).

[5] M. E. Pozin, I. P. Mukhlenov, E. S. Tumarkina and É. Ya. Tarat, The Foam Method for Treatment of Gases and Liquids [in Russian] (Leningrad, Goskhimizdat, 1955).

[6] A. V. Dumanskii, Colloid Science [in Russian] (Goskhimizdat, 1948) p. 316.

[7] S. Yu. Elovich and G. M. Zhabrova, J. Phys. Chem. 19, 239 (1945).

[8] A. A. Balandin, Bull. Acad. Sci. USSR, Div. Chem. Sci. 339 (1945).

Received April 3, 1957

CHEMICAL CONVERSIONS OF MERCURY SALTS AND THEIR ROLE IN THE HYDROFLUORINATION OF VINYLACETYLENE*

I. M. Dolgopol'skii, I. M. Dobromil'skaya, and B. A. Byzov

As the result of researches carried out in our laboratory in recent years [1], a method has been developed for synthesis of fluoroprene, based on the reaction of vinylacetylene with hydrogen fluoride, with a catalyst consisting of a suspension of mercuric oxide in vaseline oil. The influence of various factors on the hydrofluorination of vinylacetylene was studied, and a technological scheme for continuous synthesis of fluoroprene was worked out.

The reaction proceeds as follows:

$$CH_2=CH-C\equiv CH+HF\rightarrow CH_2=CH-CF=CH_2.$$

The hydrofluorination process was shown to be completely reproducible, and it was found that the fluoroprene yield, calculated on the converted vinylacetylene, is 85-86% at an average output rate of 65-70 g of fluoroprene per 1 kg of catalyst mixture (10% mercuric oxide) per hour. The main reaction of fluoroprene formation is accompanied by side reactions, which give rise to difluoro-3, 3-butene-1 ($CH_2=CH-CF=CH_2+HF\rightarrow CH_2=CH-CF_2-CH_3$), methyl vinyl ketone ($CH_2=CH-C\equiv CH+H_2O\rightarrow CH_2=CH-CO-CH_3$), and resins which contain, together with fluorinated polymers (up to 40% of presumed fluoroprene polymer), polymers of copolymers of unsaturated compounds (such as vinylacetylene, methyl vinyl ketone, etc.). The principal cause of the fall in catalyst activity during the process is apparently reduction of mercury salts to metallic mercury, which is always present to some extent in the catalyst mixtures.

EXPERIMENTAL

Investigation of the Composition of Catalyst Mixture and its Changes During Hydrofluorination of Vinylacetylene

The catalyst mixture is a suspension of resinlike polymers in vaseline oil, with mercury and its salts (HgF_2 and Hg_2F_2) distributed in them.

The method used for separate determinations of mercury and its salts was based on precipitation of mercurous ions from the catalyst mixture (after separation of vaseline oil) by hydrochloric acid. The mercuric salt is converted into water-soluble $HgCl_2$, while the mercurous salt remains in the precipitate as Hg_2Cl_2. The total mercury content of the catalyst mixture is determined in a separate sample by oxidation of a weighed sample of the dry residue with nitric acid on heating, with subsequent determination of the mercuric nitrate formed. The metallic mercury content was found by difference.

Samples of the catalyst mixture were taken at definite intervals during continuous operation, in order to study the variations in the composition.

Experimental conditions. Initial mercuric oxide content of vaseline oil 10%, reaction temperature 60°, stirring rate 900 revolutions/minute, molar ratio of hydrogen fluoride to vinylacetylene, 1:1.

* Communication III in the series on the synthesis of fluoroprene.

TABLE 1

Variation of the Catalyst Mixture Composition with Time

Time of catalyst operation (hours)	2	4	6	12	24	43	55	67	79	91	103	115	127
Total mercury content of catalyst mixture (%)	7.23	7.22	6.24	5.43	4.83	4.48	4.27	4.08	4.18	4.1	3.86	3.58	2.91
Resin content of catalyst mixture (%)	20.0	23.0	25.5	27.4	33.4	34.6	34.7	36.9	37.9	38.6	38.3	38.2	37.1
Mercury contents of catalyst mixture (%) mercuric	0.13	0.12	0.16	0.15	0.26	0.21	0.21	0.15	0.16	0.19	0.15	0.18	0.17
mercurous	2.75	2.37	1.91	1.38	1.02	0.83	0.66	0.65	0.53	0.47	0.37	0.36	0.33
metallic	4.35	4.73	4.17	3.90	3.55	3.44	3.40	3.28	3.49	3.44	3.34	3.04	2.41
Average conversion of vinylacetylene into fluoroprene (%)	60	52	50.0	45.0	38.0	37.0	34.0	34.0	30.0	26.0	25.0	20.0	17.0
Vinylacetylene consumed in formation of difluorobutene (%)	0.6	0.4	0.6	0.4	0.4	0.4	1.1	1.3	1.1	1.4	1.4	1.5	1.3

TABLE 2

Effect of Catalyst Mixture Composition on the Conversion of Vinylacetylene
Initial HgO Concentration 10%

Time of catalyst operation (hours)	18	48	72	96	120	144	168	192	216	240	256
Total mercury content of catalyst mixture (%)	4.08	4.15	4.35	4.54	4.25	4.42	4.30	4.52	4.30	4.66	5.05
Resin content of catalyst mixture (%)	22.0	27.0	30.0	32.0	33.0	37.0	37.0	32.0	33.0	31.0	31.0
Mercury contents of catalyst mixture (%) mercuric	0.18	0.15	0.20	0.22	0.15	0.17	0.20	0.22	0.24	0.22	0.23
mercurous	0.99	1.30	0.80	1.02	1.10	1.20	0.96	1.10	1.06	0.95	0.98
metallic	2.91	2.70	3.35	3.30	3.00	3.05	3.14	3.20	3.00	3.49	3.94
Conversion of vinylacetylene into fluoroprene (%)	40.68	39.0	41.2	39.7	36.5	47.0	47.0	47.7	45.5	42.2	46.6
Vinylacetylene consumed in formation of difluorobutene (%)	0.7	1.5	1.86	1.76	1.9	1.0	1.4	1.5	1.4	1.8	2.0

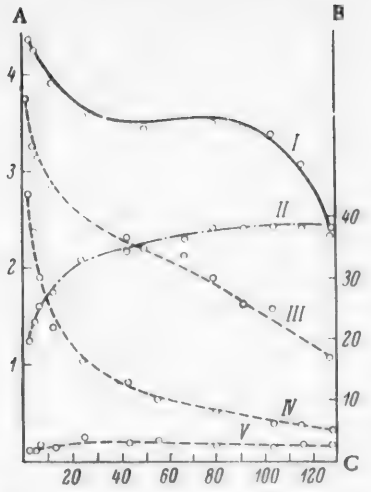

Fig. 1. Conversion of vinylacetylene and composition of catalyst mixture during the process:
A) contents of Hg (I), $Hg^{\cdot}$ (IV), and $Hg^{\cdot\cdot}$ (V) in the catalyst (%);
B) conversion of C_4H_4 (III) and resin content of suspension (%) (II).
C) duration of catalyst operation (hours).

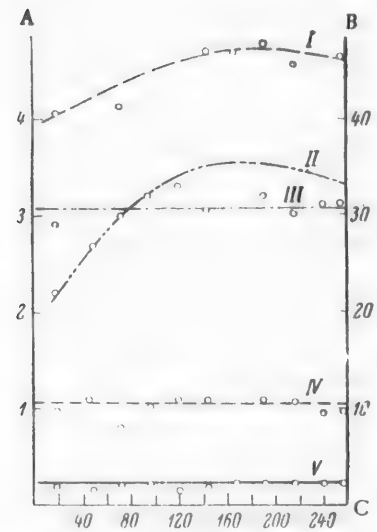

Fig. 2. Conversion of vinylacetylene and composition of catalyst mixture during the process (Table 2):
A) contents of Hg (III), $Hg^{\cdot}$ (IV), and $Hg^{\cdot\cdot}$ (V) in the catalyst (%);
B) conversion of C_4H_4 (I) and resin content of suspension (%) (II).
C) duration of catalyst operation (hours).

It follows from the results (Table 1 and Fig. 1) that after 2 hours of operation the catalytic mixture already contains mainly metallic mercury and mercurous salts. The content of the latter is 2.75%, and drops gradually in continuous operation (100 hours) to 0.4%.

The content of mercuric salts is within the range of 0.1 – 0.2%.

The total content of mercury salts gradually diminishes owing to reduction to metallic mercury. The catalyst activity gradually falls at the same time. The conversion of vinylacetylene falls from 60 to 17%.

Since the catalyst mixture contains mainly mercurous salts during operation, the possibility of using mercurous fluoride (Hg_2F_2) in hydrofluorination of vinylacetylene was investigated. The comparative results are presented in Table 3.

It follows from the results (Table 3) that hydrofluorination of vinylacetylene proceeds with mercurous salts in the same was as with mercuric salts. In either case the mercury salts evidently undergo disproportionation with formation of an active catalyst mixture containing mercurous and mercuric salts and metallic mercury.

Therefore the activity of the catalyst mixture and its service life are evidently determined by constancy of the mercuric or mercurous fluoride content in the suspension. On this assumption, the service life of the catalyst mixture in continuous operation was increased, with its activity remaining roughly constant, by periodic additions, during the process, of a freshly-prepared suspension of mercuric oxide in vaseline oil to the catalyst mixture, with simultaneous removal of an equal amount of spent mixture. The initial content of mercuric oxide in the vaseline oil was 10%, and 2% of mercuric oxide was added every 24 hours into the reactor, in the form of 10% suspension in vaseline oil.

The average conversion of vinylacetylene then remained in the 45-50% range during prolonged operation (250-400 hours). The variations of the catalyst composition under these conditions are given in Table 2 and Fig. 2.

It follows from these results (Table 2) that the contents of mercurous and mercuric salts remain almost constant, and are about 1% of mercurous and 0.2% of mercuric salts. The catalyst mixture retains constant activity with these salt contents.

Mechanism of the Reaction of Vinylacetylene Hydrofluorination

In view of the fact that a complex mixture of mercury salts is involved in the hydrofluorination of vinylacetylene, in addition to hydrogen fluoride, it was desired to investigate the influence of each reaction component individually.

a) Reaction of hydrogen fluoride with vinylacetylene in absence of mercury salts. It was found that in these conditions HF does not add on to vinylacetylene, and resin formation occurs, probably as the result of vinylacetylene polymerization under the influence of hydrogen fluoride. At the same time, fluoroprene reacts smoothly with HF in an addition reaction which yields 3,3-difluorobutene-1.

b) Reaction of mercuric fluoride with vinylacetylene in absence of HF. It was found that much heat is evolved in this reaction, with liberation of hydrogen fluoride and metallic mercury, and formation of considerable amounts of resins.

TABLE 3

Comparative Data on Hydrofluorination of Vinylacetylene with Mercurous and Mercuric Salts

Catalyst used	HgF_2	Hg_2F_2	HgF_2	Hg_2F_2	HgF_2	Hg_2F_2
Amount of catalyst (g) per 100 g of suspension	7.5	7.5	12.5	12.5	25.0	25.0
Duration of experiment (hours)	11.8	12.0	11.0	11.4	11.25	6.5
Fluoroprene yield (%) calculated on vinylacetylene passed	21.0	22.8	33.9	35.6	46.9	45.7
Fluoroprene yield (%) calculated on vinylacetylene converted	63.3	65.0	64.1	65.9	64.5	66.3

The formation of hydrogen fluoride in this case can only be due to removal of hydrogen from the vinylacetylene molecule with formation of divinyldiacetylene:

$$HgF_2+2CH{\equiv}C-CH{=}CH_2 \rightarrow CH_2{=}CH-C{\equiv}C-C{\equiv}C-CH{=}CH_2+Hg+2HF.$$

The divinyldiacetylene is readily polymerized under the influence of the liberated hydrogen fluoride, forming resinous products.

The possibility of such reactions is confirmed by the work of Zal'kind et al. [2] and of Klebanskii and Kuznetsova [3].

These authors showed that when a mixture of cupric and cuprous chlorides reacts with acetylenic hydrocarbons, diacetylene compounds are formed with reduction of cupric chloride to cuprous.

Klebanskii and Kuznetsova showed that the reaction proceeds by the following mechanism:

$$RC{\equiv}CH + CuCl_2 \rightarrow R\overset{+}{C}{=}\overset{-}{C}H\ldots\ldots\overset{++\ -}{Cu}Cl \quad (1)$$
$$\qquad\qquad\qquad\qquad\qquad\qquad\qquad\qquad\qquad\quad |$$
$$\qquad\qquad\qquad\qquad\qquad\qquad\qquad\qquad\qquad\quad \overline{Cl}$$

Coordination bonds are formed between the negatively polarized carbon atom of the acetylenic compound and the positively charged copper cation. This coordination of the acetylene molecule is due to the presence of four mobile π-electrons in the acetylenic compound.

$$R\overset{+}{C}{=}\overset{-}{C}H\text{----}\overset{++\ -}{Cu}Cl \rightarrow HCl + \overset{+}{C}uCl + RC{\equiv}C^{\cdot} \quad (2)$$
$$\qquad\qquad\qquad\qquad\quad |$$
$$\qquad\qquad\qquad\qquad\quad \overline{Cl}$$

$$RC{\equiv}C^{\cdot} + C^{\cdot}{\equiv}CR \rightarrow RC{\equiv}C-C{\equiv}CR. \quad (3)$$

By analogy, the reaction of HgF_2 with vinylacetylene may be represented as follows:

$$CH_2{=}CH-\overset{+}{C}{\equiv}\overset{-}{C}H + \overset{++\ -}{Hg}F \rightarrow CH_2{=}CH-C{\equiv}\overset{-}{C}H^{\cdot} \quad (4)$$
$$\qquad\qquad\qquad\qquad\qquad\quad |$$
$$\qquad\qquad\qquad\qquad\qquad\quad \overline{F}$$

$$CH_2{=}CH-C{\equiv}\overset{-}{C}H \quad HgF \rightarrow HF + \overset{+}{Hg}F + CH_2{=}CH-C{\equiv}C^{\cdot} \quad (5)$$
$$\qquad\qquad\qquad\quad |$$
$$\qquad\qquad\qquad\quad \overline{F}$$

$$2CH_2{=}CH-C{\equiv}C^{\cdot} \rightarrow CH_2{=}CH-C{\equiv}C-C{\equiv}C-CH{=}CH_2. \quad (6)$$

TABLE 4

Effect of Moisture on the Hydrofluorination of Vinylacetylene

Amount of water added (% of catalyst mixture)	—	1.0	5.0	10.0
Conversion of vinylacetylene into fluoroprene (%)	34.6	17.7	9.9	3.9
Amount of resins formed, calculated on fluoroprene (%)	28.8	55.4	70.5	85.8

Thus, in the first stage a complex of vinylacetylene with HgF_2 is formed. A coordination bond is formed between the electronegatively polarized carbon atom in vinylacetylene and the positively charged Hg atom.

In this complex the bond between carbon and hydrogen is weakened, and the latter interacts with a fluorine atom with liberation of HF. Hg^{++} gives up an electron to pass into Hg_2^{++}, and the free radical $CH_2=CH-C\equiv C\cdot$ is formed. The free radicals recombine to form divinylacetylene which, like most unsaturated compounds, readily polymerized under the influence of HF to form resins.

c) Reaction between vinylacetylene and mercury salts in presence of HF. As has been shown, fluoroprene is formed predominantly under these conditions.

It may be assumed that, by analogy with other mercury and also copper halides, mercuric or mercurous fluoride forms with HF complexes of the type

$$\overset{+}{H}(HgF_3^-),\quad \overset{++}{H_2}(HgF_4^{--})\quad \text{or}\quad \overset{+}{H}(HgF_2^-),\quad \overset{++}{H_2}(HgF_3^{--})\quad \text{etc.}$$

These complex compounds form coordination bonds with polar vinylacetylene molecules according to the scheme:

$$(CH_2=\overset{\curvearrowright}{CH}-\overset{\curvearrowright}{C}\equiv\bar{C}H)\cdot H(HgF_2)\quad .$$

The complex so formed decomposes under the influence of HF, with formation of fluoroprene and regeneration of the original complex

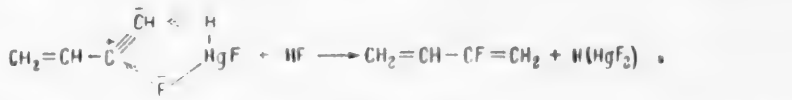

We postulated a similar mechanism for the addition of HCl to vinylacetylene in presence of CuCl, with formation of chloroprene.

The subsequent addition of hydrogen fluoride to fluoroprene takes place even in absence of mercury salts, in the 1 — 2 position with formation of 3,3-difluorobutene-1.

$$CH_2=CH-CF=CH_2 + HF \rightarrow CH_2=CH-CF_2-CH_3$$

The direction of HF addition to fluoroprene in the 1 — 2 position differs in principle from the direction of HCl addition to chloroprene, which always takes place in the 1 — 4 position. This type of HCl addition is determined by the polarity distribution in the chloroprene molecule, in which

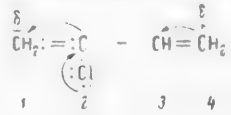

TABLE 5

Composition of Resins Formed in the Catalyst Mixture

Amount of resin, calculated on converted vinylacetylene (%)	Contents of		
	organically bound fluorine in resin (%)	"polyfluoroprene" (%)	vinylacetylene polymers (%)
11.7	11.8	45.2	54.8
7.5	9.8	39.3	60.7
14.0	11.0	41.8	58.2
16.3	12.1	46.0	54.0
8.3	9.5	39.1	60.9
8.2	9.6	40.2	59.8

TABLE 6

Composition of Resins Formed in Gas Outlet Tubes

Amount of resin (%) calculated on substance converted	Contents of			
	HF (%)	organically bound fluorine in resin (%)	"polyfluoroprene" (%)	vinylacetylene polymers (%)
4.8	3.6	21.3	78.2	18.2
2.7	7.2	18.4	62.1	30.7
2.4	3.0	17.0	62.7	34.3
3.2	3.0	16.6	61.2	35.8
2.1	4.5	16.0	59.8	36.8
2.1	8.0	15.9	57.2	34.8

The electron density is shifted toward the 1st carbon atom owing to conjugation of unpaired electrons of the chlorine atom with π-electrons of the double bond, with formation of a negative charge at the 1st carbon atom. Because of the smaller radius of the F atom and its higher electronegativity as compared with chlorine, the positive charge in fluoroprene is at the carbon atom directly linked to the fluorine atom.

$$\overset{-}{\overset{\frown}{CH_2}}=\overset{+}{\underset{\underset{F}{|}}{C}}-CH=CH_2$$

The fact that conversion of monofluoride to difluoride is more favorable thermodynamically may also favor this course of addition.

If the hydrofluorination of vinylacetylene with a mercury catalyst is performed in presence of water, the reaction of hydrogen fluoride addition to vinylacetylene is accompanied by hydration of vinylacetylene with formation of methyl vinyl ketone.

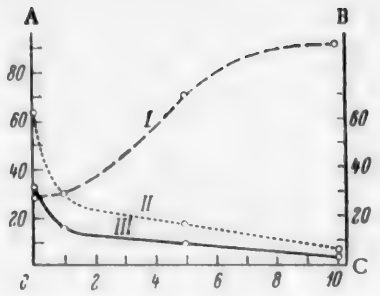

Fig. 3. Effect of moisture on hydrofluorination of C_4H_4:
A) conversion of C_4H_4 (III) and amount of resins (I) (%); B) output per 1 kg of catalyst (II) (in g/hour); C) moisture content (%).

Methyl vinyl ketone was isolated from the reaction products, and found to have the following characteristics: b.p. 80 – 82°, d^{20}_4 0.8504, $n^{20}D$ 1.4110. The condensation product with phenylhydrazine was prepared. Recrystallization from alcohol yielded crystals with m.p. 76°, which coincides with the melting point of methylphenylpyrazoline [4].

Under hydrofluorination conditions most of the methyl vinyl ketone formed polymerized under the influence of HF with formation of resinous products. This is consistant with our data on variations of the resin content on introduction of different amounts of water into the catalyst mixture (Table 4 and Fig. 3).

Resin Formation During Hydrofluorination of Vinylacetylene

One important problem in studies of the hydrofluorination of vinylacetylene is the nature and formation conditions of the resins which accumulate in the catalyst mixture.

Investigations of possible resin formation under reaction conditions in which vinylacetylene and fluoroprene were passed with hydrogen fluoride through vaseline oil without catalyst showed that resins are not formed in the oil, but gradually accumulate on the walls of the apparatus and in the gas outlet tubes.

Investigation of the composition of the resins formed in the catalyst mixture during the reaction showed that the content of polymerized compounds containing fluorine is about 40% (calculated as polyfluoroprene), regardless of the reaction conditions.

The resins accumulating in the outlet tubes have a considerably higher content, around 60%, of fluorine compounds (Tables 5 and 6).

The amount of resins formed in the catalyst mixture is roughly 3-5 times the amount formed in the outlet tubes.

It follows from the data in Table 6 that resins are formed in the catalyst mixture only in presence of mercury salts and excess of HF, and are the products of polymerization of vinylacetylene, fluorine compounds, and by-products formed in the hydrofluorination of vinylacetylene.

As was noted earlier, when HgF_2 reacts with vinylacetylene in absence of hydrogen fluoride the principal reaction is reduction of mercury salts accompanied by considerable resin formation. Evidently this reaction may partially occur during the hydrofluorination of vinylacetylene.

Investigations of the effect of moisture showed that addition of water to the catalyst mixture decreases the conversion of vinylacetylene (the hydrofluorination of vinylacetylene is almost entirely suppressed), with a considerable increase of resin formation (Table 4, Fig. 3).

Hence the main causes of resin formation in hydrofluorination of vinylacetylene by means of mercuric oxide suspensions in vaseline oil are probably the following reactions:

a) hydration of vinylacetylene, with formation of methyl vinyl ketone, by the water formed in the reaction of mercuric oxide with hydrogen fluoride: $HgO + 2HF \rightarrow HgF_2 + H_2O$;

b) reduction of mercury salts with formation of readily-polymerized diacetylenic compounds;

c) polymerization of vinylacetylene and fluoroprene under the influence of excess hydrogen fluoride.

The first two reactions evidently occur at the very start of the process, as confirmed by the data in Table 1, from which it follows that after 2 hours of operation the resin content of the catalyst mixture reaches about 20%, and the total resin content after 127 hours of continuous operation is 35-37%.

SUMMARY

1. The composition of the catalyst mixture in hydrofluorination of vinylacetylene was studied, and variations in the contents of mercury and its salts during continuous operation of the catalyst were determined.

2. It is shown that the time of continuous operation can be increased considerably, with the catalyst activity remaining constant, by periodical renewal of the catalyst composition.

3. The possible mechanism of vinylacetylene hydrofluorination and of certain side reactions taking place in the synthesis of fluoroprene from vinylacetylene is discussed.

LITERATURE CITED

[1] I. M. Dolgopol'skii, I. M. Dobromil'skaya, and B. A. Byzov, J. Appl. Chem. 31, No. 10, 1534 (1958).*

[2] Yu. S. Zal'kind and B. Fundyler, J. Gen. Chem. 6, 530 (1936); Yu. S. Zal'kind and M. I. Aizikovich, J. Gen. Chem. 7, 227 (1957).*

[3] A. L. Klebanskii and O. M. Kuznetsova, J. Gen. Chem. 27, 2977 (1957).*

[4] Wernitz, J. Am. Chem. Soc. 57, 204-206 (1935).

Received October 4, 1957

* Original Russian pagination. See C. B. Translation.

DIRECT SYNTHESIS OF PHENYLTRICHLOROSILANE IN A FLUIDIZED BED

K. A. Andrianov, S. A. Golubtsov, N. N. Tishina,

and I. V. Trofimova

Literature data on the preparation of phenylchlorosilanes by direct synthesis (from chlorobenzene and silicon in presence of catalysts) are very scanty, and the published information is generally not sufficient for estimation of two important characteristics of the process – the utilization of silicon and the yield of product per unit time (productivity). Only one patent [1] contains fairly complete data, according to which the yield of phenyltrichlorosilane (by Equation (1), given below) does not exceed 1.6% on the silicon and 40% on the chlorobenzene; the yield of phenyltrichlorosilane per 100 g of catalyst per hour does not exceed 0.14 g, and the content of the product in the liquid mixture is 9%.

According to patent information [2], 50% silicon – copper alloy oxidized by air at an elevated temperature has high activity (the reaction product contains 20% of phenyltrichlorosilane). In Rochow's detailed investigation [3] of different catalysts for the reaction between chlorobenzene and silicon the best results were also obtained with the use of oxidized silicon – copper alloy (the reaction product contained 10% of phenyltrichlorosilane and 24% of diphenyldichlorosilane); good results were also obtained with silicon – silver alloy (yields of 4 and 10% respectively). It is not possible to calculate the yield on the silicon and the productivity from the data given.

In one paper it is stated [4] that it is possible to carry out the reaction between chlorobenzene and silicon – iron alloy (ferrosilicon), and tentative schemes for the chemical reactions are presented. However, these schemes are not substantiated by any experimental data, and can hardly be accepted as representing the complex interaction of chlorobenzene with silicon.

In the present investigation we attempted to bring about the direct synthesis of phenylchlorosilanes in a fluidized bed, the solid particles of the catalyst mass being agitated by a stream of chlorobenzene vapor. We showed in the case of the preparation of ethylchlorosilanes [5] that when the reaction is effected by this method the process characteristics are much better than in, say, direct synthesis in a stirred reactor or without stirring.

Our experiments showed that the reaction of chlorobenzene with silicon in a fluidized bed proceeds with satisfactory activity at elevated temperatures (at about 600°) only in presence of appreciable amounts of hydrogen chloride, which also interacts with silicon. The catalysts used were copper or iron in the form of alloys with silicon. The main reaction product is phenyltrichlorosilane; very little diphenyldichlorosilane is formed. In addition, the reaction products contain considerable amounts of benzene and silicon tetrachloride; somewhat smaller amounts of trichlorosilane and even smaller amounts of diphenyl were found. Considerable amounts of carbon, partly as the element and partly combined with silicon as the carbide, accumulate in the spent alloy during synthesis. The gaseous reaction products consist mainly of hydrogen.

Table 1 contains the principal over-all results obtained when the reaction between chlorobenzene, hydrogen chloride, and silicon was conducted in presence of copper (Experiment No. 1) or iron (Experiment No. 2) as catalyst. If follows from these results that when the process is effected in a fluidized bed quite satisfactory productivity can be attained, with satisfactory yields of phenyltrichlorosilane.

For detailed investigation of the processes taking place in the interaction of silicon with chlorobenzene and hydrogen chloride, complete analyses of the products formed in the experiments detailed in Table 1 were

TABLE 1

Principal Process Characteristics in the Preparation of Phenyltrichlorosilane in a Fluidized Bed

Characteristics	Expt. No. 1	Expt. No. 2
Yield (in g) of phenyltrichlorosilane per 100 g of contact mass per hour (productivity)	11.1	11.2
Yield of phenyltrichlorosilane (%) by Equation (1):		
a) on the converted chlorobenzene	95	82
b) on the silicon taken	21	32
Total percentage conversion of silicon	54	66
Average contents of phenyltrichlorosilane in reaction products (%)	15.8	18.3

TABLE 2

Molar Amounts of Substances Consumed or Formed in the Direct Synthesis of Phenyltrichlorosilane

Substance	Expt. No. 1		Expt. No. 2	
	reacted	formed	reacted	formed
Silicon	2.86	—	3.64	—
Chlorobenzene	3.46	—	6.43	—
Hydrogen chloride	6.70	—	6.25	—
Phenyltrichlorosilane	—	1.09	—	1.75
Silicon tetrachloride	—	0.91	—	1.17
Benzene	—	1.30	—	2.72
Trichlorosilane	—	0.66	—	0.45
Carbon	—	5.10	—	8.00
Hydrogen	—	3.19	—	5.00
Diphenyldichlorosilane	—	0.05	—	0.05
Diphenyl	—	0.10	—	0.16
Chlorine in the form of nonvolatile compounds in the spent mass	—	0.45	—	0.72

performed, and the material balance was calculated. The results were used for calculation of the molar proportions of the reacted and formed substances (Table 2), and an attempt was made to represent the process (in the first approximation) by a series of chemical equations.

Analysis of the data in Table 2 suggests that the principal reaction in the process is interaction of chlorobenzene with silicon:

$$3C_6H_5Cl + Si \rightarrow C_6H_5SiCl_3 + 2C_6H_5. \quad (1)$$

For example, in Experiment No. 1, according to Equation (1) the formation of 1.09 mole of phenyltrichlorosilane requires the consumption of $3 \times 1.09 = 3.27$ moles of chlorobenzene and $1 \times 1.09 = 1.09$ mole of silicon. This corresponds to the interaction, in accordance with Equation (1), of $\frac{3.27}{3.46} \cdot 100 = 95$ molar % of the expended chlorobenzene and $\frac{1.09}{2.86} \cdot 100 = 30.2$ molar % of the expended silicon.

An analogous calculation for Experiment No. 2 gives 82 molar % of chlorobenzene and 48 molar % of silicon respectively. Similar calculations for the formation of the other main reaction products show that about 35% of the expended silicon reacts with hydrogen chloride according to the scheme

$$Si + 4HCl \rightarrow SiCl_4 + 4H \quad (2)$$

and about 23%, according to the scheme

$$Si + 3HCl \rightarrow HSiCl_3 + 2H. \quad (3)$$

55 – 75% of the hydrogen chloride reacts according to Equation (2), and 22 – 30% according to Equation (3).

The formation of diphenyldichlorosilane

$$2C_6H_5Cl + Si \rightarrow (C_6H_5)_2SiCl_2 \quad (4)$$

is of secondary importance in the experimental conditions studied. Less than 2% of the expended silicon and about 2% of the expended chlorobenzene take part in Reaction (4).

Of the total quantity of phenyl radicals formed in Reaction (1), the main part (60 – 75%) reacts with hydrogen formed by Reactions (2), (3), and (7)

$$C_6H_5^{\cdot} + H \rightarrow C_6H_6. \quad (5)$$

A small proportion (4 – 6%) of the phenyl radicals forms diphenyl

$$2C_6H_5^{\cdot} \rightarrow C_6H_5C_6H_5, \quad (6)$$

and the rest undergoes pyrolysis with formation of carbon:

$$C_6H_5^{\cdot} \rightarrow 6C + 5H. \quad (7)$$

(According to the balance for Experiment No. 2, rather more carbon is formed than would correspond to the remaining phenyl radicals, probably by pyrolysis of chlorobenzene). Of the hydrogen formed in Reactions (2), (3), and (7), 16 – 20% enters Reaction (5) and the rest forms elemental hydrogen

$$2H \rightarrow H_2. \quad (8)$$

It is not claimed that the suggested scheme is an accurate description of the highly complex processes taking place in the reaction between chlorobenzene, hydrogen chloride, and silicon under the conditions described below. The scheme is tentative in a number of respects; for example, it is not known whether the chlorine atoms from the hydrogen chloride molecules form silicon tetrachloride and trichlorosilane only, or whether they are also partially involved in the formation of phenyltrichlorosilane molecules, etc. However, in our opinion this scheme may be accepted in the first approximation as representing the material changes taking place in the synthesis of phenyltrichlorosilane in a fluidized bed.

TABLE 3

Composition of Original and Spent Alloy (%)

Composition of Alloy	Expt. No. 1		Expt. No. 2	
	fresh	spent	fresh	spent
Silicon	73.6	34.0	79.0	28.0
Copper	26.0	25.9	0.3	—
Iron	—	—	13.0	11.0
Aluminum	0.2	—	1.2	—
Carbon	—	31.0	—	48.4
Chlorine	—	5.1	—	12.2

TABLE 4

Material Balance (in g)

Products	Expt. No. 1		Expt. No. 2	
	taken	found	taken	found
Alloy	200	196	200	199
Hydrogen chloride	344	62	425	112
Chlorobenzene	1210	—	1783	—
Condensate	—	1452	—	2015
Gases (calculated as hydrogen)	—	8	—	10
Losses	—	36	—	72
Total	1754	1754	2408	2408

TABLE 5

Amounts and Composition of Gaseous Reaction Products

Expt. No.	Amount of gas (liters)	Composition (%)		
		hydrogen	hydrogen chloride	hydrocarbons
1	120	87.2	6.0	6.8
2	166	76.0	1.6	—

EXPERIMENTAL

Apparatus used for direct synthesis. Hydrogen chloride was prepared by the action of sulfuric acid on dry sodium chloride. The salt was put in a 3-liter round flask, and 96% sulfuric acid was gradually added from a dropping funnel. Hydrogen chloride passed through a drying column containing calcium chloride into a preheater, where it was mixed with chlorobenzene vapor; the feed rate was regulated by means of a flow meter. Chlorobenzene was supplied into the preheater from a dropping funnel. The mixture of chlorobenzene vapor and hydro-

TABLE 6

Composition of Liquid Reaction Products

Fraction No.	Boiling range of fraction (°C)	Expt. No. 1		Expt. No. 2	
		yield (wt %)	chlorine content (%)	yield (wt %)	chlorine content (%)
1	32—57	6.4	80.0	3.1	80.3
2	57—58	6.0	84.0	9.1	84.0
3	58—80	4.7	81.5	1.1	62.6
4	80—81	5.9	0.9	9.3	—
5	81—130	1.8	—	3.3	—
6	130—132	55.0	—	50.0	—
7	132—193	3.8	42.6	5.7	43.9
8	193—197	12.5	50.4	13.2	50.3
9	200—210	1.0	44.0	1.1	43.0
10	210—254	0.1	28.0	0.7	34.7
11	254—290	1.0	10.5	1.0	11.6
12	290—310	0.9	16.7	0.6	12.0
13	Residue in still	0.3	—	0.4	—
	Losses	0.6	—	1.4	—

TABLE 7

Proportions of Silicon, Chlorine, Carbon, and Hydrogen Involved in Formation of the Individual Reaction Products (molar %)

Substances formed	Elements from the original compounds, entering the reaction							
	Expt. No. 1				Expt. No. 2			
	Si	Cl	C	H	Si	Cl	C	H
Phenyltrichlorosilane	38.2	32.2	31.5	22.7	48.3	40.8	27.3	22.8
Silicon tetrachloride	31.9	35.8	—	—	32.2	36.3	—	—
Trichlorosilane	23.1	19.6	—	2.8	12.4	10.4	—	1.2
Diphenyldichlorosilane	1.8	1.0	2.9	2.1	1.4	0.8	1.6	1.3
Benzene	—	—	37.7	32.6	—	—	42.3	42.3
Diphenyl	—	—	5.8	4.2	—	—	5.0	4.2
Hydrogen	—	—	—	26.7	—	—	—	26.0
Carbon (free and as carbide)	—	—	24.5	—	—	—	20.8	—
Chlorine in nonvolatile compounds in alloy	—	4.5	—	—	—	5.6	—	—
Other compounds and losses	5.0	6.9	2.4	8.9	5.7	6.1	3.0	2.2
Total	100	100.0	100.0	100.0	100.0	100.0	100.0	100.0

gen chloride then entered the reactor. The reaction products were condensed in a condenser and collected in receivers; the uncondensed products passed to a trap cooled in a mixture of solid carbon dioxide and acetone, and the gas then passed through a wash bottle with alkali and collected in a gas holder.

Experimental procedure. 100 g of powdered silicon – copper (Experiment No. 1) or silicon – iron (Experiment No. 2) alloy was put in the reactor (the composition of the alloys is given in Table 3). The alloy was dried in a current of nitrogen, and hydrogen chloride at 20 – 25 liters/hour and chlorobenzene at 110 – 120 g/hour were then passed into the reactor at 600°. The course of the process was investigated at intervals by distillation of condensate samples from a flask with a fractionating column; when the phenyltrichlorosilane content of the condensate fell to 12%, the process was stopped (after 10 hours 30 minutes in Experiment No. 1, and after

16 hours 40 minutes in Experiment No. 2). The total amount of hydrogen chloride introduced into the reactor was found from the difference between the amounts of sulfuric acid and sodium chloride used, and the amount of acid sodium sulfate found at the end of the experiment. The spent alloy was removed from the reactor, weighed, and analyzed (the results are given in Table 3). The liquid reaction products collected in the receivers and trap were mixed and fractionated. The material balance for the experiments is given in Table 4, and analytical results for average samples of the gaseous reaction products are given in Table 5.

Separation of the liquid reaction products. The composition of the condensate was determined by rectification of a part of it (about one half of the total) through a column (20 mm in diameter and 800 mm high) packed with porcelain 3 × 1 × 1 mm rings, from a still 1 liter in capacity. Fractions boiling up to 200° were collected, after which the rectification was stopped and the residue was distilled from a column fitted with a dephlegmator, the fractions between 200 and 310° being collected. The composition of the fractions was calculated from data on their chlorine contents. The results of separation of the condensates obtained in Experiments Nos. 1 and 2 are given in Table 6.

To identify the reaction by-products – trichlorosilane and benzene – fractions 1 and 4 were rectified again and then analyzed.

Fraction 32 – 33°
Found %: Si 21.2; H 0.67; Cl 78.8
$HSiCl_3$. Calculated %: Si 20.7; H 0.74; Cl 78.9
Fraction 80 – 81°
Found %: C 92.0; H 7.7.
C_6H_6. Calculated %: C 92.2; H 7.8.

Calculations. The data in Tables 3 – 6 were used for calculation of the molar amounts of the reacting substances and products (Table 7). The losses (which did not exceed 3%) were nominally counted as hydrogen chloride in the calculations.

Table 7 shows the proportions of silicon, chlorine, carbon, and hydrogen in the reacting substances entering the various reaction products. The amounts unaccounted for (due to the formation of compounds not listed in Table 7, etc.) comprise about 5 – 6%. This degree of accuracy can be considered satisfactory in view of the complexity of the reactions, the high temperature of the synthesis, and the large number of compounds formed.

SUMMARY

The synthesis of phenyltrichlorosilane from chlorobenzene, hydrogen chloride, and silicon in a fluidized bed, in presence of copper or iron catalyst, was studied; it is shown that high yields of the product per unit time (productivity) can be obtained, with a satisfactory yield of phenyltrichlorosilane and fairly complete utilization of silicon.

LITERATURE CITED

[1] U. S. Patent No. 2,483,373; Chem. Abs. 44, 374 (1950).

[2] U. S. Patent No. 2,383,818, Chem. Abs. 40, 348 (1946).

[3] E. G. Rochow and W. F. Gilliam, J. Am. Chem. Soc. 67, 1772 (1945).

[4] L. Riccoboni and Zotta, J. Soc. Chem. Ind. 67, 235 (1948).

[5] K. A. Andrianov, S. A. Golubtsov, I. V. Trofimova and A. S. Denisova, J. Appl. Chem. 30, No. 8, 1277 (1957).*

Received May 29, 1957

* Original Russian pagination. See C. B. Translation.

SYNTHESIS OF β-METHYLNAPHTHALENE*

I. L. Kotlyarevskii and A. S. Zanina

It was shown in previous papers of this series [1 – 3] that divinylacetylene and its alkyl derivatives can undergo ring closure to form aromatic hydrocarbons under the influence of such catalysts as aluminum oxide, chromium oxide on aluminum oxide with or without an admixture of magnesium oxide, molybdenum oxide on aluminum oxide, aluminum carbide, etc. It was found that this reaction can be used for synthesis of aromatic hydrocarbons of predetermined structure; it was possible to synthesize compounds of the general formula

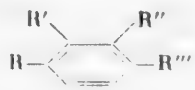

where R" is hydrogen or an alkyl group.

This method was used for synthesis of monocyclic aromatic hydrocarbons: benzene, toluene, and p-xylene; and a tricyclic hydrocarbon, phenanthrene.

It was of undoubted interest to attempt to use aromatization of divinylacetylene hydrocarbons for the synthesis of bicyclic aromatic hydrocarbons. We therefore performed the aromatization of isopropenylcyclohexenylacetylene, with the formation of β-methylnaphthalene.

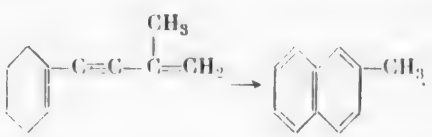

Isopropenylcyclohexenylacetylene was prepared by dehydration of cyclohexylolisopropylolacetylene, synthesized by the Favorskii method by condensation of dimethylethynylcarbinol with cyclohexanone.

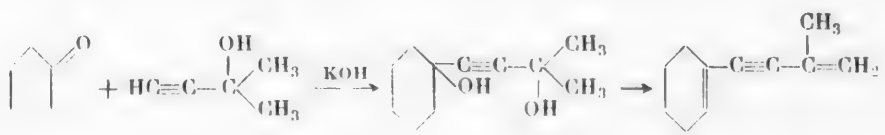

The aromatization catalysts tried were $MgO|Cr_2O_3|Al_2O_3$ (2:18:80), $Cr_2O_3|Al_2O_3$ (20:80) and an industrial molybdenum catalyst. The best results were obtained with $MgO|Cr_2O_3|Al_2O_3$ catalyst, when β-methylnaphthalene was obtained in about 18% yield at 400°; a lower yield was obtained if the temperature was increased by 50°. The yields of β-methylnaphthalene were somewhat lower with $Cr_2O_3|Al_2O_3$ catalyst than with the preceding one, while the industrial molybdenum catalyst caused such extensive cracking of the dienyne that the catalyzate yield was very low.

* Communication VI in the series on unsaturated hydrocarbons.

TABLE 1

Aromatization of Cyclohexenylisopropenylacetylene

Expt. No.	Catalyst	Temperature (°C)	Substance fed in (g)	Feed rate (g per liter catalyst per hour)	Catalyzate yield (%)	Yield of β-methylnaphthalene (%)	Melting point of picrate (°C)	Melting point of mixed sample (°C)
1	$MgO \mid Cr_2O_3 \mid Al_2O_3$	400	6.6	133.5	45.5	17.9	115—116	114.5—115.5
2		450	6.3	133.5	31.8	17.2	115—116	115—116
3*		450	6.0	267	40.0	12.5	115—116	115—116
1**	$Cr_2O_3 \mid Al_2O_3$	400	7	133.5	44.3	15.7	114—115.5	114—116
2***		450	6.7	133.5	31.4	14.9	114—115.5	114—116
3****		450	7.2	267	46.8	15.3	115—116	115—116

* 0.6 g of a mixture of the original substance with β-methylnaphthalene boiling at 95 — 107° (17 mm Hg) was also obtained.

** 1.2 g of an 88 — 107° fraction (at 15 mm Hg) was also obtained.

*** 0.5 g of a 94 — 104° fraction (at 15 mm Hg) was also obtained.

**** 1 g of an 86 — 110° fraction (at 16 mm Hg) was also obtained.

It was shown earlier [2, 3] that partial hydrogenation of divinylacetylene hydrocarbons prior to aromatization increases the yield of the required hydrocarbons and gives a more homogeneous catalyzate. For example, when two hydrogen molecules are introduced into the molecule of 2,5-dimethylhexadiene-1,5-yne-3, or three hydrogen molecules are introduced into the molecule of 2-methylhexadiene-1,5-yne-3, the yields are increased severalfold, and the catalyzates consist of almost 100% individual p-xylene and toluene respectively.

Therefore in our studies of the aromatization of cyclohexenylisopropenylacetylene it was decided to test the effect of introducing two molecules of hydrogen into the dienyne molecule on the yield and composition of the catalyzate. Accordingly, 2-methyl-4-(cyclohexen-1-yl)-butene was synthesized by dehydration of the product formed by exhaustive hydrogenation of cyclohexylolisopropylolacetylene:

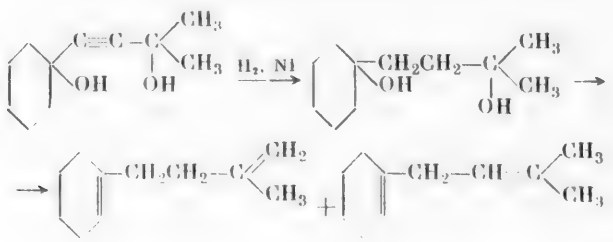

Aromatization of 2-methyl-4-(cyclohexen-1-yl)-butene was performed under various conditions with the same catalysts as those used for aromatization of cyclohexenylisopropenylacetylene.

It was shown in the preceding investigations that the optimum aromatization temperature increases with increasing saturation of the original hydrocarbon. This rule applies to the present instance also.

Whereas the optimum temperature for aromatization of cyclohexenylisopropenylacetylene is 400° aromatization of 2-methyl-4-(cyclohexen-1-yl)-butene proceeds best at 450°, and the best catalyst is $MgO|Cr_2O_3|Al_2O_3$ (2:18:80). Almost pure β-methylnaphthalene is obtained in ~30% yield with this catalyst at 450° and a space velocity of 0.15 liter/liter of catalyst per hour. At higher space velocities the yield of β-methylnaphthalene fell, and the product was contaminated with unconverted 2-methyl-4-(cyclohexen-1-yl)-butene.

TABLE 2

Aromatization of 2-Methyl-4-(cyclohexen-1-yl)-butene-1

Temperature (°C)	Substance fed in (g)	Feed rate (g per liter catalyst per hour)	Yield of β-methylnaphthalene (%)	Catalyzate yield (%)	Melting point of picrate (%)	Melting point of mixed sample (°C)
			$MgO \mid Cr_2O_3 \mid Al_2O_3$ (2 : 18 : 80)			
400	10	133.5	17	49	111.5—112	112—115
450	9.6	133.5	31	31.3	114 —115	114—115
450	8.9	200	18.4	33.7	114 —115	114—115
450	4.9	267	22.3	34.7	114 —115	114—115
500	10	133.5	0.5 g of naphthalene obtained; substance and mixed sample m.p. 79.5-80°C			
500	5.4	267	—	14.8	Not formed	
			$Cr_2O_3 \mid Al_2O_3$ (20 : 80)			
400	3.56	133.5	Not obtained	50	Original	
450	8	133.5	15.6	55	113—113.5	112—115
500	8	133.5	17.5	34	115—116	115—116
550	5.8	133.5	19.1	31	114—115	114—115
			Industrial molybdenum catalyst			
400	5.4	133.5	10	42.5	114—115	114—115
450	5.4	133.5	10	18.5	114—115	114—115.5
500	7.1	133.5	15.6	22.5	115—117and 135—136	
500	8.0	267	18.7	27.5	116—120 131—132.5	

At 500° C the substances undergo extensive changes. The only product isolated was a small quantity of naphthalene.

A higher temperature is required with the alumina – chromium oxide catalyst than with the catalyst promoted by magnesium oxide in order to bring the reaction about, but the former has a lower cracking action.

The industrial molybdenum catalyst caused extensive decomposition of the hydrocarbon molecule.

The results of experiments on aromatization of cyclohexenylisopropenylacetylene are summarized in Table 1, and on aromatization of 2-methyl-4-(cyclohexen-1-yl)-butene, in Table 2.

EXPERIMENTAL

Hydrogenation of isopropylolcyclohexylolacetylene. 150 g of the glycol, 100 ml of ethanol, and 10 g of Raney nickel were stirred together in a 0.5 liter autoclave at 100° and at 60 atmos initial pressure. 35 liters of hydrogen was absorbed. 140 g of 1-cyclohexylol-2-isopropylolethane was obtained after removal of the alcohol.

Dehydration of 1-cyclohexylol-2-isopropylolethane. 50 g of the diol and 5 ml of 90% phosphoric acid were heated together in a Favorskii flask, with distillation of the dehydration products. The substance was separated from water, dried over calcium chloride, and fractionated.

The following fractions were isolated from 40 g of the dehydration product:

Fraction I b.p. 56 – 85° (86 mm Hg) – 6 g,
Fraction II b.p. 114 – 119° (84 mm Hg), $n^{20}D$ 1.4731 – 15 g,
Fraction III b.p. 130 – 154° (85 mm Hg) – 6.8 g,
Fraction IV b.p. 119 – 129° (6 mm Hg) – 10.4 g,
Residue 1.5 g.

Fraction II was 2-methyl-4-(cyclohexen-1-yl)-butene, used for the subsequent aromatization.

Dehydration of isopropylolcyclohexylolacetylene. 26 g of the glycol and 18 g of calcined and powdered potassium bisulfate were heated together in a Wurtz flask, with distillation of the reaction products. 20.3 g of substance was obtained; it was separated from water, dried over calcium chloride, and fractionated.

The following fractions were obtained:

Fraction I b.p. 63 – 77° (27 mm Hg) – 1.21 g,
Fraction II b.p. 83 – 91.5° (27 mm Hg), $n^{19}D$ 1.5161 – 2.2 g,
Fraction III b.p. 107 – 111° (28 mm Hg), $n^{20}D$ 1.5279 – 6.63g,
Fraction IV b.p. 186.5 – 188° (28 mm Hg) – 5.4 g,
Fraction V b.p. 179° (1 mm Hg) – 3.8 g.

Fraction III was cyclohexenylisopropenylacetylene [4].

Aromatization of cyclohexenylisopropenylacetylene and 2-methyl-4-(cyclohexen-1-yl)-butene was carried out over 75 ml of catalyst contained in a quartz tube heated in a tube furnace with automatic temperature regulation to within ±2°. The substance was fed from a metering device.*

For preparation of the catalysts, pieces of industrial alumina were impregnated with a solution of the calculated amount of chromic anhydride in water (for a catalyst promoted with magnesium oxide, the calculated amount of magnesium carbonate was first dissolved in the chromic acid), dried at 105° and calcined in a current of air at 350 – 500° (for 2 hours) and 500 – 550° (for 2 hours). Industrial molybdenum catalyst was obtained from one of the local plants. The catalyst was regenerated by air at 500 – 550° after each experiment. Hydrogen was blown through the catalyst tube before introduction of the substance and after the end of the experiment. The catalyzate was collected in a receiver cooled in ice – salt mixture, and fractionated after each experiment.

For purification, β-methylnaphthalene was converted into the picrate; to isolate the substance from the picrate an alcoholic solution was passed through a column of aluminum oxide 18 – 20 mm in diameter and 100 mm long. This yielded β-methylnaphthalene with m.p. 36-37°; a mixed sample with the known compound had m.p. of 36-37°. The course of reaction was indicated by gas evolution. The catalysts did not show any noticeable loss of activity in use.

SUMMARY

1. Aromatization of cyclohexenylisopropenylacetylene yielded β-methylnaphthalene.

2. If 2-methyl-4-(cyclohexen-1-yl)-butene is used for aromatization, the yield and purity of the product are increased.

LITERATURE CITED

[1] I. L. Kotlyarevskii, A. S. Zanina and V. G. Lipovich, J. Appl. Chem. 30, No. 2, 321 (1957).**

[2] I. L. Kotlyarevskii and A. S. Zanina, J. Appl. Chem. 30, No. 9, 1356 (1957).**

[3] I. L. Kotlyarevskii and A. S. Zanina, J. Appl. Chem. 30, No. 12, 1755 (1957).**

[4] A. Babayan, Proc. Acad. Sci. Armenian SSR 56, 121 (1941).

Received March 2, 1957

* The design of the metering device was kindly provided by V. É. Vasserberg of the Institute of Organic Chemistry, Academy of Sciences USSR, to whom we offer our sincere thanks.

** Original Russian pagination. See C. B. Translation.

SYNTHESIS OF ISODECYL ALCOHOL AND PRODUCTION OF ESTERS FROM IT

A. I. Kutsenko, V. I. Lyubomilov, and R. A. Abramova

Laboratory of Organic Synthesis, Scientific Research Institute of Plastics

It is known that among the best plasticizers for polyvinyl chloride are di-2-ethylhexyl sebacate and di-2-ethylexyl phthalate; these yield the most frost-resistant plasticized products with high volume resistivity. We considered that an ester made from adipic acid, which is a cheap and abundant industrial intermediate, and an alcohol containing rather more carbon atoms in the molecule than 2-ethylhexanol, should not be inferior in quality to the above-named plasticizers. There have been several publications [1] in recent years on the use of esters of isodecyl alcohol, although the structure of the latter is not indicated. We therefore tested isodecyl alcohol — 2,6-dimethyl-3-methylolheptane — which can be easily prepared by condensation of isoamyl alcohol in presence of caustic soda and a dehydration catalyst, by the method described earlier for the preparation of 2-ethylhexanol-1 from n-butanol [2].

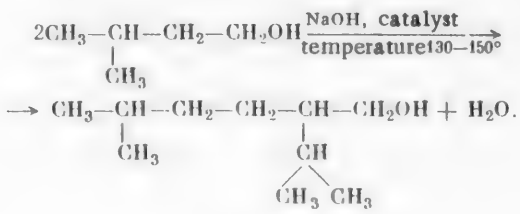

Isoamyl alcohol can also be readily available; for example, it may be made from isobutylene and formaldehyde by the Prins reaction.

EXPERIMENTAL

Synthesis of 2,6-dimethyl-3-methylolheptane. The boiler of the apparatus described for the condensation of n-butanol [2] was charged with 1500 g of isoamyl alcohol, 45 g of caustic soda, and 40 g of industrial nickel catalyst supported on chromium oxide. The reaction was conducted as for the condensation of n-butanol, but the temperature was 128° at the beginning and 148° at the end of the condensation. The reaction product was distilled in steam, and the alcohols were separated from water and rectified through a fractionating column 20 cm high. The product consisted of 524 g of unchanged isoamyl alcohol, and 574 g of a 199 — 206° fraction, with 79.2 g of residue in the still. In addition, 30 g of a substance containing 74.0% of isovaleric aldehyde was decanted earlier from the water separator of the reaction apparatus. Pure isovaleric aldehyde boiling at 92° was isolated from it by distillation. The yield of the isodecyl alcohol fraction was 67.5% of the theoretical, calculated on isoamyl alcohol. The bromine number of this fraction was 10.45 g Br/100 g.

For preparation of isodecyl alcohol, this fraction was hydrogenated in an autoclave under 120 — 150 atmos hydrogen pressure at a temperature reaching 150°, in the presence of a catalyst consisting of nickel on chromium oxide (5% on the weight of the fraction). The hydrogenation product was filtered to remove catalyst and rectified under vacuum through a packed column of about 8 theoretical plates. The rectification yielded about 0.5% of water and isoamyl alcohol, and 93% (on the weight taken) of 2,6-dimethyl-3-methylolheptane fraction; b.p. 208.5 — 209° (761 mm), d^4_{20} 0.8345, $n^{20}D$ 1.4370, bromine number 0.

TABLE 1

Physicochemical Properties of 2,6-Dimethyl-3-methylolheptane (isodecyl alcohol) Esters*

Ester	d^{20}_4	$n^{20}D$	Acid number, mg KOH/g	Saponification number		Temperature (°C)		Volume resistivity at 20° (ohm·cm)
				found	calculated	flash point	setting point	
Diisodecyl succinate	0.9215	1.4468	0.08	281.2	282	188	−57	$4.6 \cdot 10^{11}$
Diisodecyl adipate	0.9166	1.4492	0.18	266.8	262.8	200	−57	$6.3 \cdot 10^{11}$
Diisodecyl sebacate	0.9074	1.4520	0.23	230.5	232	229	−58	$5.1 \cdot 10^{11}$
Diisodecyl phthalate	0.9670	1.4830	0.58	255.0	250.6	210	—	$4.3 \cdot 10^{10}$
Diisodecyl thiodipropionate	0.9551	1.4648	0.29	244.4	244.5	213	−55	$1.9 \cdot 10^{11}$

* Constants determined for undistilled esters.

TABLE 2

Properties of Plasticized Resins*

Properties	Insulation resin	Tube resin
Ultimate tensile strength (kg/cm^2)	175	162
Relative elongation at break (%)	352	380
Decomposition temperature (°C)	210	218
Loss on heating for 6 hours at 160° (%)	3.5	2.4
Brittle point (°C)	−45	−40
Volume resistivity at 20° (ohm·cm)	$1.4 \cdot 10^{12}$	$2.6 \cdot 10^{11}$

* The tests were performed in accordance with the technical specifications of the Ministry of the Chemical Industry 1535-47 [4] for these products.

Found %: C 76.18, 76.34; H 14.24, 14.11; OH 10.65, 10.77. Calculated %: C 75.87; H 14.02; OH 10.76.

α-Naphthylurethane: m.p. 47.5°.

The constants exactly correspond to the constants reported earlier for 2,6-dimethyl-3-methylolheptane [3]. The substance is a colorless, somewhat viscous liquid with a faint peculiar odor.

Preparation of esters. The esters were prepared from succinic, adipic, and sebacic acids, and phthalic anhydride, which are the standard corresponding technical materials. The thiodipropionate ester was prepared from the acid which had the following properties: m.p. 129 − 130° and acid number 628.9 mg KOH/g.

A weighed quantity of one of the above-named acids or of phthalic anhydride, isodecyl alcohol in 20% excess over the theoretical quantity, and p-toluenesulfonic acid catalyst (2% on the weight of acid or anhydride taken), were put into a flask fitted with a stirrer, thermometer, and a trap for the water formed in the reaction. The esterification was performed at 130 − 150° with the distillation of the water formed in the reaction, periodic samples of the reaction mass being taken and their acid numbers determined. The reaction was terminated when the acid number reached 2 − 2.5 mg KOH/g.

The reaction mass was washed with water, neutralized with 0.5 N caustic soda solution, and washed with water again until the wash waters were neutral. The washed product was dried under vacuum, the residual pres-

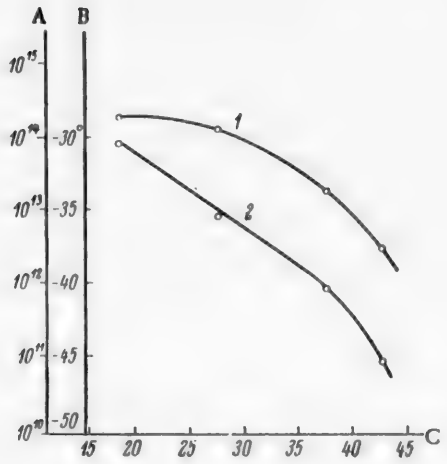

Variations of volume resistivity (1) and brittle point (2) of plasticized resins with the diisodecyl adipate content:
A) volume resistivity (ohm · cm), B) brittle point (°C), C) content of ester (parts by weight).

sure being reduced to 3 – 4 mm Hg, and excess isodecyl alcohol was distilled off. The temperature of the liquid was gradually raised to 180° during the process. The ester yields were 92 – 95% on the acids taken.

The esters were relatively viscous odorless liquids of a faint yellow color. The properties of the esters are given in Table 1.

The graph shows the variations of brittle point and volume resistivity of plasticized polyvinyl chloride with its content of diisodecyl adipate. The plasticized products were prepared as follows: 5 weight parts of lead silicate, 1 weight part of calcium stearate, and the amounts of diisodecyl adipate indicated along the abscissa axis were added to 100 weight parts of polyvinyl chloride. The mixes were masticated for 15 – 20 minutes at 150 – 160°. The diagram shows that a resin with brittle point –30° and volume resistivity $3.6 \cdot 10^{14}$ ohm · cm can be obtained. On the other hand, a resin with brittle point –45° has volume resistivity $5.5 \cdot 10^{12}$ ohm · cm.

Table 2 gives detailed characteristics of plasticized resins made by the usual industrial formulations for insulation and tube resins, with diisodecyl adipate as plasticizer.

The properties of the esters, given in Table 1, suggest that these esters may also be of interest as plasticizers.

SUMMARY

The adipate diester tested as plasticizer for polyvinyl chloride may be used industrially in the production of resins for tubing and other materials.

LITERATURE CITED

[1] Modern Plastics., 32, 2, 108 (1954); 33, 5, 248 (1956).

[2] A. I. Kutsenko and V. I. Lyubomilov, J. Appl. Chem. 31, No. 9, 1419 (1958).*

[3] V. I. Lyubomilov, J. Gen. Chem. 26, 2738 (1956).*

[4] Collected Standards and Technical Specifications for Plastics (Moscow – Leningrad, Goskhimizdat, 1950) p. 227. [In Russian].

Received May 30, 1957

* Original Russian pagination. See C. B. Translation.

BRIEF COMMUNICATIONS

DECOMPOSITION POTENTIALS OF NaCl IN THE FUSED ELECTROLYTES $NaCl-CaCl_2$ AND $NaCl-CaCl_2-BaCl_2$

K. Ya. Grachev and V. Ya. Zhuryutina

The literature contains contradictory data on the decomposition potential of pure NaCl. For example, the decomposition potential of NaCl at 800° is 2.62 – 2.65 v according to Neumann [1, 2], 2.56 v according to Tverdovskii [3], 3.18 v according to Molchanov [4], 3.20 – 3.25 v according to Cambi and Devoto [5], and (at 700°) 3.39 v according to Delimarskii [6]. The decomposition potential of NaCl at 800°, calculated from thermodynamic data, is 3.34 v according to Lyashenko, and 3.24 v according to Hamer [8].

The data of Neumann, Tverdovskii, Molchanov, and Cambi and Devoto were critically examined by Antipin et al. [9], who showed that Neumann's data must be regarded as unreliable because of considerable depolarization, and that Devoto's data are the most accurate.

In view of the discrepancies in the values for the decomposition potential of NaCl at 700 – 800°, and of the lack of such data for lower temperatures, we determined the decomposition potential of NaCl in $NaCl-CaCl_2$ and $NaCl-CaCl_2-BaCl_2$ melts at temperatures from 620 to 700°.

The experiments were performed in a U-shaped Pyrex glass vessel constricted at the bend, and containing a partition consisting of broken porcelain. NaCl and $BaCl_2$ were of the chemically pure grade, dried at 250 – 300° to complete removal of adsorbed water and water of crystallization. $CaCl_2$ was technical, anhydrous, conforming to Technical Specification 2096-50 of the Ministry of the Chemical Industry, produced at the Stalinogorsk Chemical Combine, and additionally remelted and dehydrated by dry hydrogen chloride gas.

The salt mixture was first melted in a porcelain beaker and treated with hydrogen chloride, then poured into the U-shaped vessel and treated for 1.5 – 2 hours with a mixture of hydrogen chloride and chlorine to remove traces of water and to decompose metal oxides.

The sodium electrode consisted of a thin-walled Pyrex test tube containing metallic sodium (Fig. 1). The tube was first blown through with argon or purified nitrogen; metallic sodium was then placed in the side tube, melted in a burner flame, and carefully shaken down to the bottom of the test tube while oxides remained on the side-tube walls. The test tube was closed by means of a rubber bung containing a steel rod for contact with the sodium.

The chlorine electrode was a graphite rod 5 – 10 mm in diameter, with gaseous chlorine blown endways over it. The chlorine rate was kept at 90 – 100 bubbles per minute.

New graphite rods and new sodium electrodes were used in every experiment.

The vessel is shown diagrammatically in Fig. 2.

The vessel was contained in a melt bath for reliable temperature control. The electrolyte temperature was measured by means of a platinum/platinum – rhodium thermocouple immersed in a sheath in the bath near the bend of the vessel, with the junction at the level of the chlorine and sodium electrodes. The temperature was measured to within ±2°.

The bath containing the vessel was placed in a TG-1 crucible furnace, the heating temperature of which was established and regulated by means of the EPD-17 recording and regulating potentiometer, with Kh. A. calibration.

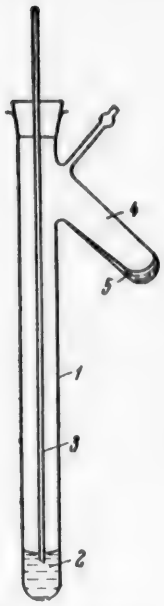

Fig. 1. Sodium electrode: 1) Pyrex test tube, 2) metallic sodium, 3) steel rod, 4) side tube, 5) sodium oxides.

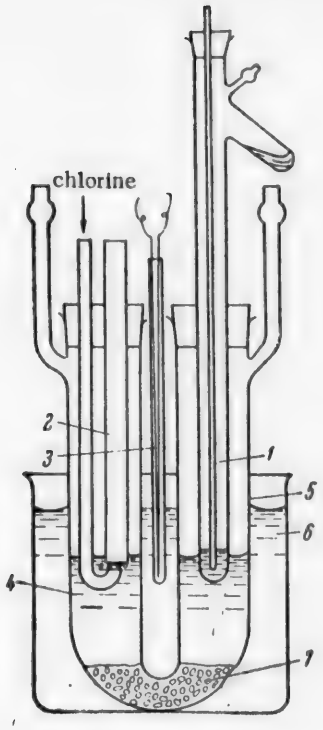

Fig. 2. Vessel for determination of cell e.m.f.: 1) sodium electrode, 2) chlorine electrode, 3) thermocouple, 4) electrolyte, 5) vessel, 6) bath, 7) partition.

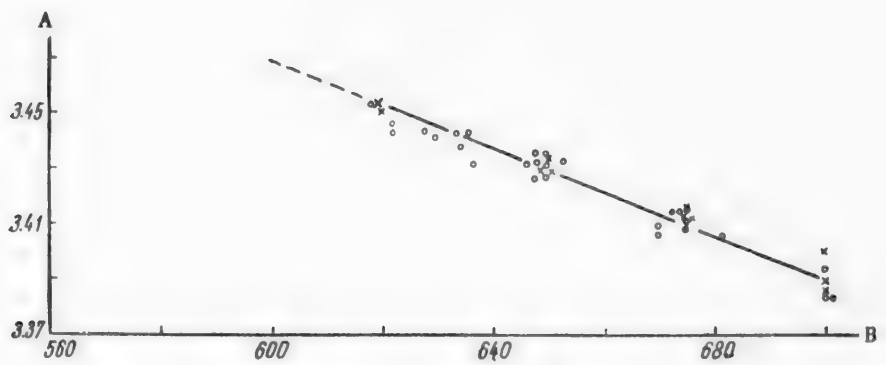

Fig. 3. The e.m.f. of the cell Na/melt, Cl_2/C at different temperatures: A) e.m.f. (v), B) temperature (°C).

After the melt had been treated with HCl and Cl_2, the graphite rod and chlorine inlet tube were immersed in it to a depth of 2 – 3 mm. Chlorine was supplied from a cylinder, chlorination of the graphite being continued for 1.5 – 2 hours. The sodium electrode was then immersed and measurements of the cell e.m.f. were commenced by means of the PPTV high-resistance potentiometer. Stable e.m.f. was established in 1 – 1.5 hours.

The cell e.m.f. was measured at 620 – 700°. The electrolytes were salt mixtures of the following compositions (wt.%): $32NaCl+42CaCl_2+26BaCl_2$ and $42NaCl+58CaCl_2$.

In Fig. 3 the results of e.m.f. measurements of the cell with $NaCl - CaCl_2$ electrolyte are indicated by points, and $NaCl - CaCl_2 - BaCl_2$ electrolyte by crosses.

It is clear from Fig. 3 that the e.m.f. (decomposition potential) is a linear function of temperature, and may be represented by a common equation for the two electrolytes

$$E = 3.43 - 0.78 \cdot 10^{-3} (t - 650)$$

with an error not exceeding ±0.01 v.

The value found for the temperature coefficient of e.m.f. is $0.78 \cdot 10^{-3}$ v/degree, which is in good agreement with Lyashenko's value [7] of $0.795 \cdot 10^{-3}$ v/degree for the temperature range from 98 to 800°.

LITERATURE CITED

[1] B. Neumann and E. Bergve, Z. Elektroch., 21, 143 and 152 (1915).

[2] B. Neumann and H. Richter, Z. Elektroch., 31, 287 (1925).

[3] I. P. Tverdovskii, Trans. Sci. Res. Inst. Light Metals 4, 71 (1933).

[4] V. S. Molchanov, Light Metals 5, 28 (1935).

[5] L. Cambi and G. Devoto, Gazz. Chim. Italiana, 57, 836 (1927).

[6] Yu. K. Delimarskii, J. Phys. Chem. 29, No. 1, 28 (1955).

[7] V. S. Lyashenko, Metallurgist 1, 95 (1936).

[8] W. J. Hamer, M. S. Malmberg and B. Rubin, J. Electroch. Soc., 103, 1, 8 (1956).

[9] P. F. Antipin, A. F. Alabyshev, B. P. Artamonov, V. P. Barzakovskii and N. A. Belozerskii, Electrochemistry of Fused Salts, 1 [in Russian] (ONTI, 1937).

Received May 3, 1957

REDUCTION OF POTASSIUM SULFATE BY METHANE

S. V. Kushnir

The reduction of potassium sulfate is becoming a problem of practical interest in connection with the development of new methods for the dry conversion of langbeinite and kainite – langbeinite deposits of the Carpathian region into concentrated potash fertilizers. A dry process for the conversion of langbeinite ($K_2SO_4 \cdot 2MgSO_4$) into potassium sulfate by gaseous reduction with natural gas (Dashava methane) is being developed in our laboratory [1].

A method has been developed* for hydrothermal conversion of kainite – langbeinite deposits into glaserite with the use of natural gas as fuel [2]. In either case it is very important to have data on the behavior of K_2SO_4 at high temperatures in a methane atmosphere (or in presence of methane). However, no data are available at all in the literature on the reduction of K_2SO_4 by methane. The present investigation was performed in order to obtain such data.

In our experiments we used fine-grained K_2SO_4 of chemically pure grade, with 0.3 – 0.6 mm grains, and natural methane (from Dashava) of the following composition (%): CH_4 97.83, C_2H_6 0.44, C_3H_8 0.18, C_4H_{10} 0.05, C_5H_{12} and higher 0.11, N_2 1.1

The apparatus and methods were similar to those used in studies of the reduction of $MgSO_4$ by methane [1]. A weighed sample of K_2SO_4 (1 – 2 g) in a porcelain boat was put into the quartz tube of an electric furnace heated to the required temperature, and reduced in a current of purified and dried methane. The methane rate was measured by means of a capillary flow meter, and the temperature of the furnace by a platinum/platinum – rhodium thermocouple.

It was found in preliminary experiments that the reduction products of K_2SO_4 consist of potassium sulfide and polysulfides; K_2SO_3, $K_2S_2O_3$ and K_2CO_3 in the solid residue; CO_2, CO, H_2S and traces of COS in the gas phase.

The H_2S content of the gas was determined iodometrically, COS by the combustion method [3], and CO_2 and CO by the usual methods of gas analysis. The solid residue was dissolved in water and analyzed by Budnikov's method (somewhat modified) for the product of reduction of Na_2SO_4 by carbon [4]. The analytical results were expressed in percentage of total sulfur of the converted sulfate for each product.

The reaction between potassium sulfate and methane commences at 800±10°. This was established by means of a series of experiments at progressively higher temperatures. In each experiment methane was passed for 10 – 15 minutes over K_2SO_4 in a porcelain boat, and the residue was tested for the $S^{=}$ ion.

The effect of temperature on the reaction rate was studied in a series of reduction experiments with equal weights of K_2SO_4 (1.13 g), equal gas rates (15 ml/minute), and equal exposure times of the salt in the reaction zone (10 minutes). The total amount of methane passed was sufficient for complete reduction of sulfate to sulfide. The reduction rate was estimated from the weight loss of the sulfate samples. The results of these experiments are given in Table 1.

These results show that reduction of K_2SO_4 by methane proceeds at an appreciable rate only at $t > 820°$. However, even at 900° the reduction rate is not high; the degree of reduction reached in 10 minutes is only about $\frac{6.8}{36.8} \cdot 100 \simeq 20\%$.**

* In the Institute of General and Inorganic Chemistry, Academy of Sciences, Ukrainian SSR.

** Here 36.8% represents the weight loss in complete $K_2SO_4 \rightarrow K_2S$ conversion.

TABLE 1

Effect of Temperature on the Reaction Rate

Temperature (°C)	Weight loss (%)	Color and nature of residue
800	0.04	White, crystalline
820	0.32	Pale yellow, crystalline
840	2.2	Yellow, crystalline, sintering commenced
860	3.5	Yellow, sintered
900	6.8	Yellow-orange, fused

TABLE 2

Effect of Reduction Time on the Reaction Rate

Time (min)	Weight loss (%)	Reaction rate (nature of residue)
10	2.2	Start of sintering
20	6.5	Much sintering
30	7.1	Fused
40	7.6	Fused

TABLE 3

Effect of Temperature on Reduction of K_2SO_4 by Methane

Expt. No.	Temperature (°C)	$\frac{CH_4}{K_2SO_4}$	Degree of reduction (%)	Distribution of reduced sulfur (%)					$\frac{K_2CO_3}{K_2SO_4 \text{ red.}}$ (molar %)	$\frac{CO_2}{CO}$
				K_2S_n			K_2SO_3 ($+K_2S_2O_3$)	H_2S + +COS		
				K_2S	S_{n-1}	Σ				
1	820	1:1	12.5	30.8	31.3	62.1	28.6	9.3	19.2	2.6
2	820	1.5:1 *	22.0	36.3	33.7	70.0	23.2	6.8	20.9	2.5
3	860	1:1	29.0	51.0	24.0	75.0	20.1	4.9	11.4	3.7
4	860	1:1	32.7	49.5	27.0	76.5	19.3	4.2	11.0	3.2
5	900	1:1	41.0	54.4	23.6	78.0	17.7	4.3	11.4	4.2
6	900	1:1	43.2	51.5	25.2	76.7	18.0	5.3	9.4	4.6

* Duration of experiment 30 minutes.

The data in Table 1 show that the residue sinters at 840° C, and melts rapidly above this temperature. However, as the eutectic temperature of the system K_2SO_4–K_2S is only 600° [5], fusion of the product could not be avoided even by reduction at 800°. Therefore reduction of K_2SO_4 by methane must always be accompanied

by fusion of the residue. It is quite obvious that the reaction rate must fall sharply at the instant of fusion, as the reaction can then proceed only at the surface of the melt.

Several experiments were performed at 840° with different reduction times (Table 2); the results confirm that the reaction rate drops sharply 20 minutes after the start, when the residue begins to melt.

A series of experiments with complete analysis of the reaction products was carried out in order to determine the quantitative proportions of the products and their variations with temperature. The experimental conditions were: weight of K_2SO_4 2 g, methane rate 15 ml/minute, total time 20 minutes (then $CH_4 : K_2SO_4 = 1 : 1$). The results of these experiments are given in Table 3.*

The results indicate that the main products of the reduction of K_2SO_4 by methane are potassium sulfide and polysulfides. Simple calculation shows that at 820°the average value of n is about 2. The value of n decreases with rise of temperature, and is about 1.4 at 900°. It follows that at low temperatures mainly potassium disulfide is formed; its yield diminishes with rise of temperature, and the monosulfide becomes the principal reaction product. The color of the residue (which changes from pale yellow to dark brown) suggests that it also contains some higher polysulfides [6].

Quite appreciable amounts of potassium sulfite and carbonate are also formed; their yields slowly decrease with rise of temperature. The yield of volatile sulfur compounds (H_2S, COS) is low. The main oxidation product of methane was carbon dioxide in all experiments.

In Experiment 2 (at the same temperature and gas rate) the amount of methane passed was only 1½ times as much as in Experiment 1, but the degree of reduction was almost doubled. This is possible due to the autocatalytic nature of the process, as in the reduction of Na_2SO_4 by carbon [4].

These results show that in processes of high-temperature conversion of potassium minerals of the sulfate and chloride – sulfate type with the use of methane at temperatures above 800° there is always the possibility of more or less intensive reduction of potassium sulfate.

LITERATURE CITED

[1] Ya. P. Berkman and S. V. Kushnir, Proc. Acad. Sci. USSR 104, 448 (1955).

[2] S. D. Shargorodskii, O. I. Shor and B. S. Barabanova, Ukrain. Chem. J. 21, 152 (1955).

[3] A. A. Il'inskaia and L. M. Kontorovich, Ind. Lab. 13, 29 (1947).

[4] P. P. Budnikoff, Z. anorg. Ch., 170, 255 (1928).

[5] J. Goubeau and H. Kolb, Z. anorg. Ch., 236, 45 (1938).

[6] F. Feher and H. J. Berthold, Z. anorg. Ch., 274, 223 (1953).

Received April 27, 1957

* In the case of K_2CO_3 the molar yield on the converted K_2SO_4 is given in Table 3.

PROCESSES LEADING TO GENERATION OF DROPLETS IN THE RUPTURE OF BUBBLES AT LIQUID – GAS INTERFACES

V. G. Gleim, I. K. Shelomov and B. R. Shidlovskii

Chair of Chemistry, The Rostov-on-Don Institute of Railroad Engineers

In studies of the effects at interphase boundaries during bubbling and boiling, which determine the rational regime of such processes [1 – 4] it is naturally necessary to consider the geometry of the bubbles in relation to their stability at the interface and to generation of moisture in their rupture.

Photographs show that bubbles consist of pairs of segments with a common circular base (Fig. 1). Careful measurements of air bubbles (from photographs) show that the upper segment is approximately a hemisphere. It seems that the thinner the film of the upper segment, the nearer it is to a hemisphere.

The conditions for detachment of droplets from the liquid surface are determined only by the pressure distribution in the lower segment. Equilibrium of the two segments, with the weight of the upper segment film ignored, is represented by the equation

$$x \cdot dg + \left(\frac{2\sigma}{\rho}\right)_x = \left(\frac{4\sigma}{r}\right)_x , \tag{1}$$

where ρ is the radius of curvature of the lower segment; r is the radius of an equivalent hemisphere; σ is the surface tension; x is a subscript indicating projection onto the corresponding axis.

It follows from Equation (1) that the lower segment can be replaced by a hemisphere of radius r, equivalent to it in pressure distribution.

The pressure which detaches the drop from the liquid surface is normal to that surface and, by Equation (1) is

$$P_{\text{norm}} = \left(\frac{4\sigma}{r}\right)_x . \tag{2}$$

Clearly, for every element of mass to be detached, the normal component of the pressure must exceed a certain critical value P_{cr}, determined by the forces of intermolecular cohesion in the liquid. However, P_{cr} is a function of the hemisphere radius, and therefore at a certain value of this radius (r_{cr}) the drop cannot become detached. The existence of such a radius has been demonstrated experimentally [2, 5].

Evidently all the surface energy of any point which conforms to the condition

$$\left(\frac{4\sigma}{r}\right)_x < \frac{4\sigma}{r_{cr}} , \tag{3}$$

is expended in overcoming the forces of internal friction and gravity, and is converted into heat at the instant when the bubble bursts.

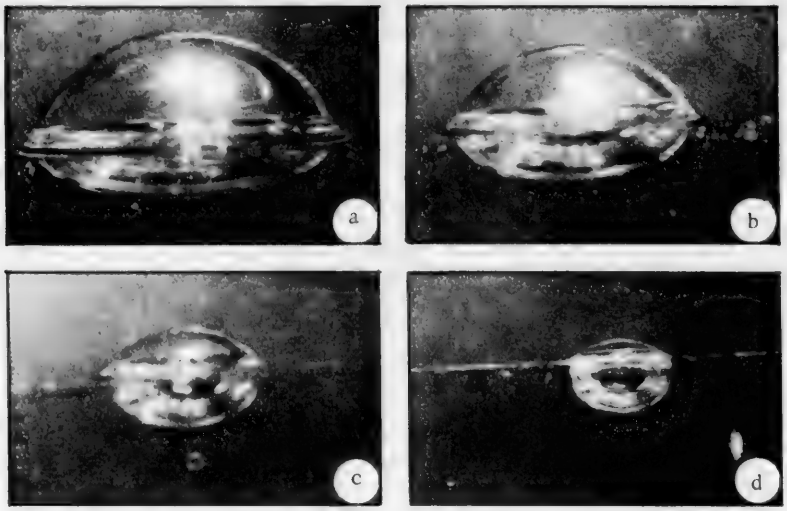

Fig. 1. Photographs of air bubbles of different diameters (in glycerol): R (in cm): a) 0.6, b) 0.5, c) 0.29, d) 0.19

At the points in the surface at which

$$\left(\frac{4\sigma}{r}\right)_x > \frac{4\sigma}{r_{cr}} \tag{4}$$

there is a certain excess of energy, which is expended to detach the drop and to impart kinetic energy to it. The kinetic energy of the drop must be proportional to the energy of the surface under a pressure exceeding the critical value.

The boundary of the detaching surface must be the geometrical situation of the points conforming to the condition

$$\left(\frac{4\sigma}{r}\right)_x = \frac{4\sigma}{r_{cr}} . \tag{5}$$

It follows from Fig. 2 that

$$\left(\frac{4\sigma}{r}\right)_x = \frac{4\sigma}{r} \cdot \cos\theta = \frac{4\sigma x_{cr}}{r^2} , \tag{6}$$

where x_{cr} is the abscissa of the boundary point.

From Equations (5) and (6) we have

$$x_{cr} = \frac{r^2}{r_{cr}} .$$

Then

$$S = 2\pi r (r - x_{cr}),$$

where S is the surface ejecting the drops.

Rearrangement gives

$$S = 2\pi \frac{r^2}{r_{cr}} (r_{cr} - r). \tag{7}$$

The condition of proportionality between the energy of the drop and the energy of the surface S is expressed in the form

$$mgh = KS\sigma, \tag{8}$$

where m is the mass of the drop and h is the height of its ascent. Stated otherwise,

$$mgh = K \frac{2\pi r^2}{r_{cr}} (r_{cr} - r)\,\sigma. \tag{9}$$

The coefficient K indicates the relationship between the kinetic energy of the drop and the energy expended when it is detached. This coefficient may serve as a relative measure of the energetic advantage of drop generation in a particular solution.

Comparison of Experimental and Calculated Data

Solution	r (cm)	$m \cdot 10^6$ (g)	h (cm)	$mgh \cdot 10^3$ (ergs)	$S\sigma$ (ergs)	$K \cdot 10^2$	$K_{cr} \cdot 10^2$
Na_2SO_4 0.1 N	0.105	2.5	17.8	4.36	3.52	1.240	1.24
	0.124	4.0	13.5	5.30	4.51	1.172	
	0.234	11.2	9.5	10.45	8.35	1.250	
	0.340	22.3	0.9	1.96	1.52	1.290	
	0.350	—	0	0	0	—	
NaCl 0.1 N	0.105	2.5	17.6	4.32	3.52	1.230	1.23
	0.124	4.0	13.5	5.30	4.51	1.175	
	0.234	10.3	9.7	10.51	8.35	1.260	
	0.340	24.1	0.8	1.89	1.52	1.245	
	0.350	—	0	0	0	—	
H_2O	0.105	2.6	17.0	4.38	3.52	1.245	1.22
	0.124	3.9	14.5	5.60	4.51	1.241	
	0.234	9.8	9.5	9.15	8.35	1.100	
	0.340	25.0	0.8	1.96	1.52	1.290	
	0.350	—	0	0	0	—	
NaOH 0.1 N	0.105	2.1	16.4	3.38	3.52	0.960	0.96
	0.124	3.3	13.5	4.36	4.51	0.967	
	0.234	8.5	9.5	7.91	8.35	0.950	
	0.340	21.0	0.7	1.44	1.52	0.951	
	0.350	—	0	0	0	—	
Na_2CO_3 0.1 N	0.105	2.0	17.2	3.38	3.52	0.960	0.95
	0.124	3.1	14.0	4.25	4.51	0.943	
	0.234	8.4	9.5	7.84	8.35	0.940	
	0.340	20.9	0.7	1.44	1.52	0.940	
	0.350	—	0	0	0	—	

EXPERIMENTAL

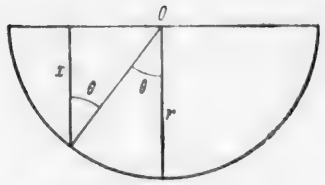

Fig. 2. Force distribution in a hemisphere equivalent to the lower segment of an air bubble (explanation in text).

To test the foregoing theoretical considerations, experiments were performed on determinations of the weight of drops and the height of their ascent in relation to bubble radius.

The experimental technique is described in an earlier paper [2].

The results are summarized in the table and are compared with results calculated from Formula (9). The value of r_{cr} was taken to be 0.35 cm, which is the mean of many experimental determinations.

It follows from the results that Equation (9) accurately reflects variations of kinetic energy as a function of bubble diameter, while the coefficient K for each solution remains constant, within the limits of experimental error, over the whole range of radius variations.

The solutions studied fall into two groups according to the average value of the coefficient: the group of neutral salts and water ($K_{av} \simeq 1.23$), and the group of alkaline solutions ($K_{av} \simeq 0.95$).

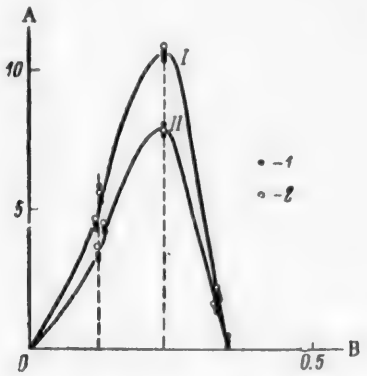

Fig. 3. Curves showing variations of the kinetic energy of drops with bubble radius:
A) kinetic energy of drops, B) radius of bubble base (cm); points: 1) experimental, 2) theoretical; solutions: I) neutral, II) alkaline.

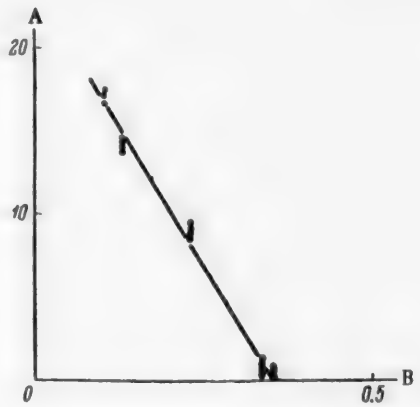

Fig. 4. Plot of the height of drop ascent as a function of radius:
A) height of drop ascent (cm), B) radius of bubble base (cm).

It follows that drop generation by the evaporation surface is less advantageous from the energy standpoint in alkaline than in neutral media.

It follows from the same equation that the kinetic energy of the drop is at a maximum when $r = 2/3\ r_{cr}$. When $r = 2/3\ r_{cr}$ the function $mgh = f(r)$ has an inflection when the sign of the curvature changes from plus to minus. Fig. 3 shows variations of the kinetic energy of the drops with the bubble radius for both groups of solutions. The values of kinetic energy were calculated from experimental data (m and h) and also found from Equation (9). Fig. 3 shows that these results completely coincide.

Fig. 4 shows how the height of drop ascent decreases with increase of bubble radius.

The value of h can be approximately represented by the equation

$$h = A(r_{cr} - r), \qquad (10)$$

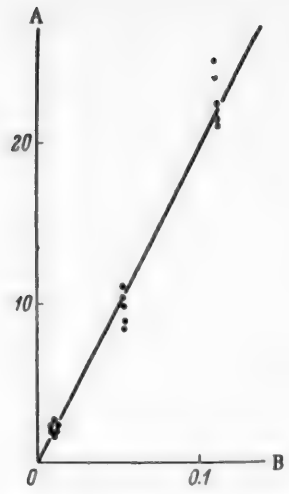

Fig. 5. Variation of the mass of drops formed with the radius of the bursting bubble: A) drop mass, B) radius of bubble base (cm).

where A is a constant. Then it follows from Equations (9) and (10) that

$$m = B \cdot r^2, \tag{11}$$

where B is a constant.

This rectified equation is represented by the straight line in Fig. 5, which also shows experimental values for the mass of drops generated by bursting bubbles of different diameters.

The agreement between the theoretical and experimental values is quite satisfactory.

SUMMARY

1. A bubble at a liquid – gas interface consists of two segments. If the film is thin, the upper segment can be approximately regarded as a hemisphere.

2. Generation of droplets from a liquid surface can occur only until the bubble radius reaches a certain critical value.

3. Experimental data on the kinetic energy of a generated drop, its mass, and height of ascent as functions of the bubble radius can be interpreted theoretically.

4. Under equal conditions, drop generation is energetically less advantageous in alkaline than in neutral media.

LITERATURE CITED

[1] V. G. Gleim, J. Appl. Chem. 26, No. 11 (1953).*

[2] V. G. Gleim, J. Appl. Chem. 28, No. 1 (1955).*

[3] V. G. Gleim and I. K. Shelomov, J. Appl. Chem. 30, No. 1 (1957).*

[4] M. E. Pozin, I. P. Mukhlenov, E. S. Tumarkina and E. Ya. Tarat, The Foam Method for Treatment of Gases and Liquids [in Russian] (Goskhimizdat, 1955).

[5] F. H. Garner, S. R. Ellis and L. A. Lacey, Trans. Inst. Chem. Eng., 32, 4 (1954).

Received July 19, 1957

* Original Russian pagination. See C. B. Translation.

SOLUBILITY OF PEAT HUMIC ACIDS

S. E. Burkat

The question of the solubility of humic acids, apart from the theoretical interest, is of great practical importance, as the isolation of these acids from peat and studies of their composition, properties, and structure are all associated with their behavior toward various solvents. The solubility of humic acids in caustic and carbonate alkalies and ammonia is well known [1 – 3]. Their behavior with organic solvents has been studied much less [4 – 7].

This paper contains data on the solubility of peat humic acids in acetone – water and alcohol – water mixtures.

EXPERIMENTAL

A preparation of humic acids obtained from lowland peat by the usual alkaline method [8] was used for the investigation. The preparation was not treated in order to isolate the so-called hymatomelanic acids, soluble in ethyl alcohol. The humic acids taken for the investigation had the following characteristics: moisture content 8.25%, ash 0.8%; amount of KOH combined with 1 g of acids in the reaction with alcoholic alkali solution, by the Fuchs method [9], 6 meq.

For the solubility determinations 50 ml of solvent was added to a weighed quantity (1 g) of the finely ground preparation in a bottle with a ground-glass stopper, and the mixture was kept for 24 hours at room temperature with frequent shaking. The amount of acids dissolved was found from the weight of dry residue obtained after evaporation of a known volume of solution.

The behavior of the preparation with pure organic solvents and with water was first studied. The experiments showed that humic acids are insoluble in ligroine, gasoline, chloroform, carbon tetrachloride, isobutyl alcohol, ethyl ether, benzene, toluene, and m-xylene. The solubility of humic acids was 27.2% in methyl alcohol, 21% in ethyl alcohol, 19% in acetone, and 1.9% in distilled water. The organic solvents used in these experiments conformed to the purity specifications of the State Pharmacopeia or the All-Union Standards.

The same procedure was then used in determinations of the solubility of humic acids in aqueous mixtures of acetone, methyl alcohol, and ethyl alcohol, with different contents of the organic solvents, namely: 20, 40, 60, and 80 vol.%. The results of these experiments are given in Table 1. The solubilities are expressed as percentages of the weight taken. The surface tensions of the aqueous alcohol and acetone mixtures at 20° are also given.

It follows from Table 1 that the solubility of humic acids in aqueous mixtures of alcohols and acetone increases with the contents of organic solvents in the mixtures. Compared with the pure solvents, 60% mixtures of ethyl alcohol and acetone with water have considerably higher solvent power. The almost complete solubility of humic acids in 60% aqueous acetone is especially noteworthy.

Comparison of the surface tensions of aqueous alcohols and acetone with their solvent effects on humic acids shows (Table 1) that mixtures with the lowest surface tension have the highest solvent power. This suggests that the solvent action of alcohols and acetone in mixtures with water is associated with their surface activity [10].

TABLE 1

Results of Determinations of the Solubility of Humic Acids in Aqueous Acetone and Aqueous Alcohols

Content of organic solvent in aqueous mixture (vol.%)	Methyl alcohol		Ethyl alcohol		Acetone	
	Solubility of acids (%)	Surface tension (dynes·cm^{-1})	Solubility of acids (%)	Surface tension (dynes·cm^{-1})	Solubility of acids (%)	Surface tension (dynes·cm^{-1})
20	3.4	49.20	7.4	41.60	5.6	44.01
40	4.2	39.00	9.9	31.90	37.3	35.72
60	9.8	33.00	37.3	28.10	98.2	32.40
80	24.9	29.30	39.6	25.70	98.3	27.16

TABLE 2

Analytical Data for Different Humic Acid Preparations

Humic acid preparation	Contents (%)			Amount of KOH (meq)
	moisture	ash	carbon	
1	8.25	0.80	59.26	6.00
2	6.90	0.72	61.00	6.67
3	4.65	0.21	62.30	6.97

Humic acids dissolve slowly in 60% aqueous acetone at room temperature; the particles swell, forming a resinous mass which gradually passes into solution. Similar effects are observed, to a lesser extent, in the action of aqueous ethyl alcohol.

Experiments showed that the solubility of humic acids in ethyl alcohol and its mixtures with water increases considerably with temperature. About 80% of the acid sample taken dissolves in boiling 60% alcohol (with 1 g acids to 50 ml solvent).

1% solutions of humic acids in 60% aqueous solutions of acetone and ethyl alcohol are dark liquids, reddish-brown in color and transparent in thin layers, with a distant acid reaction to litmus. Removal of the organic solvents from the solutions by evaporation leaves turbid aqueous suspensions of humic acids, brown in color and with a scarcely perceptible acid reaction.

The fact that acetone – water and alcohol – water solutions of humic acids, in contrast to aqueous suspensions, have a distinct acid reaction, suggests that when humic acids dissolve they form solvated groups with acetone and ethyl alcohol, which tend to dissociate and split off hydrogen ions [11 – 12].

The aqueous suspension of humic acids passes through a paper filter without visible change, and becomes clear again on addition of organic solvent. If the aqueous suspension is concentrated by evaporation on a boiling water bath, a dark brown resinous film is formed on the surface, while the suspension under it retains its brown color. This indicates that humic acids can be oxidized not only in alkaline solutions [13] but also under other conditions.

Humic acids, isolated from aqueous acetone or aqueous alcohol solutions and dried, consist of shiny dark brown flakes which are easily ground to a brown powder. The solubility in the above-named solvents decreases considerably after exposure to air, sunlight, or heat.

On the basis of the modern view that humic acids are mixtures of large numbers of organic compounds – polycyclic hydroxycarboxylic acids [14] – it seemed likely that different fractions of such mixtures may be dissolved. It was therefore of interest to compare the characteristics of the original humic acids (Preparation 1) with those isolated from aqueous acetone (Preparation 2) and aqueous alcohol (Preparation 3) solutions.

Experiments showed that the humic acid preparations are similar in external appearance, are completely soluble in excess aqueous alkali, and give precipitates with salts of alkaline-earth and heavy metals; this, of course, is the principal characteristic of humic acids. The different humic acid preparations were also compared by their carbon contents determined by Tyurin's method [15], and by the amounts of KOH combined with 1 g of the acids in the Fuchs reaction with alcoholic alkali.

The results of these experiments are given in Table 2.

It follows from Table 2 that humic acids isolated from aqueous acetone (Preparation 2) are similar to the original acids (Preparation 1) in carbon content and amount of combined alkali. Preparation 3, isolated from aqueous alcohol, shows somewhat greater differences from the original humic acids. However, even these differences are not very large. The chemical equivalent of the humic acids before and after solution, calculated from the KOH data, varies from 140 to 166, in agreement with literature data [16].

The almost complete solubility of humic acids in 60% aqueous acetone at room temperature, their high solubility in boiling 60% aqueous ethyl alcohol, and the above comparative data for the different preparations, all lead to the conclusion that humic acids behave as a single entity toward these solvents. Even if peat humic acids comprise a mixture of compounds, these compounds are evidently very similar in chemical nature and have a common form of structure. This conclusion is consistent with the results of other investigations [17].

SUMMARY

The solubility of peat humic acids was studied and it was found that they are completely soluble in 60 and 80% aqueous acetone solutions at room temperature, and somewhat less soluble in boiling 60% aqueous ethyl alcohol. Aqueous methyl alcohol had the lowest solvent power.

These solvents – mixtures of acetone or ethyl alcohol with water – may prove useful for isolation of humic acids from peat and for studies of their physicochemical characteristics.

LITERATURE CITED

[1] G. L. Stadnikov, Chemistry of Peat [in Russian] (State Tech. Press, 1932).

[2] S. Oden, Kolloidchemische Beihefte, 11, (1919).

[3] V. E. Rakovskii, General Chemical Technology of Peat [in Russian] (Gosenergoizdat, 1949).

[4] F. Hoppe – Seyler, Z. physiol. Ch., 13 (1889).

[5] D. Kreulen, Brennstoffchemie, 12 (1928).

[6] J. Jodl, Brennstoffchemie, 5 (1930).

[7] F. F. Dragunova, Proc. Acad. Sci. USSR 96, 1 (1951).

[8] V. E. Rakovskii and M. M. Zhuravleva, Collected Papers on the Chemistry and Genesis of Solid Mineral Fuels [in Russian] (Izd. AN SSSR, 1953).

[9] W. Fuchs, Brennstoffchemie, 12 (1928).

[10] P. A. Rebinder, Jubilee Volume of the Academy of Sciences USSR on the 30th Anniversary of the October Revolution, 1 [in Russian] (1947).

[11] A. V. Dumanskii and T. A. Granskaia, Colloid J. 4, 4 (1938).

[12] N. A. Izmailov, Trans. Sci. Res. Inst. Chem. Khar'kov State Univ. 7 (1950).

[13] P. K. Mél', Trans. Sci. Res. Inst. Peat 1 (1928).

[14] N. M. Karavaev, Collected Papers on the Chemistry and Genesis of Solid Mineral Fuels [in Russian] (Izd. AN SSSR, 1953).

[15] I. V. Tyurin, The Organic Matter of Soils [in Russian] (Agricultural Press, 1937).

[16] T. A. Kukharenko, Trans. Inst. Combustible Minerals Acad. Sci. USSR 5 (1955).

[17] M. M. Kononova, The Problem of Soil Humus and Modern Tasks in its Investigation [in Russian] (Izd. AN SSSR, 1951).

Received (for the second time) July 29, 1958

SIMULTANEOUS CONDENSATION OF SUBSTITUTED ORTHOSILICATE ESTERS AND AN ORTHOSILICATE ESTER WITH A POLYESTER

V. B. Losev

The polyester formed from glycerol and adipic acid taken in 2:1 molar ratio is a compound of high molecular weight containing hydroxyl groups in the molecule.

These hydroxyl groups can interact with the functional groups of organosilicon compounds [1]. On the basis of these considerations, we used glycerol – adipic acid polyester as the original organic polymer, and alkyl (aryl)-, di(tri)ethoxysilanes and an orthosilicate ester as the organosilicon compounds.

EXPERIMENTAL

The polyester was prepared in a five-necked flask fitted with a stirrer, thermometer, dropping funnel, inlet tube for carbon dioxide and a reflux condenser for removal of water liberated in condensation or of alcohol liberated in esterification.

A mixture of adipic acid (analytical grade, Technical Specification No. 2618-51) and glycerol (GOST 6259-52), the latter being in excess, was heated in the flask at 200 ± 2° in a continuous stream of carbon dioxide. The water formed in the process was continuously removed from the reaction zone. The reaction proceeded at a high rate at first, but the rate gradually diminished. The acid number was determined every 30 minutes; it was initially 340, and fell to below 10 at the end of the reaction (see diagram).

The reaction of polyester formation can be schematically represented as follows:

$$2x\mathrm{HO{-}CH_2{-}\underset{\displaystyle OH}{\underset{|}{CH}}{-}CH_2{-}OH} + x\mathrm{HOOC{-}(CH_2)_4{-}COOH} \longrightarrow$$

$$\longrightarrow \mathrm{HO}\left[\mathrm{-CH_2-\underset{\displaystyle OH}{\underset{|}{CH}}-CH_2-O-\overset{\displaystyle O}{\overset{\|}{C}}-(CH_2)_4-\overset{\displaystyle O}{\overset{\|}{C}}-O-CH_2-\underset{\displaystyle OH}{\underset{|}{CH}}-CH_2-O-}\right]_{3x}\mathrm{-H} +$$

$$+ (3x-2)\mathrm{H_2O}.$$

The group of atoms in the square brackets is the structural unit of the polyester ($n^{20}D$ = 1.4865, d^{20}_4 = 1.2633)[2].

When the acid number fell below 10, phenyltriethoxysilane, or a mixture of phenyltriethoxysilane with diethyldiethoxysilane or with tetraethoxysilane, was added (Table 1).

When these substances or mixtures were added, the reaction temperature fell from 200 to 165°. Further heating for 15-20 minutes at 200° was then necessary to complete the reaction [3]. The end of the reaction was indicated by gelation. The reaction mass frothed strongly and the resin adhered to the stirrer. When cooled, the contents of the flask consisted of a transparent brittle resin of a pale yellow color.

For lacquer preparation, the resins were dissolved in ethyl Cellosolve. The lacquers were applied onto brass plates and glass test tubes. They had good adhesion to these materials. The coated glass test tubes were

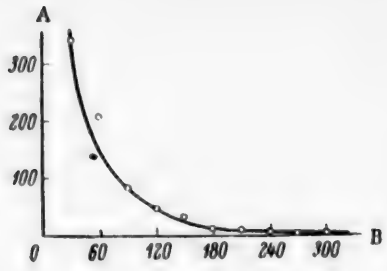

Decrease of the acid number of the polyester with time at 200°;
A) acid number, B) time (minutes).

tested for water resistance by immersion in a vessel containing water at room temperature. The lacquered test tubes showed no visible changes after 9 days; the weights of the tubes when dried with filter paper were unchanged. The lacquer films on brass plates did not show any visible changes after several hours in a thermostat at 200°; they remained transparent and elastic (Table 2).

The polyester and the products of combined condensation were analyzed by the usual methods: silicon was determined by saponification of a sample with hydrochloric acid and subsequent oxidation of the saponification products by nitric acid, and the acid number was found by titration of a sample in alcohol with 0.1 N KOH in presence of phenolphthalein (Table 3).

TABLE 1

Amounts of Starting Materials (in moles)

Substance	Variant		
	I	II	III
Glycerol	0.4	0.8	0.4
Adipic acid	0.2	0.4	0.2
Phenyltriethoxysilane	0.2	0.15	0.15
Diethyldiethoxysilane	—	0.18	—
Tetraethoxysilane	—	—	0.05

TABLE 2

Elasticity Changes of Lacquer Films During Drying at 200°

Characteristics	Variant		
	I	II	III
Drying time of lacquer film, imprint method (minutes)	20	15	20
Heat resistance of lacquer film, 3 mm bend test on the NIILK scale (hours)	18	200	120

Note: NIILK = Scientific Research Institute of Lacquers and Paints. (Publisher's note).

The analytical results suggest that the twofold decrease of acid numbers and silicon contents of the products of simultaneous condensation, as compared with the acid number of the original polyester and the silicon contents of the ethoxysilanes, is the result of interaction of the polyester with phenyltriethoxysilane, diethyldiethoxysilane, and ethyl orthosilicate. This interaction probably occurs in accordance with the following scheme:

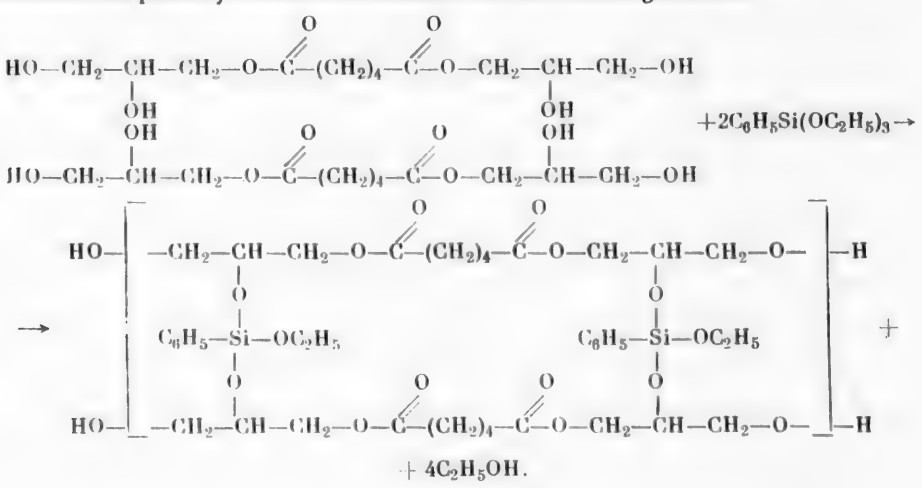

This is partially confirmed by the fact that the theoretical amount of ethyl alcohol is distilled off in all instances of simultaneous condensation of Variants I, II, and III.

TABLE 3

Analyses of Starting Materials and Final Products in Simultaneous Condensation

Sample No.	Substance	Si content (%)			Acid number (ml KOH/g)		
		I	II	III	I	II	III
1	Phenyltriethoxysilane	11.93	11.93	11.93	—	—	—
2	Diethyldiethoxysilane	—	16.75	—	—	—	—
3	Tetraethoxysilane	—	—	13.55	—	—	—
4	Polyester	—	—	—	8.66	5.93	8.00
5	Product of simultaneous condensation of 1 and 4	6.49	—	—	5.17	—	—
6	Product of simultaneous condensation of 1 and 2 with 4	—	6.37	—	—	3.09	—
7	Product of simultaneous condensation of 1 and 3 with 4	—	—	5.65	—	—	4.42

SUMMARY

Phenyltriethoxysilane, or a mixture of phenyltriethoxysilane with diethyldiethoxysilane or tetraethoxysilane, reacts chemically with the polyester by interaction of the ethoxyl groups of the aryl (alkyl) ethoxysilanes or their mixtures with hydroxyl groups of the resin, giving rise to new organosilicon compounds.

LITERATURE CITED

[1] K. A. Andrianov, Organosilicon Compounds [in Russian] (Moscow, Goskhimizdat, 1955) pp. 209, 472; A. P. Kreshkov, G. S. Petrov and A. D. Saenko, J. Appl. Chem. 22, 747 (1949).

[2] I. P. Losev and G. S. Petrov, Chemistry of Synthetic Resins [in Russian] (Goskhimizdat, 1951) pp. 346, 347.

[3] C. R. Hiles, B. Golding and R. N. Shreve, Ind. Eng. Ch., 1418 (1955).

Received December 31, 1957

PURIFICATION OF ADIPONITRILE

A. E. Kulikova, E. N. Zil'berman, Ts. N. Roginskaya and
M. M. Smirnova

Adiponitrile is an intermediate in the industrial synthesis of hexamethylene diammonium adipate (nylon salt), which is used in the production of polyamide resins. The production of adiponitrile stable on keeping and containing the minimum amounts of impurities is very important for the manufacture of polyamide resins of high quality. However, the production of such a material involves certain difficulties. The use of vacuum distillation does not ensure the production of adiponitrile of adequate purity. The constants of such adiponitrile fluctuate over a very wide range, and on keeping it turns yellow and then brown. Therefore adiponitrile conforming to the requirements of the polyamide industry is made by treatment of the vacuum-distilled product with various reagents. The patent literature contains a number of chemical methods for purification of adiponitrile: by means of potassium permanganate [1], sulfuric acid [2], bisulfite [3], etc.

This paper gives a method for purification of distilled adiponitrile, based on the results of chemical analyses and investigation of its ultraviolet absorption spectrum.

The ultraviolet spectrum of freshly-distilled adiponitrile shows very pronounced absorption at 265 mμ (Fig. 1, Curve 1). This absorption increases after storage for two weeks (Fig. 1, Curve 2). The considerable absorption shown by unpurified adiponitrile is due to the presence of compounds with conjugated double bonds. One such compound may be [1, 4] 1-amino-2-cyanocyclopentene-1,2 (I) or, as it is more often called, 1-imino-2-cyanocyclopentane, which is formed by isomerization of adiponitrile.

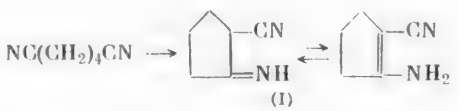

(I)

Indeed, the absorption spectrum of 1-amino-2-cyanocyclopentene-1,2 shown in Fig. 2 (λ_{max} = 265 mμ, ϵ_{max} = 17,600) differs little from the absorption spectrum of unpurified adiponitrile. The presence of (I) in unpurified adiponitrile is also confirmed by the fact that it requires much more hydrochloric acid for titration than does purified adiponitrile. Moreover, after hydrolysis by dilute hydrochloric acid under conditions in which nitrile groups are stable [5], unpurified adiponitrile gives a positive reaction with Nessler's reagent.

The small hump at 300 mμ in the absorption spectrum of unpurified adiponitrile (Fig. 1) indicates that it also contains cyclopentanone [6]. The results of chemical analysis indicate that such adiponitrile also contains compounds with carboxyl groups; probably δ-cyanovaleric, adipic, and other acids [5].

Since (I) is easily hydrolyzed by acids, we concentrated mainly on the sulfuric acid method for purification of adiponitrile. Purification of the original adiponitrile, containing 0.05 – 0.06% of easily hydrolyzed nitrogen, under conditions described in patents [2] yielded adiponitrile which was stable on keeping, and which contained 0.01% of easily hydrolyzed nitrogen. However, the spectrum of the purified product still indicated the presence of impurities in the adiponitrile (Fig. 1, Curve 3); probably 2-cyanocyclopentanone-1 (II) and cyclopentanone, formed by hydrolysis and decomposition [7] of 1-amino-2-cyanocyclopentene-1,2.

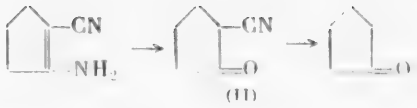

(II)

The presence of 2-cyanocyclopentanone-1 in adiponitrile purified by sulfuric acid is indicated by the similarity of its spectrum (Fig. 3) to the spectrum of adiponitrile (Fig. 1, Curve 3) in the 220 – 250 mμ region.

In view of the fact that after treatment of adiponitrile with sulfuric acid the predominant impurities in it contain carbonyl groups, the sulfuric acid method for purification of adiponitrile was supplemented by washing with ammonium bisulfite solution; this yielded adiponitrile of a high degree of purity (Fig. 1, Curve 4), similar to adiponitrile purified by the permanganate method (Fig. 1, Curve 5). After the sulfuric acid treatment and the subsequent washing with bisulfite solution, the adiponitrile contained 0.001% of easily hydrolyzed nitrogen.

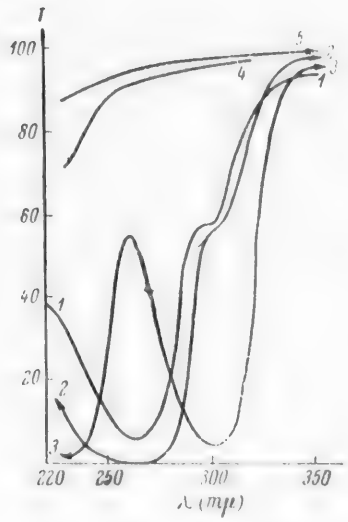

Fig. 1. Ultraviolet absorption spectra of adiponitrile: characteristics of adiponitrile: 1) unpurified, 2) unpurified, after two weeks of storage, 3) purified by means of sulfuric acid, 4) purified by the sulfuric acid – bisulfite method, 5) purified by the permanganate method.

The 1-amino-2-cyanocyclopentene-1,2 used in this investigation was prepared by cyclization of adiponitrile by the action of a suspension of sodamide in benzene [8].

We thank A. I. Finkel'shtein for his interest and valuable advice.

EXPERIMENTAL

Preparation and purification of adiponitrile. The original adiponitrile was prepared by the reaction of adipic acid with ammonia; after vacuum distillation it had d^{20}_4 = 0.9610, $n^{25}D$ = 1.4370, m.p. 2.1 – 2.3°, with permanganate number 4.0, acidity 0.001 meq/g, contained 0.05 – 0.06% of easily hydrolyzed nitrogen, and became brownon keeping. Its ultraviolet spectrum before and after storage is given in Fig. 1.

30 ml of 10% sulfuric acid was added to 200 g of adiponitrile, and the liquid was stirred at 30-35° for 30 minutes. The lower layer was then separated off, and the top layer was washed with 35 ml of 10% aqueous ammonia, then twice (with 30 ml for 1 hour each time) with ammonium bisulfite solution (800 g/liter), twice with water (30 ml each time), and twice with 10% aqueous ammonia (30 ml each time), and then distilled under vacuum; 136 g of a fraction boiling at 156° at 10 mm, d^{20}_4 = 0.9620, $n^{25}D$ = 1.4369, m.p. 2.40°, with permanganate number 0.15, acidity 0.002 meq/g, containing 0.001% of easily hydrolyzed nitrogen, was collected. Up to 10 g of substance was left in the distillation flask. An additional quantity of adiponitrile was extracted from the residue in the flask and the wash liquors.

Adiponitrile purified by sulfuric acid alone [2] solidified at 2.2° and had permanganate number 1.2, acidity 0.002 meq/g, and contained 0.01% of easily hydrolyzed nitrogen. The product purified by potassium permanganate had the same constants as adiponitrile purified by the sulfuric acid – bisulfite method. The ultraviolet spectra of adiponitrile purified by the permanganate, sulfuric acid, and sulfuric acid – bisulfite methods are given in Fig. 1. The infrared spectrum of adiponitrile with the maximum transmission in the ultraviolet region is given in Fig. 4.

Methods of adiponitrile analysis. The acidity of adiponitrile was determined by titration with 0.01 N alkali in presence of phenolphthalein.

For determination of easily hydrolyzed nitrogen, 10 g of adiponitrile was dissolved in water, 20 ml of 0.1 N hydrochloric acid was added, the mixture was shaken vigorously, and excess acid was titrated with 0.1 N alkali in presence of Methyl orange.

The permanganate number was determined by titration of adiponitrile solution with 0.01 N potassium per-

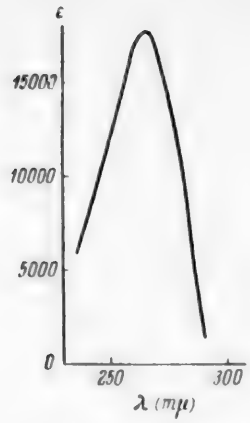

Fig. 2. Absorption spectrum of 1-amino-2-cyanocyclopentene-1,2 in the ultraviolet region.

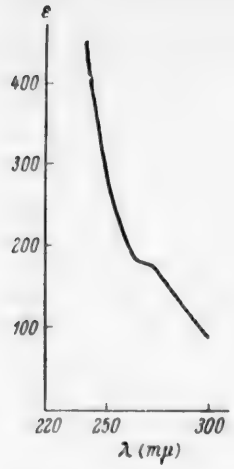

Fig. 3. Absorption spectrum of 2-cyanocyclopentanone-1 in the ultraviolet region.

manganate in presence of sulfuric acid to a faint pink color persisting for 1 minute. The permanganate number was expressed in meq $KMnO_4$ per g adiponitrile.

The ultraviolet absorption spectra were determined by means of the SF-4 photoelectric spectrophotometer. The concentration of the substance in methanol was 0.3%, and the thickness of the absorbing layer was 1 cm.

Infrared spectra were determined by means of the IKS-11 spectrophotometer. A LiCl prism and a KCl cell 0.06 mm thick was used in the 3-4.5μ region, and a NaCl prism and a KCl cell 0.1 mm thick in the 6.5-12μ region.

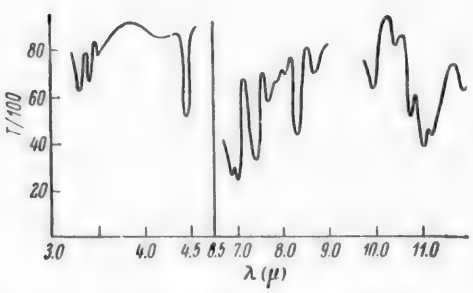

Fig. 4. Absorption spectrum of adiponitrile in the infrared region.

Synthesis of 1-amino-2-cyanocyclopentene-1,2 (I). The catalyst for synthesis of 1-amino-2-cyanocyclopentene-1,2 was a suspension of sodamide in benzene, made by addition of metallic sodium to liquid ammonia in presence of cobalt nitrate [9]. The benzene suspension of $NaNH_2$ (15.2 g sodium and 100 ml benzene) was heated to the boil, and a solution of 30 g of adiponitrile in 40 g of benzene was added during 2 hours. The reaction mass was carefully decomposed by means of 100 ml of water; two layers were formed, with solid 1-amino-2-cyanocyclopentene-1,2 at the boundary between them. The product was filtered off and washed with water. Additional small amounts of 1-amino-2-cyanocyclopentene-1,2 were isolated from the aqueous and benzene layers; the yield of (I) was 12-15 g (40-50%), m.p. 147.5° (from water); literature data [10], 147°.

Synthesis of 2-cyanocyclopentanone-1 (II). To 5 g of 1-amino-2-cyanocyclopentene-1,2 at room temperature 100 ml of 0.5 N hydrochloric acid was added and 2-cyanocyclopentanone-1 was extracted with ether from the resultant homogeneous solution. The ether extract was dried by calcium chloride and distilled under vacuum. The yield of product with b.p. 123-124° at 10 mm) and $n^{14}D = 1.4700$ was 4 g (80%); literature data [11]: b.p. 137-140° at 14 mm), $n^{14}D = 1.4701$.

SUMMARY

It is shown that if adiponitrile is treated with sulfuric acid and then washed with ammonium bisulfite solution it is possible to obtain a pure product, stable on keeping, with virtually no absorption of ultraviolet radiation in the 220-400 mμ region.

LITERATURE CITED

[1] U. S. Patent 2,305,103.

[2] Federal German Patent 901,887; Ref. Zhur. Khim. 38472 (1955); Federal German Patent 921,937, Ref. Zhur. Khim. 48259 (1956); U. S. Patent 2,711,991, Ref. Zhur. Khim. 66166 (1956).

[3] U. S. Patent 2,242,309, Chem. Abs. 35, 5517 (1941).

[4] C. F. Hamer and R. A. Hines, J. Am. Chem. Soc. 77, 3649 (1955).

[5] E. N. Zil'berman, J. Gen. Chem. 29, 2127 (1955).*

[6] G. Förster, R. Skrabal and J. Wagner, Z. Elektrochemie, 43, 290 (1937).

[7] O. Riobé and L. Govin, C. r., 238, 1235 (1954).

[8] M. S. Newman and R. D. Closson, J. Am. Chem. Soc. 66, 1553 (1944).

[9] T. H. Vaughn, R. R. Vogt and J. A. Nieuwland, J. Am. Chem. Soc. 56, 2120 (1934).

[10] S. R. Best and J. F. Thorpe, J. Chem. Soc., 95, 685 (1909).

[11] O. Riobé and L. Govin, C. r., 234, 1889 (1952).

Received May 16, 1957

* Original Russian pagination. See C. B. Translation.

PRODUCTION OF METHYL CHLORIDE BY CATALYTIC HYDROCHLORINATION OF DIMETHYL ETHER

R. M. Flid, K. S. Minsker and N. F. Skvortsova

Dimethyl ether is formed as a by-product in a number of industrial processes; this poses the problem of its efficient utilization. One of us [1] showed that it is possible to obtain carboxylic esters by catalytic reactions of dimethyl ether with carboxylic acids.

In the present investigation we studied the possibility of catalytic production of methyl chloride by the reaction

$$(CH_3)_2O_g + 2HCl_g \rightarrow 2CH_3Cl_g + H_2O_g$$

EXPERIMENTAL

Experimental and analytical procedures. Dimethyl ether (DME) was prepared by catalytic dehydration of methanol over γ-Al_2O_3 at 250-270° and was kept over saturated $CaCl_2$ + NaCl solution. Its purity was tested by the completeness of its absorption by concentrated H_2SO_4. Gaseous HCl, prepared by the action of concentrated H_2SO_4 on NH_4Cl, was kept in a gas holder over kerosene previously saturated with HCl.

Accurately measured amounts of DME and HCl were passed through drying columns with $CaCl_2$ and tubes with silica gel to adsorb kerosene vapor, mixed, and passed into the catalytic furnace with automatic heat control (±0.5°).

TABLE 1

Effect of Preliminary Saturation of the Catalyst with the Reaction Components HCl : $(CH_3)_2O$ ratio between 2 : 1 and 3 : 1; catalyst, $ZnCl_2$ on AR-3 activated carbon, t = 160° C, v = 350 liters/liter of catalyst · hour

Experimental conditions	Variation of CH_3Cl yield on the DME passed (%) with time (min)				
	30	60	90	150	240
Without preliminary saturation	83.2	68.2	52.3	43.5	65.2
Preliminary saturation with dimethyl ether	0.6	0.8	5.0	7.5	25.0
Preliminary saturation with hydrogen chloride	97.2	94.7	85.4	82.2	84.4

The reaction products passed successively through a condenser where water vapor was condensed, a wash bottle with concentrated H_2SO_4 to absorb unchanged DME, a wash bottle with water to absorb HCl, and traps

cooled in solid carbon dioxide with acetone for collecting the CH_3Cl formed.

The unchanged HCl was determined by titration with 0.1 N NaOH, and DME from the weight increase of the traps containing concentrated H_2SO_4. The purity of the CH_3Cl was checked by its boiling point (− 24.5 to − 24°) and occasionally by absorption in glacial acetic acid. The amount of CH_3Cl formed was found by evaporation of the product into a graduated gas holder. In no instance were any products formed other than those indicated above.

As a rule, the material balance agreed in all cases.

Catalysts were prepared by impregnation of the support with the appropriate salt solution, followed by evaporation and drying. The effects of temperature and DME: HCl ratio on the yield of methyl chloride were studied.

TABLE 2

Results of Comparative Tests on Different Catalysts in Relation to the Temperature Space velocity 300 − 400 liters/liter of catalyst · hour, $(CH_3)_2O$: HCl = 1:3 to 1:4

Catalyst	Yield of CH_3Cl on the dimethyl ether passed (%) at various temperatures (°C)							
	110	120	160	200	275	300	375	400
Pumice	—	13.5	—	13.2	—	13.6		
Glass					8.1	7.3	7.2	6.8
BAU carbon		—	15.4	18.2	24.6	24.8		
Mercuric chloride (10%) on AR-3 activated carbon	5.1	6.5	15.8	23.4				
Zinc chloride (30%) on BAU carbon	38.9	—	—	52.3	—	59.5	54.7	—
Zinc chloride (30%) on AR-3 carbon	—	95.0	97.7	93.2	90.8	71.5	—	—
Zinc chloride (30%) on aluminosilicate	—	—	—	47	84	81	—	—
Zinc chloride (30%) on kaolin	—	—	—	29	36	32	—	—
Cadmium chloride (30%) on AR-3 carbon	—	—	—	65	87	87	—	—
Cadmium bromide (30%) on AR-3 carbon	—	—	—	57	52	56	—	—
Cadmium iodide (30%) on AR-3 carbon	—	—	—	52	55	58	—	—
Zinc iodide (30%) on AR-3 carbon	—	—	—	44	65	60	—	—
Calcium chloride (30%) on AR-3 carbon				—	47	41	43	38
Bismuth chloride (30%) on AR-3 carbon				46	44	56	—	—
Ferric chloride (30%) on AR-3 carbon	—	—		74	60	60	—	—
Magnesium chloride (30%) on AR-3 carbon	—		—		30	46	51	—
Active alumina	—			—	—	73	96	95

Experimental Data and Discussion of Results

Effect of preliminary saturation of the catalyst. In tests on different catalysts it was found that the catalysts retain high and constant activity only after preliminary saturation with hydrogen chloride. In experiments without preliminary saturation the activity gradually fell and the material balance for hydrogen chloride did not agree. Preliminary saturation of the catalyst with hydrogen chloride led to almost complete inactivation during the initial period of operation. In such cases the yield of methyl chloride rose somewhat with time, but the catalyst activity remained very low. Table 1 contains data on the effects of preliminary saturation of the catalyst with the reaction components on the time variations of activity of $ZnCl_2$/carbon catalyst (t = 160° V = 350 liters/liter of catalyst · hour). Similar results were obtained in tests on other catalysts. Therefore in all the subsequent experiments the catalyst was first saturated with hydrogen chloride in order to ensure high and constant activity. It was found in further tests that after preliminary saturation of the catalyst with hydrogen chloride variations of the HCl: $(CH_3)_2O$ ratio between 3:1 and 6:1 have no effect on the yield of methyl chloride.

Effects of the nature of the catalyst and temperature on the CH_3Cl yield. The relative activities of different catalysts and supports were studied over a wide temperature range. The space velocity varied from 300 to 400 liters/liter of catalyst · hour in all cases. The HCl: $(CH_3)_2O$ ratio was from 3:1 to 4:1. The results are summarized in Table 2.

It is clear from the above results that methyl chloride can be obtained in considerable yields (90-95%) with the use of the following catalysts: γ-Al_2O_3, in the 375-400° C range; $ZnCl_2$ on AR-3 activated carbon, at 120-200° C; $CdCl_2$ on AR-3 activated carbon, at 275-300° C.

Preliminary saturation of the catalyst with gaseous HCl is necessary in all cases. The chlorides can be arranged in the following sequence according to activity:

$$ZnCl_2 > CdCl_2 > FeCl_3 > BiCl_3 > MgCl_2 > CaCl_2 > HgCl_2.$$

With a given cation, chlorides are more active than bromides and iodides. The nature of the support is also significant. Coarsely porous AR-3 activated carbon has the best properties. It must be pointed out that the high activity of γ-Al_2O_3, with CH_3Cl yields up to 95-96% on the dimethyl ether passed, is not reached at once. The catalyst activity gradually arises from 60% after the first hour of operation to 95-96% at the fourth hour, and then remains constant. The activity of $ZnCl_2$ catalyst on AR-3 carbon decreases with time from 93-95% to 78-82%, and does not rise even after regeneration by a current of HCl gas.

The need for preliminary saturation of the catalyst with hydrogen chloride was not unexpected.

We consider that under steady conditions activation of the components (DME and HCl) should result in the formation of a ternary complex with the composition: $(CH_3)_2O$ – catalyst – HCl [2].

No data are available on the possibility of complex formation between catalyst and DME or catalyst and HCl. However, by analogy with hydrate formation or with the tendency of salts to undergo hydrolysis, and as the result of approximate calculations, it was concluded that of the two initial components (DME and HCl), dimethyl ether should be the one predominantly activated; this should have high affinity with the above-named chlorides and γ-Al_2O_3.

Therefore, in order to avoid the formation of a stable binary complex of the catalyst with DME, leading to inactivation, the catalyst surface must first be saturated with hydrogen chloride, which tends to form a less stable complex than dimethyl ether with the catalyst.

SUMMARY

1. It is shown that methyl chloride can be produced by the catalytic reaction of dimethyl ether with hydrogen chloride.

2. The most effective catalysts are γ-Al_2O_3 (375-400°), $CdCl_2$ on AR-3 activated carbon (275-300°), and $ZnCl_2$ on AR-3 activated carbon (120-200°). At a space velocity of 300-400 liters/liter of catalyst · hour the respective CH_3Cl yields reach 95 – 96, 85 – 97, 78 – 82%.

3. The catalyst surface must first be saturated with hydrogen chloride to ensure retention of high activity.

LITERATURE CITED

[1] R. M. Flid, A. N. Protasova and E. A. Trakhtenberg, J. Gen. Chem. 6 (1957).*

[2] R. M. Flid, J. Phys. Chem. 32, 2339 (1958).

Received May 13, 1957

* Original Russian pagination. See C. B. Translation.

PRODUCTION OF ANHYDROUS SODIUM ACETATE FROM AN AQUEOUS METHANOL SOLUTION OF METHYL ACETATE

A. G. Sayadyan and A. E. Akopyan

The Erevan Polytechnic Institute

In the production of polyvinyl butyral, when polyvinyl alcohol is dissolved in water a mixture of approximately the following composition is distilled off: methanol 60-65%, methyl acetate 8-12%, acetaldehyde 0.3 – 0.6%; the residue is water and small amounts of impurities.

At the present time this aqueous methanol solution of methyl acetate is treated with caustic soda, so that methyl acetate is converted into methanol and sodium acetate. Methanol is then distilled off, rectified, and recycled, and the dilute and impure aqueous solution of sodium acetate remaining after distillation of the methanol is discharged to waste.

Therefore the alkaline treatment of the aqueous methanol solution of methyl acetate results merely in recovery of methanol, while the acetic acid consumed in the formation of the original vinyl acetate and converted to methyl acetate in the production of polyvinyl alcohol is almost all lost as sodium acetate. The recovery of sodium acetate from impure dilute aqueous solutions involves technical difficulties and is uneconomic when the production scale is small.

In this paper we propose a new and very simple method for regeneration of aqueous methanol solutions of methyl acetate, which yields pure anhydrous sodium acetate in addition to methanol. The essential difference between this method and the existing process is that a mixture of methyl acetate and methanol obtained from the aqueous methanol solution of methyl acetate by rectification is saponified, and not the original solution.

Patent information is available on the production of sodium acetate from methyl acetate. According to one patent [1], sodium acetate is made by treatment of acetate esters with sodium carbonate or bicarbonate at high temperatures (125 – 130°) and pressures, in presence of small amounts of water. This temperature range and the presence of water are necessary because of the poor solubility of the alkali in the original esters. In our proposed method, because of the presence of large amounts of methanol in the reaction mixture methyl acetate can be saponified in absence of water at an adequate rate at the boiling point of the reaction mixture, 55-60°.

EXPERIMENTAL

A series of experiments was performed in order to study processes for removal of acetaldehyde from the original mixture, and saponification of methyl acetate in relation to its concentration in the methanol solution and the relative proportions of methyl acetate and caustic soda. Although these reactions have already been studied in detail, in view of the special conditions it was necessary to conduct some check experiments.

Removal of acetaldehyde from the original mixture. It is necessary to remove aldehyde from the aqueous methanol solution of methyl acetate because acetaldehyde passes into the methanol – methyl acetate fraction during rectification; when methyl acetate is saponified by alkali the acetaldehyde is resinified and colors the sodium acetate. It was shown that sodium acetate is not colored if the acetaldehyde content of the mixture does not exceed 0.08%.

Sodium bisulfite was used for the purification. From 1 to 5 vol.% of 40% sodium bisulfite solution was added to the aqueous methanol solution of methyl acetate, the mixture was gently warmed and stirred for

0.5 hour. The mixture was then distilled through a laboratory column 35 mm in diameter and 1200 mm high, acetaldehyde being determined in the distillate. It was found that after addition of 2.5 – 3.0 vol.% of 40% sodium bisulfite solution the aldehyde content of the methanol – methyl acetate mixture is 0.05 – 0.07%.

Effect of Methyl Acetate Content on Saponification

Methyl acetate content of original mixture (%)	Methyl acetate contents of samples (%) after time (hours)				
	0.5	1	2	3	4
5	0.85	0.51	0.31	0.26	0.12
10	0.99	0.66	0.40	0.29	0.14
15	1.08	0.65	0.38	0.28	0.14
20	1.56	0.88	0.43	0.34	0.17

Effect of methyl acetate concentration on the saponification process. A methanol – methyl acetate mixture containing 20% methyl acetate and 0.07% acetaldehyde was used in these experiments. Solutions containing 5, 10, and 15% methyl acetate were prepared from this solution for the separate experiments by dilution with methanol. To 200 ml of each of these solutions was added caustic soda in an amount equivalent to the methyl acetate present, and the mixture was heated on a water bath in a flask under reflux. Samples were taken at various time intervals with a pipet, and the amounts of unchanged methyl acetate in them were determined.

The results of these experiments are given in the table.

The results in the table show that saponification of methyl acetate in methanol solution proceeds fairly readily, and variations of the methyl acetate concentration in the original mixture in the 5-20% range have almost no effect on the saponification time. Most of the methyl acetate (over 90%) reacts within 0.5 hour in all cases. Saponification of the remaining methyl acetate requires much more time (3-4 hours).

Effect of alkali concentration on saponification. The purpose of these experiments was to determine the effects of excess alkali in the solution on the rate and extent of the process. A solution containing 14% methyl acetate and 0.06% acetaldehyde was used for these experiments. The solution was prepared from aqueous methanol solution of methyl acetate by purification with bisulfite and subsequent distillation. The experimental conditions were the same as in the preceding experiments, but in presence of 5, 10, and 15% excess alkali. It was found in these experiments that the effect of up to 5% excess alkali on saponification is very slight (after 4 hours 0.08% free methyl acetate remains in solution). If more than 10% excess alkali is present, the reaction is already complete after 2-3 hours. However, excess alkali increases the alkalinity of the product (sodium acetate) which is not permitted by GOST 208-43. Therefore additional experiments were performed on saponification of methyl acetate with a deficiency of alkali. In these experiments the amounts of alkali taken were 3-5% below the theoretical. In experiments lasting 4-5 hours the free alkali content of the sodium acetate samples was 0.05 – 0.08%, and the methanol distilled off after the reaction contained 0.5 – 0.7% methyl acetate. The presence of this amount of methyl acetate in the recycled methanol does not cause any difficulties in its use for the production of polyvinyl alcohol, while the sodium acetate obtained has an admissible alkali content.

Another feature of the proposed method is that it can be easily performed in existing equipment for methanol recovery, only small changes in the connections being necessary. The technological details of the process are as follows: 2.5 – 3.0 vol. % of 40% sodium bisulfite solution is added to the aqueous methanol solution of methyl acetate, the mixture is stirred for 0.5 – 1 hour, and distilled. The distillate, consisting of 12 – 15% solution of methyl acetate in methanol, is saponified with caustic soda, the amount of the latter being 3 – 5% below the amount equivalent to the methyl acetate present. The process is continued at the boil for 4-5 hours in a reactor fitted with a stirrer, heater, and reflux condenser. At the end of the process methanol is distilled off completely and returned to the polyvinyl alcohol cycle. If it should be necessary to use the recovered methanol as solvent for vinyl acetate polymerization, it should probably be rectified. After distillation of the methanol, the sodium acetate present in the reactor is cooled and discharged.

SUMMARY

1. A new process for regeneration of aqueous methanol solutions of methyl acetate has been developed, which yields pure anhydrous sodium acetate in addition to methanol.

2. The method can be easily used with existing equipment for methanol recovery in polyvinyl butyral production.

LITERATURE CITED

[1] German Patent 472,123 (1926).

Received May 8, 1957

SYNTHESIS OF QUATERNARY AMMONIUM SALTS FROM A BROAD FRACTION OF HIGH-MOLECULAR ALIPHATIC ALCOHOLS MADE BY OXIDATION OF PARAFFINIC HYDROCARBONS FROM PETROLEUM

V. P. Érekaev and M. P. Gerchuk

The G. V. Plekhanov (Order of the Red Banner of Labor) Institute of National Economy, Moscow

Quaternary ammonium salts of the type $[b\overset{a}{\underset{R}{N}}c]\,x$; where a, b, and c are relatively short radicals (CH_3, C_2H_5, $C_6H_5CH_2$); R is a radical containing from 8 to 18 carbon atoms, and x is one of the following anions: Cl', Br', I', SO_4", or CH_3', have become widely used in industry, agriculture, and medicine in foreign countries in recent years. Compounds of this type have surface-active and bactericidal properties and are used in dyeing and scouring of fabrics, in ore flotation, in the manufacture of rubber and paper, for washing of equipment in the food industry, and as disinfectants, herbicides, and fungicides [1].

The existing methods for production of quaternary ammonium salts essentially consist of the condensation of pyridine [2], quinoline [3], dimethylbenzylamine [4], amino ethers [5] or other tertiary amines with alkyl halides of high molecular weight. Difficulties in carrying out synthesis of this type on the large scale arose because of shortages of high-molecular alcohols or acids required for the production of alkyl halides of high molecular weight. Coconut oil, whale oil, edible fats, products of hydrocarbon chlorination, and natural higher fatty acids were generally used for this purpose. Shortages of all these materials constituted the main obstacle to the large-scale production of quaternary ammonium salts. In the USSR cation-active substances are still not being widely used.

We have developed a convenient method [6] for the production of quaternary ammonium salts on the industrial scale. The starting material was a broad fraction of high-molecular aliphatic alcohols made by catalytic oxidation of paraffinic hydrocarbons by the method worked out in the Institute of Petroleum of the Academy of Sciences USSR by Bashkirov et al. [7]. Halogenation of the broad alcohol fraction yielded a mixture of alkyl halides of high molecular weights. Treatment of pyridine or pyridine bases with this mixture of high-molecular alkyl halides gave a mixture of alkylpyridinium salts. Treatment of diethylbenzylamine with the mixture of high-molecular alkyl halides yielded a mixture of diethylalkylbenzylammonium salts.

For characterization of our quaternary ammonium salts, we determined their surface tension and wetting power. The results were compared with the corresponding data for cetylpyridinium bromide. It is clear from Table 1 that alkylpyridinium halides lower the surface tension of water considerably and have high wetting power.

The microbiological properties of our alkylpyridinium halides were tested at the All-Union Scientific Research Institute of Pharmaceutical Chemistry (Table 2). Pure cetylpyridinium bromide was taken for comparison. It is clear from the data in Table 2 that our quaternary ammonium salts have pronounced bacteriostatic effects on a number of microorganisms. It was also found that these substances have bactericidal and fungicidal effects.

We developed methods for preserving fresh hides by means of quaternary ammonium salts, on the basis of their bacteriostatic properties.

Our experiments, performed jointly with V. G. Leites in the Department of Animal Raw Materials of the Veterinary Academy, showed that our quaternary ammonium salts, used in quantities of 0.1 – 0.4% on the fresh

TABLE 1

Surface Tension and Wetting Power of Quaternary Ammonium Salts

Substance	Solution concentration (%)	Surface tension (ergs/cm²)	Wetting power
Alkylpyridinium bromide (solid product)	0.5	30.6	0.81915
	0.25	34.2	0.78079
	0.125	42.0	0.73924
Alkylpyridinium iodide (liquid product)	0.5	28.4	0.80212
	0.25	31.16	0.78801
	0.125	33.28	0.75851
Diethylalkylbenzylammonium bromide	0.5	34.73	0.78801
	0.25	44.13	0.74314
	0.125	53.25	0.72837
Cetylpyridinium bromide	0.5	30.56	0.73135
	0.25	30.67	0.69151
	0.125	31.95	0.67559

TABLE 2

Bacteriostatic Action of Quaternary Ammonium Salts

Microorganism	Growth of microorganisms inhibited at dilution		
	alkylpyridinium bromide	alkylpyridinium iodide	cetylpyridinium bromide
Staphylococcus aureus	1 : 819200	1 : 1638000	1 : 1024000
Hemolytic streptococcus	1 : 409600	1 : 409000	1 : 1204000
Escherichia coli	1 : 51200	1 : 204000	1 : 128000
Flexner's bacillus	1 : 102400	1 : 204000	1 : 128000
Diphtheria bacillus	1 : 204800	1 : 409600	1 : 512000
Anthracoid spores	1 : 51200	1 : 102400	1 : 64000
Mycobacterium tuberculosis var. hominis (extensive growth)	1 : 1638400	1 : 1638000	1 : 8192000
Avian tubercle bacillus	1 : 65536000	1 : 1638000	1 : 4096000
Acid-fast saprophyte B_5	1 : 3276800	1 : 1638000	1 : 256000
Trichophyton	1 : 204800	1 : 204000	1 : 256000
Achorion	1 : 204800	1 : 204000	1 : 2048000
Actinomycetes	1 : 204800	1 : 1638000	1 : 512000

hide weight, preserved the hides for longer times than were achieved in a control experiment on hides salted by the usual process [8], and it was found that the quaternary salts are suitable for disinfection of equipment used in the fish and yeast industries for sterilization of surgical instruments.

As our method for the production of quaternary ammonium salts is based on the use of readily available oxidation products of paraffinic hydrocarbons from petroleum, it opens up extensive possibilities for the use of these compounds as disinfectants, preservatives, detergents, wetting agents, herbicides, and fungicides.

EXPERIMENTAL

Preparation of mixed alkyl halides of high molecular weight from mixtures of high-molecular alcohols. The starting material was a broad fraction of alcohols made by catalytic oxidation of paraffinic hydrocarbons (C_{10}—C_{30}), boiling in the 130-230° C range (15 mm). 121 g of this fraction was boiled with stirring for 5 hours

with 168 g of 48% hydrobromic acid. The bromides were washed with sulfuric acid and aqueous ammonia solution, and distilled. The boiling range was 165-295° C (17 mm), yield 125 g (82% of theoretical). 121 g of the alcohol fraction was heated with 5 g of red phosphorus and 67 g of iodine to give a mixture of alkyl iodides. Boiling range 135 – 210° C (5 mm), yield 128 g (72% of theoretical).

Preparation of alkylpyridinium salts. To 30.5 g of the alkyl bromide fraction, heated on an oil bath to 150° C, 8 g of pyridine was added during 2 hours. The precipitate was crystallized from ethyl acetate. The liquid product was washed with ethyl acetate. The solid reaction product was a colorless crystalline mass, readily soluble in water and alcohol. Yield 5.7 g. The liquid product was a viscous mass, readily soluble in water and alcohol and insoluble in ether. Yield 8.8 g. The total yield of solid and liquid alkylpyridinium bromides was about 40% of theoretical.

Alkylpyridinium iodides, a brown mass, were prepared analogously from 35.2 g of alkyl iodides and 8 g of pyridine. Yield 20.0 g (54.5% of theoretical).

Preparation of diethylalkylbenzylammonium salts. 16.3 g of diethylbenzylamine was added to 35.2 g of the alkyl iodide fraction heated on an oil bath to 150° C. The mixture of diethylalkylbenzylammonium iodides was a faintly yellowish crystalline mass, readily soluble in water. Yield 23.5 g (45% of theoretical).

SUMMARY

In the development of an industrial method for the production of quaternary ammonium salts from mixtures of high-molecular alcohols made by direct oxidation of petroleum paraffins it was found that diethylalkylbenzylammonium and alkylpyridinium salts prepared by this method have bactericidal, bacteriostatic, fungicidal, wetting, surface-active, and preservative properties.

LITERATURE CITED

[1] G. Domagk, Münch. Med. Wochenschr., 61, 829 (1935); Vashkov, Manual of Disinfection and Insect and Rat Control [in Russian] (Medical Press, 1956) p. 102; P. V. Naumenko, Oil and Fat Ind. 3, 44; 7, 44 (1957); A. I. Gershenovich, Chem. Sci. and Ind. 1, 3, 298 (1956); A. Schwartz and J. Perry, Surface Active Agents IL, (1953) pp. 448, 489, 153-195 [Russian translation]; R. Vuillaume, Recueil de Médicine vétérinaire, 606 (1951).

[2] British Patent 79,396; G. S. Fawcett, J. Chem. Soc., 396 (1934); S. V. Zhuravlev, N. D. Sukhareva and E. K. Chadova, Trans. TsNIDI 8, 125 (1954).

[3] U. S. Patent 2,048,885; British Patent 401,707.

[4] G. Domagk, U. S. Patent 2,108,765; German Patent 680,599, 708,076 French Patent 806,662; R. A. Reck and H. J. Harwood, Ind. Eng. Ch., 45, 1022 (1953).

[5] German Patent 704,338; U. S. Patents 1,987,228, 2,098,203, 2,115,192, 2,231,502, 2,334,517, 1,290,880 2,297,221, 2,312,135; British Patent 517,114; French Patents; 832,288, 837,604; H. Sturm, E. Konermann, Ind. Eng. Ch., 45, 186 (1953).

[6] V. P. Érekaev and M. P. Gerchuk, Chem. Sci. and Ind. 2, 5, 666 (1957); Certificate No. 7633 of the Committee for Inventions and Discoveries SM USSR priority from September 1, 1957.

[7] A. N. Bashkirov, Chem. Sci. and Ind. 1, 3, 273 (1956).

[8] M. P. Gerchuk, V. G. Leites and V. P. Érekaev, Authors' certif. 103,707 (1953).

Received April 15, 1957

ALL-UNION CONFERENCE ON THE CHEMISTRY AND PRACTICAL USES OF ORGANOSILICON COMPOUNDS

V. B. Losev

The 2nd All-Union Conference on the Chemistry and Practical Uses of Organosilicon Compounds was held in Leningrad from September 25 to 27, 1958.

The Conference was organized by the Division of Technical Sciences and the Institute of Silicate Chemistry of the Academy of Sciences USSR, the D. I. Mendeleev All-Union Chemical Society, the State Committee for Chemistry of the Council of Ministers USSR, and the National Economy Council of the Leningrad Economic Administrative Region; it was attended by more than 650 specialists in the organic chemistry of silicon, representing various institutions of the Academy of Sciences USSR, a number of universities, and many branch institutes.

Papers by eminent scientists were presented and discussed at the Conference; the authors included Academicians A. N. Nesmeyanov and A. V. Topchiev; Corresponding Members of the Academy of Sciences K. A. Andrianov and A. D. Petrov; Doctors of Science B. N. Dolgov and A. P. Kreshkov and Scientists from China, Czechoslovakia, Poland, Hungary, and Yugoslavia; there were more than 100 papers in all.

The Conference was opened by a plenary session at which Corresponding Member (AN SSSR) K. A. Andrianov presented a review paper. In his paper K. A. Andrianov considered the most important stages and trends in the synthesis of organosilicon polymers and described the great potentialities latent in this interesting field of polymer chemistry. Synthesis of the following polymers are the main stages in the production of high-molecular organosilicon compounds.

1. Synthesis of polymers containing elements such as Ti, Al, Ni, etc., with molecules of linear and branched structure, and especially of linear crystalline polymers, for the production of rubbers, greases, and plastics of high thermal stability.

2. Synthesis of polymers with heteroorganic molecular chains, containing hydrocarbon, ester, isocyanate and similar groups in the molecular chains together with siloxane groups. The production of linear polymers of the fiber-forming type may be expected in this group.

3. Synthesis of polymeric organosilicon compounds with organic molecular chains. For this active catalysts must be sought, for conversion of unsaturated silicon derivatives of hydrocarbons into polymers of high molecular weights.

Organosilicon compounds and materials based on them are widely used in various branches of the national economy. They are used as lubricants, liquids for hydraulic systems, heat-transfer media, antifoaming additives, pump oil, etc. They are used with success as adhesive, impregnating, water- repellent, and heat-resisting coatings with good dielectric properties.

The development of organosilicon chemistry is determined by the demands of modern technology. The trend for the immediate future is the creation of new highly thermostable organosilicon polymers for use at temperatures in the 200-500° range.

The work of the Conference was concentrated in four main sections: organosilicon monomers, organosilicon polymers, analysis and physicochemical methods for investigation of organosilicon compounds, and practical applications.

The extensive industrial uses of various organosilicon polymers have made it necessary to develop new methods for the production of organosilicon monomers — alkyl and aryl halosilanes — which are the starting materials for these polymers. The section of organosilicon monomers was concerned with this problem.

A paper on the phenylation of trichlorosilane, presented by N. N. Tishina, K. A. Andrianov, S. A. Golubtsov, M. I. Kafyrov, R. L. Darashkevich, et al., was of great practical interest.

They showed that phenyltrichlorosilane can be produced by a new technological process with technical and economic characteristics approximating to those of direct synthesis in a fluidized bed.

The paper by I. V. Trofimova, K. A. Andrianov, and S. A. Golubtsov contained new data on the synthesis of trichlorosilane by the action of hydrogen chloride on silicon in a fluidized bed, with agitation of the silicon powder by the current of hydrogen chloride; in this way productivity can be increased more than 10-fold, and the composition of the reaction products can be regulated more economically by variations of temperature.

Reactions of compounds containing Si — H bonds form a promising branch of the chemistry of organosilicon compounds. A paper by M. E. Dolgaya, E. A. Chernyshov, and Li Kuang-lian dealt with development of methods for the synthesis of aromatic organosilicon monomers by reactions of hydrosilanes with aromatic hydrocarbons in presence of catalysts, with formation of Si — C bonds and liberation of hydrogen, and by reactions of hydrosilanes with aryl halides at elevated temperatures with formation of Si — C bonds and liberation of hydrogen chloride.

Research into new methods for synthesis of trialkyl(aryl) siloxy derivatives of elements of groups III, IV, and V of Mendeleev's periodic systems, and studies of the reactions of triorganosilanols with titanium and vanadium halides and alkoxy derivatives, with orthoboric and phosphoric acids, and with oxides of boron, phosphorus, vanadium, and antimony were described in an extensive paper by N. F. Orlov, B. N. Dolgov and M. S. Voronkov.

Papers were presented on the behavior of various dichloro alkanes and dichloro alkenes with chlorine atoms at the same carbon atom or at different carbon atoms in symmetrical and asymmetrical molecules under conditions of direct synthesis (G. I. Nikishin, A. D. Petrov and S. I. Sadykh-zade); on the catalytic addition of hydrosilanes to unsaturated compounds (V. A. Ponomarenko, V. G. Cherkaev, G. V. Odabashyan, N. A. Zadoroshnyi and A. D. Petrov); on the catalytic reactions of alkyldichlorosilanes with benzene and its derivatives (E. P. Mikheev, G. N. Mal'nova, et. al.); on the synthesis of organogermanium compounds (V. F. Mironov, V. A. Ponomarenko, G. Ya. Vzenkova, I. E. Dolgii and A. D. Petrov); on new methods for the synthesis of organosilicon vinyl ethers (S. I. Sadykh-zade and A. D. Petrov); and on thermal telomerization of silicon hydrides with ethylene (A. N. Nesmeyanov, R. Kh. Friedlina, A. A. Karapetyan and E. Ts. Chukovskaya).

Papers presented at the section of organosilicon polymers included new data on the simultaneous hydrolysis of equimolecular mixtures of diethyldichlorosilane with phenyltrichlorosilane, which is the principal reaction in production of polyorganosiloxane resins (A. G. Kuznetsova, K. A. Andrianov and D. Ya. Zhinkin) and the results of a study of the catalytic polymerization of di- and trifunctional compounds for the production of soluble polymers of high viscosity, which influences the properties of the resultant varnishes and electrical insulating materials (S. N. Dzhenchel'skaya, K. A. Andrianov and Yu. K. Petrashko).

Several papers at the organosilicon polymer section dealt with the synthesis and properties of polysiloxane rubbers. K. A. Rzhendzinskaya and I. K. Stavitskii reported on the synthesis of SKT-Kh5 chlorinated polysiloxane rubber, with higher adhesion to metals and better frost and heat resistance than SKT dimethylsiloxane rubber.

N. B. Baranovskaya, A. A. Berlin, M. S. Zakharova and A. I. Mizikin reported on the development of a method for vulcanization of liquid and rubberlike polydimethylsiloxanes at room temperature, based on the interaction of hydroxyl end groups of the polymer in presence of organometallic compounds — orthotitanate esters and a mixed catalyst, a solution of an organotin compound in tetraethoxysilane. Sealing compositions which harden at room temperature were developed from the liquid polydimethylsiloxanes. They can pass in a few hours from the viscofluid state to become rubberlike materials with good dielectric properties.

An interesting communication was presented by A. I. Glukhova, K. A. Andrianov, L. N. Kozlovskaya and K. F. Kalushenina on the production of a rubberlike material, based on the tendency of polydimethylsiloxane and heat-resistant organic polymers to undergo degradation under the influence of mechanical forces and heat. The resultant rubberlike material has high mechanical strength, 100-180 kg/cm^2 as against 30-40 kg/cm^2 for the

polymethylsiloxane rubbers 5R-129, MR-2, etc., and it retains these properties between −75° and +350°.

An important step in the development of organosilicon polymers is the synthesis of polymers with inorganic chains. A. A. Zhdanov and K. A. Andrianov described methods for the synthesis of polymers the molecular chains of which contained alternating atoms of silicon, oxygen and metals, and also oxygen and aluminum atoms.

Interesting data on the synthesis of polyamides from dicarboxylic acids containing silicon were presented in a paper by V. V. Korshak, G. M. Frunze, E. V. Kukharskaya and D. I. Andreeva. These polyamides have higher reversible elasticity than the analogous polymers.

A serious disadvantage of the organosilicon polymers used in industry is their low mechanical strength, due to the small intermolecular forces. Various methods are used to eliminate this defect; one of these is the introduction of polar groups into the organic radical at the silicon atom. This changes the polarity of individual segments of the polymer chain, and the intermolecular forces are thereby increased (L. M. Volkova, K. A. Andrianov, G. E. Golubkov, L. N. Makarova and V. A. Odinets).

A subject of great interest is the development of methods for using organosilicon polymers in conjunction with polymeric organic compounds, whereby the technical properties of various materials based on compounds from both these classes are improved. N. Ya. Guretskii, A. P. Kreshkov and P. A. Andreev studied the chemistry of the interaction of a number of organosilicon compounds with cellulose under various conditions. Tests of the combined products showed them to be of practical value as film formers.

Extensive utilization of organosilicon polymers in the national economy was considered in the papers at the section on the practical applications of organosilicon compounds.

A paper by N. P. Kharitonov and B. N. Dolgov dealt with new heat, moisture, and electrical insulating materials based on organosilicon compounds, which ensure prolonged protection at 300-350°, have high resistance to the effects of sharp temperature changes in the range of −70 to +350° and good water resistance and dielectric properties. These materials can replace ordinary and vitreous enamels, and are very resistant to oxidizing agents, corrosive media and solvents.

Very interesting communications dealt with the production of water-repellent glass fabrics with polyester binders containing organosilicon compounds with groups, capable of undergoing hydrolysis in presence of moisture present on the glass fiber surface, attached to the silicon atom, and also with unsaturated groups such as methacrylate, allyl and vinyl (B. A. Kiselev, Z. A. Zinov'eva, Ya. D. Avrasin and P. V. Davydov); and with the production of thermostable and strong foam materials based on organosilicon resins combined with phenol–formaldehyde and epoxy resins and nitrile rubbers (M. Ya. Borodin, Z. I. Kazakova, A. P. Koroleva and V. A. Popov).

N. V. Kalugina and M. G. Voronkov reported on the use of the organosilicon preparations A-4, A-19 and MSN as water-repellent treatments for cotton fabrics; E. K. Mamin ov discussed the use of organosilicon preparations MN-1, EN-1, A-3, A-4, A-11, A-12, MSN, ESN, FSN and others for water-repellent impregnation of leather and leather substitutes; N. A. Afonchikov, G. V. Kolobova, P. N. Mikhailov and M. G. Voronkov described the use of organosilicon preparations for paper sizing, and V. N. Khramova and A. P. Kreshkov discussed the increase of the frost resistance of cements by organosilicon additives.

In the section dealing with analysis and physicochemical investigation methods, communications by S. V. Syavtsillo, E. A. Bondarevskaya, A. P. Kreshkov, B. M. Luskina, A. P. Terent'ev, V. T. Shemyatenkova and L. M. Shtifman were concerned with the development of modern rapid control methods in the production of monomers and polymers; the paper by K. K. Popkov was on quantitative determination of alkylchlorosilanes by a spectroscopic method; Yu. Ya. Mikhailenko reported on infrared spectroscopy of organosilicon compounds; and papers by A. V. Topchiev, G. M. Panchenkov, N. S.Nametkin, A. A. Gundyrev and Ku Ch'ang-li dealt with studies of the effects of temperature on the viscosity and density of certain classes of organosilicon compounds and the relationship between the structure and the energy of interaction of these molecules.

The resolution adopted by the Conference noted both the achievements and the failures in the field of synthesis of organosilicon monomers and polymers. There were no papers on the theory of technological processes, equipment design calculations and planning, or new types of equipment for the production of organosilicon compounds, and only a few papers on the synthesis of methylchlorosilanes.

The Conference elected a commission for the adoption of a unified nomenclature of organosilicon compounds.

It was proposed to hold the 3rd All-Union Conference on the Chemistry and Practical Uses of Organosilicon Compounds in 1960.

ERRATA

Volume 31, Number 9, June 1958

Page	Line	Reads	Should Read
1376	The footnote was omitted. It should read as follows:		
	*The values obtained for degree of polymerization and molecular weight of cellulose are somewhat low, as the specific viscosity was determined with access of air.		
1380	11 from top	n_T	η_T
1381	12 from top	phthalate (DEP) phthalate (DEP) sebacate (DBS)	phthalate (DBP) phthalate (DOP) sebacate (DOS)
1386	1-2 of Table 1	CYT	days
1406	10	$3\underset{\downarrow}{\overset{\times}{PbSO_4}} + 2K_3PO_4 \rightleftarrows \underset{\downarrow}{Pb_3(PO_4)_2} + 3\overset{\times}{K_2SO_4}.$ $La_2O_3 + 7C = 2LaC_2 + 3CO.$	
1410	14	$La_2O_3 + 7C = 2LaC_2 + 3CO.$ $3\underset{\downarrow}{\overset{\times}{PbSO_4}} + 2K_3PO_4 \rightleftarrows \underset{\downarrow}{Pb_3(PO_4)_2} + 3\overset{\times}{K_2SO_4}.$	

SIGNIFICANCE OF ABBREVIATIONS MOST FREQUENTLY ENCOUNTERED IN SOVIET CHEMICAL LITERATURE

Abbreviation (Transliterated)	Significance
FIAN	Phys. Inst. Acad. Sci. USSR
GIPKh	State Institute of Applied Chemistry
GIREDMET	State Rare Metals Scientific Research Institute
GITI	State Sci.-Tech. Press
GITTL	State Tech. and Theor. Lit. Press
GLAVKhIM	Main Administration of the Chemical Industry
GOI	State Optical Institute
GONTI	State United Sci.-Tech. Press
Goskhimizdat	State Chem. Press
GOST	All-Union State Standard
Gostoptekhizdat	State Scientific and Technical Publishing house of the Petroleum and Mineral Fuel Industry
GTTI	State Tech. and Theor. Lit. Press
IFKhA	Institute of Physicochemical Analysis
IL	Foreign Lit. Press
IOKhAN	Institute of Organic Chemistry of the Academy of Sciences of the USSR
IONKh	Institute of General and Inorganic Chemistry (N. S. Kurnakov)
IONKhAN	Institute of General and Inorganic Chemistry of the Academy of Sciences of the USSR
INBI	Institute of Biochemistry
IREA	Institute of Chemical Reagents
ISN (Izd. Sov. Nauk)	Soviet Science Press
IVKhTI	Ivanovo Chemical Engineering Institute
Izd. AN SSSR	Acad. Sci. USSR Press
Izd. MGU	Moscow State Univ. Press
KEIN	Colloid Electrochemical Institute
Khimizdat	Chemistry Press
LGU	Leningrad State University
LIM	Leningrad Institute of Metals
Metallurgizdat	Metallurgy Press
MITKhT	Moscow Institute of Fine Chemical Technology
OIYaI	Joint Institute of Nuclear Studies
OKhN	Division of Chemical Science
ONTI	United Sci.-Tech. Press
OTI	Division of Technical Information
OTN	Division of Technical Science
RIAN	Radium Institute, Academy of Sciences of the USSR
RZhKhim	Chemical Abstract Journal (USSR)
VKhO	All-Union Chemical Society (Mendeleev)
ZhFKh	Journal of Physical Chemistry (USSR)
ZhRKhO	Journal of the Russian Chemical Society

Note: Abbreviations not on this list and not explained in the translation have been transliterated no further information about their significance being available to us. — Publisher.

SCIENTIST - TRANSLATORS WANTED

For over a decade, Consultants Bureau, Inc. has provided Western scientists with high quality cover-to-cover translations of Soviet scientific journals. Our unique contracts with the Soviet government are constantly revised to include more extensive coverage of technical activity in the USSR. In order to produce these journals at the high standards set down by both the Soviet and American governments, it is of prime importance to maintain a large staff of scientist-translators who can translate with precision in their specific scientific field. It is our strict policy to assign a translator only that material which is within his scope.

As part of our current and future* expansion programs, we have openings for a limited number of scientist-translators who can translate in the fields covered by the following journals:

Journal of General Chemistry

Antibiotics
Biochemistry
Bulletin of Experimental Biology and Medicine
Entomological Review
Microbiology
Pharmacology and Toxicology
Plant Physiology

Automation and Remote Control
Industrial Laboratory
Instruments and Experimental Techniques
Measurement Techniques

Czechoslovak Journal of Physics
Soviet Journal of Atomic Energy
Soviet Physics - Acoustics
Soviet Physics - Crystallography
Soviet Physics - Technical Physics

Our basic requirements are that the scientist-translator have a native command of English, a minimum degree of B.S. in his specific field, and a thorough knowledge of the contemporary technical terminology of his scientific discipline.

Translation may be done at home on a full or part-time basis.

For further information, please contact:

Translation Editor
CONSULTANTS BUREAU, INC.
227 West 17th Street
New York 11, New York

*We expect, in the near future, to initiate a program of translation from the growing amount of important Chinese scientific literature available. In preparation, we are accepting applications from Chinese to English translators.